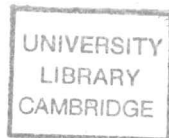


PhD 14685

Radio Echo Sounding Studies of Svalbard Glaciers

Jonathan Louis Bamber



A dissertation submitted for the degree of
Doctor of Philosophy in the University of Cambridge

Jesus College
Cambridge
June 1987



FRONTISPIECE

A glacier in central Spitsbergen—Bakaninbreen—during the active phase of a surge, photographed in May 1987 (courtesy of J.A. Dowdeswell).

PREFACE

The work presented in this thesis was undertaken by the author at the Scott Polar Research Institute between October 1983 and June 1987 under the supervision of Dr D.J. Drewry. The dissertation does not exceed the regulations on length and has not been submitted for a degree at any other university. The collection of radio echo sounding data in 1983 and 1985 were collaborative projects involving many individuals. The analyses and interpretation presented here is, however, the original work of the author unless otherwise stated.

ACKNOWLEDGEMENTS

I would like to thank my supervisor, Dr D.J. Drewry, for his guidance, criticism and help. I have also benefited greatly from discussions with Dr J.A. Dowdeswell, M.R. Gorman, A.P.R. Cooper, Dr G. de Q. Robin and Dr M.J. Hambrey and other members of the university. I wish to thank the staff of the Institute, who have kept it running so efficiently while I have been here and members of the British Antarctic Survey for their advice and help and the use of their facilities. I am grateful to Dr R. Mulvaney for chemical analysis of ice samples and to members of the Chemical Laboratories workshop for building apparatus used in the 1985 field season.

Finally I would like to thank my parents who have been of such support and encouragement during my time in Cambridge.

SUMMARY

Radio Echo Sounding Studies of Svalbard Glaciers

The objective of this study was to investigate the radio echo sounding properties of Svalbard glaciers and to use these data to obtain information about the glaciological environment. Particular emphasis was placed on obtaining an understanding of the dielectric properties of the ice and reflecting boundaries present. These were then used to elucidate the physical processes causing them.

First, a theoretical model, describing the dielectric properties of a wet bed, was developed. The ice/bed interface was then investigated using, as the primary data source, radar reflection coefficients. From these data inferences about the presence of water and/or debris, roughness of the interface and geographical trends were made. A number of geological divides were detected.

Second, the dielectric properties of Svalbard ice were considered using i) radio echo sounding data on the bulk *in situ* radar absorption and ii) measurements made on the dielectric properties of a sample of Spitsbergen ice. Data were collected between 20 Hz and 100 kHz in the temperature range -2.5 to -44.0°C . From these and other data deductions about the thermal regime of the ice masses were made and a geographical trend, linked to the reflection coefficients, observed. The theory of dielectric absorption in ice was discussed with an emphasis on the high frequency, radio echo sounding characteristics.

Third, the properties of an extraordinary internal reflecting horizon (observed on 60% of the glaciers sounded in 1983) were investigated. A model was developed to describe the scattering properties of inhomogeneities (of arbitrary size) within ice. Using this, and data on the reflecting properties of the horizons, they were attributed to the presence of a finite quantity of water. The implications of this finding were considered. Finally, the surface and, where available, bedrock profiles of 40 glaciers and six ice caps, in Spitsbergen, were presented.

TABLE OF CONTENTS

Title page	i
Frontispiece	iii
Preface	iv
Acknowledgements	iv
Summary	v
Table of Contents	vi
List of Figures	ix
List of Tables	xii
List of Symbols	xiii
List of Abbreviations	xv
Chapter 1 THE SVALBARD ENVIRONMENT	
1.1 Introduction	1
1.1.1 Aims of the thesis	1
1.2 Svalbard	3
1.2.1 Introduction	3
1.3 Climate of Svalbard	7
1.3.1 Long Term Trends	8
1.4 Geology	8
1.5 Glaciological Studies in Svalbard	9
1.5.1 Introduction	12
1.5.2 Mass Balance	12
1.5.3 Thermal Regime	17
1.5.4 Other Relevant Glaciological Studies	23
1.5.5 Surging	26
1.6 Introduction to Radio Echo Sounding	28
1.6.1 Recording	31
1.7 Radio Echo Sounding in Spitsbergen	31
Chapter 2 RADIO ECHO SOUNDING IN SPITSBERGEN	
2.1 Introduction	35
2.2 The 1983 and 1985 Field Seasons	35
2.3 Equipment and Recording Techniques	39
2.3.1 The RES Equipment in 1983	39
2.3.2 Recording in 1983	39
2.3.3 RESEquipment 1985	42
2.3.4 Recording in 1985	45
2.4 Data Reduction in 1985	46
2.5 Navigation	47
2.6 Ice Surface and Bedrock Elevations	47
2.6.1 EM Velocity in Ice	48
2.7 Power Calibration	50
2.8 General Results- Topography	52
Chapter 3 THEORY AND APPLICATIONS OF ELECTROMAGNETIC PROPAGATION IN ICE	
3.1 Introduction	57
3.1.1 The Debye Dispersion	57
3.1.2 Propagation of EM waves through a Lossy Dielectric	58
3.1.3 The Radar Equation	60
3.2 Applications	61

3.2.1	Fresnel Reflection	61
3.2.1.1	Bedrock Roughness	62
3.2.2	Reflections from Dielectric Mixtures	65
3.2.3	Dielectric Properties of Water-Saturated Rocks	66
3.2.4	Internal Reflecting Horizons	70
3.2.5	Scattering	72
3.3	Summary	77
Chapter 4 CONDUCTION AND ABSORPTION IN ICE		
4.1	Introduction	78
4.2	Point Defects and Charge Carriers	79
4.3	Jaccard's Theory of Electrical Conduction	80
4.3.1	Relative importance of σ_{DL} and σ_{\pm}	82
4.3.2	HF doping	83
4.3.3	Other Impurities	84
4.4	Polar versus Temperate Ice	87
4.5	Radar Absorption in Ice	88
4.5.1	Laboratory Results	88
4.6	Dielectric measurements on a Spitsbergen Core	92
4.6.1	Introduction	92
4.7	Description of the Core	93
4.8	Results	96
4.8.1	Introduction	96
4.8.2	Modified Complex Conductivities	101
4.9	Discussion	108
4.9.1	Spectrum 2	108
4.9.2	Spectrum 3	109
4.9.3	Static Conductivities	111
4.9.4	Relevance to RES	112
4.10	Summary and Conclusions	114
Chapter 5 RADIO ECHO SOUNDING RESULTS		
5.1	Introduction	117
5.2	Calculation of In Situ Dielectric Absorption	117
5.2.1	Spitsbergen	118
5.2.2	Nordautlandet	122
5.3	Models for Calculating Absorption	128
5.3.1	Errors	129
5.3.2	Calculation of Reflection Coefficients	131
5.3.3	Errors	131
5.4	Reflection Coefficients	133
5.4.1	Spitsbergen	133
5.4.2	Nordautlandet	137
5.5	Internal Reflecting Horizons	139
5.5.1	Introduction	139
5.5.2	Interpretation	142
5.5.2.1	RC values	142
5.5.3	Factors affecting the level of the IRH	143
5.5.3.1	Rothlisberger Channels	146
5.5.3.2	Thermal Regulation	147
5.5.3.3	Extraordinary Glacier Profiles	150
5.6	Summary	158
Appendix 1 GLACIER PROFILES AND RC DATA		
		160

Appendix 2 THEORY AND EXPERIMENTAL PROCEDURE FOR DIELECTRIC MEASUREMENTS MADE ON A SPITSBERGEN CORE	
1	Experimental Procedure..... 180
1.1	Apparatus..... 180
1.2	Bridge Measurements..... 181
1.3	Sample Preparation..... 182
1.4	Temperature measurement..... 185
1.5	Calibration of the Electrodes..... 185
1.6	Experimental Procedure..... 188
2	Theory..... 189
3	Errors..... 191
Appendix 3 DIELECTRIC DATA..... 192	
REFERENCES..... 198	

LIST OF FIGURES

1.1	Map of the Svalbard archipelago showing the major islands.....	4
1.2	Major place names in Spitsbergen.....	5
1.3	Major place names and physiographic features in Nordaustlandet	6
1.4	A simplified geological map of Svalbard	10
1.5	Total accumulation on Nordaustlandet in the winter of 1957-'58	14
1.6	Net mass balance and altitude of equilibrium lines on Austre Brøggerbreen and Midre Lovenbreen between 1966 and 1983.....	15
1.7	Altitudes of equilibrium lines in Svalbard.....	16
1.8	Weight of snow cores in Svalbard.....	16
1.9	Location of temperature measurements in Spitsbergen.....	19
1.10	Shallow ice temperatures in Nordaustlandet and location of deeper boreholes	21
1.11	Temperature-depth profiles for the deep boreholes in Svalbard.....	22
1.12	Stratigraphic records for cores from the Fridtjovbreen-Grønfjordbreen ice divide and Lomonosovfonna plateau.....	24
1.13	Location of glaciers known to have surged in Svalbard.....	29
1.14	Analogue and digitally recorded RES records.....	32
1.15	Previous RES flightlines in Spitsbergen.....	34
2.1 a)	Location of RES flightlines in 1983 and ground-based tracks in 1985 on Spitsbergen.....	36
2.1 b)	Location of RES flightlines in 1983 on Nordaustlandet.....	37
2.2	Block diagram of the RES hardware used in 1983	41
2.3	Digitally recorded waveforms displaying the effects of scattering and ice thickness on echo power.....	43
2.4	Block diagram of RES hardware used in 1985	44
2.5	Receiver calibration data.....	51
2.6	Oscillograph record from Sefströmbreen	55
3.1	Effects of roughness on echo power.....	64
3.2	Permittivities and RCs for a wet bedrock.....	67
3.3	Scattered power from air, rock and water inclusions	75
3.4	Scattering cross section for air, rock and water inclusions.....	76
4.1	H ⁺ ion concentrations in snow samples from Svalbard	86
4.2	Arrhenius diagram of Johari and Charettes' and Westphal's dielectric data .	89

4.3	Density, electrolytic conductivity and anion concentrations down a core from Skobreen	94
4.4	Thin sections from the Skobreen core	95
4.5	ϵ_{∞} vs. temperature for the Skobreen samples.....	97
4.6	Cole-Cole plots at two temperatures for Skobreen samples.....	98
4.7	Logarithmic plot of σ vs. frequency for Skobreen samples.....	100
4.8	Arc plots for two temperatures for Skobreen samples	102
4.9	Arc plots comparing experimental and least squares fitted data applied to spectrum 2 only	104
4.10	Arc plots comparing experimental and least squares fitted data applied to spectrum 2 and spectrum 3.....	105
4.11	Arrhenius plot of $\Delta\sigma_2$ and $\Delta\sigma_3$ for Skobreen samples	108
4.12	Arrhenius plot of relaxation frequencies for Skobreen samples.....	110
4.13	Arrhenius plot of σ_0 for Skobreen samples	112
4.14	Dielectric absorption vs. temperature for Skobreen samples.....	113
4.15	Arrhenius diagram comparing the hf conductivities of a number of different ice samples, including polar, temperate and commercial ices and the Skobreen samples.....	115
5.1	Absorption vs. ice thickness for Borebreen	119
5.2	Absorption vs. ice thickness for four elevation groups on Nordaustlandet....	125
5.3	Mean absorption and temperature vs. surface elevation on Nordaustlandet..	126
5.4	Comparison between different absorption models and the data from Borebreen	130
5.5	Glacier profiles and RC data for Valhallfonna and Olav V ice cap.....	134
5.6	Areal distribution of RC values in Spitsbergen.....	136
5.7	Contour map of RC values in Nordaustlandet	138
5.8	Example of a typical IRH: Borebreen.....	140
5.9	Areal distribution of IRHs in Spitsbergen	141
5.10	RC vs. water content for small spherical water inclusions.....	144
5.11	Comparison between IRH profiles and theoretical 'water table' calculated from Darcy's law and Dupuit's assumptions	145
5.12	Comparison between IRH profiles and theoretical 'water table' calculated from R�thlisberger's theory of subglacial water flow.....	148
5.13	Glacier profile and RC data for Vonbreen	151
5.14	Glacier profile and RC data for Veteranen and Chydeniusbreen.....	152
5.15	Oscillograph record from Veteranen	153
5.16	Scattered power for moraine inclusions with $\epsilon'_r = 9$	155

5.17	'A' scopes from Veteranen indicating a change in reflecting properties.....	157
A1.0	RES records indicating the different reflecting properties of an IRH and bed	161
A1.1	RES flightlines in 1983 and ground-based tracks in 1985.....	162
A1.2	Glaciers sounded in Oscar II Land	163
A1.3	Sveabreen, Kongsvegan, Holmstrombreen and Sefströmbreen.....	164
A1.4	Uvêrsbreen, Nansenbreen, Dahlbreen, Aavatsmarkbreen and Murraybreen ..	165
A1.5	Borebreen, Wahlenbergbreen and Eidembreen	166
A1.6	Glaciers sounded in Albert I Land, Haakon VII Land and James I Land	167
A1.7	Kronerbreen-Holtedahlfonna, Abrahamsenbreen and Vonbreen	168
A1.8	Lilliehöökreen, Raudfjordbreen, Idabreen, Monacobreen, Isachsenfonna and Fjortende Julibreen.....	169
A1.9	Glaciers sounded in Olav V Land	170
A1.10	Hochsteterbreen, Akademikerbreen, Hinlopenbreen, Kvitbreen and Russe- breen.....	171
A1.11	Oxfordbreen, Lomonosovfonna, Tunabreen and Petermannbreen.....	172
A1.12	Vaigattbreen-Olav V ice cap, Fimbulisen and Negribreen.....	173
A1.13	Formidablebreen, Nordenskiöldbreen and Mittag-Lefflerbreen.....	174
A1.14	Glaciers sounded in Ny-Friesland	175
A1.15	Valhallfonna, Dunérbreen and Åsagårdfonna	176
A1.16	Veteranen, Balderfonna, Chydeniusbreen and Tommelbreen.....	177
A1.17	Glaciers sounded in 1985.....	178
A1.18	Bakaninbreen, cross profile from Paulabreen, Skobreen and cross profile from Skobreen	179
A2.1	Plan view of electrodes	183
A2.2	Sample preparation and housing	184
A2.3	Calibration graph for the three pairs of electrodes	186

LIST OF TABLES

1.1	Shallow ice temperatures in Spitsbergen.....	20
1.2	Chemical composition of ice core from Vestfonna and snow samples from Hornbreen.....	25
2.1	System parameters of the SPRI Mk IV in 1983 and 1985.....	40
2.2	Topographic, ice thickness and RC data for the ice masses sounded in Spitsbergen.....	53
3.1	Reflection and transmission coefficients for different interfaces.....	63
5.1	Mean absorption values for ice masses from Spitsbergen.....	121
5.2	Mean absorption values for different elevation groups on Nordaustlandet....	124
A2.1	Calibration data for the three pairs of electrodes.....	187
A3.1	Dielectric data, at all temperatures, for the three Skobreen samples.....	192
A3.2	Results of least squares fitting procedure for dispersion 2.....	196
A3.3	Results of least squares fitting procedure for dispersion 3.....	197

LIST OF SYMBOLS

a	scattering radius
A	effective antenna area; flow law constant
B	dielectric absorption in ice (in dB/100 m)
c	velocity of electromagnetic radiation in vacuo
C_∞	high frequency conductivity constant
d	capacitor plate separation
D	displacement current; const. in Röthlisberger's eqn.
e	charge on an electron
E	electric field vector
E_∞	activation energy of the hf conductivity
f	frequency; volume fraction of an inhomogeneity
f_r	relaxation frequency
G	antenna gain
$h_n^{(2)}$	spherical Bessel function of the 3rd kind
H	terrain clearance
i	denotes imaginary part
j_n	spherical Bessel function of the 1st kind
K	wave number; roughness coefficient in Röthlisberger eqn.
m^*	complex refractive index
$n; n_i; n'; n''$	ice flow law exponent; defect concentration; real and imaginary refractive indices
p	subglacial water pressure
$P; P_r, P_t$	overburden pressure; receiver and transmitter power
Q_i	effective charge on an ionic or Bjerrum defect
r	distance from source to scatterer; correlation coefficient
R	reflection coefficient
$S_w; S_1$	fraction of water saturation in rock pores; backscattering amplitude
T	transmission coefficient; temperature
$V_g, V_p; V_2$	group and phase velocities; volume fraction of inclusion
W	energies of reaction
x	dimensionless scattering parameter (related to scattering radius and EM wavelength)

z	ice thickness
Z	intrinsic impedance
α	attenuation const.
β	phase const.; bed slope
γ	exponent in the eqn. of a depressed arc (for modified complex conductivities)
ϵ	permittivity
ψ and ζ	Riccati Bessel functions
λ	wavelength in sounding medium
$\mu_0; \mu_i$	permeability of free space; defect mobility
ρ	density
σ	conductivity; scattering cross section
τ	relaxation time
ϕ	rock porosity
ω	angular frequency

Superscripts

*	complex quantity
'	real part; first derivative
"	imaginary part
-	mean value

Subscripts

o	dc or free space value
∞	hf value
m	value for a mixture of two dielectrics

LIST OF ABBREVIATIONS

BAS	British Antarctic Survey
BD	Bjerrum defect
EM	electromagnetic
fm	formation
Gp	Group
HH	Hecla Hoek
ID	ionic defect
IRH	internal reflecting horizon
MAAT	mean annual air temperature
NP	Norsk Polarinstitut
RC	reflection coefficient
RES	Radio echo sounding
SPRI	Scott Polar Research Institute
TCL	terrain clearance

CHAPTER 1

THE SVALBARD ENVIRONMENT

1.1 Introduction

This chapter begins with a brief introduction to the thesis, explaining its aims and how they were achieved. This is followed by a description of the environment of Svalbard, emphasising the factors that are most relevant to radio echo sounding (RES). These include the thermal regime, chemical composition of the ice and a short description of the geology of the archipelago. Other factors of glaciological importance are also discussed. The chapter is concluded by an introduction to the RES technique and a description of previous RES studies carried out in the region.

1.1.1 Aims of the thesis

This thesis investigates the radio echo sounding properties of Svalbard glaciers using data collected during an airborne field season in 1983, a ground based operation in 1985 and laboratory experiments on the dielectric properties of a Spitsbergen ice core. The geographical emphasis is directed mainly towards the ice cover over Spitsbergen although data from Nordaustlandet are also included for comparative purposes. A comprehensive study of the surface and bedrock morphology of the latter land mass, using RES and other remote sensing data, has been already undertaken (Dowdeswell, 1984). Particular emphasis is placed on obtaining an understanding of the dielectric properties of the reflecting surfaces and to use these to elucidate some of the physical processes present within and beneath the ice.

The specific objectives of this thesis are to

- (1) obtain a better understanding of the ice/bedrock interface using, as the primary data source, radar reflection coefficients. Models are developed to describe the possible bedrock environment from these data.
- (2) deduce information about the bulk dielectric properties of the ice from *in situ* RES data and to compare these with more detailed laboratory measurements on Spitsbergen ice core samples. These data are used to make inferences, where possible, about the bulk thermal regime of the ice. The theory of dielectric absorption in ice and mixtures of dielectrics

along with results from different ice samples is discussed in some detail.

(3) to present surface and, where available, bedrock topographic information for 34 glaciers and 6 ice caps, on Spitsbergen, and to investigate the cause(s) of a single, pronounced internal reflecting horizon on 25 of these ice masses.

1.2 Svalbard

1.2.1 Introduction

Svalbard comprises a group of islands that lie between latitudes, 74° and 81° N, and longitudes, 10° and 35° E. The two largest islands, and those investigated in this work, are Spitsbergen ($39,000 \text{ km}^2$, known as Vestspitsbergen until June 1969) and Nordaustlandet ($15,000 \text{ km}^2$). They are shown in Fig. 1.1 together with the other five major land masses of the archipelago. Figures 1.2 and 1.3 show the place names and some physiographic features of Spitsbergen and Nordaustlandet respectively.

The terrain of much of central and eastern Spitsbergen is characterised by plateau-type mountains divided by broad glaciated valleys. Towards the west, moving from sedimentary strata to metamorphic and igneous rocks (Fig. 1.4), the topography becomes more jagged and angular. The highest peaks, at an altitude of 1717 m, are to be found in north-east Spitsbergen. Typically the relative surface relief of glaciers is from sea level at the snout to about 700 m a.s.l. at the head and similarly on Nordaustlandet. In north-east Spitsbergen there is an area of high mountain terrain with ice cover over 1000 m a.s.l. Bedrock elevations beneath glaciers in the west can extend down to 100 m b.s.l. (App. 1).

Approximately 60% of Svalbard is ice covered and the extent of glacierization tends to increase moving north and eastward. This trend is reflected in Nordaustlandet where the largest ice caps of the archipelago are located; Vestfonna has an area of 2510 km^2 and Austfonna-Sørfonna an area of 8105 km^2 (Dowdeswell, 1984) which cover some 75% of the island. Moving further east, Kvitøya is almost completely ice covered. As with the extent of glaciation the thermal regime of glaciers in Spitsbergen is extremely varied and complex. Austre-Brøggerbreen (78.8°N , 11.5°E) on the west coast of James I Land is believed to be cold along its entire length (Liestøl, 1984) and frozen to its bed while borehole measurements on Amundsenisen (77.25°N , 15.5°E) in Wedel Jarlsberg Land further south suggest that it is close to the melting point throughout (Zotikov and Zagorodnov, 1981). The percolation and refreezing of meltwater in the accumulation zone of many glaciers is an important factor in the heat budget (e.g. Sverdrup, 1935) and can lead to higher values of ice surface temperatures at higher elevations. An added complication is the fact that over 60 glaciers in Svalbard are believed to have surged (section 1.5.5). Consequently the region should be of considerable glaciological interest yet, despite this, only a handful of glaciers have been studied in any detail and, in general, the bulk of the ice

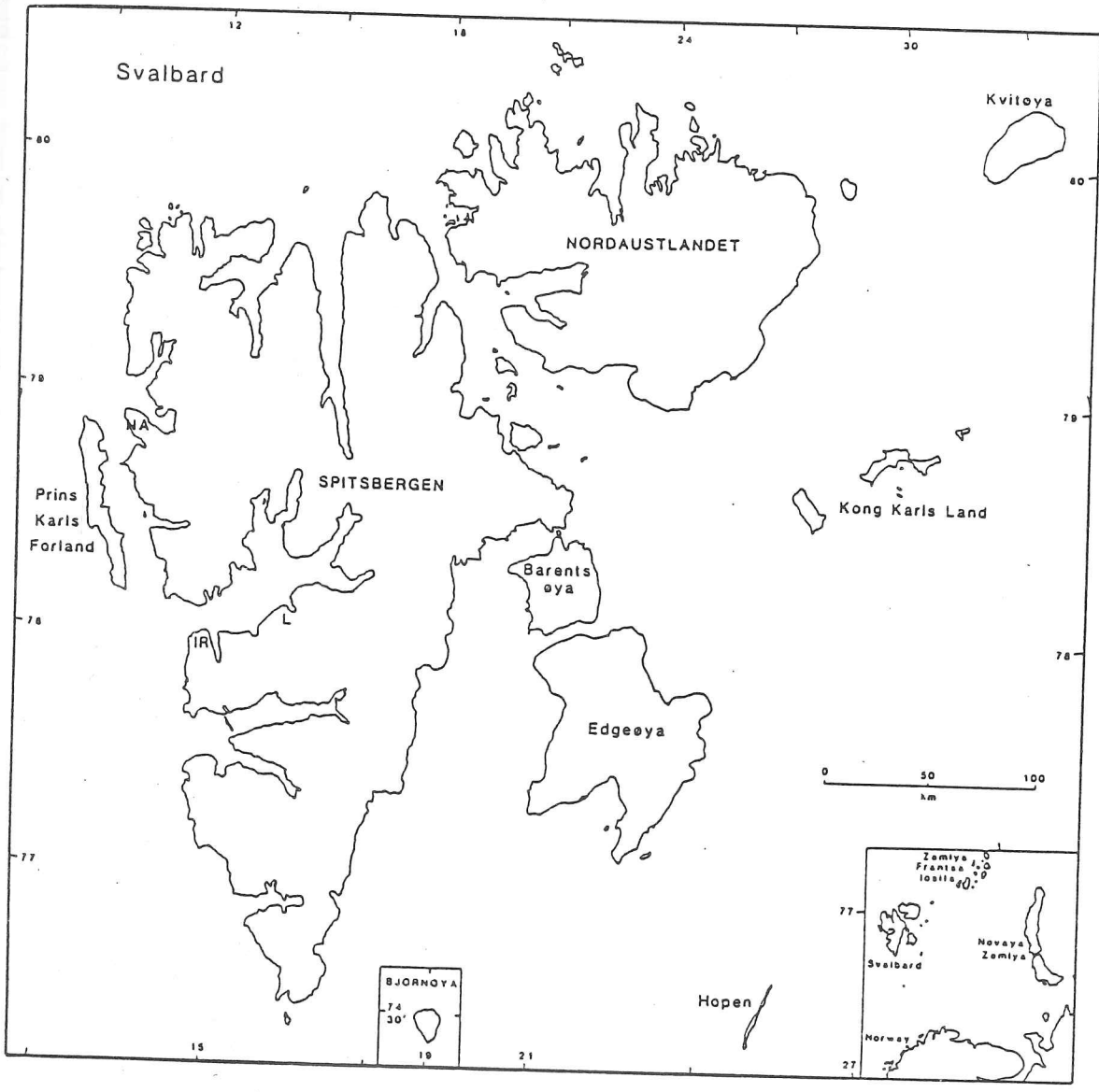


Fig. 1.1 Map of Svalbard showing the major islands of the archipelago. The inset locates Svalbard relative to Norway and neighbouring islands.

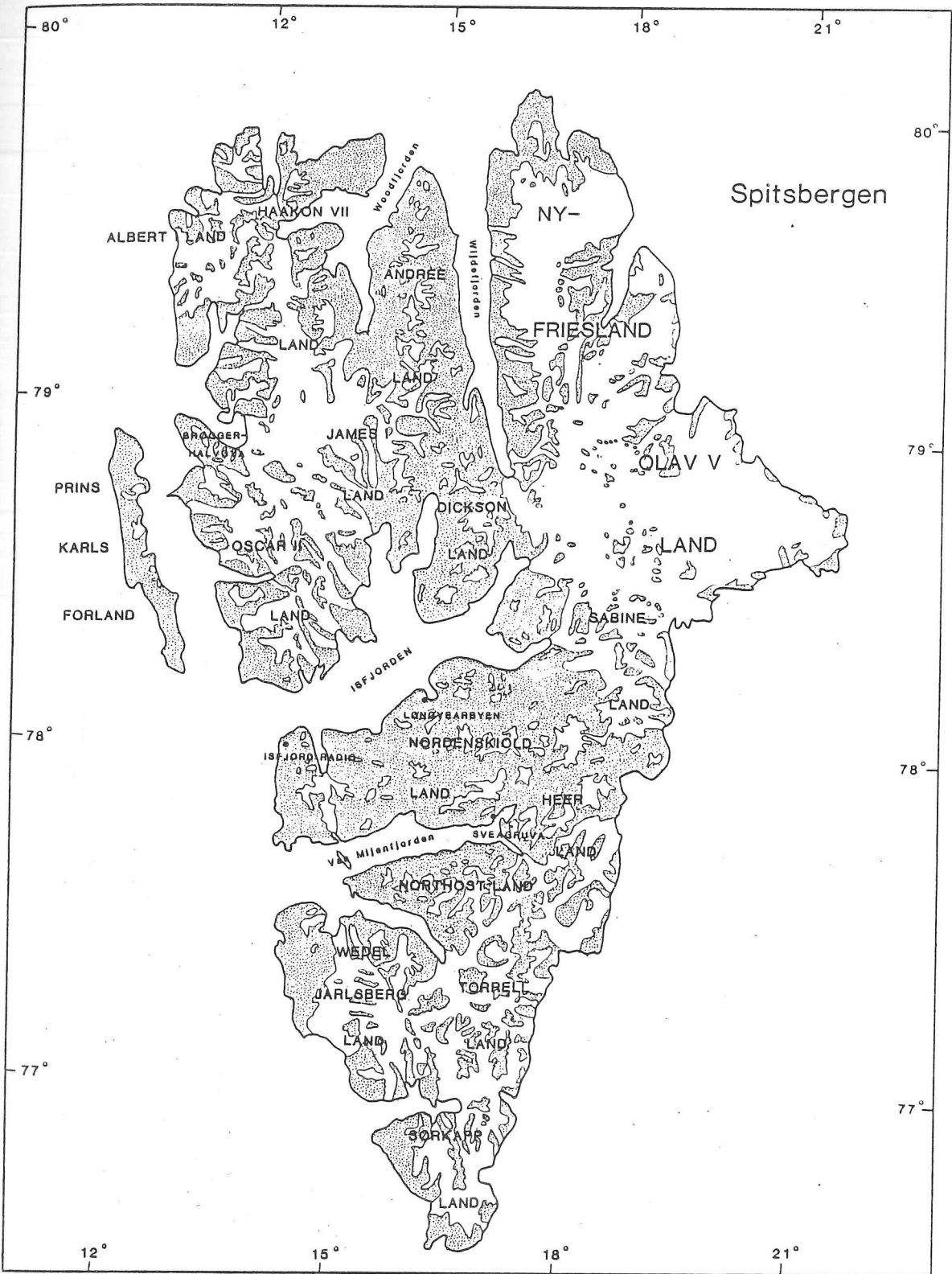


Fig. 1.2 Major place names in Spitsbergen.

cover has been little investigated. An attempt has, therefore, been made to redress this situation using data from an extensive network of RES flight-lines. In particular, deductions about the bulk thermal regime of the glaciation are made. They are shown to have an areal pattern which is reflected by the climatic variations observed across the archipelago. Consequently, a brief account of the climatic changes, that occur in both time and location, are given in the next section.

1.3 Climate of Svalbard

There are two principal data sources on climatic characteristics of Svalbard, from weather stations and from isotopic analysis of deep ice core samples. Dating of the samples also allows trends in the net mass balance to be observed. These two sources are discussed separately.

There are three permanent weather stations, the earliest continuous record starting in 1916 (for Isfjord Radio): Longyearbyen Lufthaven (78.2° N, 15.7° E) formerly Isfjord Radio (78.1° N, 13.6° E), Hopen (76.5° N, 25° E) and Bjornoya (74.5° N, 19° E). These are all located in coastal regions and consequently may not be representative of the whole of Svalbard. Cloud cover, wind speed and direction for Longyearbyen Lufthaven and monthly mean temperatures for all three stations are published annually in the Norsk Polarinstitutts Årbok.

Svalbard, and particularly the western side of Spitsbergen, experiences relatively high mean winter air temperatures compared with those for other land masses at similar latitudes. The long-term average for the coldest months (January–March) for Isfjord Radio (78.1° N, 13.6° E) is -11.9°C (Hisdal, 1985) and there is a gradual fall in this value towards the east. These comparatively warm temperatures (c.f. Isachsen station in the Canadian Arctic, at a similar latitude, which recorded a value some 20° C lower for the same months) are mainly attributed to the North Atlantic Current and the transport of air from lower latitudes. The winter temperature range is between -8 to -16° C. In summer, on the west coast, temperatures are typically about 5° C and values outside the range 1 to 10° C are not common (Hisdal, 1985).

1.3.1 Long Term Trends

Soviet scientists have undertaken detailed isotopic analyses of three cores from Svalbard giving a proxy climatic record stretching back some 800 years (Vaykmyae *et al*, 1984). The first core was retrieved from the Grøn fjordbreen–Fridtjovbreen ice divide at an elevation of 450 m. 203 m of a 213 m core to bedrock were analysed to determine the $^{18}\text{O}/^{16}\text{O}$ ratios (Punning *et al*, 1980). The second was taken from Lomonosovfonna, at an altitude of 1000 m, and reached a depth of 200 m (Gordiyenko *et al*, 1981). The third core was from Vestfonna, 580 m a.s.l. and recorded the most negative mean $\delta^{18}\text{O}$ value (implying the coldest temperature), as it is some 100 m higher, 2° further north and 5° further east of the first site (Vaykmyae *et al*, 1984). The general climatic trends seem to be similar in all their cores, although the Little Ice Age (a cold period extending from the 17th to late 19th century) began somewhat later on Nordaustlandet than on Spitsbergen.

Three distinct periods are visible in the oxygen isotope curves. Between the 13th and 16th centuries the values are close to those at present, implying a similarity in meteorological conditions. This period was followed by the Little Ice Age lasting to the beginning of this century when temperatures began to rise again.

The temperature rise in north-western Europe at the beginning of the Twentieth Century was particularly marked in Svalbard. On the west coast historical records show that the mean winter temperatures increased by 8°C (Hisdal, 1985) between 1915 and 1920 before declining again. From 1950 to 1960 there has been a further marked increase in temperatures. These observations imply a changing thermal environment with time. Hence, deep ice temperatures may reflect the non steady-state climate. Some shallow ice temperatures may thus be reflecting the warm period between 1950–60 and could lead to misinterpretation of the bulk thermal regime of the ice. Such possibilities are discussed further in section 1.5.3

1.4 Geology

The type of bedrock beneath the glacier is important in determining its RES properties (Ch. 3) and in this section a brief outline of the lithology will be given and used in Ch. 5 to aid an understanding of the bedrock reflecting properties. Only a fairly general discussion is presented, with the emphasis on the description of the rock types underlying the glaciers that were sounded by SPRI in 1983 (Ch. 2). The material for this section was obtained from the four-part geological map series—Norsk Polarinstitut Skrifter 154 (Flood *et al*, 1971; Hjelle and Lauritzen, 1982).

The lithology varies widely in its composition, age and porosity (Winsnes *et al*, 1962) and the area has often been described as a geologic picture book (Hisdal, 1985). The rocks may be conveniently grouped into six divisions according to age and are shown in Fig 1.4 (after Winsnes *et al*, 1962). These divisions do not, however, refer to the rock type which can vary considerably within each division. These are divided into a hierarchy of units of common affinities which in decreasing order of size are complexes, supergroups, groups (Gps) and formations (fms). Hence the lithology is complex and a more specific description may be obtained from papers referring to particular regions or groups. All the pre-Devonian (c. 400 Ma) rocks of Svalbard have historically been referred to as the Hecla Hoek (complex), the type area being N.E. Spitsbergen. This usage is still maintained by the Norsk Polarinstitut. Harland (1985), however, has argued that, since there is strong evidence that Svalbard consists of at least three tectonic provinces that were widely separated in pre-Devonian times, the use of the term Hecla Hoek (HH) outside the type area is unwarranted. For the purposes of this work, however, the broader Norwegian usage is followed (e.g. Hjelle and Lauritzen, 1982). In this classification the HH is divided into Lower, Middle and Upper.

The HH complex is most widely developed in north-east and north-west Spitsbergen and Nordaustlandet. The Lower Hecla Hoek (LHH), also known as the Stubendorffbreen Supergroup, exposed in the north and north-west of Spitsbergen and on Nordaustlandet mainly consist of feldspathic and amphibolitic gneisses. In north-west Nordaustlandet, however, quartzites, siltstones and shales overlain by a basal conglomerate consisting of intermediate to basic extrusives are also present. The Middle Hecla Hoek (MHH or Lomfjorden Supergroup) in Ny-Friesland and Olav V Land is divided into two groups. The Veteranen Gp comprises mostly greywackes and quartzites and underlies Valhallfonna and part of Veteranen (Fig. 2.1). The Akademikerbreen Gp, underlies five ice masses sounded in 1983—Kvitbreen, Russebreen,

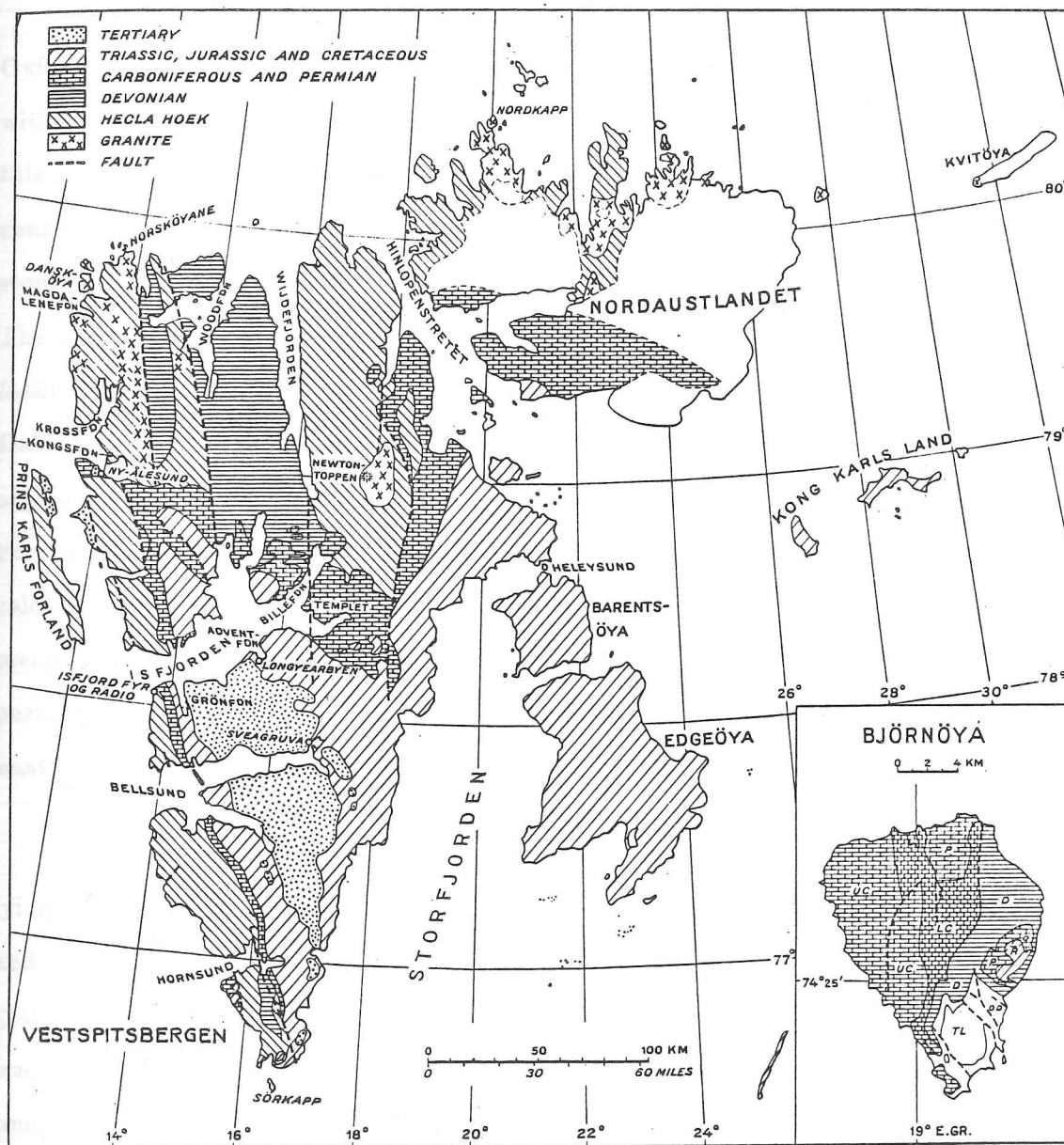


Fig. 1.4 Generalised geological map of Svalbard (source Winsnes et al, 1962).

Oxfordbreen, Akademikerbreen and Lomonosovfonna. It consists predominantly of carbonates with some stromatolite beds. The Upper Hecla Hoek (UHH or Hinlopenstretet Supergroup) of this region comprises carbonates, tillites, sandstones and shales, with some graptolitic limestone near the top. In north-west Nordaustlandet the LHH consists of a sequence of quartzites, siltstones and shales overlain by a basal conglomerate made up of intermediate to basic extrusives. The MHH consists of mudstones, sandstones and shales, and the UHH of tillites, shales and fossil-bearing beds. South of Engelskbukta (incorporating Uvêrsbreen, Aavatsmarkbreen and Dahlbreen) MHH and UHH rocks comprising, from bottom to top, the Quartzite-Shale, Calcargillo Volcanic, Tillitic conglomerate and Bulltinden fms. north and south of St Jonsfjorden. Further north, beyond Kongsfjorden, is an extensive area of LHH which consists primarily of calcareous, gneissose, amphibolitic marble and quartzite rocks. Moving further north these merge into marbles and pelitic rocks with subordinate quartzite. North-east of Lilliehöökreen paragneisses and pelitic rocks prevail. Some granites are also present. The thin wedge of LHH east of Isachsenfonna (Fig 1.4) comprises pelites in the north and migmatite moving south.

The next most extensive development of rocks (in the area of interest) is of Devonian age, lying in central northern Spitsbergen and encompassing Abrahamsenbreen, Holmstrombreen and part of Holvedahlfonna. It is interrupted in the west by a narrow 'finger' of LHH (gneisses, granites and pelites) and is finally terminated by a faultline running down the Monacobreen-Isachsenfonna valley. It extends south as far as the Wijdefjorden-Billefjorden fault zone and comprises mainly continental and fresh or brackish water deposits. Around Raudfjordbreen and Monacobreen (at its northern limit) coarse conglomerates and sandstones predominate. Southwards, sandstones are most common although the Mimer valley Gp has a more varied lithology.

Rocks of Carboniferous and Permian age probably underly the greatest proportion of glaciers sounded in '83 (Sveabreen, Sefströmbreen, Hinlopenbreen, Balderfonna, Tommelbreen, Tunabreen, Petermannbreen, Fimbulisen and parts of Akademikerbreen, Chydeniusbreen and Negribreen). These rocks are bounded by Brøggerhalvøya in the north-west, Mittag-Lefflerbreen in the north-east and Fimbulisen in the south. They are made up of a number of groups. The Billefjorden Gp (the oldest) consist of sandy fluvial deposits, interfingered with fine grained coal-bearing, flood-plain deposits. South of this is the Gipsdalen Gp divided into a lower limestone part-Nordenskiöldbreen fm, and an upper dolomite-evaporite unit—the Gipshuken fm (gypsum/anhydrite and dolomites with local conglomerates and breccias, which are sul-

phitic sediments). Triassic and Lower Jurassic beds are also widely exposed throughout the archipelago comprising mainly shales, siltstones and sandstones. Five fms have been identified. Among these are the Vardebukta fm in the Sassendalen Gp which is made up of sandstones with varying amounts of interbedded siltstone and clay. The Sticky Keep and Botneheia fms consist of dark grey shales. The De Geerdalen Gp (south of Sassendalen) alternates between grey-green sandstones and sandy shales.

In conclusion it can be stated that generalisations about the lithology underlying a particular glacier are not possible. It can be seen, however, that the majority of glaciers sounded in 1983 lie on relatively unresistant sedimentary deposits (with comparatively high carbonate concentrations)— sandstones, shales, siltstones, tillites and conglomerates being the most common. Harder metamorphics (granites, gneisses, pelites etc.) are only present in significant quantities in north-east Spitsbergen and Nordaustlandet. These rocks generally have a smaller carbonate content and are consequently likely to be less soluble (M.J. Hambrey, personal communication). This fact will be seen to be of importance when discussing the regional variations in the radar reflectivity of the bed (Ch. 5).

1.5 Glaciological Studies in Svalbard

1.5.1 Introduction

Modern glaciological work in Spitsbergen began with the Swedish-Norwegian expedition of 1931. Snow stratification was studied in shallow pits on Isachsenfonna (Ahlmann, 1935) allowing an estimate of the net mass balance to be made and these were combined with measurements of 10m temperatures and ablation (Sverdrup, 1935).

More recent work includes a detailed and long-term investigation of Werenskioldbreen (77°N, 15°E) by Polish scientists started in 1957. Yearly measurements of mass balance along the length of the glacier have been made (Baranowski, 1975) and in the first two years surface velocities were also measured. In later seasons hydrological and geomorphological studies were carried out (Baranowski, 1975).

Other glaciers that have received attention include Midre Lovenbreen and Austre Brøggerbreen (77.8°N, 12°E), where mass balance data have been collected continuously since 1966 (Liestøl, 1984). Measurements on Finsterwalderbreen (77.3°N, 15°E) began in the early 1950's and included a gravimetric survey carried out in 1963 (Husebye *et al*, 1965), surface velocity, mass

balance and 10 m temperatures (Liestøl, 1969, 1976).

Of particular relevance to this thesis are data on the thermal regime and chemical composition of Spitsbergen ice. Studies on these and related topics will now be discussed. The mass balance has an important rôle in determining the temperature profile within a glacier (e.g. Clarke *et al*, 1977) and hence its thermal regime. The heat budget above and below the equilibrium line can be markedly different (section 1.5.3) and in the next section measurements on the mass balance are described.

1.5.2 Mass Balance

In 1958 Schytt made a traverse across Nordaustlandet as part of the Swedish IGY expedition to Svalbard (Schytt, 1964). He measured the total accumulation in 75 snow pits at different locations and produced, from this data, a contour map of total accumulation over the island (Fig. 1.5). Measurements were accurate to about $\pm 100 \text{ kg m}^{-2}$. Combined with field measurements, collected by SPRI in 1983, these data imply that the equilibrium line lies at an approximate elevation of 300 m a.s.l. (Dowdeswell, 1984).

In Spitsbergen several glaciers have had mass balance studies. The most comprehensive and extensive work has been carried out by the Norsk Polarinstitut on Midre Lovenbreen and Austre Brøggerbreen. These two glaciers lie on the west coast of central Spitsbergen on a small peninsula—Brøggerhalvøya (78.8°N , 12°E)—and are situated close to a number of the glaciers that were sounded in 1983 (Fig. 1.9 and 2.1). Snow stake measurements along the length of the glaciers have been made since 1966 and in the period 1966 to 1983 both glaciers have shown a net deficit of -350 and -440 kg m^{-2} respectively. Figure 1.6 shows the net mass balance and location of the equilibrium line for this period. Both glaciers have clearly been depleting over the last 16 years and Austre Brøggerbreen has never been recorded as having a positive balance since measurements began. It is a thin glacier ($< 75\text{m}$) and Liestøl (1983) observes that it drains no water in winter. It has negative 5 m temperatures in both the accumulation and ablation zones in summer and combined with its slow velocity, he concludes that it must be cold throughout and frozen to its bed.

On a more general scale, Liestøl and Roland (unpublished) have produced a map of equilibrium lines for the archipelago (Steffenson, 1982) based on Landsat imagery, aerial photographs and a limited ground dataset (Fig. 1.7). The height of the equilibrium line is dependent upon several factors, though Steffenson believes that the primary influence is the level of precipita-

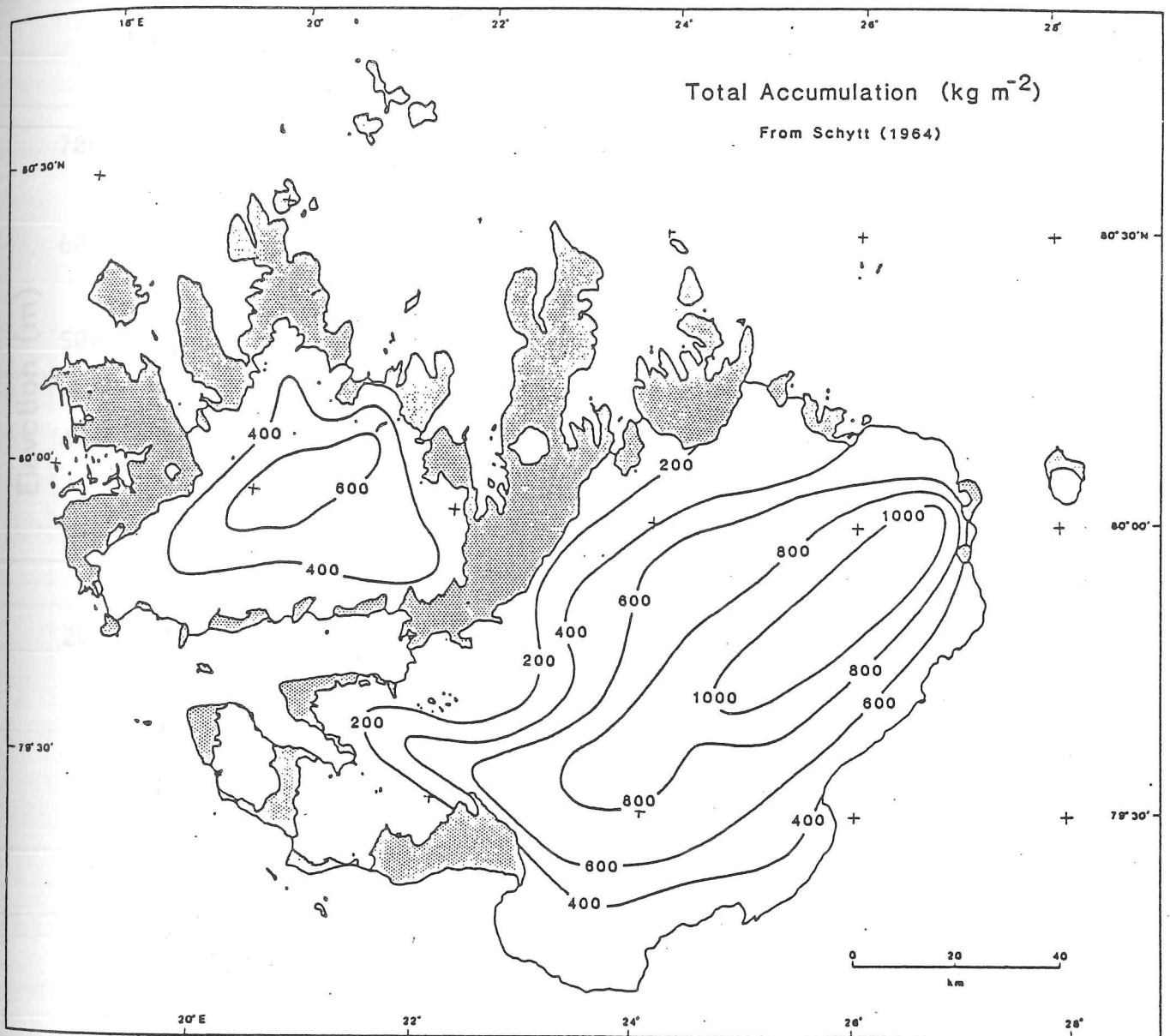
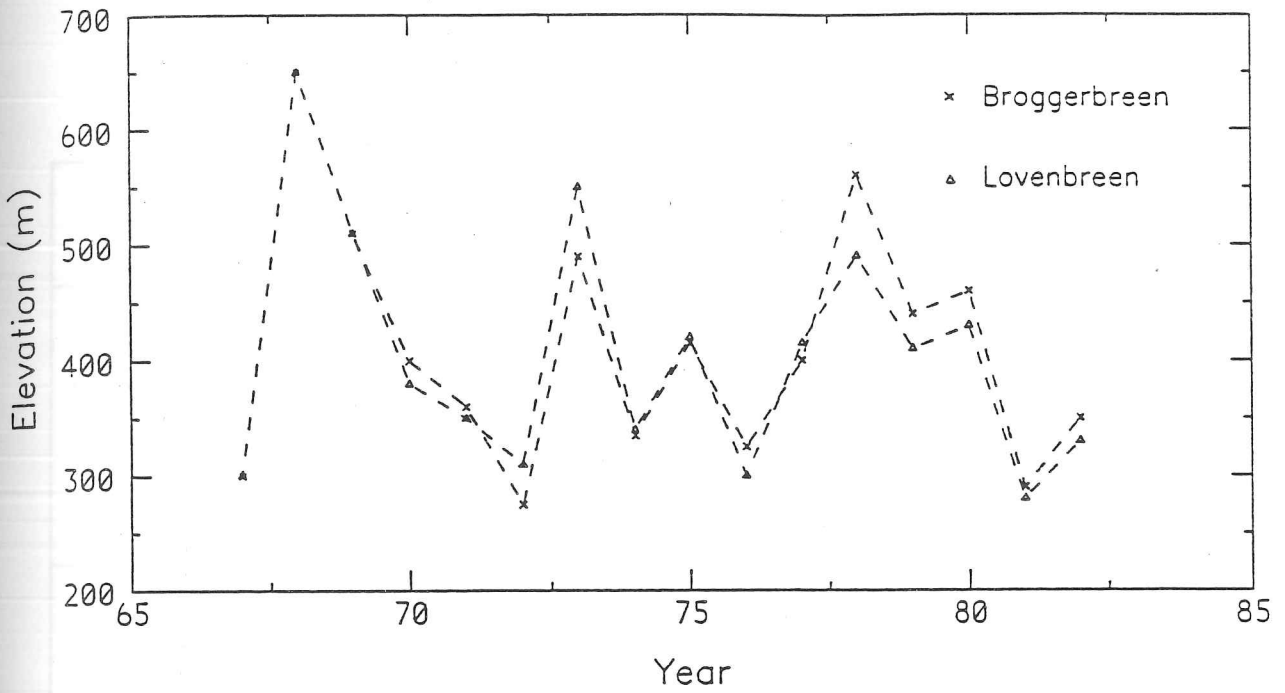


Fig. 1.5 Total accumulation on Nordaustlandet in the winter of 1957-58 (source Schytt, 1964).

Elevation of Equilibrium Line



Net Mass Balance

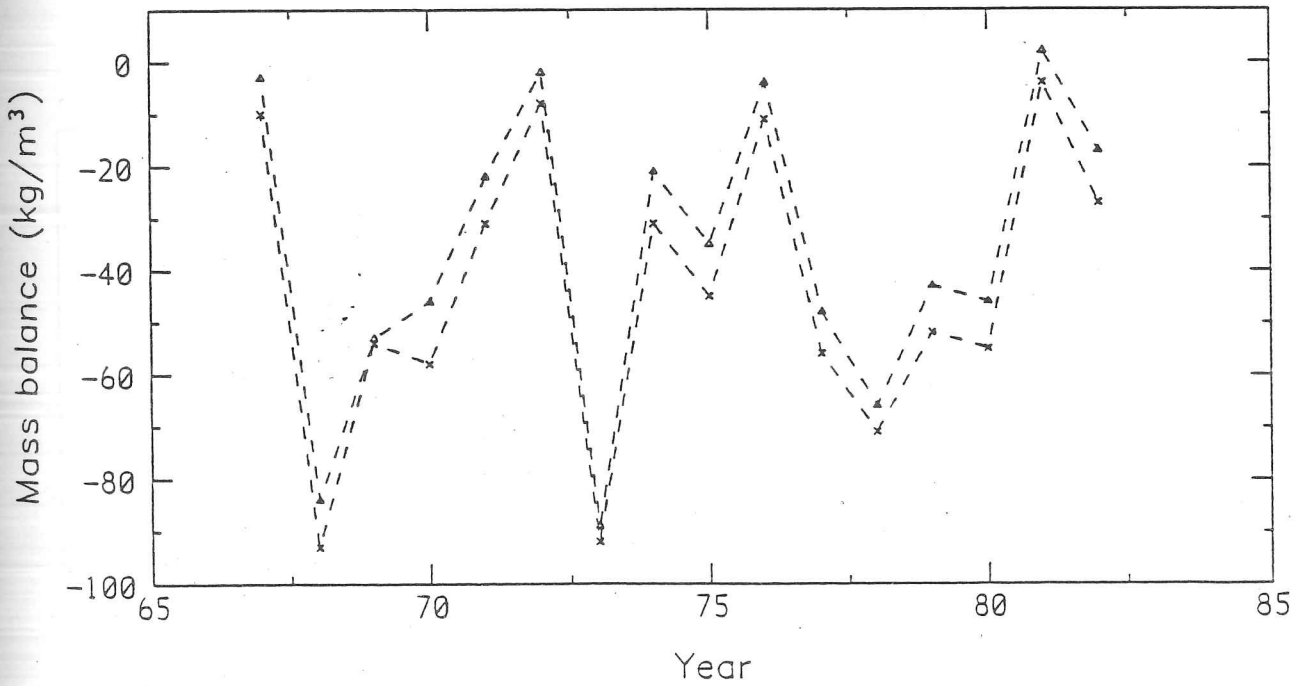


Fig. 1.6 Elevations of the equilibrium line and mass balance data for Lovenbreen and Auste-Brøggerbreen between 1966 and 1982. (source Norsk Polarinstitut Årbok 1966-'83).

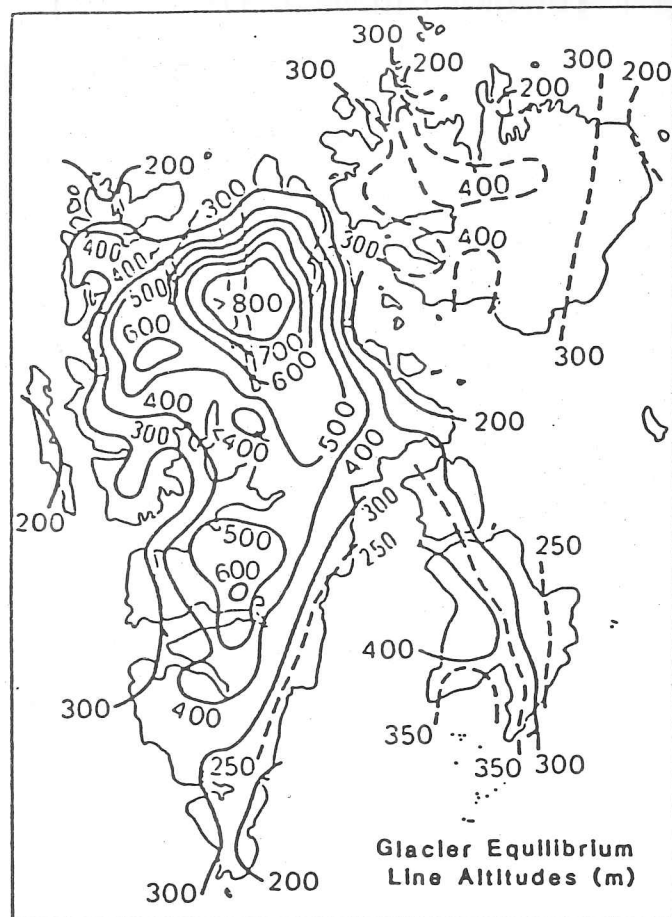


Fig. 1.7 Altitude of glacier equilibrium lines, derived from aerial photographs, Landsat imagery and direct observations (source Steffenson, 1982).

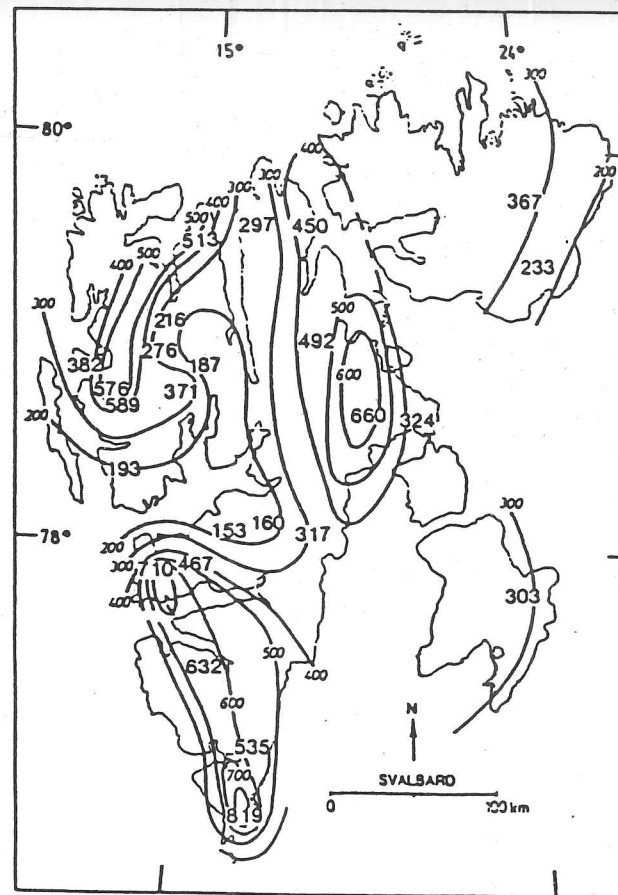


Fig. 1.8 Weight of snow cores plotted in precipitation equivalents (mm) collected in April 1983 (source Semb et al, 1984).

tion. Hence the 'desert region' of Svalbard is to be found in northern Spitsbergen where the equilibrium lines lie at 800 m a.s.l. and above. Data from this source are used in Ch. 5 and App. 1 to estimate the approximate equilibrium lines of specific glaciers.

Semb *et al* (1984) collected snow samples at the end of the winter, from sites throughout Spitsbergen and Nordaustlandet. Cores were taken down to the ice layer representing the previous summer's surface, usually from the middle of the accumulation zone. The level of precipitation was estimated from the weight of snow and the regional pattern is shown in Fig 1.8. It is consistent with the results of Liestøl and Roland and again indicates a relatively arid zone in the north of Spitsbergen. The orographic nature of the snow fall is also evident—the largest values coming from locations facing south or east and generally increasing with altitude between 600 and 800 m a.s.l.

1.5.3 Thermal Regime

Before discussing the thermal regime of Svalbard glaciers, a short discussion on some of the commonly used terms is required. In general the terms that describe the thermal characteristics of an ice mass will not be adopted. Many of the glaciers in Svalbard are polythermal, displaying properties of both 'temperate' and 'polar' ice— terms originally defined by Ahlmann (1933) as part of a geophysical classification of glaciers. The former term is used to describe any glacier, or part thereof, that is at its melting point. The term 'cold' will be used to refer to any ice that is below this temperature. In Ch. 4 when dealing with the dielectric properties of ice, the term 'polar' is used to describe ice possessing certain electrical characteristics which are generally associated with cold glaciers. This is in keeping with the literature, which uses the term 'polar' for such samples (e.g. Glen and Paren, 1975). The term 'sub-polar' will be avoided wherever possible.

The single most important variable that influences the propagation of radio waves through ice is temperature (e.g. Johari and Charette, 1975). A reduction from the melting point to -8°C can halve the dielectric absorption. It is, however, a poorly known parameter for the majority of Spitsbergen glaciers and the available deep (> 50 m) borehole data is limited to three glaciers on Spitsbergen (Zagorodnov and Zotikov, 1981) and one site on Austfonna (Vallon, personal communication).

Despite the specific variability from glacier to glacier, the general trend in lower mean annual air temperatures (MAATs) moving north and east across Svalbard (Hisdal, 1985) is

supported by these deep ice temperatures and the results of RES data in 1983 (Dowdeswell, 1984) and it will be shown (in Ch. 5) that this is reflected in the RES characteristics of the ice masses. The pattern is, however, not universal as glaciers in southern/central Spitsbergen have been observed to be colder than many of their counterparts further north. For example Austre Brøggerbreen, in James I Land ($78^{\circ}50' \text{ N}$, $11^{\circ}30' \text{ E}$), and Foxfonna (78°N , 16°E) are both believed to be frozen to their beds (Liestøl, 1984; 1974) while RES data (Ch. 5) suggests that many of the glaciers sounded in Haakon VII Land (i.e. further north) have a considerable part of their thickness (100–200 m) at the melting point. Generalisations about the thermal regime, due to geographical location, are clearly not possible and other factors are often more important (as in the examples quoted, where the thinness of the glaciers allowed penetration of the cold winter wave to bedrock) (Paterson, 1981). 10 m temperatures may also be misleading as they may not represent a stable value locally or seasonally (e.g. the results of Sverdrup (1935) on Isachsenfonna and data from the crest of Austfonna). This is a consequence of the percolation and refreezing of meltwater in the firn during the summer (Muller, 1963). The variability of this contribution to the heat budget could explain the markedly different values for the 10 m temperatures near the summit of Austfonna, which range from -1°C (Semb, private communication) to -6.4 (Dowdeswell, 1984).

Shallow ice temperatures are thus of limited use for describing the bulk thermal regime of glaciers and may lead to erroneous conclusions if treated without caution. They can, however, give useful information about the thermal regime of the surface layer of ice and if collected at several different locations, above and below the equilibrium line, will help elucidate trends with elevation. Values from above the firn line, where the surface is more permeable, are more likely to be the most variable. They cannot be used to represent the MAAT or as the surface boundary condition in a steady state temperature model. In fact for many of the glaciers in Svalbard which are known to surge such a model is of very limited use whether well defined boundary conditions are available or not. All the available data are listed in Table 1.1. Fig. 1.9 shows the location of the temperature measurements in Spitsbergen that are described in the table. In Fig 1.10 the shallow ice temperature measurements that have been made on Nordaustlandet and the location of the deeper boreholes are marked. Temperature depth profiles are shown in Fig. 1.11 for the deeper data from Nordaustlandet and Stollbreen (Fig. 1.9).

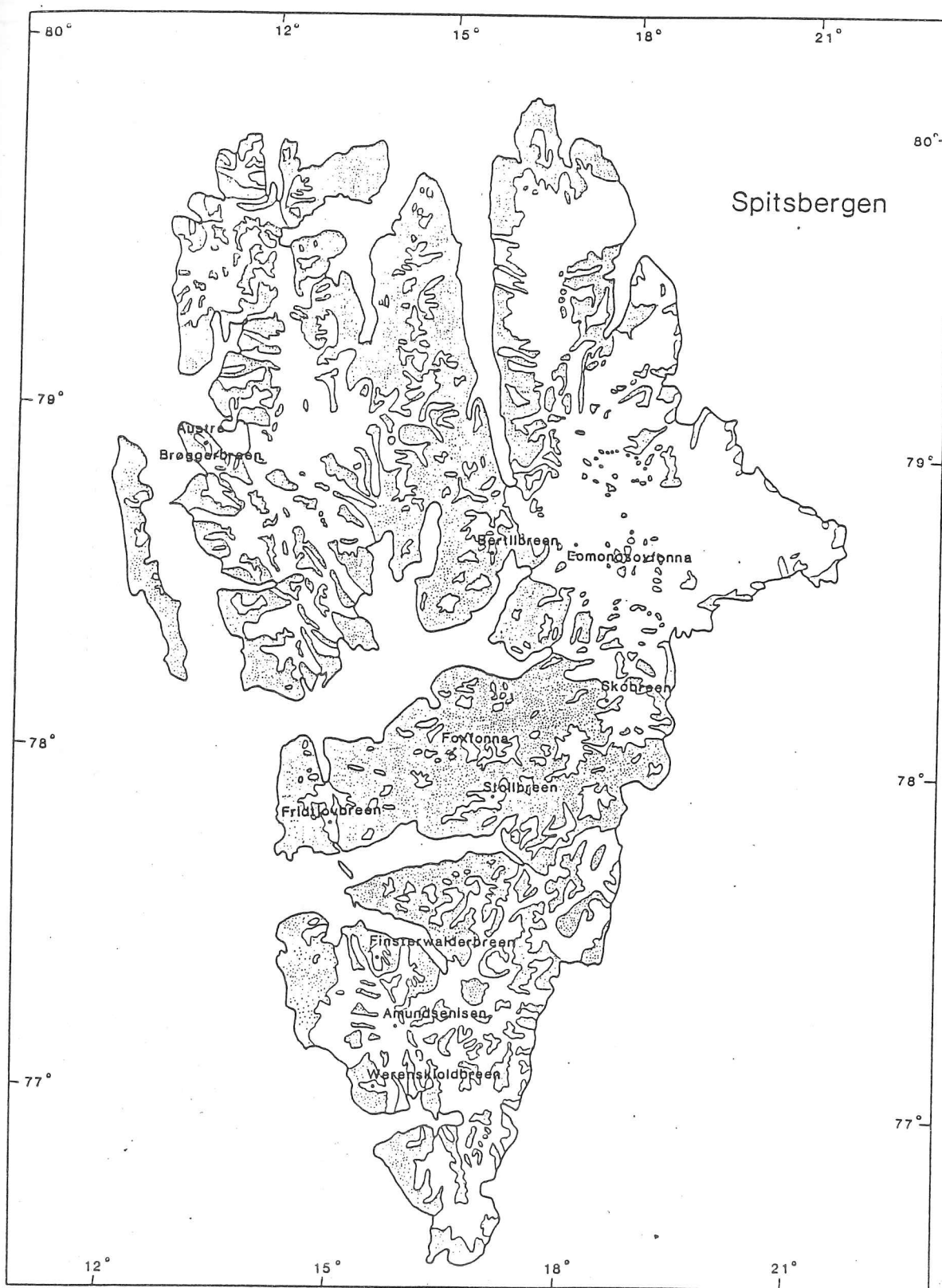


Fig. 1.9 Location of temperature measurements in Spitsbergen.
(Data are presented in Table 1.1 and Fig. 1.11).

Table 1.1 Shallow ice temperature measurements in Spitsbergen.

Glacier	Altitude of site (m)	Latitude in degrees	Longitude in degrees	10 m temperature (°C)	Mass balance zone	
a) Werenskioldbreen	i)	50	77.1	15.3	-2.5 (8 m)	ablation
	ii)	225	"	"	-4.2 (8 m)	"
	iii)	380	"	"	-3.2 (8 m)	equil. line
	iv)	550	"	"	0 (15 m)	accumulation
b) Amundsenisen	700	77.3	15.5	-0.7	accumulation	
c) Finsterwalderbreen	i)	95	77.3	15	-4.2	ablation
	ii)	320	"	"	-3.5	"
	iii)	410	"	"	-3.0	"
	iv)	470	"	"	0	"
	v)	600	"	"	0	"
d) Fridtjovbreen	410	78.8	14.4	-0.16 (17 m)	accumulation	
e) Stollbreen	i)	335	77.9	16.7	-4.6 (8 m)	
	ii)	444	"	"	-4.7	
	iii)	503	"	"	-3.2 (8 m)	
f) Foxfonna†	i)	500	78.2	16.4	-6.5 (30 m)	ablation
	ii)	580	"	"	-3.3 (70 m)	"
g) Skobreen	495	77.75	17.2	-2.8	accumulation	
h) Bertilbreen	i)	340	78.7	16.3	-4.2	ablation
	ii)	470	"	"	-4.8	equil. line
i) Lomonosovfonna	1120	78.7	17.6	-2.25 to -3	accumulation	
j) Austre Brøggerbreen	600	78.9	11.9	-6.5 (8 m)	ablation	

† Both measurements from Foxfonna were from the base of the glacier.

Sources: a) Baranowski (1975); b), h) and j) Zagorodnov and Zotikov (1981b); c) Liestol (personal communication); d) and i) Zagorodnov and Zotikov (198i) e) A. Stensrud (personal communication); f) Liestol (1976); g) SPRI 1985.

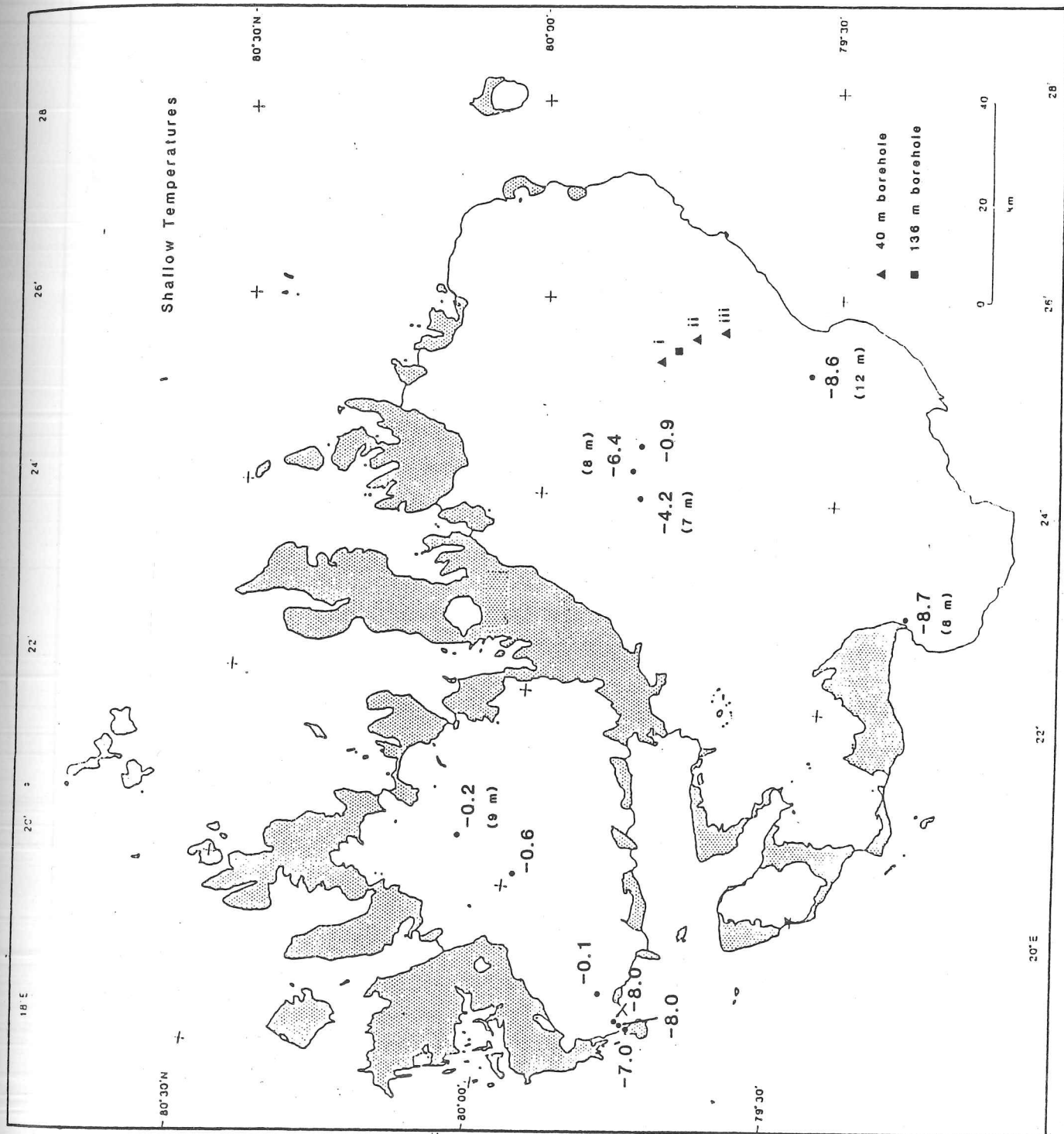


Fig. 1.10 Shallow ice temperatures in Nordaustlandet and the location of deeper borehole measurements.

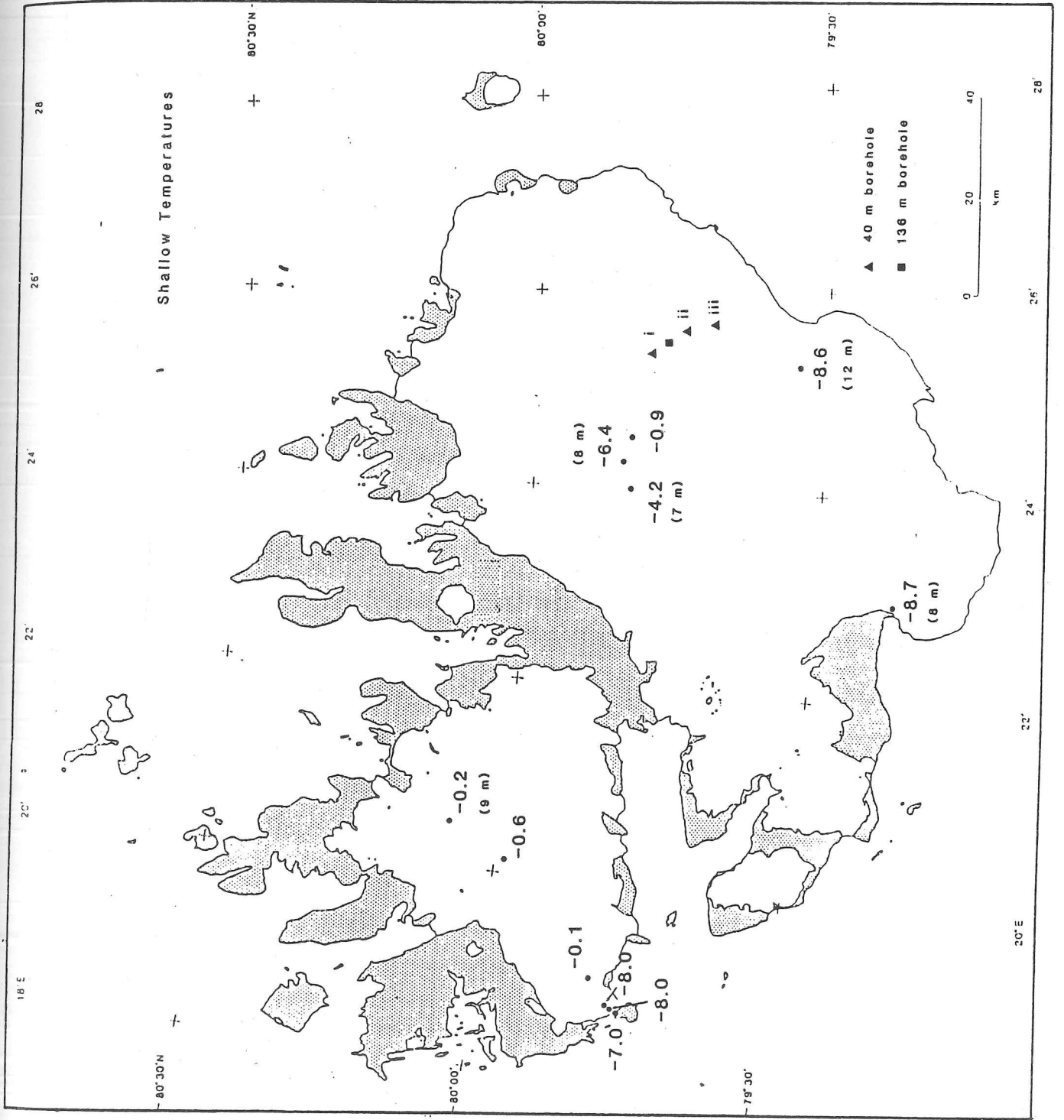


Fig. 1.10 Shallow ice temperatures in Nordaustlandet and the location of deeper borehole measurements.

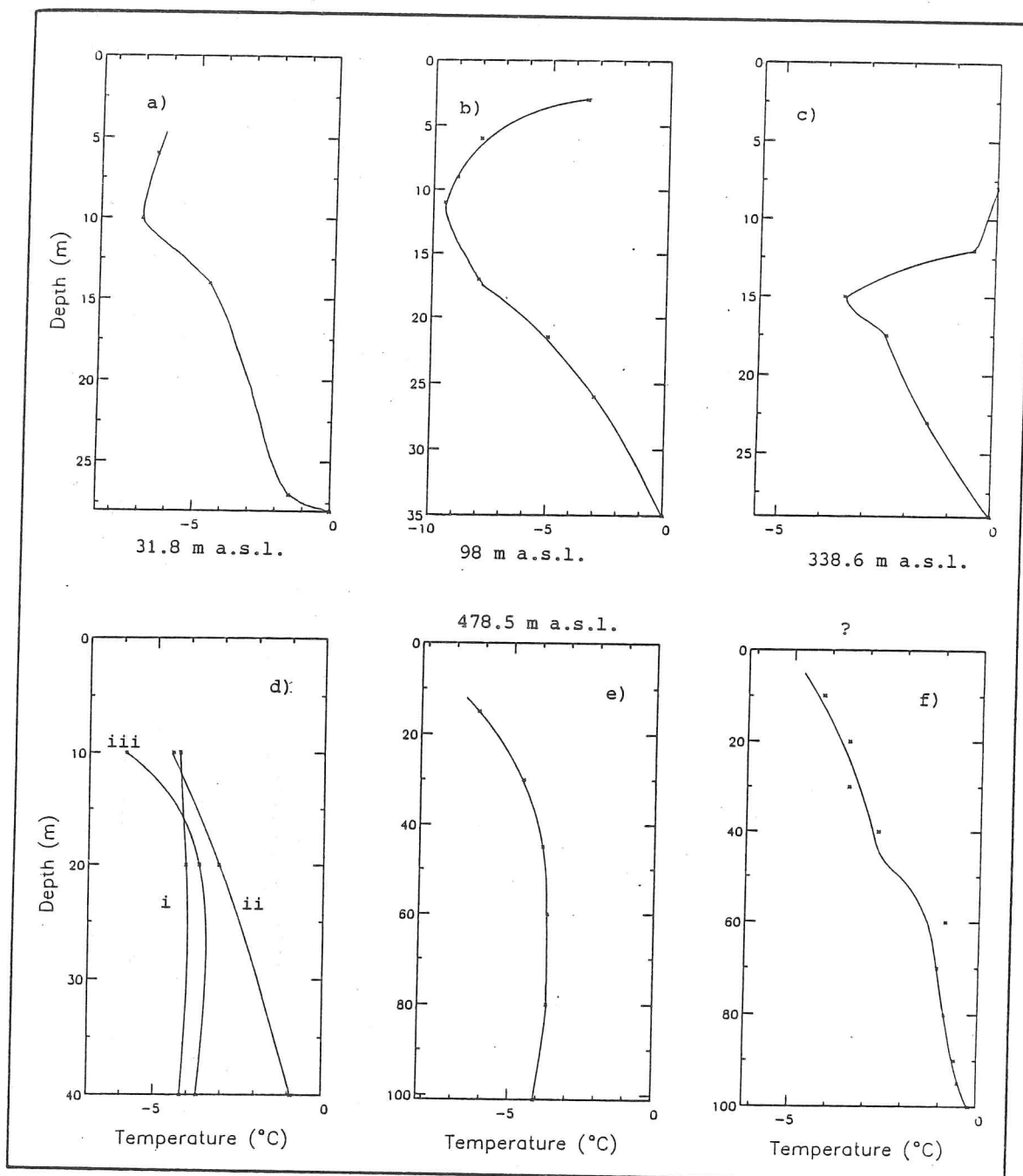


Fig. 1.11 Temperature-depth profiles from Svalbard. Figs. a)-c) come from south west Vestfonna (source J.T. Hollin, personal communication). Fig d) shows the data from the 40 m boreholes indicated in Fig. 1.10. Their altitudes are: i 585.3 m a.s.l.; ii 418.5 m a.s.l.; iii 350 m a.s.l. (source M. Vallon, personal communication). Fig. e) is the 136 m borehole shown in Fig. 1.10 (source as for d)). Fig. f) is from a borehole in Stollbreen (Fig. 1.9), its altitude was not given (source A. Stensrud, personal communication).

1.5.4 Other Relevant Glaciological Studies

Other parameters that are of relevance to radio echo sounding are the crystal structure and impurity content. The concentration and species of ions in the ice are an important determinant in explaining its electrical properties (Ch. 3) and some of the values given shortly are used to try and understand the results of RES absorption data from Nordaustlandet and Spitsbergen. Also in Ch. 3 it is suggested that the strain history and imperfections in the crystal may influence its dielectric response and therefore the small number of studies concerning these variables will be described below.

A stratigraphic record of the core from Fridtjovbreen was made (Zagorodnov and Zotikov, 1981) and is shown in Fig. 1.12 along with the classifications of ice stratigraphy that were used. The form and dimension of ice crystals and air bubbles and the presence of mineral particles were studied. Alternating layers of bubbly ice with small and large bubbles were observed and at depths of 20, 50, 100 and 200 m visible mineral particles were found which were assumed to originate from dust blown onto the glacier during the summer when there is a considerable amount of exposed rock (Zagorodnov and Zotikov, 1981). Below 154 m fourteen bands of clear ice were detected varying in thickness from 0.4 to 3 m. They therefore distinguished three types of ice: "young" ice with a large air bubble content, "transparent" ice with a low concentration of small bubbles and "crystal" ice containing no air.

Observations were also made on the level of the drilling fluid in the borehole. Initially the level sank but then after a few days reached a fairly constant level 27 m below the surface. They found that if no more fluid was added during further drilling, then the level of the solution sank by 5–8 m but after several hours returned to its original level. They suggest that the observations can be explained by a system of interconnecting conduits.

β -activity was used to identify a number of horizons, the earliest of which was believed to be 1951. The net mass balance, in the period 1951–57, was estimated as 0.75m/a water equivalent at the ice divide from the total ice thickness that was assumed to have accumulated during this period (Vaykmyae *et al*, 1977).

Oxygen isotope ratios down to a depth of 12 m were published along with the analysis of dissolved salts down to a depth of 146 m. The chemical analysis included measuring CO_2 , HCO_3^- , Cl^- , Ca^{++} and Mg^{++} concentrations and heavy metal concentrations in suspended material were also examined.

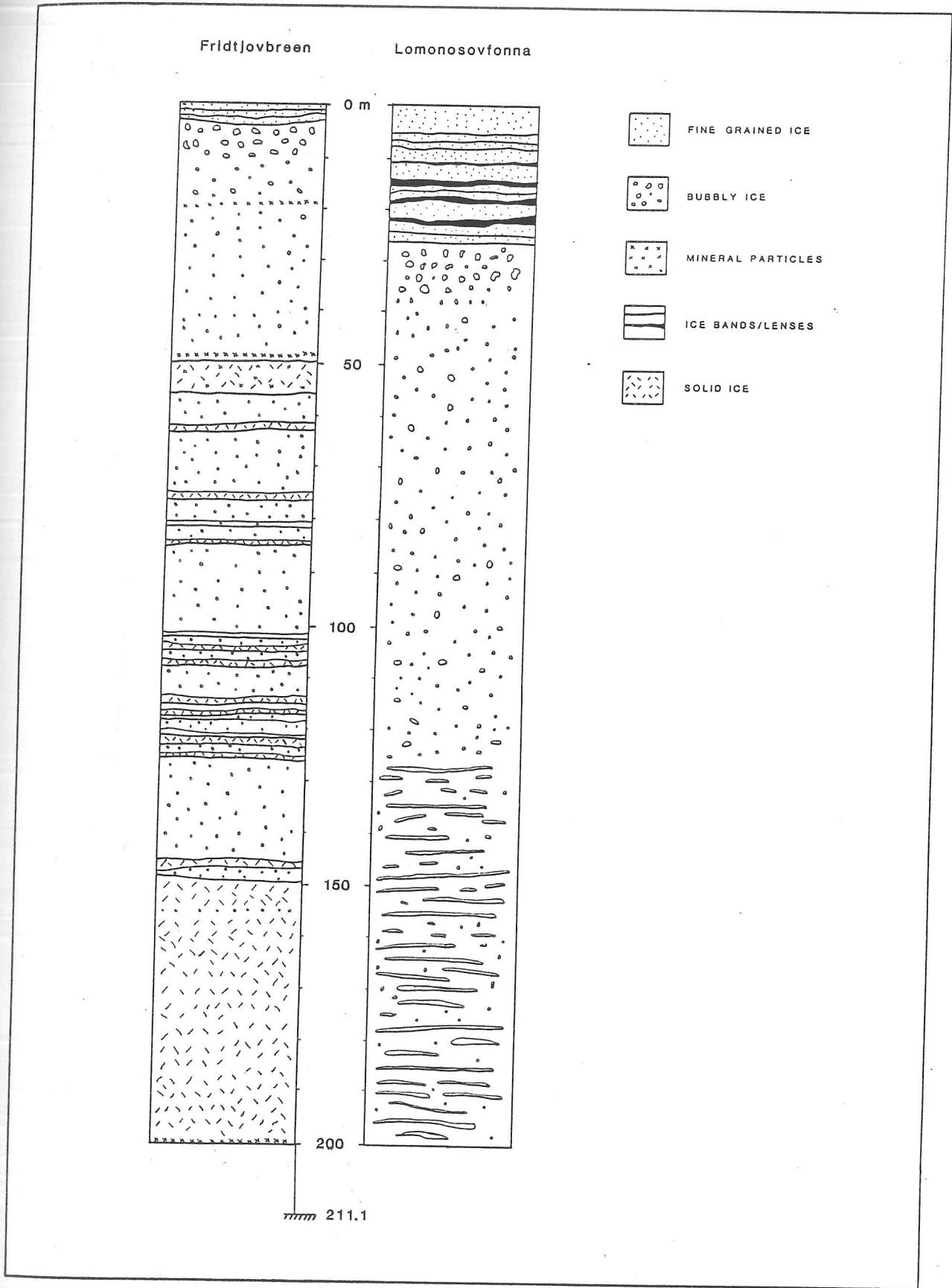


Fig. 1.12 Stratigraphic records from the Fridtjovbreen-Grønfyordbreen ice divide (altitude 450 m a.s.l.) and the Lomonosovfonna plateau (altitude 1000 m a.s.l.). Source Zagorodnov and Zotikov (1981).

Table 1.2 Chemical composition of samples from Svalbard

Concentrations (in μM) of dissolved chemicals in snow samples from Hornbreen (77°N , 16°E) (source Semb *et al*, 1984).

Depth (m)	H ⁺	SO ₄ ^{- -}	NO ₃ ⁻	Na ⁺	Mg ⁺⁺	Ca ⁺⁺	Total
0-0.25	31	16	1	44	3	2	97
0.25-0.38	25	20	4	55	7	4	115
0.38-0.57	15	7	<1	59	7	2	90
0.57-0.68	12	4	1	30	2	1	50
0.68-0.79	11	5	<1	54	6	2	79
0.79-0.90	15	8	2	26	3	1	55
0.90-1.0	12	7	1	38	5	1	63
1.0-1.23	12	19	2	206	24	8	271

Maximum, minimum and mean concentrations (in μM) of dissolved chemicals from a 206 m core from Vestfonna (source Yevseyev and Korzun, 1985).

	HCO ₃ ⁻	SO ₄ ^{- -}	Cl ⁻	Na ⁺	Ca ⁺⁺	Total
Minimum	40	4	11	6	10	71
Maximum	100	20	41	37	24	222
Mean	69	5	20	17	13	124

Similar work on the chemical composition was also carried out on the core from Vestfonna (Yevseyev and Korzun, 1985). Table 1.2 shows the minimum, maximum and mean values of ion concentrations for the whole length of the core. The results of the chemical analysis showed a level of mineralisation of 4–10 mg/l, and they found that the lowest salt contents were in relatively old ice layers at depths > 80 m and the highest values in the surface snow. They recorded pH and Na⁺ ranges of 5.1–6.2 and 0.14–0.31 mg/l (6.1–13.5 μM) respectively from their ice core samples.

Snow samples collected by Semb *et al* (1984) were processed to determine H⁺, SO₄²⁻, NO₃⁻, NH₄⁺, Na⁺, Mg⁺ and Ca⁺⁺ concentrations. Presence of sea salt was found to decrease with height (i.e. away from the coast, as expected) while excess sulphate, ammonium and nitrate concentrations decreased from south east to north-west, though the highest individual values were measured on Nordaustlandet, where the pH was as low as 4.53 and H⁺ concs. were up to 30 μM compared with typical values of 1 to 10 μM in Spitsbergen. Na⁺ values did not show such a marked difference, but non marine SO₄ was again much higher on Nordaustlandet (4.8 μM compared with 0.2–2.1 μM). The results of their analysis of snow samples from Hornbreen (77°N, 16°E) are shown in Table 1.2.

Stratigraphic analysis of the 586 m core from Amundsenisen (Zagorodnov and Zotikov, 1981b) was also undertaken and led to the discovery of small “water-filled canals and channels” ranging in cross section from 10–200 mm². “Thin horizontal crevasses” were also detected. The stratigraphy consisted of alternating layers of clear and bubbly ice anywhere between 0.1 and 3 m thick. These observations will be seen to be of relevance when interpreting the possible causes of internal reflecting horizons in later chapters.

1.5.5 Surging

A glacier surge is a term that is used to describe a sudden rapid advance when the velocity of the ice increases by a factor of 10–100 and which lasts from anywhere between a few months to a few years (Paterson, 1981). Typically the ice in the lower reaches of the glacier (the receiving area) moves forward by several kilometres in this period and is accompanied by the formation of a chaotic mass of crevasses and ice contortions. Surges are cyclic phenomena and the active period is usually followed by a longer, quiescent phase lasting between about 10 and 200 years. During this period the upper part of the glacier (the reservoir area) builds up to its pre-surge level while lower down the ice is often stagnant and the snout gradually retreating.

The nature of this instability has received considerable attention and a number of theories have been proposed, all of which are in some respect inadequate (Paterson, 1981). An essential part of all these hypotheses is that there is sliding at the bed. This is necessary to account for the high velocities during the active phase, which cannot be due to creep alone. Three mechanisms will be considered here that are relevant to surges in Svalbard: 1) thermal instabilities, 2) mechanical damming of water and 3) deformation of an unlithified bed.

The first can take a number of different forms, one of which is known as creep instability. This describes the positive feedback system between strain rate and temperature. The greater the strain rate the greater the internal heat of deformation. This increases the ice temperature which in turn increases the strain rate. The phenomenon has been modelled theoretically (Clarke *et al*, 1977) and it was concluded from this that it was unlikely to account for surging as the time over which the instability might develop was found to be an order of magnitude greater than the observed periods.

Another thermal instability was suggested by Clarke (1976) involving an alternation between a bed that is mainly frozen to one that is mainly melting. Surface accumulation and compressive flow cause the ice to thicken which effectively warms the bed by reducing the temperature gradient in the ice. Subglacial water would then become trapped by the damming effect of the frozen bed near the snout and this would eventually lead to a surge. This model is, however, not supported by field measurements which suggest that the frozen bed does not seem to impede the drainage of subglacial water from the glacier (Clarke *et al*, 1984).

Another possible mechanism for surging has been put forward by Robin and Weertman (1973) and involves the mechanical damming of subglacial water. They suggested that this could take place if sufficiently high negative basal shear stress gradients were present. They applied this model to Finsterwalderbreen (Fig. 1.9) and deduced that water could have been trapped by this mechanism. There were, however, a number of problems with the assumptions made and again, their model is not supported by field measurements (Clarke *et al*, 1984).

The last mechanism considered is the deformation of an unlithified bed. Clarke *et al* (1984) suggested that the accumulation of water beneath a glacier lying on a permeable bed could trigger a surge. They argued that destruction of the subglacial drainage system, due to increasing ice thickness and shear stress during the quiescent phase, could give rise to a build up of water at the bed. The condition for surging to begin was when the rate of change of the discharge capacity with time became negative.

Another possibility has been considered by Jones (1977). He has shown that once relatively impermeable sediments were saturated, very little surplus water is required to produce a slurry giving rise to a well lubricated bed. Neither this, nor the previous hypothesis, has been tested analytically however and uncertainties remain. Indeed it may well be inappropriate to attribute a single mechanism to the onset of a surge, which could be caused by a combination of any of the models described above.

Surging is a phenomenon that is restricted to a limited number of glaciers in a limited number of regions of the world. Svalbard is one such region and several glaciers in the archipelago have been observed to surge while many others show signs of having done so in the past (e.g. Schytt, 1969; Horvath and Kahn, 1975 and the most recently recorded surge that took place in 1985/86 on Bakaninbreen: Drewry, in press). The largest surge ever recorded was on Bråsvellbreen, Nordaustlandet, between 1936 and 1938 (Glen 1937, Schytt, 1969) during which time the ice front reached some 20 km beyond its pre-surge limit.

The most comprehensive inventory of surging glaciers in Svalbard was undertaken by Liestøl (in press) listing 57 glaciers in Spitsbergen and seven on Nordaustlandet where evidence for surging exists. The geographical distribution is shown in Fig. 1.13.

Surging is an instability in the glacier dynamics and makes the use of modelling of flow and temperature within the glacier very difficult. Glaciers that undergo this type of behaviour are, thus, not in a steady state and the surface profile may be dramatically altered during the active phase. These points need to be borne in mind in later discussions of internal glacier characteristics.

1.6 Introduction to Radio Echo Sounding

Radio echo sounding (RES) has been successfully used as a technique for obtaining ice thickness data since the early '60's (Robin *et al*, 1969) when a SPRI MK II system operating at 35 MHz, was used along a 100 km trail between Camp Tuto and Camp Century in northwest Greenland. Since then considerable improvements have taken place in both equipment and the physical understanding of the electromagnetic propagation effects in ice. Light aircraft are now the most common platform and the introduction of digital recording techniques (Goodman, 1975; Drewry and Liestøl, 1985) have considerably improved data handling and analysis. As equipment improved, interest also developed in the detailed interpretation of the returned

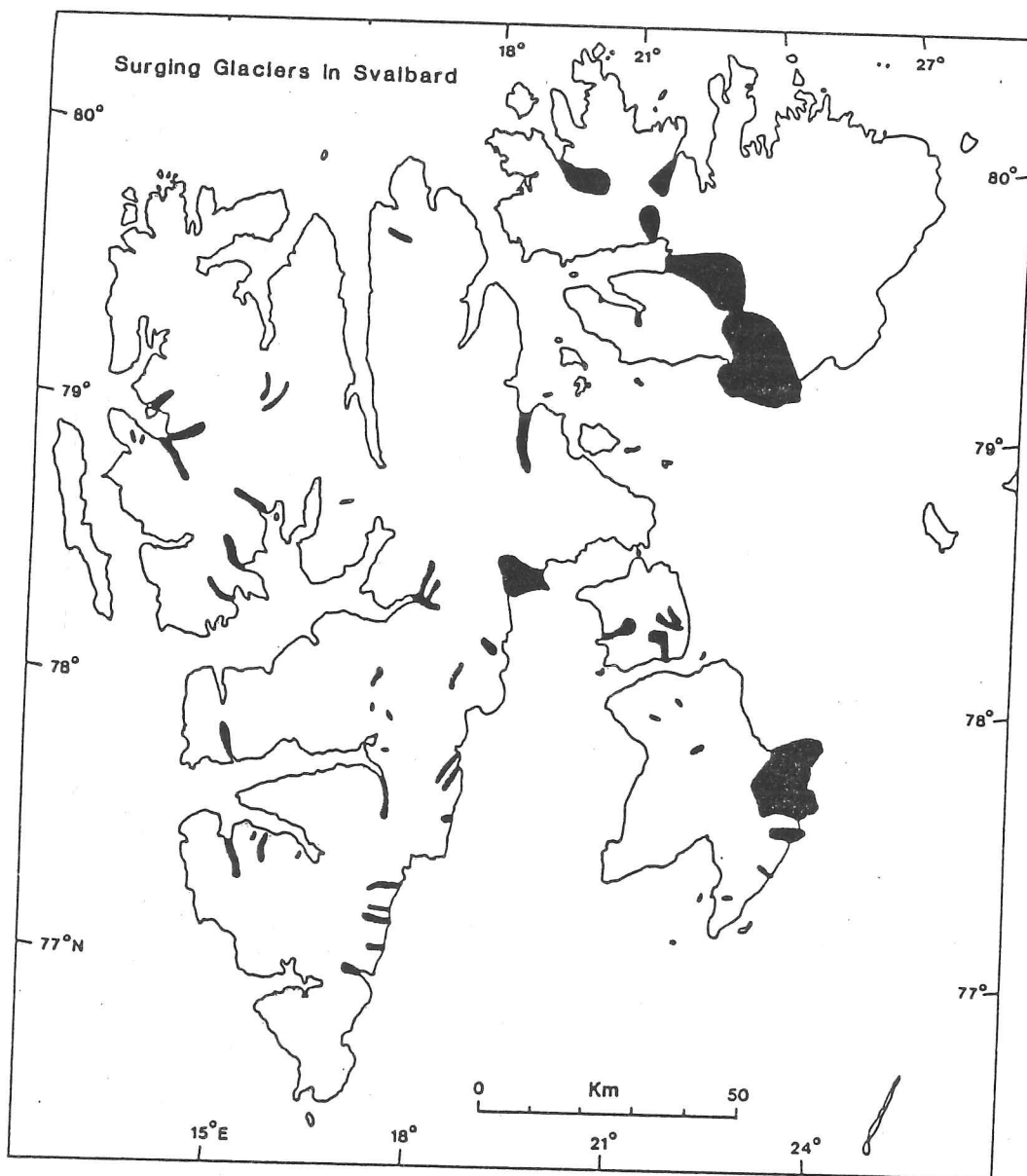


Fig. 1.13 The location of glaciers in Svalbard which have been observed to surge (source Liestøl, in press).

waveform and its fading (i.e. fluctuations in the echo strength due to diffraction processes at the reflecting boundary). Harrison (1972) and Berry (1973) developed a theory for the reflections from rough surfaces which was successfully applied to experimental data collected by Oswald (1975) in Devon Island (NWT, Canada). Neal (1977) extended the theory to more general situations where the reflecting surface may be intermediate between very rough and very smooth (relative to the radar wavelength). He also considered the effects of the ice surface and the possibility of the bedrock having more than one autocorrelation length describing its form.

The RES technique relies on two factors—first, that the ice is sufficiently transparent to radio waves and second, that there is a difference between the dielectric properties of the ice and the underlying bedrock. Between 100 kHz and 400 MHz there are no major dispersions (Johari, 1981) and attenuation of radio waves does not increase significantly. The critical frequency for penetration is consequently limited to this range—where the first criterion is satisfied. There are two more factors which influence the frequency chosen. First, the physical size of the antenna must be considered, and for airborne operations this limits the wavelength to no more than 10 m in air. The second consideration is the temperature of the ice: temperate glaciers (i.e. those at their melting point) possess a large number of internal scattering centres whose influence upon the returned echo is strongly frequency dependent (for Rayleigh scattering this frequency dependence is proportional to the fourth power of the wavelength, e.g. Smith and Evans, 1972). The choice of frequency is thus a compromise between the advantages of increased antenna gain, smaller size and finer resolution and the disadvantages of greater absorption and scattering, especially in warmer ice.

The dielectric properties of a wet bed are in part frequency dependent (Lysne, 1983) but this is a relatively small effect and certain rock types (for instance some fine grained igneous rocks) may have a similar permittivity and conductivity to that of the overlying ice thus preventing the reflection of radar waves. Such circumstances are, fortunately, rare and the reflection coefficients of most commonly found rock types lie between about -10 and -25 dB if dry (Oswald, 1975).

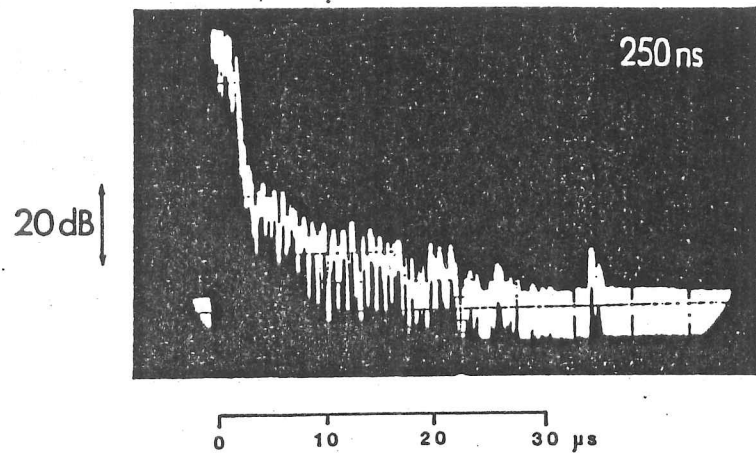
1.6.1 Recording

Two types of record are generally used for analogue recording. The first, known as an 'A' scope, is a display of delay time versus logarithmic echo power. This is photographed at frequent intervals and has the advantage of showing the detailed structure and strength of the echo but does not immediately indicate the continuity of a return and is impractical for routine ice thickness measurements over long distances. The second is an intensity modulated record called a 'Z' scope, where the returned power is represented by the intensity of the oscilloscope trace with the y axis switched off. In this case the x axis represents time delay and the photographic film is wound passed the screen at a constant rate. A third type of record, very useful in determining the variation of the peak returned power along track, was developed by C. S. Neal (1977) and is referred to as an ESM (echo strength measurement) display. A continuous record of the peak echo power is obtained by displaying the echo power along the y axis but with the time base (x axis) switched off. It is thus a hybrid of the 'Z' and 'A' modes, showing both the continuity and the quantitative strength of the signal. Examples of RES records for both analogue and digital systems are shown in Fig. 1.14.

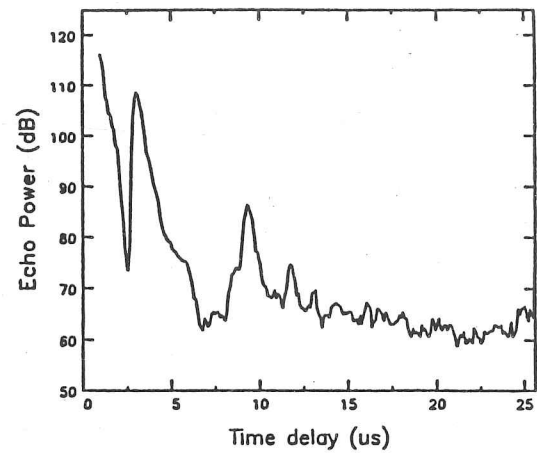
1.7 Radio Echo Sounding in Spitsbergen

The SPRI have been involved with several RES programmes in Svalbard. On all occasions the basic radar hardware has been the same, consisting of a SPRI Mk IV sounder operating at a centre frequency of 60 MHz. The major differences between each season has been the platform and recording systems used.

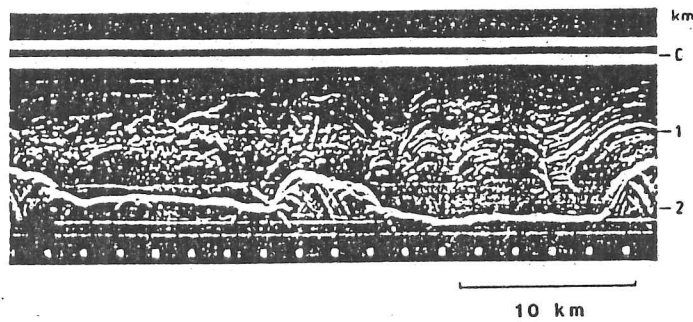
In 1980 a joint project between the SPRI and the NP was carried out, using a Bell 206 Je-tranger helicopter (Dowdeswell *et al*, 1984b). Continuous surface and bed returns were recorded in 'Z' mode on 35mm film which was then digitized in Cambridge. Glacier surface elevations were obtained from NP 1:100,000 maps, and consequently had a systematic error estimated to be approximately 100 m. 38 glaciers were sounded throughout Spitsbergen (Fig 1.15) but un-ambiguous bed echoes were only obtained from about 50% of the complete dataset. The main reasons for this were associated with obscuration by internal and surface scattering (Dowdeswell, 1984). The former was particularly prevalent in the warmer ice of the accumulation zone of the glaciers. Internal reflections were observed on 9 glaciers and were shown to have been misinterpreted as bed returns on some Soviet records (Dowdeswell *et al*, 1984a).



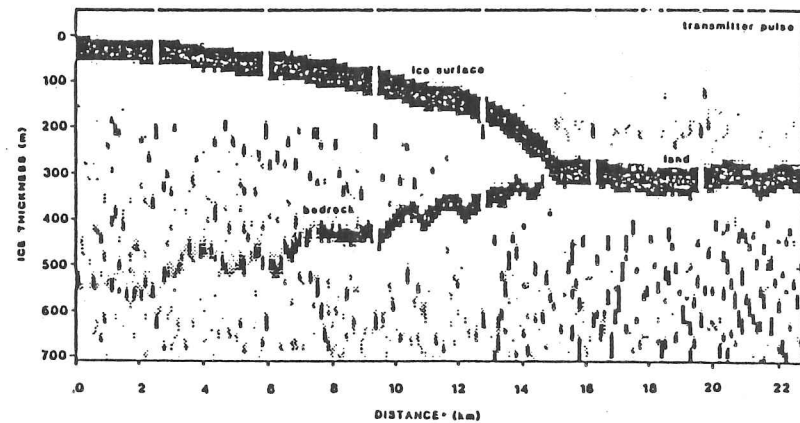
a) analogue recorded 'A' scope



b) Digitally recorded 'A' scope



c) analogue 'Z' scope



d) digital differentiated 'Z' scope.

Fig. 1.14 'A' scope and 'Z' scope records from both analogue and digital RES data.

In April 1983 a second airborne programme was undertaken, this time using a BAS de Havilland Twin Otter fixed wing aircraft (Drewry and Liestøl, 1985). This improved the stability in flying height and the surface elevation was recorded in real time from the aircrafts pressure altitude and the SPRI Mk IV. The wings acted as reflectors for the antennae which were mounted beneath them, improving their directionality. The most important advance, however, was the employment of a digital recording system which is described further in Ch. 2. It has allowed quantitative estimates of echo power and hence bedrock reflection coefficients and has removed the need to manually digitize the data. An extensive network of flight-lines over Nordaustlandet as well as 37 glaciers and 7 ice caps in Spitsbergen were covered. The third season took place in 1985 and was a ground based survey of three glaciers—Bakaninbreen, Skobreen and Paulabreen—in central Spitsbergen (Fig. 2.1). The radar and recording unit were housed in a caboose towed by one or two snow scooters. The antenna consisted of a single wave dipole which trailed approximately 5 m behind the caboose. Individual echoes were digitally recorded for some 20 km of track. Additional radio echo sounding was carried out in 1986 in central Spitsbergen but is not considered in this thesis.

An extensive RES programme has also been carried out by Soviet workers since 1974 (Macheret *et al*, 1985). During the first two seasons a 440 MHz aircraft altimeter was used, recording data on 35 mm film. The bulk of the Soviet data, however, was collected between 1978 and '79 with a purpose built sounder operating at 620 MHz. This allowed a high spatial resolution with an antenna beamwidth of 18° and a system performance of 185 dB (c.f. the SPRI Mk IV value of 160 dB) (Macheret *et al*, 1985). The narrow beamwidth is useful in reducing the effects of wide angle surface scattering but at such high frequencies internal scattering from inhomogeneities from within and near the ice surface can outweigh this advantage, especially if sounding is carried ^{out} during the melt season (Dowdeswell *et al*, 1984a). All the airborne work was carried out in helicopters using primitive navigation and NP maps to determine surface elevations. 50 km of ground based data were also collected around the ice divide of Austre Grønfjordbreen and Fridtjovbreen and from several other glaciers in the area. To aid the interpretation of these data a radio echo logging experiment was carried out in a borehole near the divide (Macheret *et al*, 1984). The results of this experiment are discussed in detail in section 2.6.1. The tracks flown in these studies and those of the SPRI 1980 field season are shown in Fig. 1.15. The SPRI 1983 and '85 field seasons form the core of the experimental data of this thesis and are described in the next chapter.

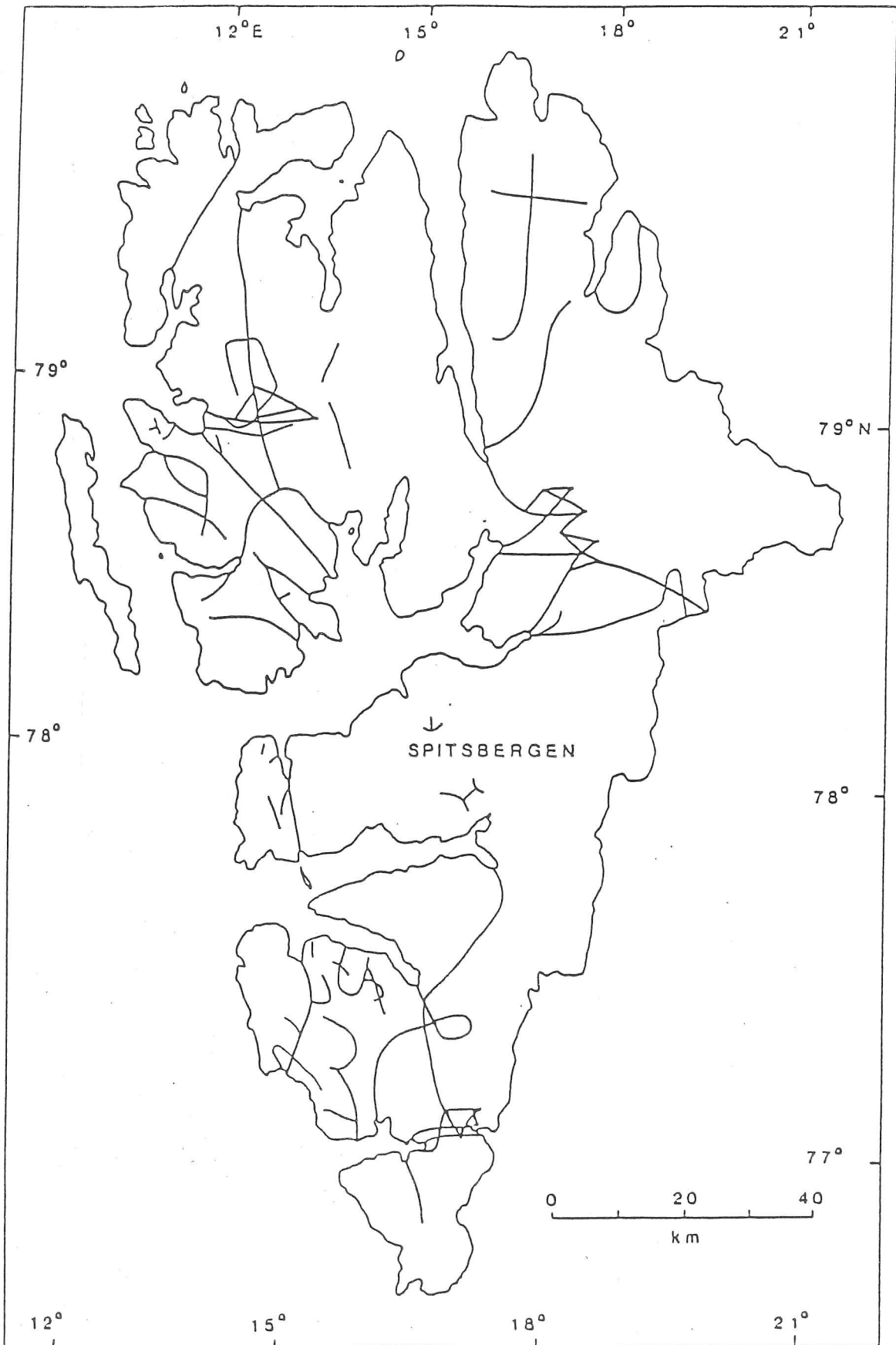


Fig. 1.15 Previous RES flight lines in Spitsbergen including the SPRI 1980 field season.

CHAPTER 2

RADIO ECHO SOUNDING IN SPITSBERGEN

2.1 Introduction

In this chapter RES equipment, data collection and reduction are described. It will be seen that the method and timing of collection influences many of the results. The single most important advance, with respect to this work, has been the use of digital recording techniques which has allowed evaluation of reflection coefficients (RCs).

A brief outline of the general topographic characteristics of glaciers sounded in Spitsbergen is given, although the bulk of the glacier profiles are presented in App. 1. A feature observed on a number of glaciers was a single internal reflecting horizon extending for several kilometres along the glacier. An introductory description of this phenomenon is provided with a more detailed discussion being held over to Chapter 5.

2.2 The 1983 and 1985 Field Seasons

During April 1983 a joint airborne RES programme was carried out by members of the SPRI and Norsk Polarinstitut (NP) (Drewry and Liestøl, 1985). Approximately 3,400 km of track were covered over the Nordaustlandet ice caps and 1,500 km over 37 glaciers and 7 ice caps in northern and central Spitsbergen (Figs. 2.1 a) and b)). This field season represented the follow-up to a preliminary season in 1980, when the effectiveness of the SPRI Mk IV sounder (centre frequency of 60 MHz) on Spitsbergen glaciers had been tested. There was considerable success in obtaining bedrock returns from the ice cap— Austfonna (90% of track flown) but only 52% from the smaller ice cap— Vestfonna, where greater internal scattering was observed and attributed to warmer ice (Dowdeswell, 1984). Of the ice masses sounded in Spitsbergen, six had no resolvable returns at all and three others had such heavy scattering that the bed echo could not be satisfactorily resolved. From the remaining 35 the bed was usually not present for the whole length of the glacier and was most commonly absent from the accumulation zone. A detailed morphological study of the ice caps in Nordaustlandet has been produced by

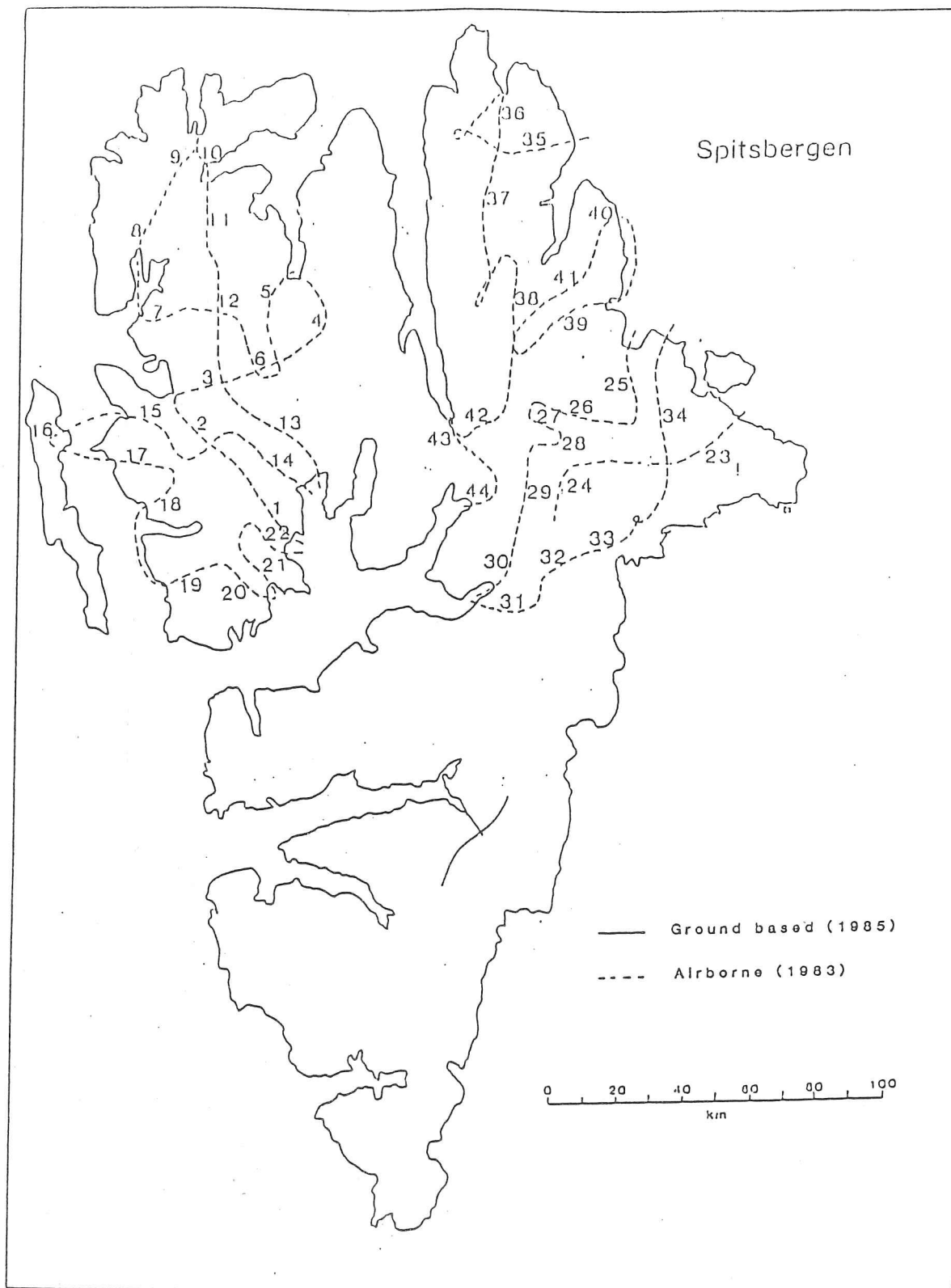


Fig. 2.1a) Location of RES flightlines in 1983 and ground-based tracks in 1985. Numbering system is explained in App. 1. The glacier names are given in Table 2.

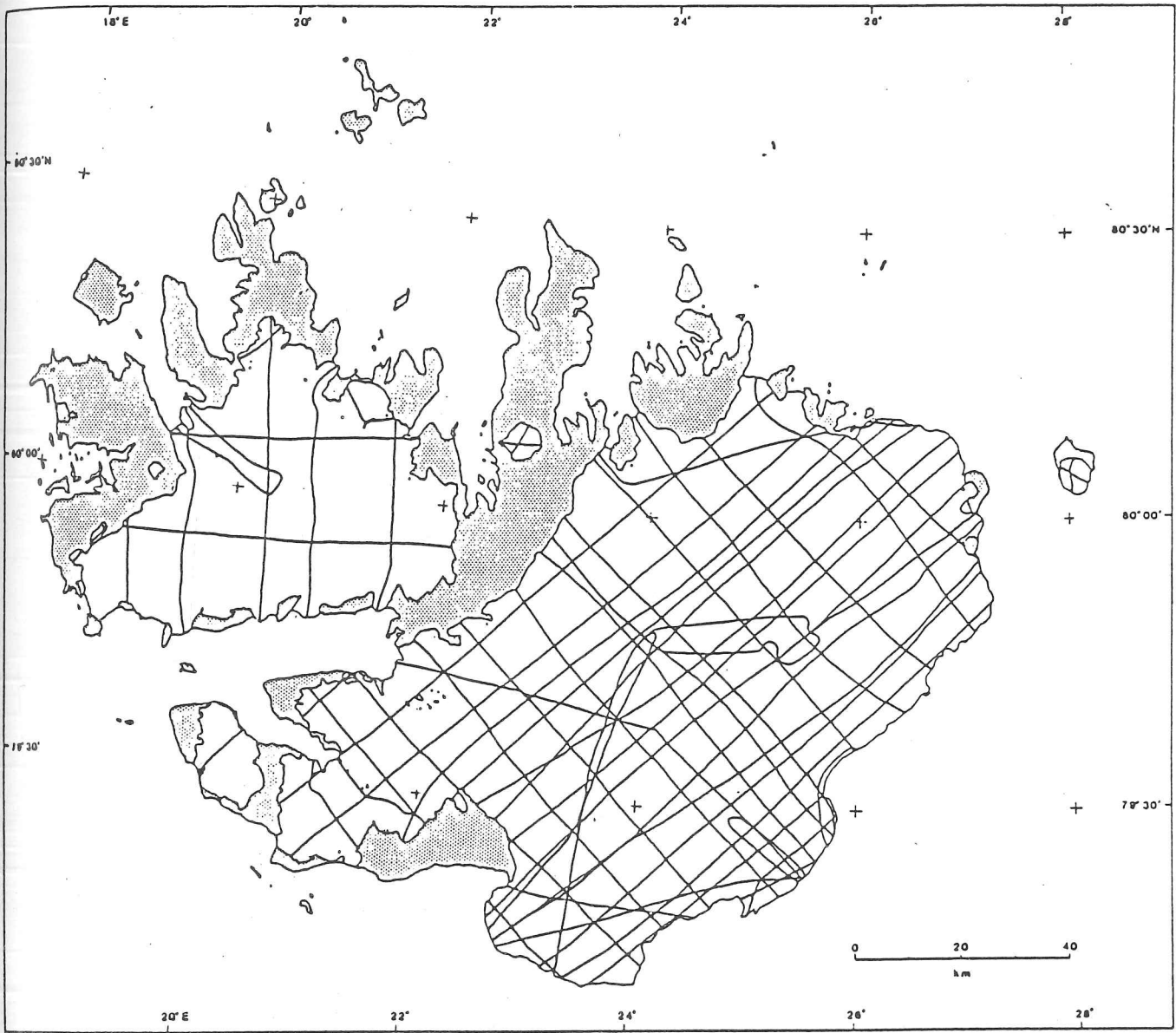


Fig. 2.1 b) Location of RES flightlines over Nordaustlandet in 1983.

Dowdeswell (1984). Greater emphasis is placed here on the data from Spitsbergen, which have not been presented before, and on an investigation of variations in echo power.

In 1985 a comprehensive ground-based RES survey was carried out on three glaciers situated near the small mining settlement of Svea ($77^{\circ} 54'$, $16^{\circ} 43'$): Paulabreen, Skobreen and Bakaninbreen. The primary objective of the work was to obtain continuous ice thickness profiles along the lengths of the glaciers and, for the latter two, these followed a line of stakes that had been laid out previously by BP (Norway), who funded the operation and provided certain logistical support. At the same time it was hoped that a ground-based survey would provide an opportunity to obtain a detailed power profile of bed echoes, allowing the fine-scale roughness characteristics of the bed to be studied and a separation of these effects from dielectric properties. A total of 20 km of track were recorded (Fig. 2.1 a)). Only the profiles along Skobreen and part of Bakaninbreen were recorded digitally however, the remainder being recorded on super 8mm ciné film. This was due to an intermittent fault in the RCU (recording and control unit). A ROM mounting could not sustain the vibrations encountered while traversing the rough terrain despite the shock-mounted housing. The unit eventually failed completely. Both 1983 and 1985 soundings were carried out using a centre frequency of 60 MHz. A 440 MHz transmitter and receiver had been taken in 1985 with a view to repeating the lines sounded at this higher frequency. The shorter wavelength would not only have a greater resolution of bed roughness but would also have helped in interpreting the ice and bed properties. Internal scattering is strongly frequency dependent and to a lesser extent so is the bed reflection coefficient. Due to time constraints and the aforementioned problem it was not possible to complete this part of the work and it still remains an unanswered question as to what degree internal scattering might modulate the signal and whether this would outweigh the increased directionality of the antenna and obscure the bed echo.

2.3 Equipment and Recording Techniques

2.3.1 The RES Equipment in 1983

A SPRI Mark IV pulse-modulated receiving and transmitting unit was employed throughout the field season. The hardware circuits are described at length in Oswald (1975). The pulse length was a nominal 250 ns with a rise time of 60 ns and approximated to a square wave envelope. The antennae consisted of two half-wave dipoles, one to transmit and the other to receive. They were mounted under each wing of a de Havilland Twin Otter, which acted as plane reflectors and produced a total theoretical forward gain of 8.4 dB. This configuration gave an overall system performance (including mismatch losses but excluding antenna gain) of 160 dB. On some flights over Spitsbergen a 10 dB attenuator was required to reduce receiver saturation thus reducing the system performance to 150 dB. The equipment was flown at a fairly constant pressure altitude of 750–1000 m. Over rough ground it was sometimes necessary to reduce the terrain clearance to prevent the bed returns being obscured by surface scattering. The system parameters are given in Table 2.1 and a block diagram of the radar hardware is displayed in Fig. 2.2.

On one of the later flights only one antenna was operational and consequently a T/R switch had to be used. The leakage from this into the receiver substantially reduced its recovery time and necessitated an increased terrain clearance to observe the surface return. During this flight some bed echoes were not observed where on previous flights they had been and this can be attributed to the increase in altitude and consequent increased surface scattering and geometrical losses.

2.3.2 Recording in 1983

Digital recording facilities were developed for 1983 by Mr M R Gorman. The data were recorded in the form of 'A' scopes comprising the geometric mean of 8 individual waveforms. It is the **geometric** mean as the average of the logarithmic power is taken. Each of the waveforms was built up of 256 samples taken at 100 ns intervals. Every consecutive sample was taken from a consecutive pulse. Thus with a pulse repetition period of 60 μ s the individual 'A' frames took 15.6 ms to accumulate, in which time the aircraft had moved 0.9 m. A delay of about 100 ms before the next cycle of sampling gave a total collection time for all 8 pulses of 1 sec (60 m in distance along track). Some examples of recorded waveforms for various sounding situations are

Table 2.1 System parameters of the SPRI Mk IV echo sounder in 1983 and 85.

	1983	1985
Carrier frequency (MHz)	60	60
Transmitter power (W)	300	300
Receiver bandwidth (MHz)	15	20
Pulse length (ns)	300	300
Antenna type	single 1/2 wave dipole	single folded dipole
Reflector for antenna	plane	1/2 wave parasitic
1/2 power beamwidth	100°	100°
Forward gain (dB)	8.3	4.5
System Performance [†] (dB)	160	130

† The system performance quoted excludes antenna gain. On some of sections of flight, in 1983, a 10 dB attenuator was employed which is not included in the figure quoted. The 30 dB reduction in system performance in 1985 is due to the use of a 30 dB attenuator during all soundings.

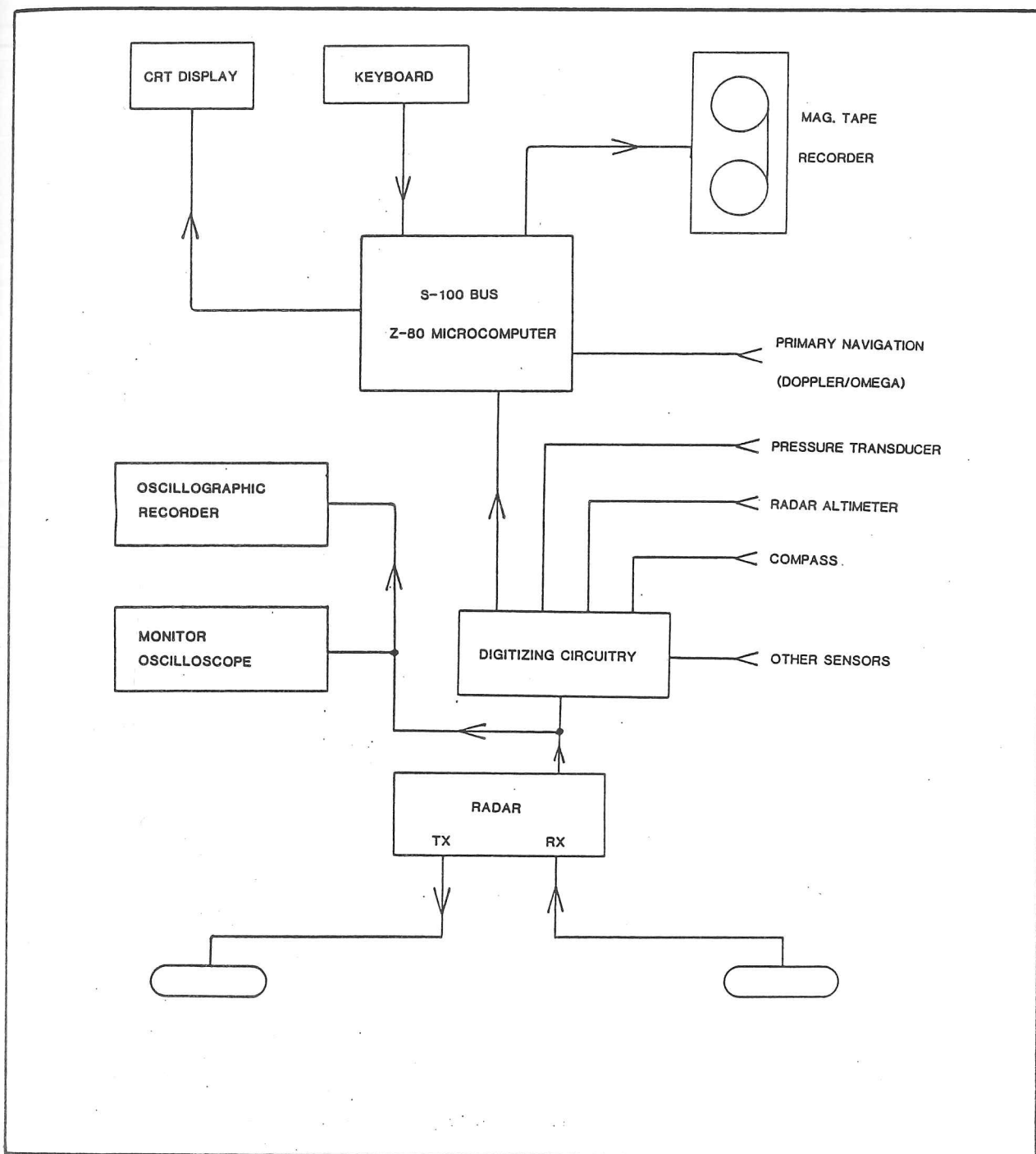


Fig 2.2 Block diagram of the RES hardware used in 1983.

shown in Fig. 2.3. The effects of scattering on the signal to noise ratio are clearly illustrated in a) from Sveabreen. Fig. 2.3 b), from Holmstrombreen, shows how the receiver can be saturated by a strong bed return from relatively thin ice. The second peak in Fig. 2.3 d) is due to an IRH, the third being from the bed.

The 8 'A' scopes were stored in a 2048×8 RAM until the interrupt trigger from a Z-80 microcomputer initiated the recording sequence. In the next second both navigation and radar data were written to magnetic data cartridges controlled by a Penny and Giles recorder. Each cassette could hold 3.2 Mbytes, representing about 4 hours continuous recording. Data rate and storage restrictions prevented the 8 unaveraged pulses being recorded individually and has consequently limited the use of the data in assessing fading rates, power variance and other parameters associated with the roughness of the interface. The precise recording of average peak echo power has, however, enabled less statistically sensitive parameters to be investigated on a scale not previously possible. It has allowed reflection coefficients and absorption rates over large areas of Nordaustlandet and Spitsbergen to be estimated. To achieve this, however, accurate calibration of the receiver response is necessary and the procedure is described in section 2.7. The digitized data were displayed in either 'Z' scope or 'A' scope mode on an oscilloscope and a backup analogue intensity modulated record was produced by a Honeywell oscillograph on heat-developed paper. In Cambridge the data were transferred to IBM 9 track compatible tape for reduction on a main-frame computer.

2.3.3 RES Equipment 1985

The radar hardware again consisted of a SPRI Mk IV transmitter and receiver. The system parameters are summarised in Table 2.1 along with those of the 1983 equipment. A wide-band preamplifier (Oswald (1975) p.70) was used having a 20 MHz bandwidth and, equally importantly, a fast recovery time allowing resolution of the bed echo, from the transmitter breakthrough, for delay times equivalent to approx. 80 m of ice (i.e. this represents the minimum ice thickness measurable). To achieve this it was also necessary to use a 30 dB attenuator. A block diagram of the hardware configuration is shown in Fig 2.4.

It was important for the echoes not to be antenna-limited and the antenna used consisted of a single folded dipole with a half wavelength parasitic reflector mounted a $1/4 \lambda$ above it. This configuration gives a theoretical forward gain of 4.5 dB. Its half power point is approximately 100° and hence sufficiently broad to eliminate any possibility of antenna limiting. The

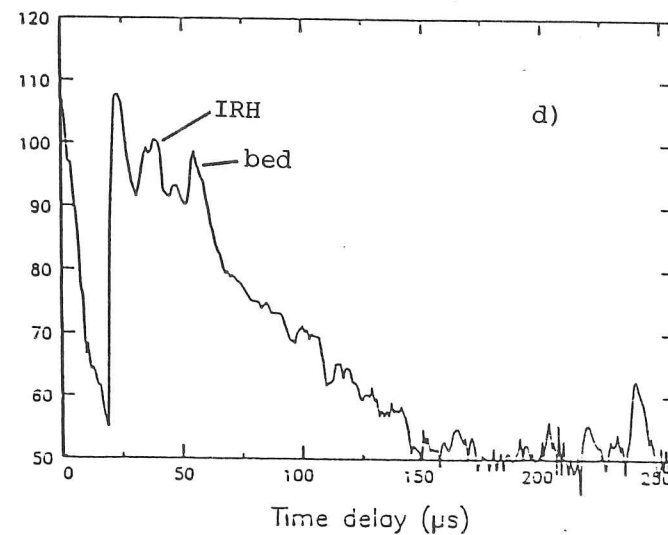
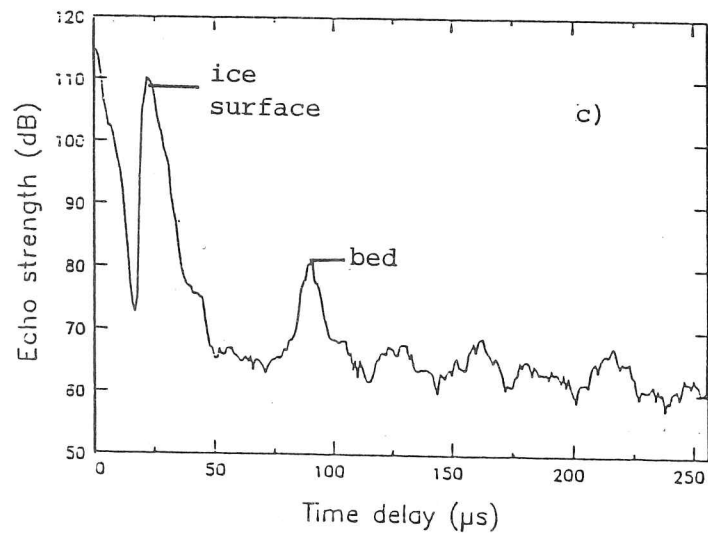
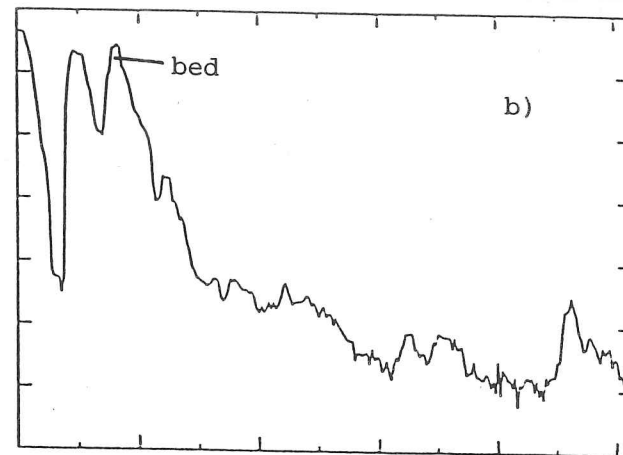
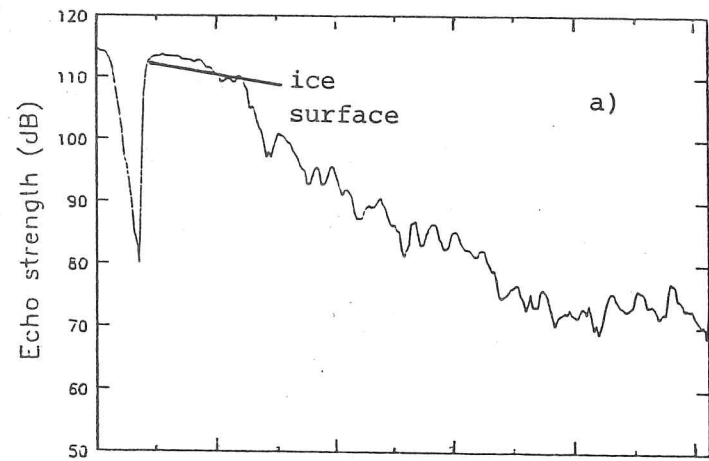


Fig. 2.3 Digitally recorded waveforms displaying a) heavy surface scattering from Sveabreen, b) thin ice from Holmstrombreen, c) deep ice from Veteranen (> 500 m) and d) an IRH echo from Sef strömbreen. The lower noise level in Fig. d) is due to the use of a 10 dB attenuator during this flight (flt. 09).

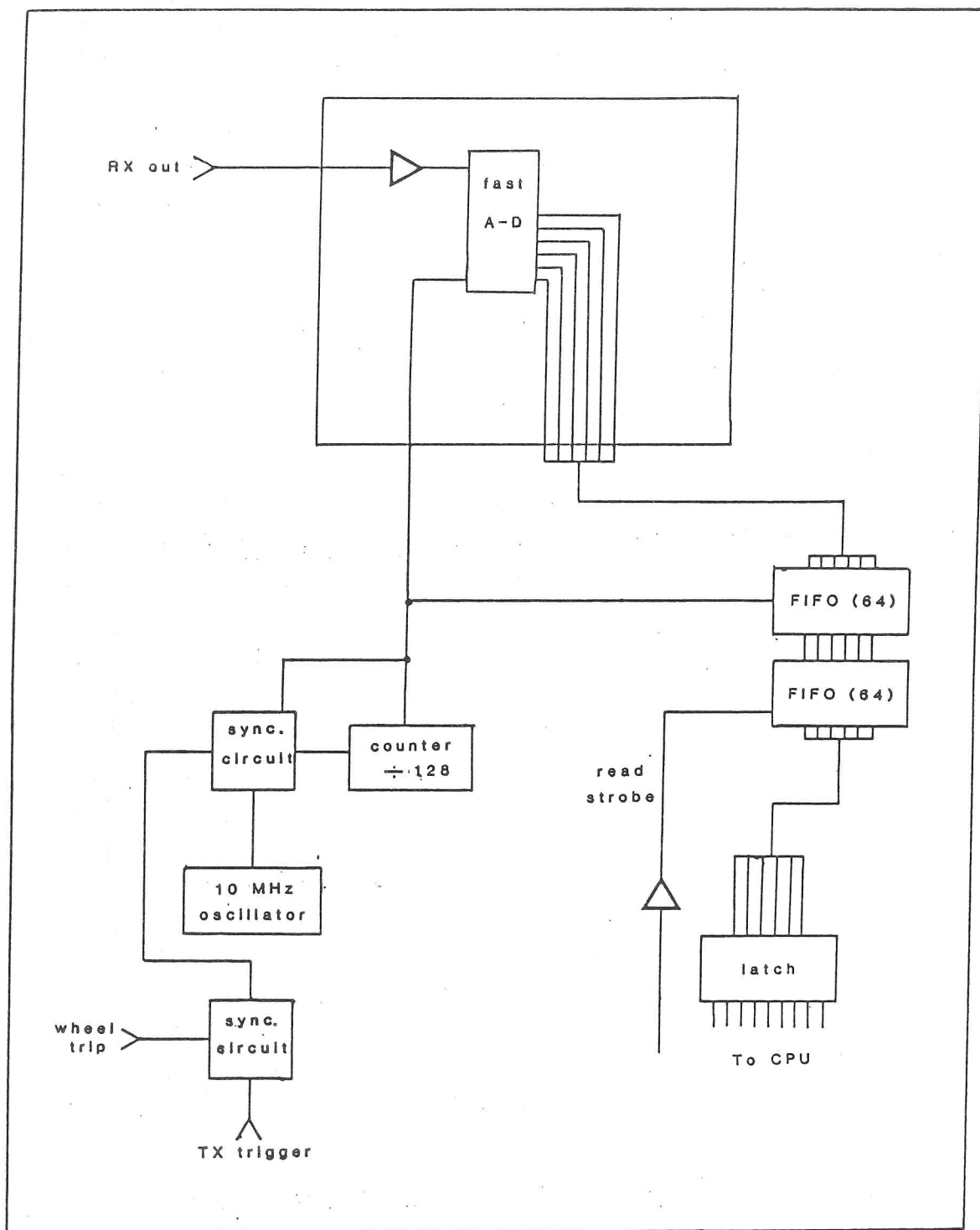


Fig. 2.4 Block diagram of the RES hardware used in 1985.

radar hardware and RCU were housed in a plywood caboose and kept at approximately room temperature by a catalytic heater using unleaded petrol. The antenna was drawn approximately 3 m behind the caboose. Power was supplied by two 120 amp hour lorry batteries which also ensured the stability of the sledge and provided a seat for the operator. When fully charged they allowed approximately 12 hours continuous sounding. An odometer was mounted on a two-way hinge at the rear end of the caboose and consisted of a bicycle wheel and trigger mechanism. Initially an infrared opto-electric switch was used to trip on the spokes of the wheel. It was found to be too sensitive to interference by snow flakes and a magnetic read relay was finally adopted. The caboose was drawn by one or, on steeper terrain, two snow scooters. The speed was restricted to about 2 ms^{-1} by data rate limitations.

2.3.4 Recording in 1985

The digital recording system was designed to obtain maximum information about the detailed echo shape and strength while maintaining a sensible over-snow velocity. Recording was undertaken in a similar manner to 1983 (3.2 Mbyte magnetic tape cartridges) but certain modifications to the sampling procedure were made. Waveforms were sampled after receiving a trigger from the wheel trip and were consequently related to distance and not time. The next transmitter pulse after the trip was synchronised with a 10 MHz oscillator which fed a counter. The oscillator was used to control sampling of the receiver voltage so that 128 samples could be taken at 100 ns intervals starting at zero delay time. Thus each waveform was made up from a single transmitter pulse and was $12.8 \mu\text{s}$ in extent (equivalent to 2,150 m path in ice). The sampled voltage was converted to a 6 bit number (0-63) by a fast A-D converter and was fed to two FIFO stacks in series, having 128 single byte storage locations. These were read upon receipt of the read strobe trigger from the CPU. Each byte was written to tape before the next value could be acquired. The action of the receiver was to amplify the signal by some 35 dB and rectify it.

Hard copy records were available in either 'Z' or 'A' mode from a small Epson thermal printer whose speed limited it to recording about every fifth waveform. This was not considered a problem as the hard copy output had been designed as a 'rough and ready' printout to check satisfactory operation of the digital recording system. The analogue signal was continuously displayed on an oscilloscope screen to which the ciné camera could be mounted if required. Each magnetic tape was able to store about 10^4 ($\equiv 10 \text{ km}$) waveforms.

2.4 Data Reduction in 1985

The ciné films were digitized using the projected image of each frame and a solid state camera linked to a microcomputer. Every 'A' scope was stored as 128 consecutive samples whose value could vary between 0 and 63 (constraints imposed by the number of pixels on the camera interface). If a trace was greater than one pixel in width then the centre of the image was recorded.

Data were transferred to standard 9 track IBM tape for use on the main-frame computer. On close examination of the digitally recorded data, striking discontinuities were seen between successive samples of an 'A' frame, the majority of which were unambiguously 'non-physical'. Investigations of the recording unit in the laboratory revealed an intermittent fault in the A-D converter such that, on the first occasion when bits 3, 4 and 5 (i.e. 8, 16 and 32 in decimal) should have been set to 1, they remained unset. Hence in regions of increasing power, values were found to be too small by either 8, 16 or 32. It is also possible that this was the case for bits 1 and 2 but was not determined unambiguously.

An algorithm to correct the data was devised so that each 'A' scope was compared with a corrected template. If the difference between the two was greater than 6 then 8, 16 or 32 was added to that value depending on the size of the difference and whether the relevant bit was set or not. The template was then weighted by the corrected 'A' scope and the whole process repeated for the next waveform. A certain variation in the time when sampling began, after the start of the transmitter pulse, was also observed. This was corrected by maximising the cross correlation between the template and sample 'A' frame in the region of the transmitter signal (i.e. at the start of the record) which does not vary with position on the ground. This procedure achieved reasonable success in removing any obvious 'spikes' in the data but was not able to reproduce the original waveform to the necessary degree of accuracy to be able to determine the peak echo power. It seems likely that bits 1 and 2 also suffered from this fault and from the calibration data it can be seen that an error of 4 in the digital reading is equivalent to 6.3 dB error in the power. It is also the case that the part of the waveform most susceptible to this fault is where the power is increasing significantly (i.e. in the region of the bed echo). The peak power cannot, consequently, be satisfactorily determined for these data and it was found that their only reliable use was in the determination of ice thickness.

2.5 Navigation

In Nordaustlandet in 1983 a combination of the aircraft's Tactical Airborne Navigation system (TANS), timed sightings of known landmarks and a Motorola ranging system from the aircraft to a network of ground-based transponders were employed and gave an accuracy of between 30 and 250 m depending upon the number of transponders in range (Dowdeswell, 1984). On Spitsbergen the use of a transponder network was impractical but the diverse terrain of the island made regular visual fixes possible. Sightings were made by one or sometimes two observers in the aircraft and timed to an accuracy of 1 sec random error. A certain amount of human error in assessing exactly when a given crossing or sighting had occurred is involved with this method but the short spacing (approximately 3–10 minutes) between fixes on most flights reduces the significance of this error, which at worst was no greater than 6 sec (360 m). NP 1:100,000 maps were used to locate the landmarks and these were then combined with the TANS data to correct for drift. The greatest errors were in across-track position and were typically < 200 m but over some of the more featureless areas such as Åsgårdfonna and Olav V Land this could rise to 800 m. Along-track errors were predominantly due to timing and depending on the fix were between 1 and 6 sec (60 to 360 m). The flight lines and glaciers sounded are shown in Fig. 2.1.

2.6 Ice Surface and Bedrock Elevations

Surface elevations were calculated from a corrected pressure altitude and the SPRI Mk IV terrain clearance, a method described in detail in Dowdeswell (1984). Pressure altitude was accurate to ± 1 m (manufacturers figure) and fixed by flying over regions of known altitude, usually the sea. The surface radar return was taken as the first positive gradient after the transmitter pulse on the 'A' frame. Interpolation between samples enabled random error in terrain clearance (TCL) to be reduced to ± 2 m (Drewry and Liestøl, 1985). Local surface elevation was taken as the difference between pressure altitude and TCL.

Bed returns could not be tracked automatically due to the noisy and/or intermittent nature of the signal and were typically some 50 dB down on the surface return. In some areas it was only the continuity of a signal that would distinguish it from the noise.

An interactive semi-automatic tracking routine was tried, using a microcomputer to display a continuous array of 'A' frames stacked one above the other. This made it possible to

distinguish isolated targets and noise from a genuine reflecting horizon. Due to the manner in which the data were read from tape and stored, however, it was necessary to track the most recent waveform displayed so that breaks in continuity of a reflecting interface made it difficult for the operator to decide on the tracking point before it had already been accomplished. The process also proved rather slow but with further development interactive tracking could become a powerful reduction technique.

The method finally adopted involved manual digitizing of a differentiated and filtered 'Z' mode display obtained from the digital data. Digitizing errors were ± 0.5 mm, equivalent to 0.5 samples—4.2 m in ice. Thus no loss in accuracy was encountered by the use of this method as the maximum resolution for the bed was ± 1 sample (or 8.4 m of ice).

The calculation of ice thickness for the 1985 data was considerably more simple—being an oversnow operation, any inaccuracies introduced by altimetric errors were eliminated. The navigational accuracy was increased due to the availability of a detailed ground survey which had located each stake to an accuracy of ± 0.01 m. Local surface elevations were accurate to ± 5 cm.

2.6.1 EM Velocity in Ice

In calculating ice thickness from RES data it is necessary to know the velocity of electromagnetic waves in ice. This is a function of the relative permittivity ϵ_{∞} and hence of temperature and density, none of which are precisely known for most Spitsbergen glaciers but vary from accumulation to ablation zone and with depth. A value of 168 m/ μ s ($\equiv \epsilon_{\infty} = 3.17$) was used as representative of the mean ice properties encountered. Although the firn layer has a considerably lower density than ice the errors involved in ignoring this difference are negligible in Spitsbergen as the thicknesses of snow/firn involved are relatively small. A far more important consideration is the value of ϵ_{∞} used as this determines the velocity of propagation of the waves in the ice. It is conceivable that ϵ_{∞} will vary depending upon the thermal and hydrological regime within the ice. Measurements from both temperate and cold glaciers have provided very similar values however (Robin, 1975; Blindow and Thyssen, 1986). The consistency of ϵ_{∞} has also been validated by a number of comparative results between borehole and RES data (Bogorodsky *et al*, 1985). Blindow and Thyssen (1986) used a monopulse sounder, (at a relatively high frequency for a monopulse system—34 MHz) on the temperate Vernagtferner (Öetzel Alps), to obtain a series of multiple internal reflections at different depths. A reflection

from the "water table" was observed and a value, for the water content, of 2% calculated. Common midpoint profiles (used in reflection seismics) were produced to enable the calculation of a velocity-depth profile. A number of sites were sounded, varying from the accumulation zone (20 m thick firn layer) to below the equilibrium line (2-3 m snow) but the same mean velocity (within $1 \text{ m } \mu\text{s}^{-1}$) was obtained— $171.5 \text{ m } \mu\text{s}^{-1}$.

Accurate velocity data has also been obtained from cold ice, with little difference in the results. An interferometric technique was used in a borehole on Devon Island (Robin, 1975). The mean velocity, at a mean temperature of -20°C and frequency of 425 MHz, was found to be $168.6 \pm 0.2 \text{ m } \mu\text{s}^{-1}$, a result similar to that obtained from a glacier possessing a finite quantity of water.

A radio-echo logging experiment has been carried out in a borehole on Fridtjovbreen by Macheret *et al* (1984). This glacier possesses an internal reflecting horizon at a depth of 120 ± 10 m, which was present in the region of the borehole. In their experiment a dielectric discontinuity at a depth of 117 ± 10 m was observed with an estimated value for ϵ_∞ of 3.035 above the IRH and 4.125 below. The latter value was deduced from only four measurements, to which a straight line was fitted. They calculated that such a change could be explained by the presence of 3.8% of water. If the values of ϵ_∞ are correct (no errors were given) they could have important implications on the ice thicknesses calculated from RES travel times.

It is difficult to envisage a mechanism by which such a high water content could be maintained throughout the lower ice layer and SPRI echo sounding in 1980 obtained a value of 205 m for the ice thickness near a Soviet borehole, on Fridtjovbreen, that reached bed at 211 m (Dowdeswell *et al*, 1984). If the radio-echo logging results are used to calculate the depth then it would be 220 m. This still lies within the RES error value of ± 10 m but the overestimate implies too high a value for the mean permittivity. Water contents of 4% have not been found even on temperate glaciers where maximum values are about 1.4% (Raymond and Harrison, 1975). Using Rayleigh's mixture formula (section 3.2.2) this predicts an ϵ_∞ of 3.26 which would introduce a 1% error into the estimated ice thickness of a 'wet' layer of ice.

The permittivity of dry ice is reasonably constant (Paren, 1970; Glen and Paren, 1975) and the only factor that is likely to reduce it to 3.035 is a lower density. Taking the permittivity of solid ice as 3.2 and using Looyenga's mixture formula ^(eqn. 3.26) gives a mean density for the upper 120 m of ice of 870 kg m^{-3} . Although not implausible for polar regions this is lower than expected for glaciers in Spitsbergen where the firn layer is not usually very deep even in the accumulation

zone. For example, a 25 m borehole made on Skobreen in 1986 (Ch. 4) reached solid ice (density 870 kg m^{-3}) at a depth of 15 m and a fairly constant density of 900 kg m^{-3} below about 20 m (Simoes, personal communication). This borehole was situated at approximately 3 km above the equilibrium line. It is considered reasonable, therefore, to assume the value of ϵ_{∞} does not vary significantly from 3.17 and that this value may be used in calculating the ice thickness.

2.7 Power Calibration

Calibration of the logarithmic receiver was achieved by flying over a nominally calm sea surface, with an assumed reflection coefficient of unity, at a constant terrain clearance of 600 m. A variable attenuator with 10 dB steps placed in front of the receiver allowed the relationship between the digitally recorded power level and attenuation to be determined. The procedure was carried out once at the start of field-work and again at the end.

A discrepancy of up to 7 bits ($\approx 4 \text{ dB}$) was observed between the two flights. There are several possible causes for this difference. Firstly, on examination of the 'A' scopes it was observed that on the first run there was an extended tail to the echo at lower attenuation settings. This implies that the sea surface was not as smooth as had been hoped and consequently could reduce the returned power by several dB. Indeed, the flight over Isfjord (flt. 01) took place during bad weather when the sea state was high. This is consistent with the lower values recorded on this flight. It was also noted that on the second calibration the average noise level at the lowest attenuation settings was a function of the attenuation. This suggests an external, 'atmospheric' noise source. A radio beacon at Longyearbyen operating close to 60 MHz could have been the cause of this interference. However at larger attenuations ($> 30 \text{ dB}$, at which stage the receiver is just coming out of saturation) this extraneous noise was reduced to the background noise level and is thus considered to have no influence on the most relevant part of the calibration curve. Due to an interrupt circuit used to write text on the oscilloscope screen the dc offset applied to the receiver was prone to a drift, equivalent to ≈ 3 samples. This can be corrected by adjusting all average noise levels (barring those containing external signals) to some arbitrary fixed value. Where a rough surface is encountered or a corner reflector is within the antenna footprint, echoes are received at delay times up to and beyond the $25.6 \mu\text{s}$ length of the recorded pulse. It was often not possible, therefore, to obtain an average noise level for every pulse: reducing the ability to correct the rest of the data for any dc shift. The average difference between the two calibrations was 3.4 bits (about 2 dB) and by using the mean of

zone. For example, a 25 m borehole made on Skobreen in 1986 (Ch. 4) reached solid ice (density 870 kg m^{-3}) at a depth of 15 m and a fairly constant density of 900 kg m^{-3} below about 20 m (Simoes, personal communication). This borehole was situated at approximately 3 km above the equilibrium line. It is considered reasonable, therefore, to assume the value of ϵ_{∞} does not vary significantly from 3.17 and that this value may be used in calculating the ice thickness.

2.7 Power Calibration

Calibration of the logarithmic receiver was achieved by flying over a nominally calm sea surface, with an assumed reflection coefficient of unity, at a constant terrain clearance of 600 m. A variable attenuator with 10 dB steps placed in front of the receiver allowed the relationship between the digitally recorded power level and attenuation to be determined. The procedure was carried out once at the start of field-work and again at the end.

A discrepancy of up to 7 bits ($\approx 4 \text{ dB}$) was observed between the two flights. There are several possible causes for this difference. Firstly, on examination of the 'A' scopes it was observed that on the first run there was an extended tail to the echo at lower attenuation settings. This implies that the sea surface was not as smooth as had been hoped and consequently could reduce the returned power by several dB. Indeed, the flight over Isfjord (ft. 01) took place during bad weather when the sea state was high. This is consistent with the lower values recorded on this flight. It was also noted that on the second calibration the average noise level at the lowest attenuation settings was a function of the attenuation. This suggests an external, 'atmospheric' noise source. A radio beacon at Longyearbyen operating close to 60 MHz could have been the cause of this interference. However at larger attenuations ($> 30 \text{ dB}$, at which stage the receiver is just coming out of saturation) this extraneous noise was reduced to the background noise level and is thus considered to have no influence on the most relevant part of the calibration curve. Due to an interrupt circuit used to write text on the oscilloscope screen the dc offset applied to the receiver was prone to a drift, equivalent to ≈ 3 samples. This can be corrected by adjusting all average noise levels (barring those containing external signals) to some arbitrary fixed value. Where a rough surface is encountered or a corner reflector is within the antenna footprint, echoes are received at delay times up to and beyond the $25.6 \mu\text{s}$ length of the recorded pulse. It was often not possible, therefore, to obtain an average noise level for every pulse: reducing the ability to correct the rest of the data for any dc shift. The average difference between the two calibrations was 3.4 bits (about 2 dB) and by using the mean of

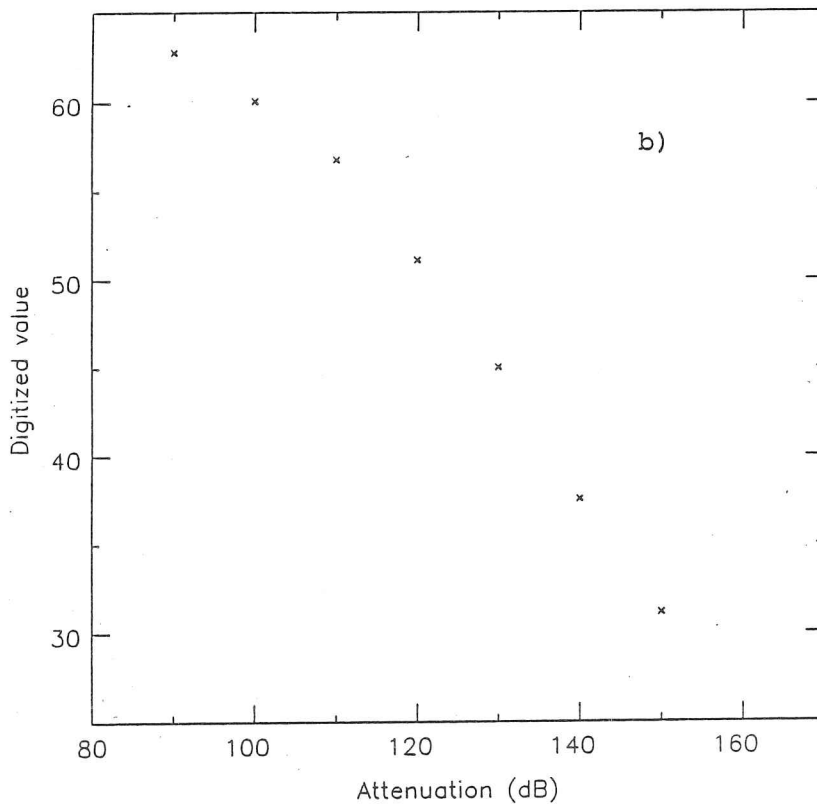
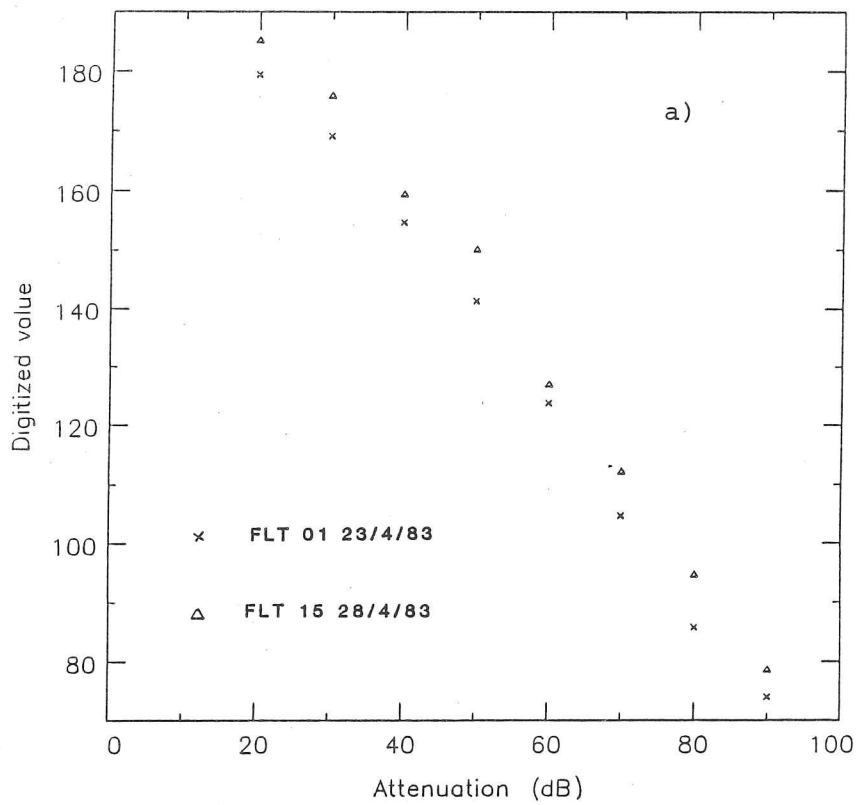


Fig. 2.5 Receiver calibration data for a) 1983 and b) 1985.

the two sets of data it is hoped that any drift would not induce an error, in absolute power calculated, of > 1 dB.

In 1985 system calibration was achieved by feeding the TR signal through a stepped attenuator directly into the receiver. This eliminates the problems encountered in the method described above but does not in any way incorporate the antenna characteristics or any cable losses. For oversnow sounding extended scatterers are not such a problem and it is consequently possible to relate all data to a standard noise level defined by the power calibration. The calibration data for the two seasons are shown in Fig. 2.5.

In general, for accurate power determination, it would seem preferable to feed the signal directly into the receiver. Uncertainties with regard to external noise sources and the reflecting properties of the surface are eliminated with the only disadvantage that the antenna is not included in the circuit. It is shown in Ch. 5 that the system parameters, such as the antenna gain and transmitter power, are not required to determine RCs, so no advantage is obtained in using the 1983 procedure. It was found that the noise level remained constant during the field-work supporting the belief that the drift in d.c. offset is not significant over the time scale of a field season.

2.8 General Results— Topography

Table 2.2 has been constructed so as to indicate the general topographic features of each ice mass sounded. The numbering system is the same as that in Fig. 2.1. Ice caps have been marked by an asterisk, although the difference is not always obvious. Maximum surface and bed elevations are given to help indicate the type of topography encountered although the latter may not be very representative in areas where only limited bed returns were received. The RC data are the mean values.

In general, the valley glaciers, especially in the west, have bed of low slope and elevation, in contrast to much of Olav V Land and Ny-Friesland (Valhallfonna and Åsgårdfonna), where bed elevations reach 1000 m (Fig. A1.15)—a mountainous area covered by thin (100–200 m) ice and possessing quite different RES properties to the valley glaciers.

Extended, single internal reflecting horizons (IRHs) (with high reflection coefficients) were observed on some 60% of the glaciers sounded in 1983. It is suggested in Ch. 5 that the presence of an IRH may indicate a region of temperate ice and the percentage of bed that can be detected

Table 2.2 Topographic, ice thickness and RC data for the ice masses sounded in Spitsbergen in 1983.

Glacier	Max. surface elevation (m)	max. and mean ice thickness (m)	Min. bed elevation (m)	% bed tracked	mean IRH depth (m)	Bed RC (-dB)	IRH RC (-dB)
1 Sveabreen	600			0			
2 Kongsvegan	660	310; 273	-74	25	158	9.1	18.0
3 Kronebreen	770	434; 289	-71	15	203	7.4	18.4
4 Abrahamsenbreen	470	307; 279	-23	90	200	10.7	20.8
5 Vonbreen	620	385; 285	-73	50	172	10.6	22.0
6 Holtedahlfonna*	1170			0			
7 Fjortende Julibreen	800	431; 378	-112	60	193	9.2	20.0
8 Lilliehöökibreen	730			0			
9 Raudfjordbreen	730			0			
10 Idabreen	210			0			
11 Monacobreen	930			0	156		19.1
12 Isachsenfonna*	930			0			
13 Holmstrombreen	880	225; 199	+32	100		9.5	
14 Sefströmbreen	640	370; 292	-41	80	157	12.2	24.7
15 Uvérsbreen	640	370; 289	-32	75	137	11.6	22.2
16 Murraybreen	370			0			
17 Aavatsmarkbreen	560			0	110		21.4
18 Dahlbreen	480			0			
19 Eidembreen	580	426; 392	-92	40	136	9.7	20.5
20 Nansenbreen	430	257; 238	-59	60	131	8.0	18.0
21 Borebreen	730	438; 328	-71	70	151	7.7	19.8
22 Wahlenbergbreen	505	401; 352	-104	65	154	9.8	22.5
23 Hochsteterbreen	760	386; 280	-103	75		16.3	23.4
24 Akademikerbreen	760	305; 284	+110	70		13.4	
25 Hinlopenbreen	314	365; 280	-160	70		15.0	
26 Kvitbreen				0			
27 Russebreen	900	517; 450	-100	20		15.7	
28 Oxfordbreen	1026			0			
29 Lomonosovfonna*	1026			0			
30 Tunabreen	620	334; 280	-110	35	114	15.9	27.1
31 Fimbulisen	854			0	163		27.6
32 Petermannbreen	575	317; 229	-102	80		19.2	
33 Negribreen	960	250; 199	-164	100		18.1	
34 Olav V ice cap*	510	390; 200	-60	80		26.4	
35 Valhallfonna*	732	355; 197	-54	80		26.4	
36 Dunérbreen†	413	322; 217	-33	40	186	21.6	27.5
37 Åsgårdfonna*	1150	334; 206	+224	95		26.4	
38 Veteranen†	940	654; 586	-64	35	359	19.6	25.5
39 Chydeniusbreen†	899	517; 467	-45	75	277	19.0	24.1
40 Tommelbreen	172	146; 124	-19	95		22.2	
41 Balderfonna*	1082	181; 256	+71	70		26.6	
42 Formidablebreen	1007			0	170		23.3
43 Mittag-Lefflerbreen	953			0	147		24.7
44 Nordenskiöldbreen	762			0	129		24.4

Note that blank spaces are present where no data were available. Grouped ice masses were plotted as continuous profiles in App. 1.

* denotes an ice cap. The literal translation of the Norwegian term—fonna—is snowfield or plateau glacier.

† Glaciers possessing IRHs but which were discontinuous and/or non uniform in depth.

is often inversely linked with the existence of this feature. The reason for the absence of a bed echo is twofold. The first is due to obscuration by **surface** scattering which is only important in regions of heavy crevassing. Such areas can be seen on oscillographs (or to a lesser extent on the differentiated 'Z' scopes) with heavy clutter from the ice surface extending in range to, and below, the nominal bed. The second factor is the intense internal scattering associated with the presence of water and other inhomogeneities **within** the ice. Such scattering is often found below an IRH. Fig. 2.6 shows an oscillograph record from Sefströmbreen, which displays this feature.

Dielectric absorption and a low bed RC, in themselves, are only sufficient to eliminate detection of the bed for ice thicknesses greater than about 500 m. Consider a 500 m column of ice with a mean value of absorption of 5 dB/100 m and an RC of -30 dB. These would reduce the reflected signal by 80 dB, added to the geometrical term (typically 70 dB) this gives a total attenuation of 150 dB. The system performance is 160 dB (150 dB when operating with a 10 dB attenuator, which was only used on flt. 09 and some sections over Nordaustlandet) so that P_r should still be 10 dB above the noise level.

Ten ice masses possessed no or poorly resolved bed echoes: Sveabreen, Holtedahlfonna, Isachsenfonna, Lilliehöökreen, Raudfjordbreen, Idabreen, Dahlbreen, Russebreen, Oxfordbreen and Lomonosovfonna, the latter three are situated in the west of Olav V Land and heavy scattering was observed on all of them. The other seven are all from western Spitsbergen but are not particularly localised extending from Lilliehöökreen in the north to Sveabreen, lying almost at the southern extremity of the covered area. Qualitatively, the absence of any reflecting horizons suggests that these ice bodies are relatively close to the melting point over a large part of their mass.

Two other glaciers of interest are Negribreen and Holmstrombreen (Figs. A1.12 and A1.3). Both these need care in assigning the tracked surface to either an IRH or bed. In the former case the values of the RCs were similar to those from an IRH (Ch. 5) of a valley glacier. It was noted, however, that the shape of the tracked surface is not typical of other IRHs found and that its elevation is very low (reaching 160 m b.s.l.), which would mean that the bed would have to lie at an even lower elevation. For Holmstrombreen, the tracked surface bears sufficient resemblance to an unambiguous IRH that further investigation is warranted. If this does represent the bed then the maximum ice thickness (220 m) is less than typical of the area and the bed gradient considerably more. Examination of the RC data (mean value of ≈ -10

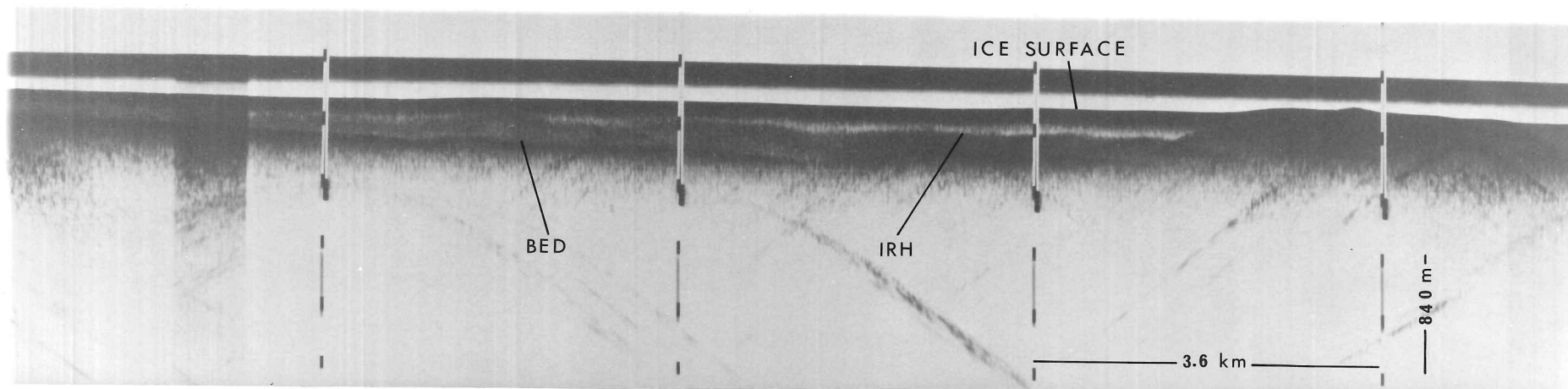


Fig. 2.6 Part of an oscillograph record from Sef strömbreen displaying the extended scattering found below many of the internal reflecting horizons (IRHs) in Spitsbergen.

dB) precludes the possibility that the surface is an IRH and the low ice thickness can then be seen as a consequence of the high bed slope. The reason that so little RC data are available, for this glacier, is not because of a poor signal to noise ratio (which is the usual cause), but because the returned echoes were so strong that they saturated the receiver, thus preventing calculation of the power. As a final check, the oscillograph and 'A' scope records were examined. Neither indicated signs of the heavy internal scattering that tends to be a property of the IRHs.

More detailed discussion of the origin of the IRHs and the RC data is left until Ch. 5, after certain principles of radio-wave propagation in ice have been introduced in the next chapter, which also includes applications of these principles to commonly found physical environments.

CHAPTER 3

THEORY AND APPLICATIONS OF ELECTROMAGNETIC PROPAGATION IN ICE

3.1 Introduction

In the first part of this chapter general aspects of the theory of electromagnetic (EM) propagation in, and at the boundary of, a lossy dielectric are considered and in the second part such theory is applied to some practical situations found in the radio echo sounding of Svalbard glaciers.

Glacier ice is a conductive and hence dispersive dielectric. To understand how EM radiation propagates through such a medium it is necessary to understand its electrical properties. These may be described by a complex relative permittivity:

$$\epsilon^* = \epsilon' - i\epsilon'' \quad (3.1)$$

The real part of ϵ^* , ϵ' , is termed the ordinary relative permittivity or the dielectric constant and represents the displacement current due to the polarization of the ice.

The imaginary part, ϵ'' , known as the dielectric loss factor, represents the conduction current due to the motion of charge carriers.

3.1.1 The Debye Dispersion

Between approximately 0 and 500 MHz the dielectric behaviour of ice can be adequately described by a Debye dispersion (e.g. Johari, 1981) of the form

$$\epsilon^* = \epsilon_\infty + \frac{\Delta\epsilon}{1 + i\omega\tau} - \frac{i\sigma_0}{\omega\epsilon_0} \quad (3.2)$$

where ϵ_∞ = high frequency value of ϵ^* , ω = angular frequency, τ = relaxation time, $\Delta\epsilon$ = dispersion strength ($\epsilon_s - \epsilon_\infty$), σ_0 = d.c. conductivity and ϵ_s = static permittivity.

This equation is a simplification of the actual behaviour as it has been shown that pure ice may possess up to seven separate dispersions (Von Hippel *et al*, 1972) and that a given

dispersion may not have a single relaxation frequency but is more satisfactorily modelled by a spread of τ s (Fitzgerald and Paren, 1978). These points are discussed further in Ch. 4, equation 3.2 serving as a useful approximation. If the real and imaginary parts of this equation are separated we obtain-

$$\epsilon' = \epsilon_{\infty} + \frac{\Delta\epsilon}{1 + \omega^2\tau^2} \quad (3.3)$$

$$\epsilon'' = \frac{\omega\tau\Delta\epsilon}{1 + \omega^2\tau^2} + \frac{\sigma_0}{\omega\epsilon_0}. \quad (3.4)$$

The relaxation time ($\equiv 1/2\pi f_r$, where f_r = relaxation frequency), for ice, is an exponential function of temperature but even at the melting point f_r is still a factor of 100 or more smaller than the frequencies used in echo sounding and hence is almost dispersion free (i.e. the absorption is low).

Above 1 MHz water may also be described by eqn. 3.2 with the appropriate values of ϵ_s , ϵ_{∞} and τ . For pure water at 0°C, $\epsilon_s = 88.15$, $\epsilon_{\infty} \sim 5.0$ and $\tau = 17.7 \times 10^{-12}$ s (Kaye and Laby, 1975). At 60 MHz this gives $\epsilon'_w \sim 83$ and $\epsilon''_w \sim 0.55$. To calculate the change in ϵ' with electrolyte concentration the Falkenhagen formula (Parkhomenko, 1967) may be used;

$$\epsilon'_w = \epsilon'_p + 3.79\sqrt{C_l} \quad (3.5)$$

where ϵ'_p is the permittivity of pure water and C_l = molar electrolyte concentration.

A third material whose electrical properties are important is rock. The permittivity and conductivity of rocks vary widely (Parkhomenko, 1967), depending on factors such as mineral content and porosity, as seen in sections 3.2.1 and 3.2.3 dealing with Fresnel reflections and water saturated rocks.

3.1.2 Propagation of EM waves through a Lossy Dielectric

Throughout this thesis non-magnetic materials are considered in which case the relative permeability, μ , is unity. Maxwell's wave equations then give a differential equation, for the electric field, of the form -

$$\nabla^2 E = \frac{\epsilon'}{c^2} \frac{\partial^2 E}{\partial t^2} + \mu_0 \sigma' \frac{\partial E}{\partial t} \quad (3.6)$$

where c = velocity of light in vacuo, μ_0 = permeability of free space and σ' = the conductivity. It can be seen that the first term on the right is due to the displacement current and the second to the conduction current. One solution of this equation is -

$$E = E_0 e^{i\omega t - Kx} \quad (3.7)$$

where $K = \text{complex wave number} (\equiv \alpha + i\beta)$ and the wave is travelling in the +ve x direction, and

$$K = (\omega^2 \mu_0 \epsilon_0 \epsilon' + i\omega \mu_0 \sigma')^{1/2} \quad (3.8)$$

Separating real and imaginary parts and substituting, $\epsilon'' = \sigma' / \omega \epsilon_0$, yields the following expressions for α and β :

$$\frac{\alpha}{\beta} = \omega \left(\frac{\mu_0 \epsilon_0 \epsilon'}{2} \left((1 + \tan^2 \delta)^{1/2} \mp 1 \right) \right)^{1/2} \quad (3.9)$$

The variable $\tan \delta = \epsilon'' / \epsilon'$ is known as the loss tangent. For a poor conductor such as ice $\omega \mu_0 \sigma' \ll 1$. In fact for ice, at 60 MHz, $\omega \mu_0 \sigma' \approx 3 \times 10^{-3}$ and

$$K \approx \frac{\omega}{c} \sqrt{\epsilon'} + i \frac{\tan \delta}{2} \quad (3.10)$$

giving the group velocity, V_g , equal to the phase velocity, V_p , which is strictly only true for a non dispersive medium;

$$V_g = \frac{d\omega}{dK} = \frac{c}{\sqrt{\epsilon'}} \quad (3.11)$$

Separating eqn. 3.7 into real and imaginary parts yields:

$$E = E_0 e^{-\alpha x} e^{i(\omega t - \beta x)} \quad (3.12)$$

from which the significance of α and β is apparent; α is the attenuation constant and β the phase constant. A useful approximation to eqn. 3.9, for low loss materials is:

$$\alpha \approx \frac{\omega}{2c} \sqrt{\epsilon'} \tan \delta \quad (3.13)$$

and the attenuation in dB/100 m is $= 868.6 \alpha$.

The intrinsic impedance, Z , (necessary in determining the Fresnel reflection coefficient) is defined as $\frac{E_y}{H_z}$ (H_z is the magnetic field strength in the z plane) and in this case is:

$$Z = \frac{\mu_0 \omega}{K} = \left(\frac{\mu_0}{\epsilon_0 \epsilon' - i \epsilon_0 \epsilon''} \right)^{1/2} \quad (3.14)$$

3.1.3 The Radar Equation

Some terms are defined here which are used extensively in the analysis of the RES data. The equations, used for calculating the power returned from a scattering target are also presented.

The gain, G , of an antenna is defined as the solid angle of a sphere (4π) divided by the solid angle subtended by the transmitted power. In the RES field work considered here, the receiving and transmitting antennae were always identical so that the forward and backward gain are the same. The effective area of the antenna can be defined as:

$$A = \frac{G\lambda_0^2}{4\pi} \quad (3.15)$$

where λ_0 = free space wavelength.

If the transmitter power is P_t and the range to the object is r then the power incident on the target is:

$$P_i = \frac{P_t G}{4\pi r^2} \quad (3.16)$$

and the scattered power is:

$$P_{sc} = P_i \sigma = \frac{P_t G}{4\pi r^2} \sigma. \quad (3.17)$$

This defines the radar cross section, σ , and gives the returned power, P_r , as

$$P_r = P_t \frac{G^2 \lambda_0^2}{(4\pi)^3 r^4} \sigma. \quad (3.18)$$

3.18 is usually termed the 'radar equation' for an isolated target of radar cross section σ in free space. If the medium being sounded has a permittivity ϵ' then the wavelength is divided by the square root of this (i.e. $\lambda = \lambda_0 / \sqrt{\epsilon'}$). Now consider the case of a perfectly reflecting, infinite plane. Using the method of electrostatic images it can be shown that the returned power is equivalent to that from a source of strength, P_t , situated $2r$ from the receiver, and gives (from eqn. 3.16):

$$P_r = P_t \left(\frac{G\lambda}{8\pi r} \right)^2. \quad (3.19)$$

For a surface with a power reflection coefficient, R , eqn. 3.19 is simply multiplied by this factor.

If the medium being sounded consists of a thickness, H , of air and a thickness, z , of ice then r is replaced by $(H + z/\sqrt{\epsilon'_i})$ (Smith, 1971) and eqn. 3.19 finally becomes

$$P_r = P_t R \left(\frac{G\lambda_0}{8\pi(H + z/\sqrt{\epsilon'_i})} \right)^2. \quad (3.20)$$

If antenna mismatch and cable losses are included in the term L and the absorption in dB/ m is $B(z)$ then eqn. 3.20 is, in logarithmic form,

$$10 \log \frac{P_r}{P_t} = 20 \log \frac{G \lambda_0}{8\pi(H + z/\sqrt{\epsilon'})} + 10 \log R - 2 \int_0^z B(z) dz - 10 \log L. \quad (3.21)$$

This equation forms the basis for the calculation of R . In future, P_r , P_t , G , R and $B(z)$ will be quoted in decibels unless otherwise stated and for convenience the prefix 10 log will be dropped.

3.2 Applications

3.2.1 Fresnel Reflection

In this section the reflection coefficients of a number of different interfaces are investigated using the Fresnel equation for reflection from a smooth, flat dielectric boundary. The terms "smooth" and "flat" are relative to the radar wavelength in the medium and mean that any departure from a plane surface must be $\ll \lambda$ (more strictly $< \lambda/16$). This approximation is discussed briefly below. It will suffice, for the present, to state that surface roughness will reduce the signal strength by an amount between 0 and ≈ 15 dB maximum (Neal, 1977). Under certain circumstances focussing effects can produce localised 'bright' points (Oswald, 1975) but this is not relevant when considering the mean received power returned from an extended area.

For an arbitrarily polarized wave, the well known equations for the Fresnel reflection coefficient, R , and transmission coefficient, T , are (for an infinite plane at normal incidence),

$$R = \left| \frac{Z_t - Z_i}{Z_t + Z_i} \right|^2 = \left| \frac{n_i - n_t}{n_i + n_t} \right|^2 \quad \text{and} \quad T = \left| \frac{2Z_t}{Z_t + Z_i} \right|^2 \quad (3.22)$$

where Z = intrinsic impedance, n = refractive index and the subscripts i and t refer to the incident and transmitting medium respectively. Later it will be seen that the dielectric boundary may consist of a layer of one material embedded in another (e.g. moraine). In this case, for a layer of thickness d ,

$$R_{layer} = 4 \sin^2 \left(\frac{2\pi d}{\lambda_i} \right) \times R \quad (3.23)$$

(Paren and Robin, 1975).

In section 1.4 the typical rocks that are found in Svalbard were described. The dielectric properties of Svalbard rock samples have not been measured but, in general, the relative permittivities of these different rock groups vary from about 4-5 for sandstone up to 15 for some gneisses (Parkhomenko, 1967) so that it might be expected that the reflection coefficients (RCs) from different regions will (in the absence of other effects) also vary considerably. Some examples of RCs for typical surfaces and rocks of the type encountered in Svalbard are shown in Table 3.1 along with the transmission coefficient, where applicable. Values for ϵ^* for the different rocks were taken from Parkhomenko (1967) while the dielectric properties of water were calculated from eqns. 3.4 and 3.5. The ice/rock RCs can be seen to vary from anywhere between -25 and -5 dB. The presence of water will increase the upper limit while roughness will effectively reduce both (roughness does not affect the **reflectivity** properties as such but it **does** reduce the received power (Neal, 1977)).

3.2.1.1 Bedrock Roughness

Unless it is easily deformed or erodable, the sub-ice bedrock is quite likely to be uneven on a scale comparable to the radar wavelength in ice. Irregularities cause scattering and reduce the power returned to the receiver. The surface can be treated as a phase modulating screen so that diffraction theory can then be used to determine the backscattered energy (Neal, 1977). Before taking this approach it is necessary to assign a distribution function to describe the rms surface slope. Two functions are favoured— Rayleigh and Gaussian. The former is best suited to a completely random arrangement of slopes whereas the latter is more appropriate to a surface that has been preferentially smoothed in one direction (Neal, 1977).

Fig. 3.1 shows the effect of roughness for various values of the rms tangential slope, β , for a) a Rayleigh distribution and b) a Gaussian one. The curves were calculated for a square pulse of 250 ns duration and an ice thickness of 500 m (Oswald, 1975). It can be seen that, even for slopes of 45° , the reduction in peak echo power is only of the order of 10 dB, and for a Gaussian distribution, the effect is smaller still (4 dB). The maximum reduction in power, from a very rough surface, was estimated by Neal (1977) as about 15 dB but this is the most extreme situation and it is reasonable to assume that the likely loss will lie between 0 and 10 dB.

So far the effects of the presence of water at the bedrock interface have been ignored. It will be shown in Ch. 5 that this may have a stronger influence on regional RC variations

Table 3.1 Reflection and transmission coefficients for different interfaces.

Boundary	Reflection coefficient (dB)	Transmission coefficient (dB)
air/snow	-15.3	-0.1
air/ice	-11	-0.4
ice/pure water	-3.4	-2.7
ice/sandstone	-25.2 to -10.4	
limestone	-14.2	
granite	-25 to -15	
gneiss	-13 to -8.6	
shale	-11.1 to -5.2	

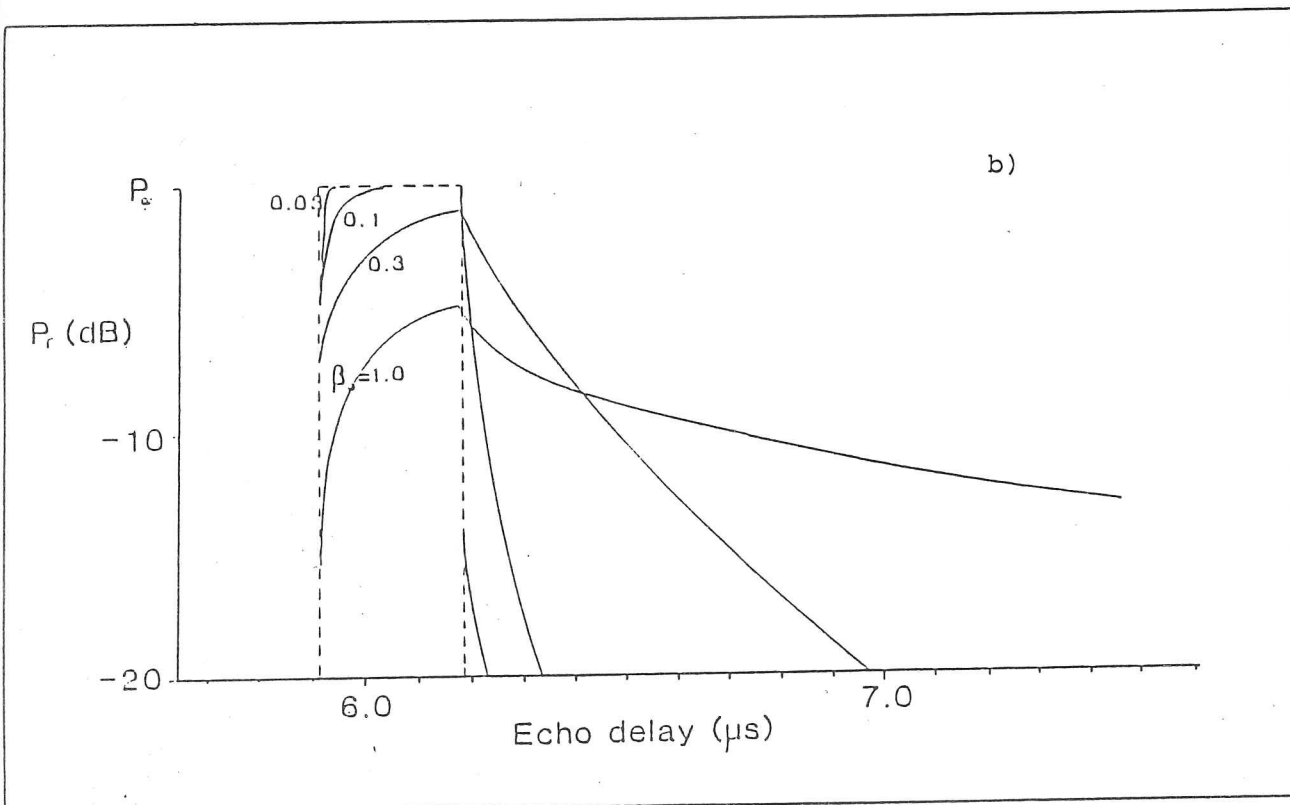
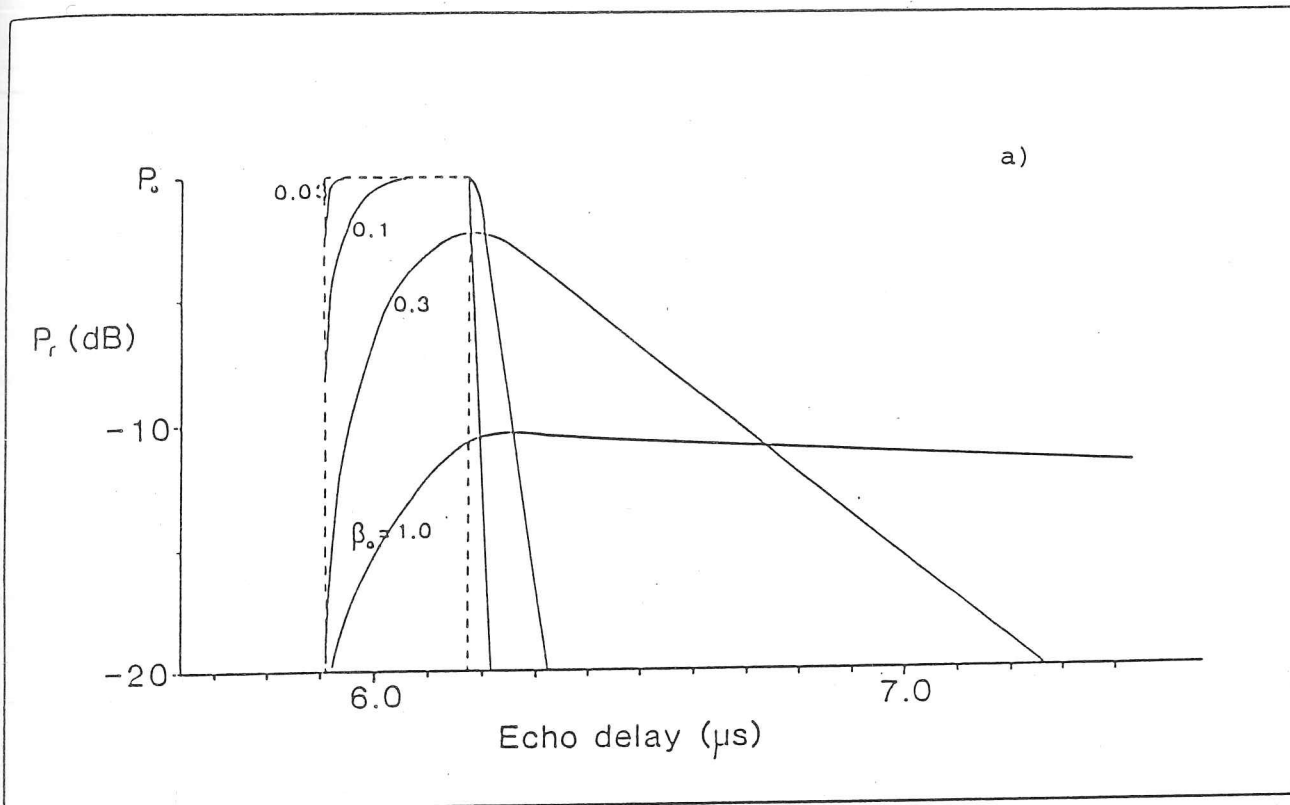


Fig. 3.1 The effects of bedrock roughness on the returned power for a) a Rayleigh distribution of slopes and b) a Gaussian distribution (source Oswald, 1975).

than differences in the rock permittivity and will be especially pronounced for acidic or basic species such as limestones. It is important to consider analytically, therefore, how water might influence the complex permittivity of a wet bedrock and this is done in section 3.2.3. Prior to this, however, it is useful to introduce some equations that can be used to determine the dielectric response of a heterogeneous system.

3.2.2 Reflections from Dielectric Mixtures

In this section we shall be considering how the Maxwell-Wagner effect modulates the complex permittivity, ϵ_m^* , of a mixture of ice with another dielectric (e.g. air). The dispersion due to this effect is present in all heterogeneous systems and is due to the trapping of charges at the boundary between two dielectrics (Maxwell, 1891; Wagner, 1914). It is sometimes also referred to as interfacial polarization. As long as the average size of the dispersoid (the minor constituent of the mixture) is $\ll \lambda$ then it is unnecessary to consider the scattering properties of the system (section 3.2.5) but one can, more appropriately, treat it in terms of dielectric theory. The equations presented here will prove useful in elucidating the possible origins of internal reflecting horizons, discussed in section 3.2.4 and Ch. 5. Van Beek (1967) has made a comprehensive review of the theory of dielectric mixtures and presents a number of equations that can be used to describe their properties. In their most general form these equations include a constant that is shape dependent (the depolarization factor). Because, in most cases, there is very little information about the shape of the inclusions, they have been assumed, unless otherwise stated, to be spherical and the equations quoted below are strictly only applicable to this case. In this section subscript 1 refers to the matrix medium and subscript 2 to the inclusion. The permittivity of the former, $\bar{\epsilon}_1$, is not necessarily the same as ϵ_1 (the value for the medium without any inclusions) but probably has a value intermediate between ϵ_1 and ϵ_m (i.e. $\epsilon_1 < \bar{\epsilon}_1 < \epsilon_m$).

Van Beek has suggested an equation derived from electrostatic theory that, in its most general form, for spherical inclusions is—

$$\epsilon_m - \epsilon_1 = \frac{3V_2(\epsilon_2 - \epsilon_1)\bar{\epsilon}_1 / (2\bar{\epsilon}_1 + \epsilon_2)}{1 - V_2(\epsilon_2 - \epsilon_1) / (2\bar{\epsilon}_1 + \epsilon_2)} \quad (3.24)$$

where V_2 = the volume fraction of the inclusion. ¹

¹ The permittivities in eqn. 3.24, and the following three equations are complex but for convenience the * has been dropped.

When $\bar{\epsilon}_1 = \epsilon_1$ (which is most likely to be true for small V_2) then eqn. 3.24 reduces to

$$\frac{\epsilon - \epsilon_1}{\epsilon + 2\epsilon_1} = V_2 \left(\frac{\epsilon_2 - \epsilon_1}{2\epsilon_1 + \epsilon_2} \right) \quad \text{or} \quad (3.25)$$

$$\epsilon = \epsilon_1 + 3V_2 \frac{(\epsilon_2 - \epsilon_1)\epsilon_1}{2\epsilon_1 + \epsilon_2 - V_2(\epsilon_2 - \epsilon_1)}.$$

This is known as Rayleigh's mixture formula. At the other extreme when $\bar{\epsilon}_1 = \epsilon_m$ (applicable to high V_2) then Böttcher's mixture formula is obtained. One more equation is considered—Looyenga's mixture formula:

$$\epsilon_m^{1/3} = V_2(\epsilon_2^{1/3} - \epsilon_1^{1/3}) + \epsilon_1^{1/3}. \quad (3.26)$$

This has proved very successful in modelling the behaviour of ice/air mixtures ranging in density from 200–800 kg m⁻³ (Paren, 1970) which is equivalent to volume fractions of air of 0.78–0.13. It is, however, most suited to relatively high dispersoid concentrations (greater than ≈5%) and is used in Ch. 4 to convert dielectric data, obtained from bubbly ice, to the solid ice equivalent ($\rho = 920 \text{ kg m}^{-3}$).

3.2.3 Dielectric Properties of Water-Saturated Rocks

Empirical results from water saturated rocks, even at quite low concentrations ($\approx 2\%$) show that water can have a dramatic influence on the permittivity. For example ϵ' of a siltstone was found to rise from ≈ 5 to 32 for a moisture content between 0 and 4% (Parkhomenko, 1967). This effect is strongly frequency dependent, however, and to investigate this dependence (so that its influence at RES frequencies may be established) a simplified model based on that of Lysne (1983) is employed.

The large changes in ϵ' are due to a new dispersion being produced by the presence of a second dielectric (water). Lysne suggests that the Maxwell-Wagner relaxation process is responsible. In the analysis that follows it will be useful to represent the conduction current, induced by the electric field, as the sum of two components—the first due to the dielectric constant, ϵ''_r , of the rock and the second due to the ionic conduction. This gives,

$$\epsilon_m^* = \epsilon'_m - i \left(\epsilon''_r + \frac{\sigma_m}{\omega\epsilon_0} \right) \quad (3.27)$$

To obtain ϵ^* we need to find ϵ'_m , ϵ''_r and σ_m . The latter has been shown to be virtually independent of frequency, in the range considered here, and may be calculated from an equation known as Archie's rule (Archie 1942);

$$\sigma_m = (\phi S_w)^2 \sigma_w \quad (3.28)$$

Permittivities vs. log Frequency

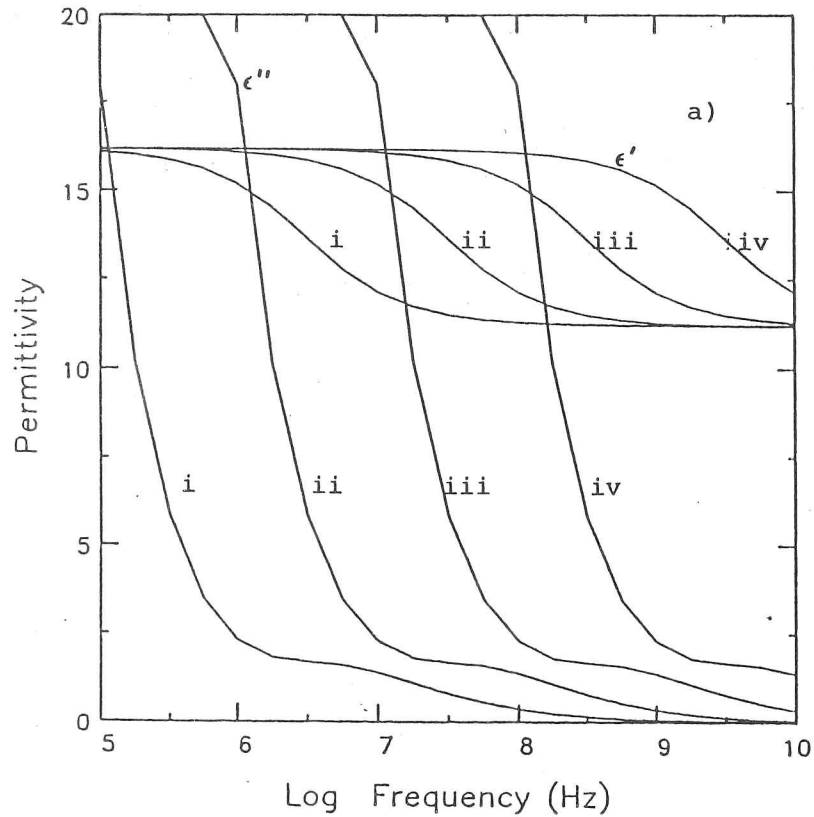


Fig. 3.2 a) Real and imaginary permittivities of water saturated rock plotted against log frequency for four different values of water conductivity; i 2.5×10^{-3} , ii 2.5×10^{-2} , iii 0.25 and iv 2.5 Sm^{-1} .

Refln. Coeffs. vs. log Frequency

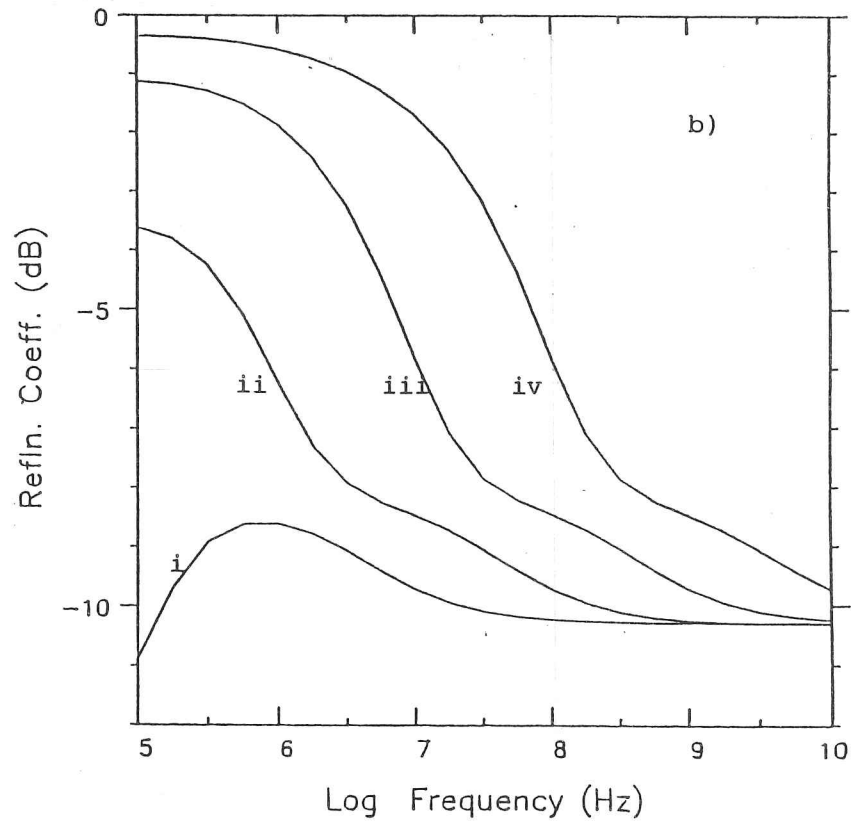


Fig. 3.2 b) Reflection coefficients plotted against log frequency, calculated from the data in fig. a).

where ϕ = porosity and S_w = fraction of water saturating the pores (assumed to be 1.0 in the following analysis) and σ_w = water conductivity. Lysne found that $\epsilon^*(f)$ can be described by the equation,

$$\epsilon_o \epsilon^*(f) = \epsilon_o \epsilon_\infty + \int_0^\infty \alpha(\tau) \frac{d\tau}{1 - if\tau} \quad (3.29)$$

where $\alpha(\tau)$ is a distribution function describing the shape of the rock pores and $\tau = 1/(2\pi f_r)$. If we assume all pores are the same and completely saturated we can write $\alpha(\tau) = \alpha_o \delta(\hat{\tau} - \tau)$ then eqn. 3.24 may be readily integrated to give,

$$\epsilon_o \epsilon^* = \epsilon_o \epsilon_\infty + \frac{i\alpha_o}{f} \ln(1 - if\tau) \quad (3.30)$$

Substituting $(1 + (f\tau)^2)^{1/2} e^{-i\theta}$ for $(1 - if\tau)$ with $\theta = \tan^{-1}(-f\tau)$ and separating real and imaginary parts yields,

$$\epsilon' = \epsilon_\infty + \frac{\alpha_o}{f} \tan^{-1}(f\tau) \quad (3.31)$$

$$\epsilon'' = \frac{\alpha_o}{2f} \ln(1 + (f\tau)^2). \quad (3.32)$$

ϵ_∞ can be calculated using a suitable mixture formula (van Beek, 1967) depending on the amount of water present.

The frequency dependence is given by the equation,

$$\tau = \epsilon_o (\epsilon'_r (n - 1) + \epsilon'_w) \sigma_w^{-1}. \quad (3.33)$$

n is a shape factor whose minimum value is 1 and has been found to be typically about 3. The most interesting feature of eqn. 3.33 is that $\tau \propto 1/\sigma$, so that the the higher the pore water conductivity, the higher the relaxation frequency, f_r . Lysne has deduced, from experimental data, a value of $\sigma_w = 2.5 \times 10^{-2} \text{ S m}^{-1}$ for fresh water in contact with clay and for a porous siltstone or carbonate bedrock it may well be possible to exceed this value.

The conductivity of subglacial meltwater is an uncertain quantity, however, and the most useful data comes from studies on the conductivity of proglacial meltstreams. This has been measured by a number of authors (e.g. Collins and Young, 1981; Slatt, 1972). It is dependent upon several factors, the most important of which are flow rate (which is correlated with time of year) and bedrock type. The highest conductivities were measured in winter, when the flow, Q , is at a minimum, and can be as much as 10 times the summer values. Plots of conductivity versus discharge invariably indicate an inverse relationship which is often non linear and appears

to be dependent upon the basin characteristics or rock type (Gurnell and Clark, 1987). Values range anywhere between about $5 \times 10^{-4} \text{ S m}^{-1}$ and $6 \times 10^{-2} \text{ S m}^{-1}$ and are obviously strongly influenced by the erosional processes at, and chemical properties of, the bed. The minimum value of τ occurs for $n = 1$ and taking $\sigma_w = 2.5 \times 10^{-2} \text{ S m}^{-1}$ and $\epsilon'_w \approx 83$ gives $f_{r_{max}} = 5.4$ MHz. This is about a factor of 10 less than the RES frequency of the SPRI Mk IV. A ten fold increase in σ_w , however, will produce the same increase in f_r : an effect that is illustrated in Fig. 3.2 a) where the real and imaginary parts of ϵ^* have been plotted against frequency for four values of σ_w ranging from $2.5 \times 10^{-3} \text{ S m}^{-1}$ to 2.5 S m^{-1} (a value typical of sea water (Smith, 1971)). Shown below this in Fig. 3.2 b) are the corresponding RCs for an ice/rock interface. The constants used in the calculations were: $\phi = 0.2$, $S_w = 1.0$, $\epsilon'_r = 5.0$, $\epsilon'_w = 83$ (the change in ϵ'_w with conductivity has not been included as it has a negligible effect on the results) and $\alpha_o = 6/\tau \text{ s}^{-1}$ (an empirical result obtained by Lysne).

It can be seen that the frequency dependence of the RC is not relevant unless the water conductivity is significantly greater than $2.5 \times 10^{-2} \text{ S m}^{-1}$ at which value increasing the sounding frequency from 10 to 100 MHz reduces the RC by only 1.5 dB. For $\sigma_w = 0.25 \text{ S m}^{-1}$ it becomes 2.4 dB. A higher rock porosity would increase these values as would a larger value for the distribution function, α_o , but for realistic water conductivities the RC will only be significantly different from its high frequency (hf) value for sounding frequencies below about 10 MHz.

It is difficult to predict the nature of the bedrock environment, depending not only upon the rock type but also on the thermal regime. If water is in contact with a deformable bed (unconsolidated sediments) then it may be more appropriate to consider a rock/water mixture of similar proportions which could be treated using an equation such as the Looyenga mixture formula (section 3.2), as long as the water conductivity remains sufficiently low. If this is done for a water content of 30% (the maximum realistic value (Drewry, 1986)) and a rock permittivity of 5 then an RC of -11 dB is obtained (the water conductivity has a negligible effect for realistic values) compared to -19 dB, for a solid rock boundary.

3.2.4 Internal Reflecting Horizons

The phrase "internal reflecting horizon" (IRH) is an umbrella term used to describe any reflection from beneath the ice surface, but above the bed, which appears to be continuous on a scale comparable to the pulse length (42 m) or greater. This phenomenon was detected as early as 1964 in northwest Greenland and described by Robin *et al* (1969) as weak echoes at a minimum depth 275 m but usually occurring at depths of about 500 m below the surface. Estimates of the RCs ranged from a maximum of -43 to -80 dB, with values of about -70 dB being typical. They were noted to have "the character of weak specular reflexions of slowly varying intensity and appear to be caused by layers of wide areal extent approximately parallel to the surface". A number of possible causes were considered including variations in density and layers of volcanic ash.

An IRH surface may be composed of a number of discrete scatterers or may be due to an homogeneous change in dielectric properties. There is a fundamental difference between these two cases; in the first there are two contributions to the returned power— one from **surface scattering** and the second from **volume scattering**, while in the second case the problem can be treated as a boundary between two dielectrics and Fresnel's equation (3.22) may be used to find the RC. The distinction between these cases is not always clear and can often not be distinguished from RES data alone.

A good example of this difficulty is presented by air bubbles in ice. A change in the bubble content produces a corresponding change in the relative permittivity and a Maxwell-Wagner dispersion and hence represents a dielectric discontinuity. The bubbles also act as scattering centres, but because the scattered power is so small (Smith and Evans, 1972) this component is usually ignored and to the echo sounder air bubbles would fall into the second category (i.e. a dielectric discontinuity) despite the fact that they are discrete scatterers. In the next section it will be shown that under certain circumstances (i.e. for large scatterers) the scattering component has a significant contribution to the returned power and may be the dominant factor.

The causes of IRHs can be broadly separated into three groups

- 1 Air bubbles. A change in bubble content alters the relative permittivity although orientation and shape can also influence the dielectric behaviour. Paren and Robin (1975) calculated the RCs from a boundary between bubbly and bubble-free ice for different over-

burden pressures (i.e for different layer depths). They found that the RC varied between -51 and -85 dB from depths of 100 to 4000 m. Ackley and Keliher (1979) made a detailed study of the possible causes of IRHs observed in ice from Cape Folger, east Antarctica. They considered a variety of factors: density changes (due to variations in bubble content), bubble geometry, crystal orientation and crystal fabric. They compared their RES data with core data from the same area and concluded that the parameter that showed the best correlation was density. The magnitudes of the RCs were typically -80 dB. Millar (1981), following the procedure of Paren and Robin (1975), obtained an equation for the maximum RC, R_{max} , for a boundary between bubbly and bubble-free ice;

$$R_{max} = 0.717 / z^2. \quad (3.34)$$

The IRHs observed in Spitsbergen are typically 100-200 m below the surface. For such thicknesses eqn. 3.34 gives a maximum RC of between -41 and -47 dB. The observed values are between 10 and 20 dB greater than these.

2 Chemical impurities. Ionic impurities dissolved in the ice have a strong effect on its conductivity (e.g. Gross *et al*, 1978) and hence can produce a reflection. Millar (1981) has correlated multiple layers observed on RES records from Greenland with the acidity levels measured in an ice core taken from the same area and he associated the increased acidity with a rise in volcanic activity. He also deduced, from Jaccard's (1959) theory of electrical conduction in ice, a semi-empirical formula for the variation of the loss tangent with acidity ($[H^+]$). For ice at 0°C he obtained,

$$\Delta \tan \delta = \frac{\Delta \sigma_{\infty}}{2\pi f \epsilon_0 \epsilon_{\infty}} = \frac{1.02 \times 10^{10}}{f} [\Delta H^+] \quad (3.35)$$

where $[H^+]$ is measured in M (mol/l). This equation allows the approximate calculation of the RC due to variations in $[H^+]$ and will be used in Ch. 4 to investigate the likely causes for the regional variations in radar ice absorption that have been observed (Ch. 5). Layer echoes caused by chemical impurities have also been found widely in the Antarctic and their strength is typically between -65 and -80 dB (Robin *et al*, 1969; Millar, 1981).

3 Presence of water. A separate category is given to water for three reasons. i), water is not strictly an impurity although it may contain a significant proportion of them (e.g. Wolff and Paren, 1984). ii) it is unlikely that the water will exist as a thin layer within the ice (though it may be distributed as a random collection of discrete scatterers) so that

the reflections cannot appear as a large number of closely spaced continuous layers. iii), because of the high relative permittivity of water (≈ 83) it is only necessary for it to be present in fairly small quantities ($< 1\%$) to produce an RC considerably greater than any of the previous mechanisms. This is discussed further in Ch. 5.

3.2.5 Scattering

In other parts of this thesis (especially Ch. 5) scattering from water bodies, within the ice, is identified as a likely cause of IRHs. It is also postulated that these are **discrete** water bodies. While drilling on a temperate glacier Hodge (1976) observed a number of 'cavities' of average size 0.25 m. For typical inhomogeneities of these dimensions the assumptions necessary to be able to apply the arguments of Rayleigh scattering (i.e. $2\pi a/\lambda \ll 1$, where a is the radius of the scatterer) are no longer valid and a more exact solution is necessary.

Mie's theory of scattering by light, from particles of arbitrary size, is just such an approach and the only assumptions that need to be made are that the scatterers are spherical and that they act as independent sources (i.e. there is no interference between the power radiated by different scatterers) so that the total scattered power is the sum of that from each target. The latter restriction is satisfied if the distance between each source is greater than approximately three times the radius of the scatterer and is not a restrictive criterion. The former is less likely to be obeyed but the results are not significantly affected because of this (van de Hulst, 1957).

We shall use Mie's theory to calculate, by numerical analysis, the backscattering cross section, σ , of a body of arbitrary size, and from this, the returned power is found using the radar equation,

$$P_r = P_t \frac{G^2 \lambda^2}{(4\pi)^3 r^4} \sigma. \quad (3.18)$$

The analysis follows that of van de Hulst (1957) and will be described here so that the significance of the parameters involved and the computational procedure may be understood.

For backward scattering ($\theta = 180^\circ$) the scattering amplitude for arbitrarily polarized radiation is,

$$S_1(\theta) = - \sum_{n=1}^{\infty} (n + 1/2) (-1)^n (a_n - b_n) \quad (3.36)$$

where a_n and b_n are the Mie coefficients,

$$a_n = \frac{\psi'_n(y)\psi_n(x) - m^*\psi_n(y)\psi'_n(x)}{\psi'_n(y)\zeta_n(x) - m^*\psi_n(y)\zeta'_n(x)} \quad (3.37)$$

$$b_n = \frac{m^* \psi'_n(y) \psi_n(x) - \psi_n(y) \psi'_n(x)}{m^* \psi'_n(y) \zeta_n(x) - \psi_n(y) \zeta'_n(x)} \quad (3.38)$$

Three new variables have been introduced: $x = 2\pi a/\lambda = Ka$ and $y = m^*ka$, where m^* is the complex refractive index;

$$m^{*2} = \epsilon' - i\epsilon'' \quad m^* = n' - in''$$

For $\epsilon' \gg \epsilon''$ this gives the familiar result $n' \approx \sqrt{\epsilon'}$ and $n'' \approx \epsilon''/2\sqrt{\epsilon'}$. If the matrix medium is not a vacuum ($m^* = 1$) then the value of m^* used in the equations should be m_{sc}^*/m_{matrix}^* . In the case of ice and water at 60 MHz and close to the melting point ($\epsilon_w^* = 83 - i0.027$ and $\epsilon_i^* = 3.17 - i0.014$) $m^* = 5.12 - i0.0088$. $\psi_n(z)$ and $\zeta_n(z)$ are known as the Riccati Bessel functions and are defined as:

$$\psi_n(z) = zj_n(z)$$

$$\zeta_n(z) = zh_n^{(2)}(z)$$

where j_n and $h_n^{(2)}$ are the spherical Bessel functions of the 1st and 3rd kind (tabulated in e.g. Abramowitz and Stegun, 1964).

To obtain the n^{th} Riccati function it is possible to use the recurrence relations derived for the spherical functions;

$$f_{n+1} = (2n+1)1/zf_n - f_{n-1} \quad (3.39)$$

$$\text{and } \frac{d}{dz}f_n = f_{n-1} - \frac{n+1}{z}f_n \quad (3.40)$$

where $f_n = j_n$ or $h_n^{(2)}$. Eqn. 3.40 must be adapted so that it can be applied to the Riccati functions (for eqn. 3.39 this is trivial) and doing this we obtain:

$$\frac{dg_n}{dz} = g_{n-1} - ng_n/z \quad (3.41)$$

where $g_n = \psi_n$ or ζ_n .

Given the first two spherical Bessel functions it is thus possible to calculate any number of Riccati functions from eqns. 3.39 and 3.41, and hence the scattering amplitude, $S_1(180^\circ)$.

If we define the radar cross section, σ , as 4π times the power scattered back per steradian divided by the power incident on a unit area (equivalent to eqn. 3.18) then,

$$\sigma = \frac{4\pi}{k^2} |S_1(180^\circ)|^2 = \frac{\lambda^2}{\pi} |S_1(180^\circ)|^2 \quad (3.42)$$

where k = wave number. Therefore for an isotropic scatterer, σ = the geometric cross section (πa^2).

Combining eqns. 3.42 and 3.18 gives P_r for a single target. Let us assume that there are f scatterers per m^3 (if their volume fraction is 0.01 then $f = 0.01 \times 3/(4\pi a^3)$). The volume illuminated is $2\pi r^2 l/G$, where l is the pulse length in ice (in units of length) and the total scattered power at the receiver is then,

$$P_r(\text{scat}) = \frac{P_t G \lambda^2 l}{32(\pi r)^2} f \sigma. \quad (3.43)$$

The reflection coefficient, R , of a plane surface has been defined as

$$P_r = P_t R \left(\frac{G\lambda}{8\pi r} \right)^2 \quad (3.19)$$

and thus the effective RC due to layer scattering is

$$R_{sca} = \frac{2l}{G} f \sigma. \quad (3.44)$$

In Fig. 3.3, R_{sca} is plotted against the target radius, a , for a volume fraction of 0.01 for three different scattering materials. In a) the inhomogeneity is air, in b) it is rock ($\epsilon^* = 5 - i0.003$) and in c) it is water ($\epsilon^* = 83 - i0.027$). It should be noted that the complex refractive index is frequency dependent and that the data are only applicable for a value of 60 MHz. Marked on the y axes are the RCs calculated using Rayleigh's mixture formula (eqn. 3.25) combined with Fresnel's equation (eqn. 3.22). It can be seen that $R_{sca} > R_{plane}$ occurs for water when $a > 2.5$ cm, for rock when $a > 3$ cm and for air when $a > 2$ cm. Although water or air inclusions of these dimensions are probably not common for cold ice, in temperate glaciers they are more likely to exist and have been observed in a number of studies (e.g. Hodge, 1976; Schommer, 1977).

The positive RCs in Fig. 3.3 require some explanation. They occur for two reasons. The first is that the power is being returned from a volume and not a surface. The second is that it is possible for σ to be greater than one, i.e. the effective area of the scatterer is greater than its geometrical area. In Fig. 3.4, $\sigma/\pi a^2$ is plotted against x and from this we observe

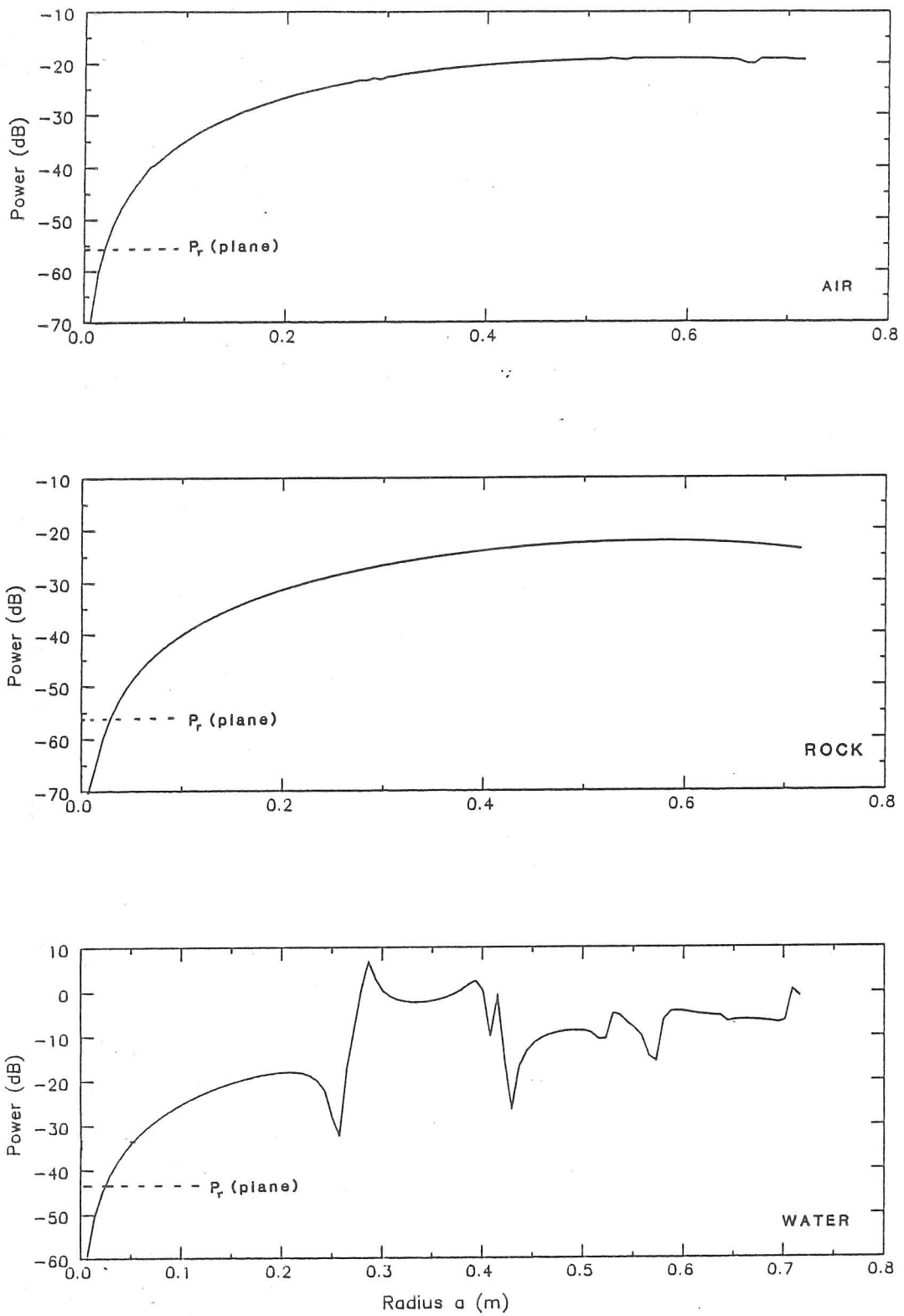


Fig. 3.3 The reflection coefficients for inclusions of air, rock and water plotted against radius. Relative permittivity of the rock was taken as 5.0 and its conductivity as $1 \mu\text{S m}^{-1}$. For water the former was 83 and the latter $90 \mu\text{S m}^{-1}$. The volume fractions, for all three types of inclusion was 0.01.

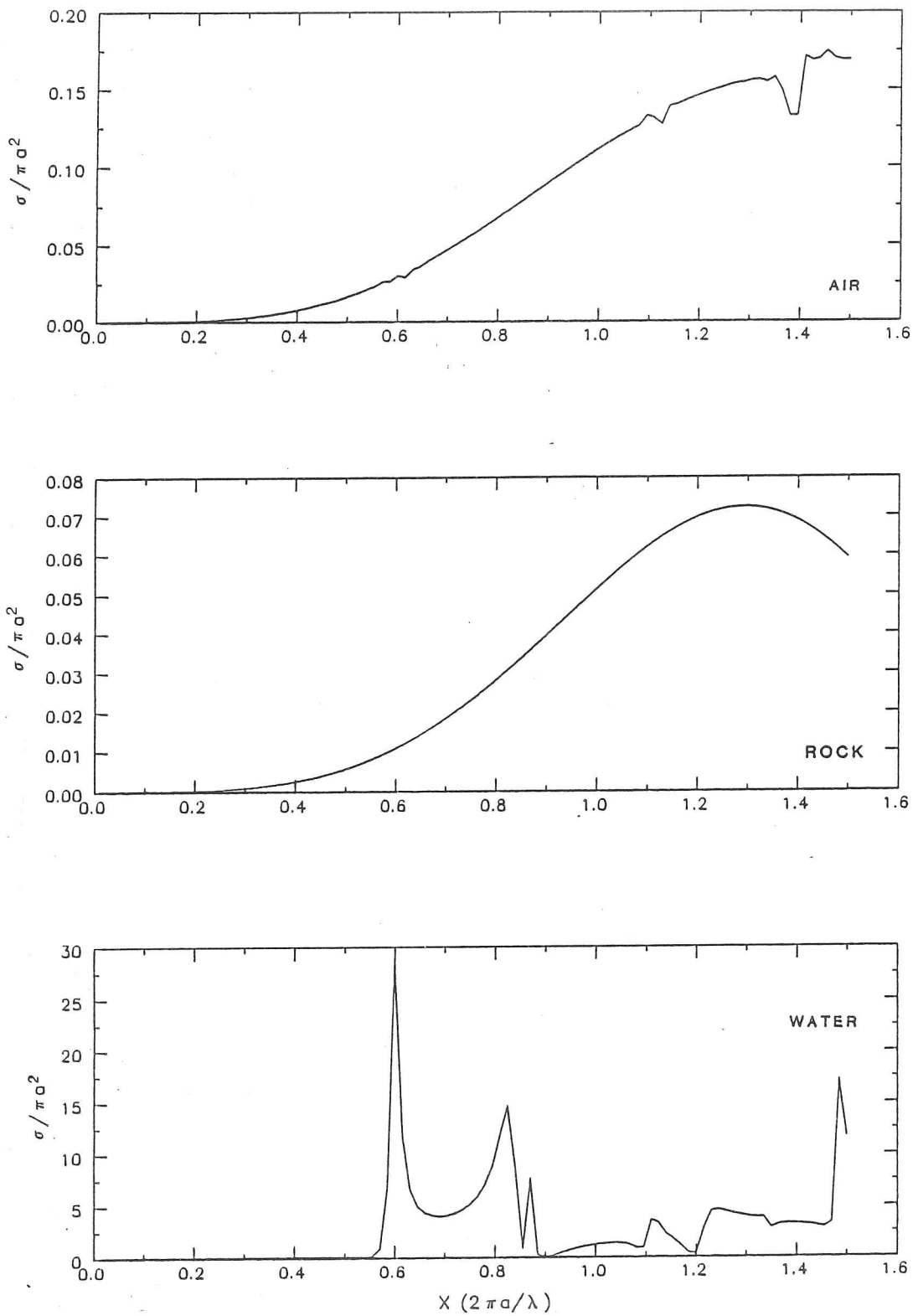


Fig. 3.4 Backscattering cross sections for air, rock and water in ice plotted against the dimensionless parameter X . Values of constants as in fig. 3.3.

the interesting result that, for certain values of a , $\sigma > 4\pi a^2$, i.e. the effective area is greater than that of a sphere. This occurs because of focussing of the radiation by the water. The remarkable scattering diagram obtained for water is a consequence of the large value of ϵ' and its finite conductivity. These combine to produce a resonant effect analogous to sound waves in water containing air bubbles (B.J. Uscinski, personal communication). The conductivity used in the calculations was $9 \times 10^{-5} \text{ S m}^{-1}$ (Wolff and Paren, 1984). Varying this value within a reasonable range can reduce the cross section by up to a factor of two but this represents a reduction in the RC of only 3 dB.

In conclusion, it can be stated that when the target radius is greater than about 5 cm the scattering power (for the dispersoids considered) will outweigh that which would be expected from a plane dielectric boundary which is assumed to obey a relaxation process due to Maxwell-Wagner effects. For the case of water bodies, if a is greater than ≈ 25 cm, the scattered power can be greater than that for any plane boundary. This result clearly illustrates the difficulties that may be encountered when sounding temperate glaciers possessing englacial water bodies. It could explain the problems that were found in obtaining bed echoes during the melt season in Svalbard by Soviet workers (Dowdeswell *et al*, 1984a) and the fact that bed returns are often absent in the accumulation zone of a glacier. It might also explain some of the results of Davis (1973) who found considerable internal scattering on temperate glaciers in the Alps. He deduced, by an empirical approach, a mean attenuation of the wave of up to 10 dB/100 m and associated this with a combination of the effects of scattering and dielectric absorption. This work strongly supports the suggestion that the most suitable sounding frequencies for temperate glaciers are the lowest ones (e.g. Watts and England, 1976).

3.3 Summary

In this chapter the principles of electromagnetic propagation in ice were introduced. They were then applied to a number of situations found in radio echo sounding and in particular to Spitsbergen glaciers where the existence of water is likely. The effects of water at the bed, and within the ice, were investigated and shown to have a very significant influence on the received echo. The work presented in this chapter forms the basis for much of the discussion of RES data in Ch. 5. Prior to this analysis, however, it is necessary to have an understanding of the dielectric properties of ice. This will allow the integral in eqn. 3.21 to be satisfactorily evaluated and hence enable the derivation of RCs. The next chapter deals with this topic.

CHAPTER 4

CONDUCTION AND ABSORPTION IN ICE

4.1 Introduction

This chapter is divided into two sections. The first of these is a brief review of the theory of electrical conduction in ice 1h and related laboratory experiments. The second part is a discussion of the results of an experiment carried out to investigate the dielectric properties (specifically the high-frequency characteristics) of a sample of Spitsbergen ice. The electrical behaviour of natural ice has been catergorised into two groups—'polar' and 'temperate'—and it was hoped that the results of this experiment would give an insight as to which, if either, group best described Spitsbergen ice (whose thermal regime typically lies somewhere between these two extremes). The methodology and theory of the data reduction are presented in App. 2.

An extensive literature exists on the theory of conduction in ice and one of the most important advances was the development of a model based on the existence of four types of point defect that could be described by the laws of mass action. This theory was developed by Jaccard (1959) and reformulated later (Jaccard, 1964) in terms of the thermodynamics of irreversible processes. More recent work has suggested certain weaknesses in his theory which will be discussed below. We shall also consider some of the studies that have been made on doped and natural samples of ice, concentrating mainly on the work of Paren (1970, 1973), Fitzgerald and Paren (1975), Camplin and Glen (1973), Camplin *et al* (1978) and Granicher *et al* (1978). The only relevant studies to include measurements at MHz frequencies are those of Westphal (Jiracek, 1965), Johari and Charette (1975) and Johari (1976) and consequently these will be discussed in some detail. An extensive review of the electrical properties of ice, up to about 1973, may be found in Hobbs (1974).

4.2 Point Defects and Charge Carriers

The term 'defect' is used to refer to any imperfection in the regular, open hexagonal crystal structure of ice Ih. There are two categories of defect—extrinsic and intrinsic. The former includes imperfections in the 'mechanical' form of the lattice due to line defects which are of two basic types—edge dislocations and screw dislocations. The first of these is where there is an extra plane of molecules in one part of the crystal while the second is where the molecules are arranged in a helical fashion around the axis of a cylinder. Combinations of the two may also exist and can be formed by deformation or during crystal growth. Dislocations are responsible for plastic deformation in solids above their yield stress. A second type of extrinsic defect, unrelated to 'mechanical' imperfections, are impurities in the crystal lattice.

Intrinsic defects are point defects (i.e. associated with a single lattice site) that are in thermal equilibrium. Their concentration can be described by a Boltzmann function of the form: $N \exp(-E/KT)$ and varies exponentially with temperature. There are several types of intrinsic defect—Frenkel defects are vacant lattice sites (a vacancy) with an associated interstitial (a molecule not in the normal location) while a Schottky defect is simply a vacancy. Four more are thought to exist in ice and are believed to be responsible for its permittivity and conductivity. The first two are termed positive and negative ionic defects and are caused by the dissociation of a water molecule into its ionic components— OH_3^+ and OH^- . The second pair are called orientational or Bjerrum defects and arise from the rotation of a water molecule through 120° around one of its O-H...O axes, which leaves two H atoms for one O-O bond (a D defect) — O-H H-O — and none between another O-O bond (an L defect). Traditionally it was believed that to obtain a d.c. conductance both defects were involved in the transfer of charge. The ionic defects (IDs) enable a proton to move along an O-O bond while the Bjerrum defects (BDs) rotate it around the O atom to the next O-O bond. Von Hippel *et al* (1973) argue that perfectly pure ice is not a protonic semiconductor but is an insulator and that proton migration is restricted to external and internal grain boundaries only and that it is the BDs alone that are responsible for internal conduction. This hypothesis will be discussed later.

4.3 Jaccard's Theory of Electrical Conduction

Jaccard (1959, 1964) developed a theory which has been widely accepted as adequately describing the general principles involved in electrical conduction in ice and has reached a fairly advanced level of investigation and analysis. More recently certain aspects of his theory (in particular some of the assumptions used to develop the model) have been called into question (Von Hippel *et al*, 1973; Mogensen and Eldrup, 1978; Bilgram and Granicher, 1978; Johari and Whalley, 1981) and these will be discussed briefly below. Despite these limitations Jaccard's work has been successful in describing many of the observations that have been made. We shall quote some of his more general results (without deriving them) as they are useful in understanding the physical principles involved in conduction and will be referred to again in later sections.

The theory starts from the assumption that the principal dispersion in ice is due to four point defects (similar to those described above, although it is not necessary to know their exact form). Assuming that the concentration, n , of a given defect is in thermodynamic equilibrium and applying the principles of statistical mechanics, probability functions for the transfer of charge by a particular defect may be found. In his analysis Jaccard assumed that there was no recombination or association between the different categories of defect with other defects. Bilgram and Granicher (1974, 1978) discuss the possibility of interaction between point defects. They postulated the existence of a BD-ID aggregate and found that it explained certain properties of highly doped crystals. Another assumption made was that the crystal is 'perfect'. i.e. that it has no vacancies, dislocations, impurities etc. or if it does that their mobility and diffusion are zero. In 1959 this did not seem a particularly restrictive criterion as the vacancy concentration was believed to be about 10^{-4} that of BDs (Hobbs 1974) and consequently could be neglected. An investigation of the vacancy concentration in pure monocrystalline ice has been carried ^{out} by Mogensen and Eldrup (1978) using a technique known as positron annihilation. This relies on an injected positron becoming trapped by a 'hole' (vacancy or void) before it is annihilated and then measuring the photon emission when this does take place. They determined a much lower activation energy for the formation of vacancies, $0.26 < E_f < 0.35$ eV (compared with a value of 0.5 eV that had been previously accepted), and that the concentration at the melting point is in the region of parts per million (ppm). This is of a similar magnitude to the calculated number of intrinsic BDs. The question of how BDs might interact with vacancies had not been considered important because of their low concentration but if the conclusions

drawn from Mogensen and Eldrup's experiment are correct it now becomes of critical importance. They suggested that a vacancy-D defect aggregate could be an energetically favourable combination and that almost all the D defects would be in a bound state and consequently unable to contribute to the relaxation process. Indeed, before this work, the location of D defects had been the subject of extensive discussion. They also proposed that the high vacancy concentration could influence the location of impurities which would otherwise not easily fit into the lattice. The full implications of their findings have yet to be fully explored but must, if correct, throw into question the validity of assuming a 'perfect' crystal of non interacting defects.

We shall, nonetheless, quote here some of the more general results obtained by Jaccard which remain effectively unchanged by these findings although his evaluation of some of the constants involved may no longer be valid. One result that will remain the same is that the total high-frequency conductivity, σ_∞ , is a sum of the contributions from each defect:

$$\sigma_\infty = \sum_{i=1}^4 \sigma'_i \quad (4.1)$$

and that each σ'_i is described by-

$$\sigma'_i = Q_i e n_i \mu_i \quad (4.2)$$

where the subscript, i , runs from 1 to 4, Q_i = the effective charge on the i th type defect, e = charge on an electron, n_i = concentration and μ_i = the mobility. Note that the effective charges on the two orientational defects are required to be equal and opposite and similarly for the ionic defects (i.e. $Q_\pm = Q_+ = -Q_-$ and $Q_{DL} = Q_D = -Q_L$) and that according to Jaccard's theory $Q_\pm + Q_{DL} = 1$. Eqns. 4.1 and 4.2 are quite general and the difficulty only comes when it is necessary to assign values to Q_i and μ_i . For example, if Mogensen and Eldrup's suggestion about the location of D defects is correct then $\mu_D \approx 0$ so that $\sigma'_D \approx 0$. Camplin *et al* (1978) undertook an experiment to investigate the effects of HF doping on conduction and polarization and from their data attempted to deduce values for the parameters involved in Jaccard's theory. They considered three possible models for how extrinsic defect populations might depend on [HF] (square brackets denote concentrations so that, for example, $n_D \equiv [D]$) and used a least squares minimization procedure to obtain best fits to the parameters in the models. Good agreement was found for the value of effective charge on a BD of 0.438 (c.f. 0.43 from Jaccard's theory) but they found that $Q_\pm = 0.73$ whereas Jaccard requires $Q_\pm = 0.57$. Jaccard's analysis also predicts that at a transition temperature, T_m , (a property that is discussed in more detail

later) when the majority carriers change from one class of defect to another, the dispersion should vanish and the conductivity of the sample become independent of frequency. This has never been observed in experimental results and Camplin *et al* attribute this fact to their higher value of Q_{\pm} .

However, what remains unchanged by these arguments is the fact that σ_{∞} is a sum of the contributions from each type of defect and that the relative magnitudes of these components vary with temperature, crystal purity and perfection.

4.3.1 Relative importance of σ_{DL} and σ_{\pm}

In almost all experiments on the dielectric properties of ice the activation energy of σ_{∞} and τ is observed to change value at a transition temperature, T_m . Jaccard's theory predicts that this temperature represents the transition of majority carrier from ionic to Bjerrum defects and because these two classes of defect have different energies of formation and mobility the value of the activation energy, E_{∞} ,¹ changes. Paren (1973) tried to separate σ_{DL} from σ_{\pm} for samples of polar ice. He did this by assuming that because the conductivity of his ice sample from the temperate Mendenhall Glacier was so low, it was almost entirely due to σ_{DL} and by removing this value, for a given temperature, from the σ_{∞} of the polar sample the remainder would be due to σ_{\pm} . He found that, at temperatures above approximately 250 K, σ_{\pm} had a zero activation energy (i.e. was independent of temperature) and that T_m was about 260 K. For Spitsbergen ice, which is always warmer than this, his findings suggest that the majority carrier will always be the BDs unless the ice is very impure. It has been postulated more recently, however, that the BDs are always the majority carrier (von Hippel, 1971).

Classically (i.e. according to Jaccard's theory) every impurity in the lattice generates a specific number of extrinsic defects, of a well defined behaviour, whose concentrations obey the laws of mass action. Some success has been achieved in using this model to explain the effects of impurities on the conduction but concomitantly inconsistencies have been found. For example, Camplin *et al* (1978) obtained good agreement between theory and experiment for Q_{DL} and μ_L (at 218 K) and were able to find a satisfactory explanation for the high value of Q_{\pm} but found that the value of E_L , the activation for the mobility of L defects, was not compatible with that obtained by Jaccard.

¹ Unless otherwise stated, activation energies are those of the hf conductivity or the conductivity dispersion strength. The activation energies of the relaxation frequency are not considered in this chapter.

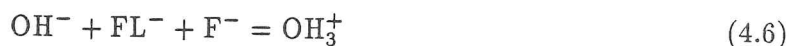
Von Hippel (1971) has suggested a completely different process of conduction which is gaining support. He proposes that the impurities in the lattice (present even in 'pure' samples) act as 'catalytic mills'. At an impurity defect site the transition probabilities are altered and the creation of ionic and Bjerrum defects is energetically 'cheaper'. Hence T_m marks the transition from extrinsic to intrinsic defects as the majority carriers. In this case σ_∞ would be due solely to the BDs, with the IDs playing no part. One of the characteristics of T_m is that, even for pure ice, its value can vary widely (Paren, 1970) and although it is rarely seen to occur below 210 K (Johari and Whalley, 1981), it can lie anywhere between this and ≈ 250 K. Second, if $\sigma_{DL} = \sigma_\pm$ at T_m then $\sigma_o = \sigma_\infty$ and the dispersion must vanish but as previously explained this has never been observed. Johari and Jones (1975) and Johari and Whalley (1981) find that their data for H_2O and D_2O ice are incompatible with the idea of a change in the type of majority carrier from ID to BD and put forward an argument similar to Von Hippel's to explain their results. The situation has not been completely resolved and despite the more recent hypotheses suggested, we shall examine some of the classical ideas about the properties of impurities in the lattice and will begin by considering one of the most commonly used dopants—HF.

4.3.2 HF doping

HF is a particularly useful doping agent because the fluorine atom is a similar size to oxygen and this means that it can be substituted into the crystal lattice with minimal distortion or energy requirements. This allows a better theoretical understanding of its effects to be obtained. It is clear that it must be an L enhancing chemical but it can also introduce ionic defects and it will be useful to investigate the possible reactions that can take place. Following the procedure of Kroger (1964), we begin with the HFL complex which may dissociate in the following ways:



where the W s are the energies of reaction. The condition of neutrality requires:



the fluorine balance requires



and the D, L balance requires

$$L = HF + F^- + D. \quad (4.8)$$

Kroger observes that $W_{OF} \approx 0$ but that $W_{IF} \sim W_{OI} \neq 0$ so that the HFL complex will be almost completely dissociated into HF and L but that the ionic dissociation will be far from complete and temperature dependent. It is, therefore, possible to make the approximation, for high [HF], that $[L] \approx [HF]$ and that this is the overriding term in σ_∞ , i.e. $\sigma_\infty \approx \mu_L Q_L e [HF]$. Hence by determining how σ_∞ varies with $[HF]$ the product $\mu_L Q_L$ can be determined.

4.3.3 Other Impurities

It is not possible to make generalisations about the effects of impurities on the conduction. HF and HCl have a more "well defined" behaviour than other salts that have not been studied in such detail. Second, it has been suggested by Bilgram (1970) that below a concentration of $70 \mu\text{M}$, [F] in the ice remains constant at $1 \mu\text{M}$ because the remaining HF is located at the grain boundaries. Above the former value, the F concentration rises linearly with doping concentration, to a limit of 2×10^{-4} M. Von Hippel *et al* (1971) dispute some of this, explaining Bilgram's results by the use of electrodes that were insensitive to fluorine concentrations below $1 \mu\text{M}$ (from the manufacturers specification). Although Bilgram's conclusion may not have been correct Wolff and Paren (1984) give good evidence for believing that impurities (particularly acids) are concentrated at grain boundaries. They suggest that the acidic impurities in natural ice (typical concentrations of $2.6 \mu\text{M}$) are sufficient to exceed a small but finite, temperature dependent solubility limit so that at above $\approx -70^\circ\text{C}$ they will be present in saturated water veins at grain boundaries.

Third, different impurities can produce different types of defect. So far we have only considered HF which creates L defects but there also chemicals, such as NH_5CO_3 or NH_4Cl , that can produce D defects. Hence, even if the number of defects created by different impurities were the same, their influence on σ_∞ will not be. Indeed, given that the product $[L].[D] = \text{a constant}$ (Kroger, 1964; Camplin *et al*, 1978), and that if a large proportion of the D defects are bound in vacancies (Mogensen and Eldrup, 1978) then it is conceivable that σ_∞ could decrease if the activation energy for ionic defects is high. Thus the most useful approach, for radio echo sounding purposes, in elucidating the effects of impurities is probably an empirical one.

A study has been carried out by Gross *et al* (1978) on the effects of a number of 'proton enhancing' solutes (HCl, HF, NaCl, KF, NH_4F) and 'proton suppressing' ones NH_4OH , NH_4Cl ,

NH_5CO_3 , NaHCO_3) in the temperature range -5 to -90°C , for frequencies between 20 Hz and 100 kHz. Teflon blocking electrodes were used and the true ice parameters extracted from linearized plots of the Debye equations. They found that all solutes, excepting NaHCO_3 , NH_4OH and CO_2 , increased σ_∞ (the three mentioned had no effect) despite the fact that the proton depressing agents considerably reduced σ_0 . They also found that ice doped with $3 \mu\text{M}$ HCl had a dispersion strength greater than that doped with $7 \mu\text{M}$ HCl, a result they were unable to explain. The static conductivities for the two samples were very similar so that σ_∞ was also greater.

These workers tentatively classified the solutes as either proton-enhancing or proton-suppressing, subdividing each of these into interacting and non interacting groups. They found that enhancing agents greatly increased σ_0 and that the alkali halides and their acids interacted with the lattice polarization and so increased σ_∞ . They suggested that this may be because they introduce L defects or lower the energy of formation of these defects (a view supported by Von Hippel, 1970).

It is worth recalling the type and concentration of impurity that is typically found in Spitsbergen. Yevseyev and Korzun (1985) obtained a total dissolved ion concentration, from a core on Vestfonna, of 4–6 mg/l. Semb (from shallow snow samples taken over the whole archipelago) quotes values of between 50 and 250 μM depending on depth. The most predominant salt is NaCl not surprisingly considering the marine setting of Svalbard and as expected, the highest values are to be found close to the coast with a maximum of 2.12 mg Na/l ($\equiv 92 \mu\text{M}$). A 23 m core retrieved from Skobreen (section 4.7) gave a mean value of 20 μM (R. Mulvaney, personal communication) although a number of individual values were considerably higher than this (the maximum was found at a depth of 2.4 m and was 76 μM).

Perhaps of greater relevance is the surface distribution of H^+ ions, shown in Fig. 4.1, as these indicate, more directly, the influence of impurities on the ionic defect concentration. As pointed out by Gross *et al*, the extrinsic ion concentration has the greatest influence on σ_0 but their presence will also affect the dispersion strength (Gross *et al*, 1978). The most striking feature of Fig. 4.1 is the large variation in the values (a factor of 40 between the lowest and highest) and that there is a $[\text{H}^+]$ gradient moving from east to west which seems to correlate reasonably well with the excess $[\text{SO}_4]$ gradient. In section 5.2 evidence will be given for believing that there are marked differences in the bulk ice conductivity between Nordaustlandet and glaciers in western Spitsbergen, possibly due to the different thermal regime of the ice. It

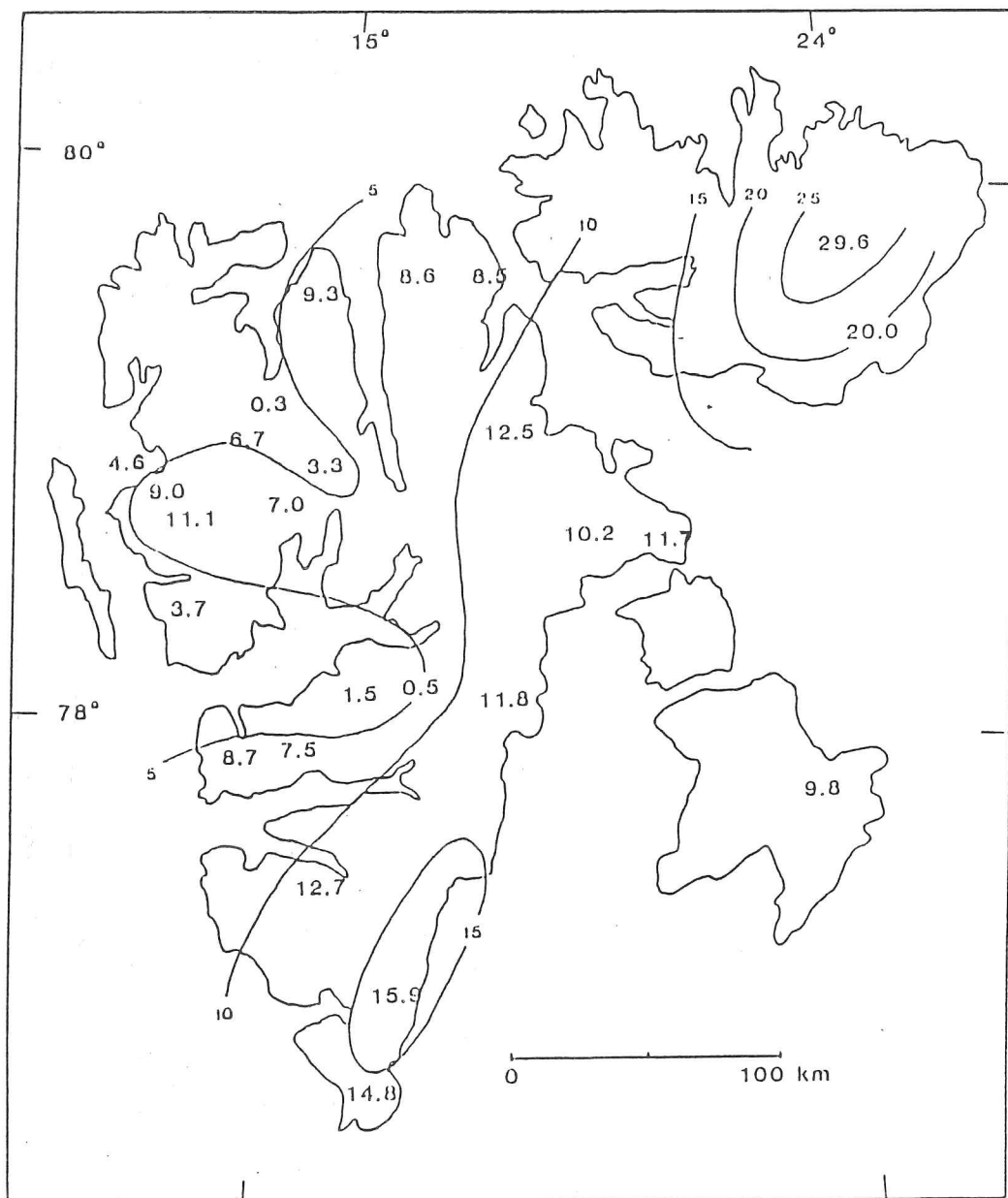


Fig. 4.1 H^+ ion concentrations (μM) in snow samples from Svalbard (source Semb et al, 1984).

is interesting to consider, however, how great an influence the $[H^+]$ gradient might have. The combination of flushing out of solutes, in the warmer glaciers, and the fact that these glaciers have a lower impurity concentration might explain the differences observed. Using eqn. 2.184 of Hobbs (1974) (for intrinsically pure ice) it is possible to estimate n_L and at 0°C a value of $13 \mu\text{M}$ was obtained. The maximum $[H^+]$ obtained by Semb was $29.6 \mu\text{M}$ which is approximately two times the intrinsic BD concentration. From the discussion of Wolff and Paren (1984), it would seem probable that much of the acids would be located at grain boundaries in saturated solutions. They deduce that, for an overall H_2SO_4 concentration of $1 \mu\text{M}$ at a temperature of -10°C , the dc conductivity is $5.32 \mu\text{S m}^{-1}$ and at higher temperatures this will be greater. If the H^+ ions are contained within the crystal lattice then eqn. 3.35 (suitable for ice at 0°C) can be used to give an estimate of $\Delta\sigma \cdot \Delta[H^+]$, between Nordaustlandet and western Spitsbergen, typically lies in the range $10\text{--}20 \mu\text{M}$. These values imply $\Delta\sigma = 18\text{--}36 \mu\text{S m}^{-1}$. The difference in absorption between temperate ice in western Spitsbergen and that in Nordaustlandet was found to be of the order of $1 \text{ dB}/100\text{m}$ (section 5.2) which is equivalent to $\Delta\sigma = 11 \mu\text{S m}^{-1}$. Thus, it can be seen that the $[H^+]$ gradient **alone** could explain the marked differences in absorption noted in Ch. 5.

4.4 Polar versus Temperate Ice

Cold, or 'polar', ice (temperatures below approximately -10°C) has a markedly different dielectric response to that of temperate or laboratory grown pure ice (Glen and Paren, 1975). The first evidence of this came from resistivity surveys (Röthlisberger, 1967) on cold glaciers where values of σ_0 were found to be up to 1000 times greater than equivalent measurements made on temperate ice. Secondly, unlike the fairly consistent values for σ_∞ (at 0°C) for laboratory and temperate samples (Glen and Paren, 1975), the values for polar specimens (at this temperature) seem to be more variable (Reynolds, 1985).

Permeable polar ice seems to possess slightly higher conductivities and values as high as $2 \times 10^{-4} \text{ S m}^{-1}$ (extrapolated from -10°C to 0°C) have been recorded (Maeno, 1973) for a sample of density $< 820 \text{ kg m}^{-3}$ although it has been suggested that this high value could be due to greater contamination (due to the higher porosity of the ice) during drilling (Glen and Paren, 1975).

The activation energy of the hf conductivity, E_∞ , of 'polar' ice is considerably less than

for 'pure' ice and is typically about 0.23 eV (below -10°C) (Reynolds, 1985). Two samples from a Byrd Station core (155 m and 1424 m depth) have been studied by Fitzgerald and Paren (1975) in the temperature range -6 to -60°C and between 60 Hz and 10 kHz. The dielectric response was observed to be markedly different to that of 'pure' ice, more closely resembling the behaviour of samples doped with $\approx 10 \mu\text{M}$ HF. They found, however, that on melting and refreezing, its characteristics had altered to those akin to samples doped with much lower concentrations ($\approx 0.5 \mu\text{M}$) and an activation energy closer to that of 'pure' ice. Reynolds and Paren (1980) have suggested that the differences between 'polar' and temperate ice (such as observed by Fitzgerald and Paren (1975)) may be due to the complete removal of meltwater and recrystallisation due to stresses—two processes which are far more extensive in the latter type of ice mass.

In the next section experiments are described that have been carried out on both 'pure' laboratory-grown and 'polar' samples at radar frequencies.

4.5 Radar Absorption in Ice

4.5.1 Laboratory Results

There have been three relevant studies made at MHz frequencies and the results will be considered below. Ambiguities exist between the findings of these experiments and although it is not possible to completely resolve them, certain useful conclusions may be drawn.

Johari and Charette (1975) published measurements made on 19 samples of polycrystalline and 5 samples of monocrystalline ice in the temperature range -0.2 to -25°C for two frequencies—35 and 60 MHz. The polycrystalline samples were prepared from double distilled de-ionized water which was evacuated in a glass container to remove the dissolved air. The water was then frozen in the coaxial cell at a temperature of -5°C and to prevent cracking the ice was subjected to a pressure of $\approx 5 \times 10^6$ Pa. Examination of the ice after the measurements showed no signs of air bubbles. The average crystal size was found to be ≈ 1 mm. The single crystals were prepared with equal care although it was necessary to machine them into a cylindrical shape in a lathe and it is conceivable that contamination was possible during this procedure. Both type of specimen had very similar hf properties, however.

The results of their measurements, at 60 MHz, are plotted on an Arrhenius diagram ($\log \sigma_{\infty}$ versus $1/T$) in Fig 4.2. There are a number of features that are worth considering. The first

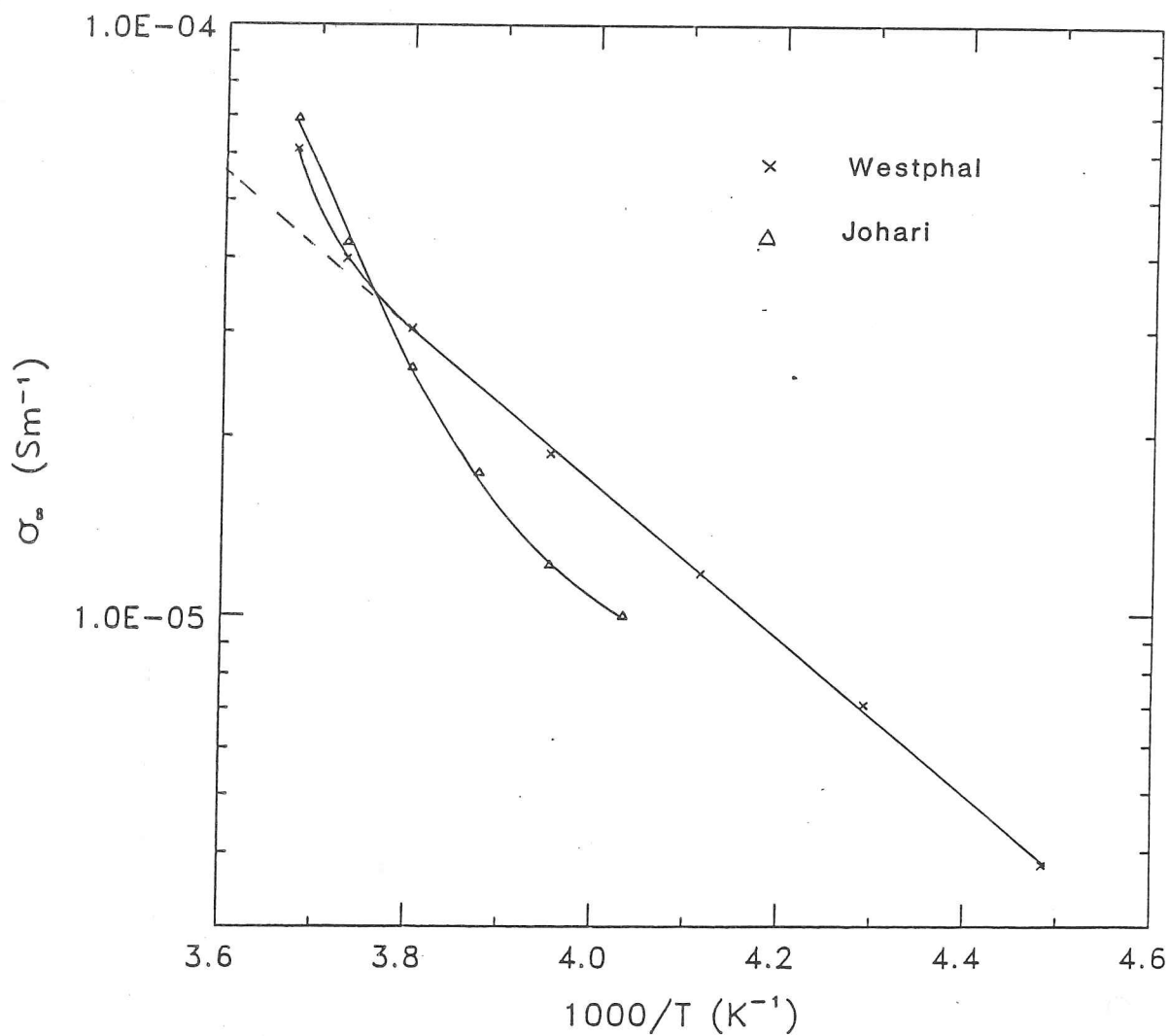


Fig. 4.2. Arrhenius diagram of Westphal's Tuto Tunnel sample at 150 MHz and Johari and Charette's laboratory grown ice at 60 MHz. Westphal's data have been corrected to a density of 920 kg m^{-3} using the Looyenga mixture formula. The crossover temperature is at $\approx -7^\circ \text{C}$.

is that extrapolation of the data to 0°C leads to a value of $70 \mu\text{S m}^{-1}$ for σ_∞ . At -1°C their data are $\approx 10 \mu\text{S m}^{-1}$ greater than those of Westphal (discussed shortly) which were natural polar samples. Second, below $\approx -7^\circ\text{C}$ their data has a lower conductivity than Westphal's. Further, it should be noted that the transition temperature of Johari and Charette's samples is in the region of 253 K, which is surprisingly high for pure ice samples (c.f. Camplin and Glen's (1973) pure ice sample, S10.11 where $T_m < -45^\circ\text{C}$ and where, even some of their HF doped samples had lower values). Whichever mechanism is taken to be the cause of T_m , it seems likely that a higher value suggests a larger number and/or mobility of extrinsic defects. It therefore seems possible that Johari and Charette's samples may have been relatively impure in comparison to Westphal's two identical 'polar' specimens. Indeed, double distilled, de-ionized water can have a considerably higher impurity concentration than 'polar' ice (J.C. Moore, personal communication).

Johari (1976) carried out a further investigation of his single-crystal samples by taking readings between 0.5 and 100 MHz and observed an hf dispersion with a relaxation frequency of 5.3 MHz and a strength, $\Delta\epsilon$, of 0.08 ($\equiv \Delta\sigma = 23.6 \mu\text{S m}^{-1}$, assuming that the dispersion obeys exactly the Debye equations) at a temperature of 268 K (-5°C). From the previous discussion it would seem possible that this dispersion may be due to the presence of impurities—a view supported by von Hippel *et al* (1972) for their hf dispersion. Johari (1976) suggests that it is "probably due to the orientation of water molecules at the grain boundaries or at the imperfection sites" but gives little evidence for this hypothesis.

The results of Westphal's data (Jiracek, 1965) are somewhat different. His measurements were made on four samples of polar land ice (and one sample of sea ice) taken from different sites in the Arctic and Antarctic. He measured the dielectric properties in the temperature range -1 to -60°C . His two higher density samples (898 kg m^{-3} and 902 kg m^{-3}) from Ward Hunt Ice Shelf (glacial ice) and the Tuto Tunnel in Greenland respectively, gave identical results. They are illustrated in Fig 4.2 against those of Johari and Charette. The only other complete dataset was for a sample from Little America V, Antarctica, which gave (when corrected for density differences) conductivities some 40% greater than the former two samples (σ_∞ at -1°C was $98 \mu\text{S m}^{-1}$ compared with $59 \mu\text{S m}^{-1}$ for the Tuto Tunnel and Ward Hunt Ice Shelf samples). The data most commonly used, however, are those from his two Arctic samples and it is these that will be discussed below.

Between -10 and -50°C the data are well described by a single activation energy of $0.259 \pm$

0.004 eV with an extrapolated melting point conductivity of $45 \mu\text{S m}^{-1}$. Above -10°C the (negative) gradient of the Arrhenius curve, begins to increase. Paren (1970) made measurements on some 13 samples of 'polar' ice from Greenland and the mean conductivity of his Camp Century samples at 100 kHz agree well with Westphal's two identical specimens measured at 150 MHz (down to a temperature of $\approx -50^\circ\text{C}$) (Evans and Smith, 1969). It can also be seen (for #357 from Camp Century) that, at a frequency of 10 kHz the conductivity appears to have stopped increasing with frequency, for temperatures up to $\approx -20^\circ\text{C}$. Paren derived, solid ice, values of conductivity and permittivity, at 0°C by linear extrapolation of Arrhenius plots for data below -10°C (which are therefore an underestimate of the true σ_∞ at 0°C) and observed a large spread in conductivities. He obtained a maximum value of $71 \mu\text{S m}^{-1}$, a minimum of $35 \mu\text{S m}^{-1}$ and a mean value of $45 \mu\text{S m}^{-1}$. The findings discussed above seem to suggest that Paren's (and by inference Westphal's) samples did not possess an hf dispersion as found by Johari. Hence it would seem that his specimens have an anomalous behaviour that may have been due to impurities in the ice.

However, an experiment that seems to support the applicability of both Westphal's and Johari and Charette's data, for 'polar' ice, has been carried out by Millar (1981). The total absorption was measured above a subglacial lake near Vostok Station, in central Antarctica, using RES data. A mean value of 86.8 dB for the two-way dielectric absorption was obtained. This was compared with theoretical predictions based on the aforementioned dielectric data and borehole temperature measurements. Excellent agreement was obtained for both dielectric datasets. This is a surprising result, considering the differences between the two datasets and it is difficult to explain why they should give the same total two-way absorption to within 0.7 dB (87.1 dB compared with 86.4 (Millar, 1981)). The ice thickness at Vostok Station is 3770 m. The surface temperature and basal temperatures used in Millar's calculation were -57.2 and -4.9°C respectively. A 0.7 dB difference in the two-way absorption, for 3770 m of ice, implies a mean difference in the dielectric data of only 1×10^{-4} dB/100 m. Millar used a basal temperature gradient of $0.018^\circ\text{C m}^{-1}$ which implies that only about 110 m of ice are above the crossover temperature between Johari's and Westphal's data. Hence it is difficult to see how both datasets could give the same results. Second, given the uncertainty of the temperature profile (at depth) at Vostok (Robin, 1985), the conclusions drawn by Millar must be called into question. For ice close to the melting point a significant disparity must occur, using the two datasets, because of the substantial differences between them at high temperatures. Hence

ambiguities in the applicability of dielectric data to different ice masses still exist.

From the foregoing discussion it has to be concluded that care must be used when applying laboratory measurements to *in situ* RES data and that significant differences may exist between ice masses possessing different thermal and hydrological regimes. In the next section the dielectric properties of samples of ice from Skobreen (Fig. 1.9), in central Spitsbergen, are investigated to establish which, if either, category they fall into.

4.6 Dielectric measurements on a Spitsbergen Core

4.6.1 Introduction

In the spring of 1985 a ground based RES survey was carried out on several glaciers near the mining settlement of Svea (Ch. 2). One year after this work, members of the SPRI and the University of Bern returned to one of these glaciers, Skobreen, to collect a core for the study of environmental glaciochemistry (i.e. determination of oxygen isotope, electrolytic conductivity, acidity, deuterium content, chemical composition and stratigraphic measurements). Concomitantly, two 10 cm sections of the core were saved with the intention of determining their electrical properties.

The dielectric properties of a Spitsbergen ice sample have not previously been investigated and (following the discussion in section 4.4 on the differences between 'polar' and 'temperate' ice) it was hoped to investigate how these properties related to those of other natural ice samples from different geographical and thermal environments. The primary aim, however, was to determine the limiting high-frequency response and to compare this with the empirical results of analyses on the *in situ* RES absorption discussed in the next chapter.

The conductivity and permittivity were measured for approximately 18 frequencies between 20 Hz and 100 kHz at ten temperatures in the range -2.5 to -44.0°C .

4.7 Description of the Core

The drilling site was located at an altitude of 630 m a.s.l., approximately 200 m in elevation above the estimated equilibrium line. Although drilling was to have been to 110 m an equipment failure resulted in only 23 m of core being retrieved. The estimated time span of this core is 27–28 years, assuming an average accumulation rate of 0.7–0.8 m/yr ice-equivalent (Simoes, personal communication).

The continuous ice phase was reached at a depth of 16.4 m and the first sample (#145) was taken from just below this level. The second section (#209) came from the lower part of the core at a depth of 22.8 m. (Note—samples were taken every 10 cm beginning at a depth of 2.0 m, so that #145 was the section at a depth of 16.4–16.5 m etc.) Their densities were found to be $863 \pm 2 \text{ kg m}^{-3}$ and $885 \pm 2 \text{ kg m}^{-3}$ respectively, which implies air bubble volumes of 6% and 4%. (Note, the densities of the ice used in the dielectric experiments were not measured directly, to prevent contamination, and the values quoted above are for specimens which were displaced from these by approximately 5 cm. This introduces a systematic error into the assumed densities estimated, from the typical local density variations, as $\pm 10 \text{ kg m}^{-3}$). One section was cut from #145 and another from #209. A third was taken from the other end of #209 to act as a “control” (i.e. to see if any differences between the two existed which might have been caused by contamination during sample preparation). The density–depth profile is shown in Fig. 4.3 a). Also shown, in Fig. 4.3 b) is the electrolytic conductivity measured at 21°C and in c) to e), the concentrations of Cl^- , NO_3^- and SO_4^{2-} for 36 samples down core. These were obtained by R. Mulvaney of the British Antarctic Survey using an ion chromatograph. Data are accurate to 10%. The values can be seen to be broadly similar to previous analyses on Svalbard ice (section 1.5.4) but at certain depths the concentrations are considerably greater than the average. Furthermore, there does not seem to be an obvious correlation between the different species. For example, sample 5 has a [Cl] 3.8 times the average yet the [NO₃] and [SO₄] are very similar. This section, however, comes from only 2.5 m below the surface and for the two other specimens with a high [Cl], all three species are larger. Electrolytic conductivity for #145 was $2.9 \times 10^{-4} \text{ S m}^{-1}$ and for #209 $3.2 \times 10^{-4} \text{ S m}^{-1}$. These values are similar to those obtained by Paren (1970) for his ‘polar’ specimens but are greater than that of his Mendenhall Glacier ice.

Thin sections were taken from both samples #145 and #209 and are illustrated in Fig. 4.4. They have been digitized to enable calculation of the ‘average’ crystal dimensions. For

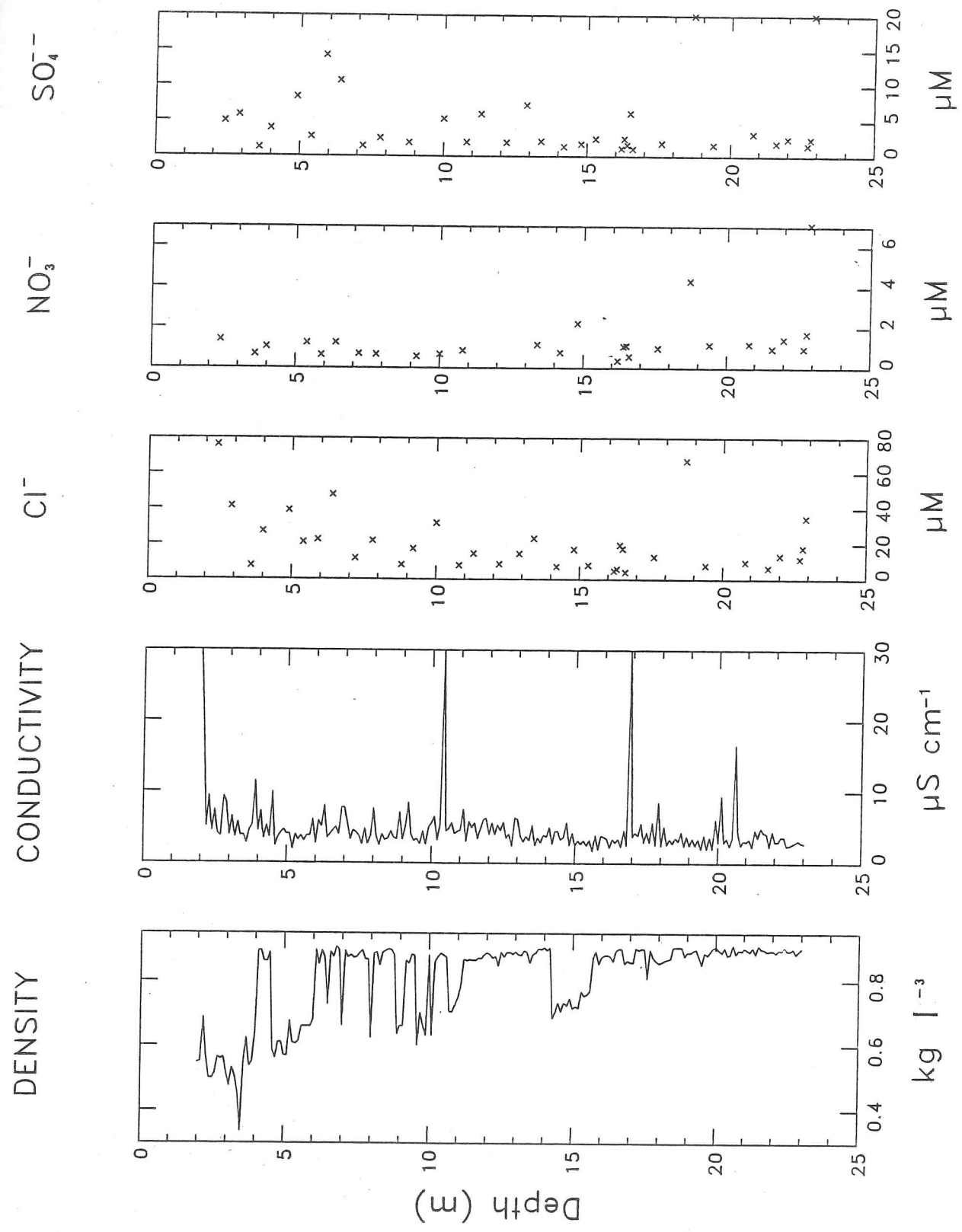


Fig. 4.3 Physical and chemical properties down the Skobreen core. Density and electrolytic conductivity data from J.C. Simoes (personal communication). Anion data from R. Mulvaney (personal communication). Note that several of the NO_3^- concentrations were below the detection threshold ($0.08 \mu\text{M}$). Two SO_4^{2-} concentrations were off scale ($>20 \mu\text{M}$). Electrolytic conductivities $> 10 \mu\text{S cm}^{-1}$ were believed to be due to contamination during sample preparation.

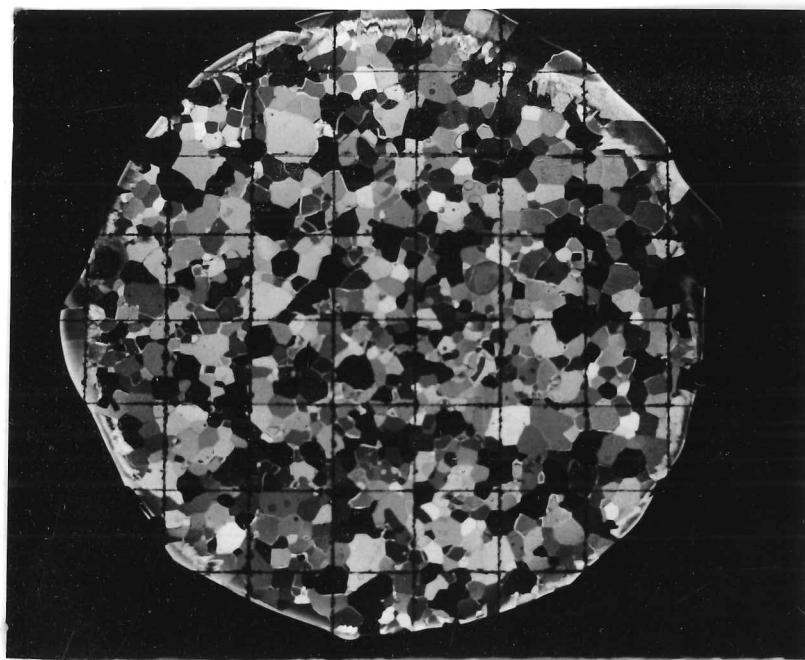


Fig. 4.4 a) Thin section from #145. The parallel lines are 10 mm apart.

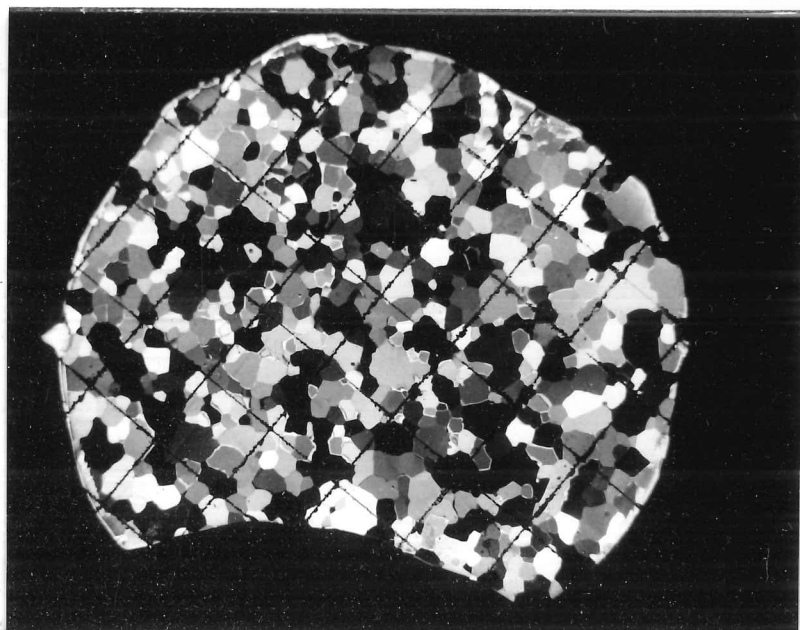


Fig 4.4 b) Thin section from #209.

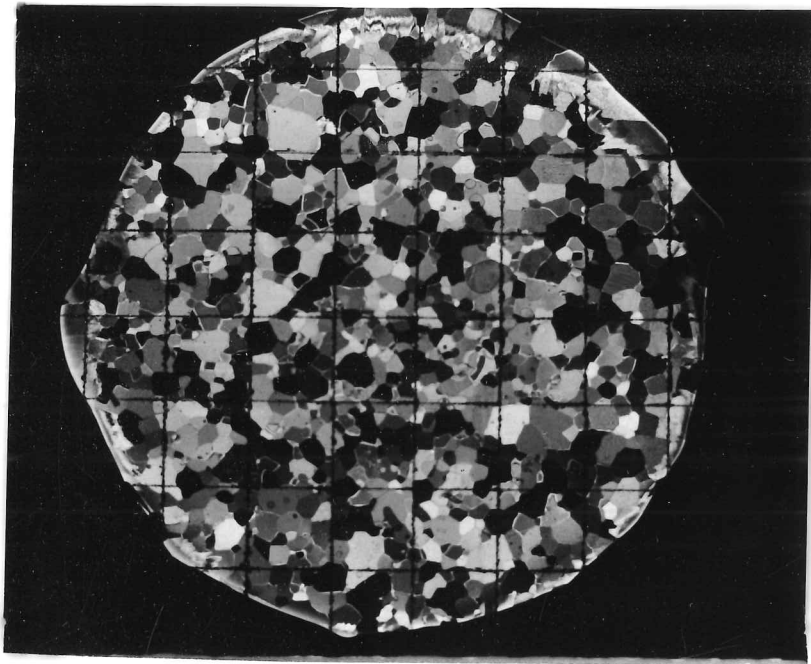


Fig. 4.4 a) Thin section from #145. The parallel lines are 10 mm apart.

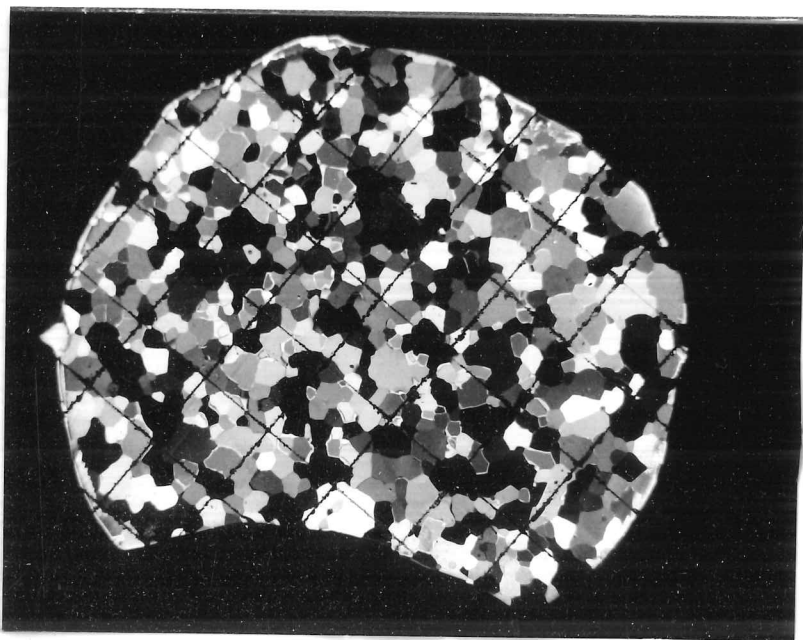


Fig 4.4 b) Thin section from #209.

#145 the mean crystal area and diameter were $9.29 \pm 9.38 \text{ mm}^2$ and $2.72 \pm 1.42 \text{ mm}$ respectively. For #209 they were $13.39 \pm 14.52 \text{ mm}^2$ and $3.035 \pm 1.76 \text{ mm}$ (Simoes, personal communication). The numbers after the \pm are the standard deviations of the mean.

4.8 Results

4.8.1 Introduction

Dielectric data can be expressed in a number of different ways (e.g. Gränicher, 1969). The most useful representation depends upon the nature of the data and the parameters that are wished to be determined. Cole-Cole plots are helpful in determining the hf permittivity, ϵ_∞ , and relaxation frequency, f_r (if σ_o is relatively small). If a sufficiently accurate estimate of σ_o is available then this component can be eliminated from ϵ'' . This should remove the low frequency tail on the plot, which can prevent a maximum in ϵ'' if $\sigma_o > \sigma_\infty / 9$.

It is also possible to deduce ϵ_∞ from another type of plot. Typical values of f_r for the main Debye dispersion (which will be referred to as spectrum 2, for reasons that will be explained shortly) lie in the approximate range 5 to 30 kHz, at 0°C (Reynolds, 1985). Thus if no higher frequency dispersions are present, then ϵ' and σ' , at 100 kHz, should be close to their hf limiting values. When $\omega^2\tau^2 \gg 1$ (i.e. $\omega^2 \gg \tau^{-2}$), $\epsilon' \approx \epsilon_\infty + \Delta\epsilon/(\omega^2\tau^2)$. Hence by plotting ϵ' vs. $1/f^2$ for values of $f > \tau^{-1}$ a linear relationship should be obtained, with the intercept on the y axis (ϵ') determining ϵ_∞ . This procedure produced some unexpected results, giving the first indication that an hf dispersion might be present. First, it was observed that, at the lowest temperatures (up to $\approx -15^\circ\text{C}$) the data were not obeying a linear relationship, even for frequencies in excess of 50 kHz. At -44.0°C the main Debye relaxation frequency, however, is in the range 0.8 to 15 kHz. ² Second, data for the highest temperatures (-8.2°C or above) gave excellent linear fits. The derived values of ϵ_∞ are plotted against temperature in Fig. 4.5. The large increases in ϵ_∞ above a temperature of -11°C cannot represent the true values of ϵ_∞ and suggest the presence of an hf dispersion which, above this temperature, has a relaxation frequency too high to allow the dispersion to be satisfactorily resolved at 100 kHz. Von Hippel *et al* (1972) observed such a dispersion in samples of both single and polycrystalline ice. At

² For these temperatures the curve was extrapolated back to the intercept on the ϵ' axis which inevitably produces a level of uncertainty to the values obtained. Independent estimates from Cole-Cole plots, however, gave the same results to within 6%, suggesting no significant loss in accuracy due to non linearity.

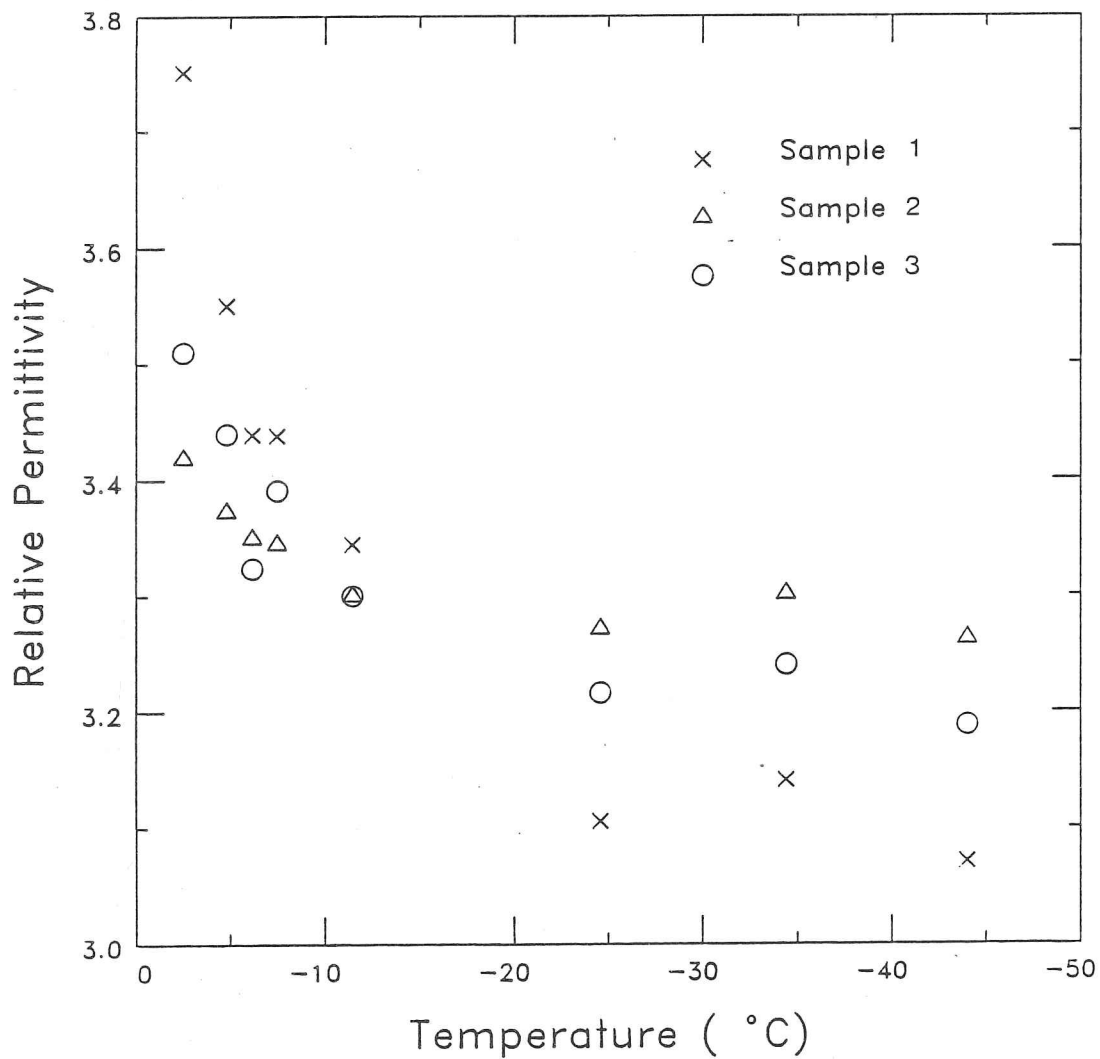
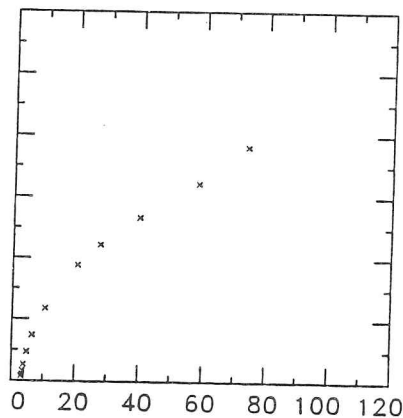
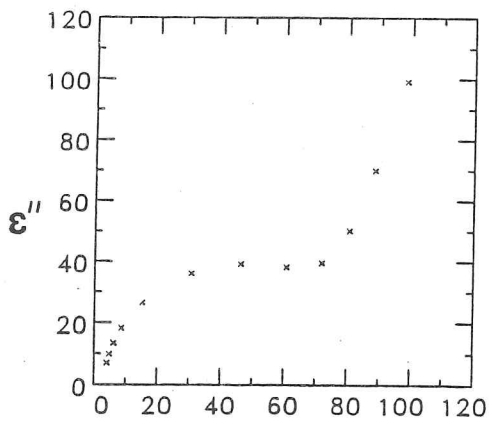
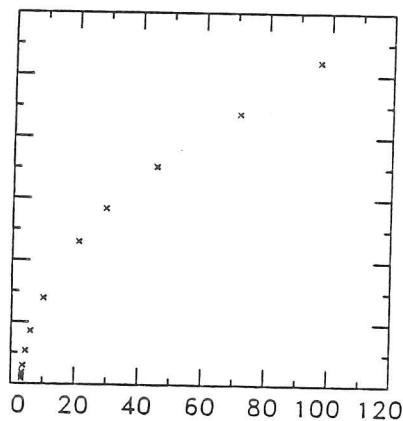
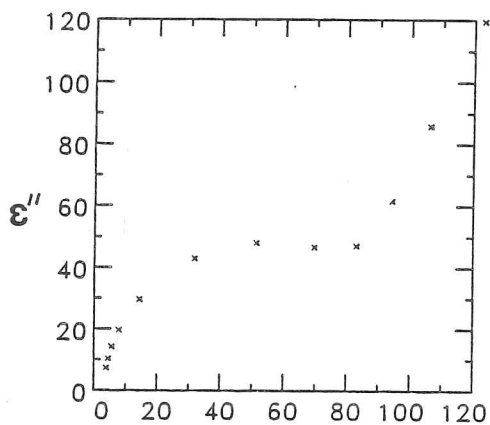


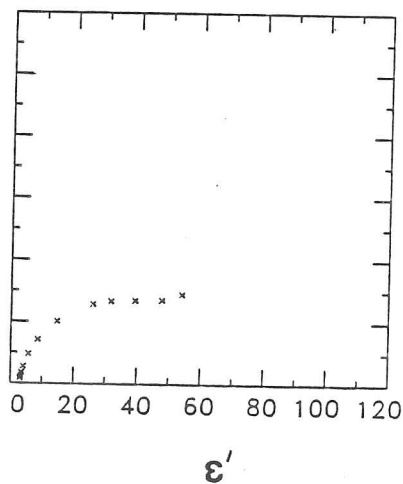
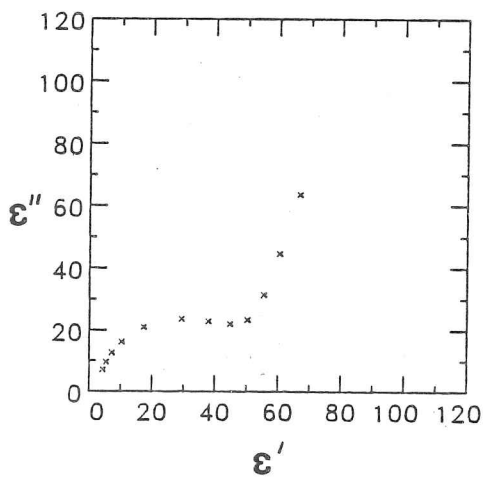
Fig. 4.5 High frequency relative permittivity extrapolated from plots of $1/f^2$ vs. ϵ' . Values have not been transposed to the solid ice equivalents and are those of the samples.



Sample 2



Sample 1



a)

b)

Fig. 4.6 Cole-Cole plots at two temperatures; a) $-2.5\text{ }^\circ\text{C}$,
 b) $-24.6\text{ }^\circ\text{C}$.

-45°C they obtained, $f_r = 18$ kHz and $E_{\infty} = 0.21$ eV so that at 0°C $f_r = 106$ kHz. They observed that the relaxation frequency of this dispersion (spectrum 1 in their terminology) was sensitive to crystal imperfections, rising by a factor of ≈ 5 for rapidly grown polycrystals compared with the single crystal data. It will be suggested shortly that the hf dispersion present in the Spitsbergen samples (denoted spectrum 3) has a number of properties similar to those of Von Hippel's spectrum 1.

A preliminary indication of the influence of spectrum 3 on the **conductivities** can be obtained by plotting a logarithmic graph of σ' against frequency. In the absence of an hf dispersion, the gradient of the curve, above f_{r2} , should tend to zero.³ This is shown clearly by Paren's Mendenhall Glacier ice (Fig. 4.1 Paren, 1970). Fig. 4.7 displays the data for the three Spitsbergen samples. From these plots it is immediately apparent that the relaxation frequencies of spectrum 2 are somewhat greater than for Paren's Mendenhall sample (i) but less than, for example, his 'polar' specimen from Camp Century (Fig. 5.6, Paren, 1970). It can also be seen that, even at 100 kHz, σ' , for the lower temperature data, is still increasing—a property not visible in either Paren's temperate or 'polar' samples. The relatively constant conductivity, above f_{r2} , for the higher temperature data, is due to spectrum 3 not having been excited. A further feature of Fig. 4.7 is the surprising lack of temperature dependence of σ' (above -35°C), in the approximate frequency range 0.5 to 5 kHz.

The preceding analyses have indicated some of the more general properties of the data but to obtain accurate values for the relaxation frequencies, hf conductivities and E_{∞} , a more rigorous approach is necessary.

³ subscripts following a variable refer to the spectrum, subscripts preceding a variable refer to the sample number. e.g. ${}_3\Delta\sigma_2$ is the dispersion strength of spectrum 2 for sample 3.

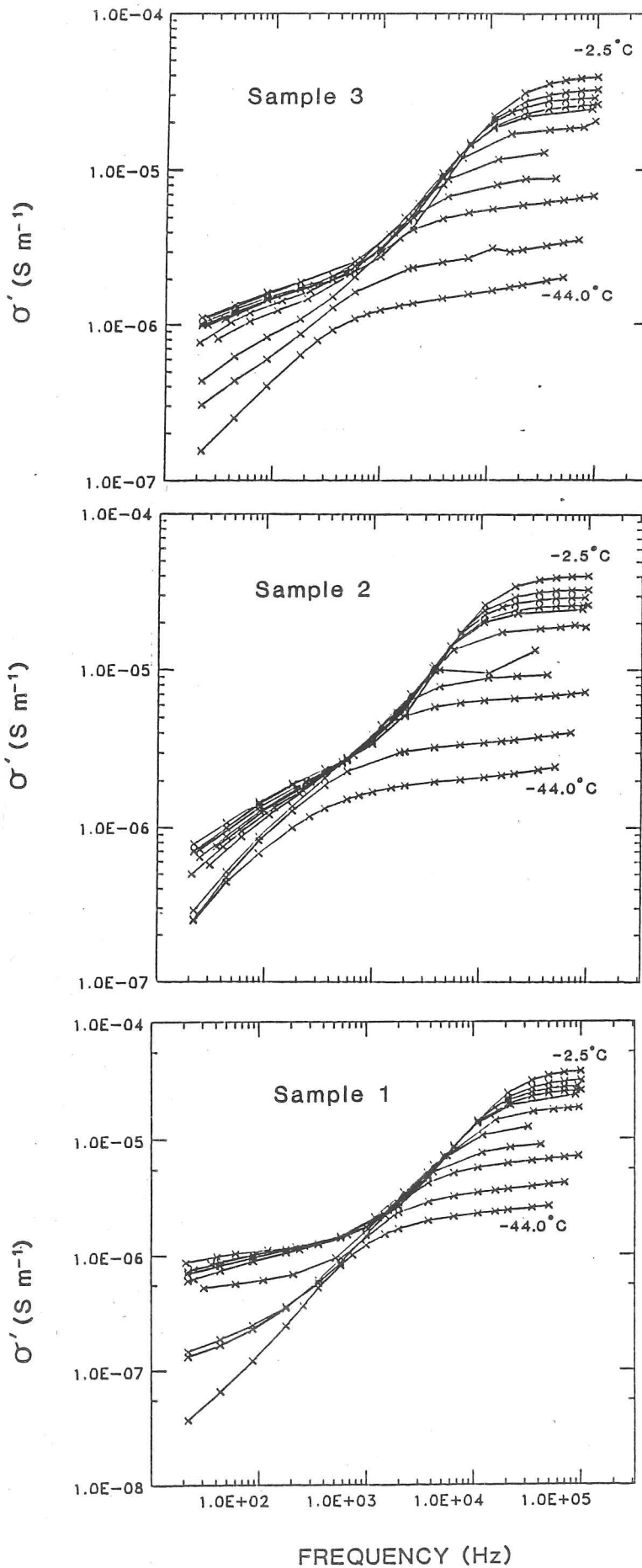


Fig. 4.7 Logarithmic plot of conductivity vs. frequency at all temperatures. The similarity in the conductivities between ≈ 1 and 10 kHz, at different temperatures, is particularly noticeable for sample 1.

4.8.2 Modified Complex Conductivities

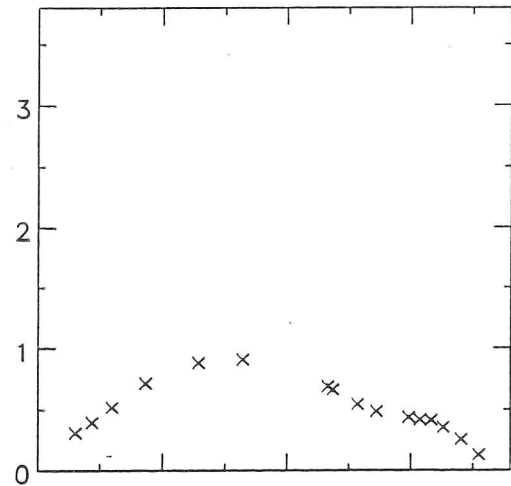
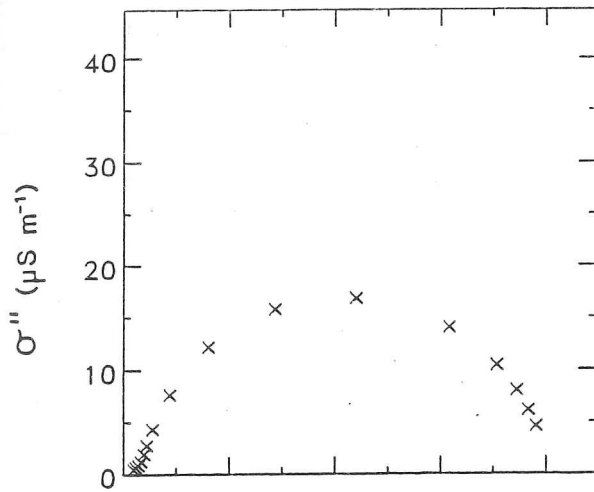
It has been shown that the dielectric properties of the Spitsbergen samples are not well described by a single Debye dispersion and that only limited information can be extracted from Cole–Cole plots. A more transparent representation of the data was found to be in terms of the modified complex conductivity, defined as:

$$\sigma_m^* = \sigma^* - i\omega\epsilon_0\epsilon_\infty. \quad (4.9)$$

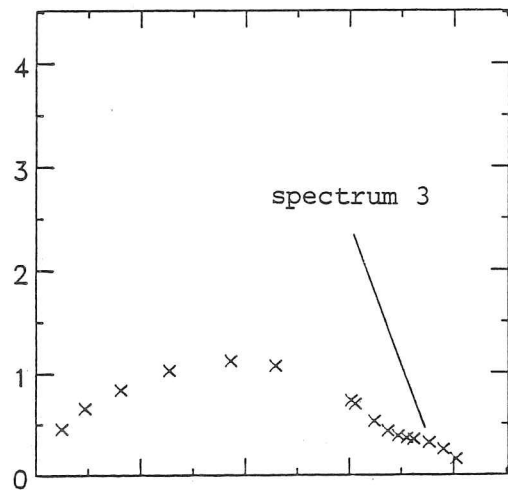
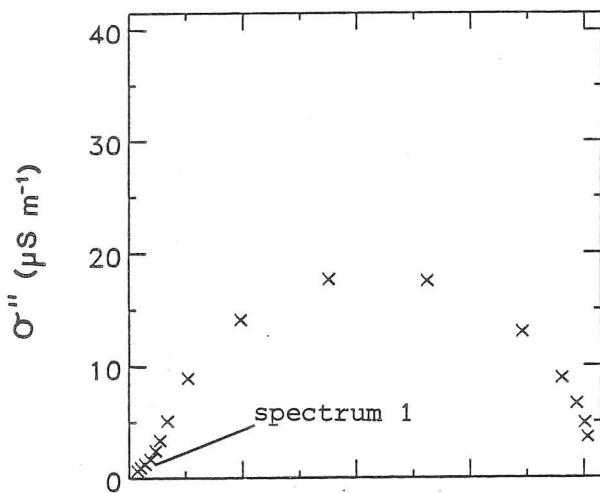
Prior to obtaining σ_m^* it is necessary to supply a value of ϵ_∞ . In the absence of a reliable experimentally determined value, ϵ_∞ was assumed to be equal to 3.2 at 0°C for ice of density 920 kg m⁻³ and $\partial\epsilon_\infty/\partial T$ to be $1.2 \times 10^{-3} \text{ }^\circ\text{C}^{-1}$ (Paren, 1970; Westphal (from Paren, 1970)). Johari (1976) obtained a value rising from 6.0×10^{-4} to 2.1×10^{-3} between 245 and 273 K (at 100 MHz) but considering the anomalous behaviour of his samples, those of Paren and Westphal are preferred. The temperature dependence of ϵ_∞ has a negligible influence on the estimated modified conductivity and any uncertainties in it introduce negligible errors. More important is the actual value of ϵ_∞ at a given temperature. This can be placed within sensible bounds (independently of experimental values) by examining its effect on the hf part of a low temperature Arc diagram. Too high a value can produce negative values of σ_m'' while if it is too low σ_m'' increases indefinitely. These 'sensible bounds' were found to lie between 3.18 and 3.26 (for solid ice).

Fig. 4.8 shows Arc diagrams (Argand diagrams of σ_m^*), for the three samples, at two different temperatures. In Fig. 4.8 a) a low-frequency dispersion (spectrum 1) is in evidence. In Fig. 4.8 b) the hf dispersion has clearly been induced and is fairly well separated from the main dispersion.

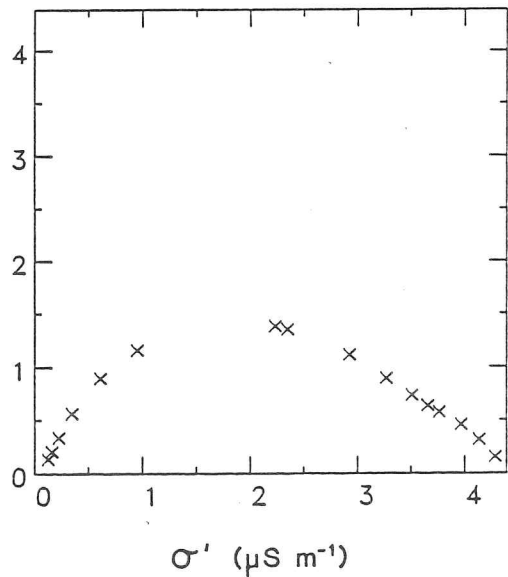
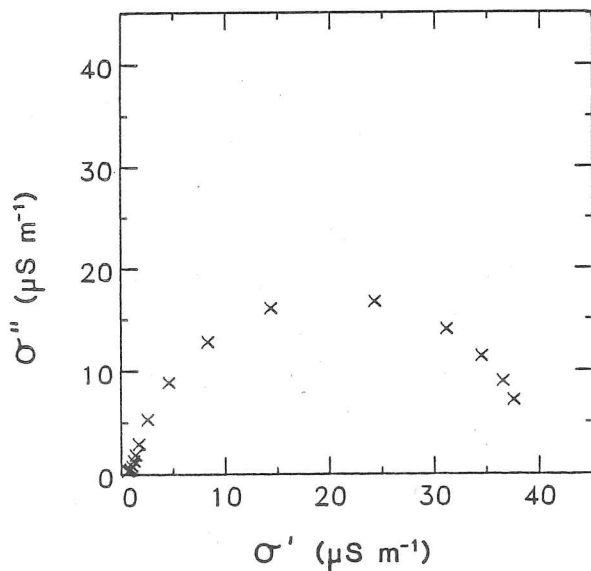
An observation, applicable to both sets of data in Fig. 4.8 is that the curves, describing spectrum 2, are not semi-circular (as would be the case for a perfect Debye dispersion) but are depressed. This property has been observed by a number of authors who have modelled this behaviour with equations for either a semi-ellipse (Paren and Glen, 1978) or a depressed arc (Camplin and Glen, 1973). The analysis preferred here is similar to that of the latter authors, who also observed three distinct dispersions, and is adopted because a semi-ellipse requires the Arc plot to cross the real axis at right angles. This did not seem to be the case for the Spitsbergen data and it was consequently felt that a depressed arc (which does not impose this condition) was more appropriate. It is also mathematically simpler to handle and makes the



Sample 2



Sample 1



a)

b)

Fig. 4.8 Arc plots (real and imaginary parts of the modified complex conductivity) at two temperatures; a) -2.5°C , when the lf dispersion becomes apparent (spectrum 1), b) -34.4°C when the hf dispersion is visible (spectrum 3).

extraction of parameters, by graphical means, easier. The details of the theory are presented in App. 2 with the experimental procedure and only a resume is given here.

σ_m^* is described by the equation:

$$\sigma_m^* = \sigma_o + \sum_{i=1}^3 \frac{\Delta\sigma_i}{1 + (1/i\omega\tau_i)^{1-\alpha_i}} \quad (4.10)$$

where the subscripts, i , refer to the three dispersions and α is a parameter that defines the angle, $\pi\alpha/2$, subtended by the real axis and the geometrical centre of the dispersion. Its physical origin probably stems from the existence of a spread of relaxation times as opposed to a single value applicable to a perfect Debye dispersion (Paren and Glen, 1978). Separating real and imaginary parts of eqn. 4.10 leads to the relations:

$$\sigma_m' = \sigma_o + \sum_{i=1}^3 \frac{\Delta\sigma_i(1 + r_i \cos \theta_i)}{\Pi_i} \quad (4.11)$$

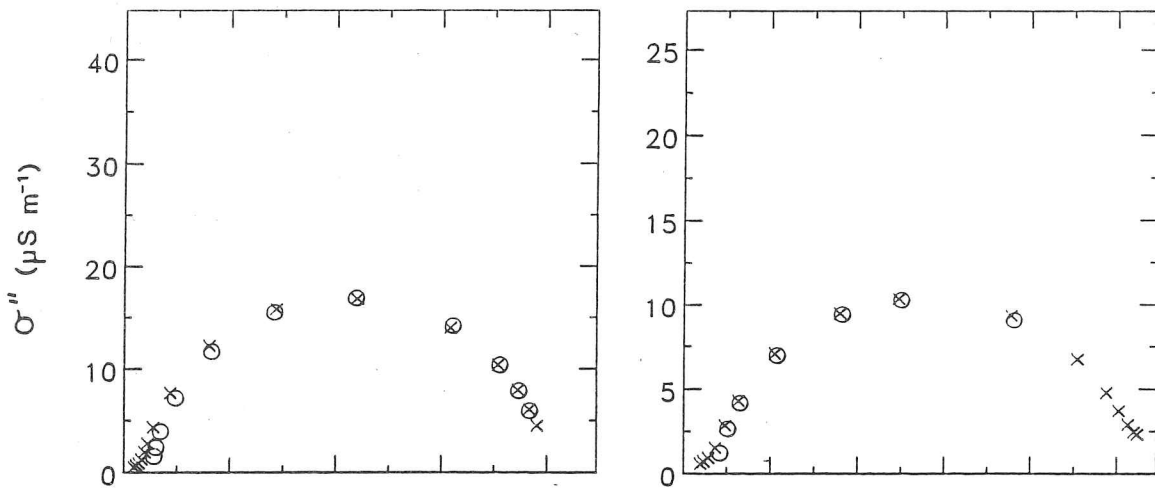
$$\sigma_m'' = \sum_{i=1}^3 \frac{\Delta\sigma_i r_i \sin \theta_i}{\Pi_i} \quad (4.12)$$

where $r_i = (1/\omega\tau_i)^{\alpha_i}$, $\theta_i = \gamma_i/(2\pi)$, $\Pi = (1 + r \cos \theta)^2 + (r \sin \theta)^2$ and $\gamma_i = 1 - \alpha_i$.

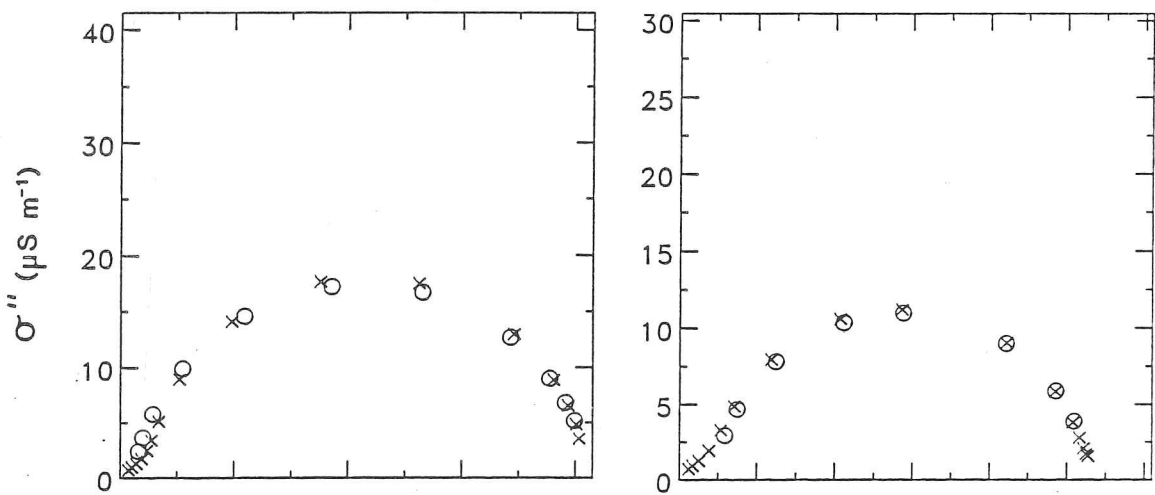
For each dispersion there are three unknowns: $\Delta\sigma_i$, τ_i and γ_i . Adding σ_o gives 10 parameters in all, that need to be determined. Due to lack of sufficient low-frequency data it was not possible to determine those for spectrum 1. This dispersion was, however, most probably due to space charge effects at the electrodes (e.g. Camplin and Glen, 1973) and was consequently an artifact of the experiment rather than the ice. For the two remaining dispersions, initial estimates of the variables were obtained by graphical means. These were then used as starting values in a least squares fitting routine (corrected Gauss-Newton method—Numerical Algorithms Group routine E04FDF). Results of the least squares fitting procedure are shown in Fig. 4.9 (for spectrum 2 only) and Fig. 4.10 (for spectrum 2 and 3).

Determination of relaxation times from conductivities are different to those obtained from permittivities when $\alpha \neq 0$. Following the standard convention, the relaxation times presented here have been converted to those that would have been deduced using permittivities (App. 2). All the relevant experimental data and results of the fitting procedure are tabulated in App. 3. The rest of this chapter will be devoted to a discussion of the results.

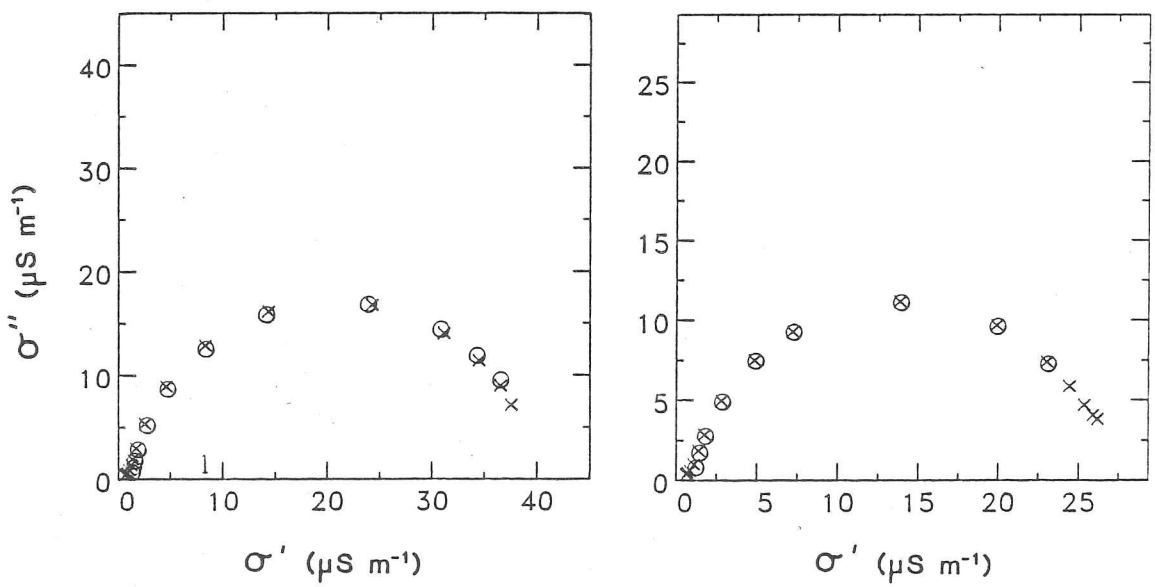
It is important to note that the objective of this experiment was to try and determine the dielectric behaviour of natural ice from a typical glacier in Spitsbergen. As such the relevant values, with respect to radio echo sounding, are those of the *in situ* ice. Consequently the data



Sample 2



Sample 1

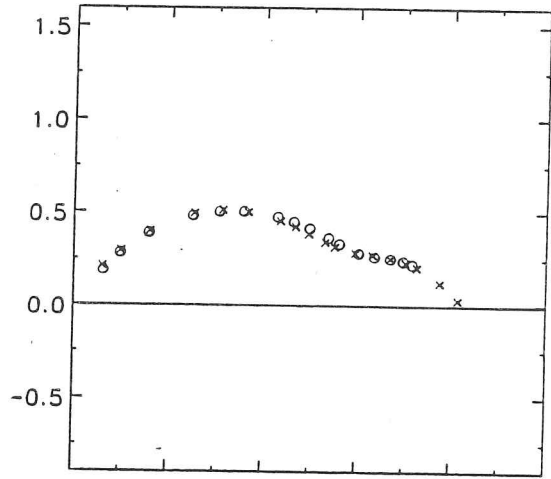
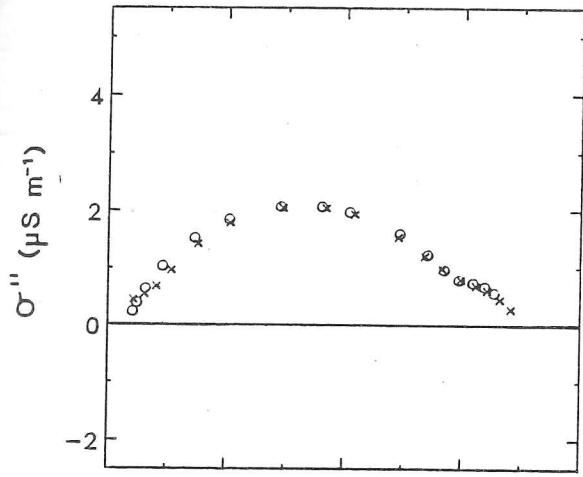


a)

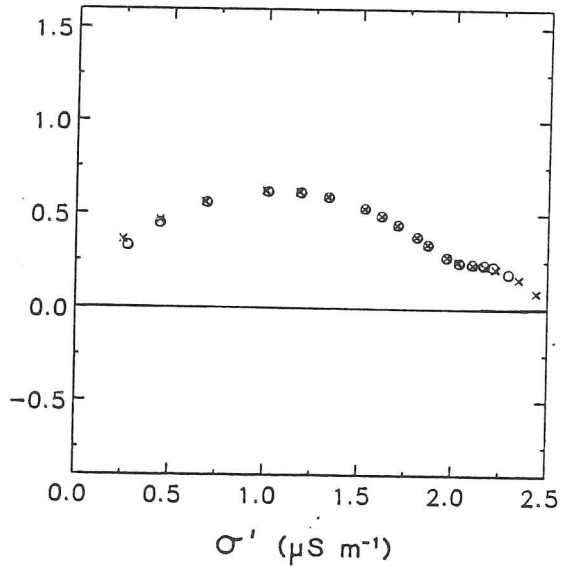
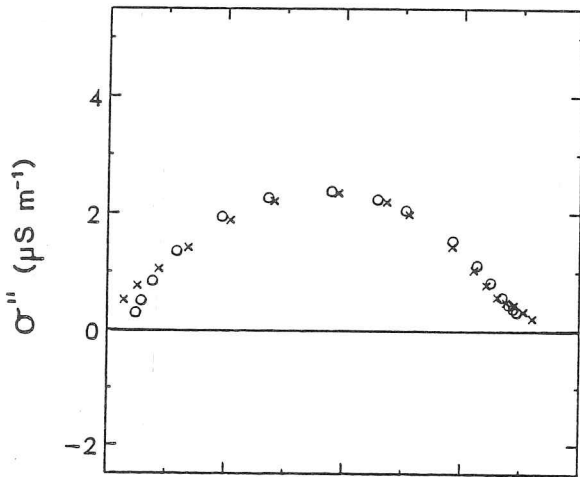
b)

Fig. 4.9 Comparison between experimental data and least squares fit (for spectrum 2 only) at two temperatures; a) -2.5°C and b) -7.5°C .

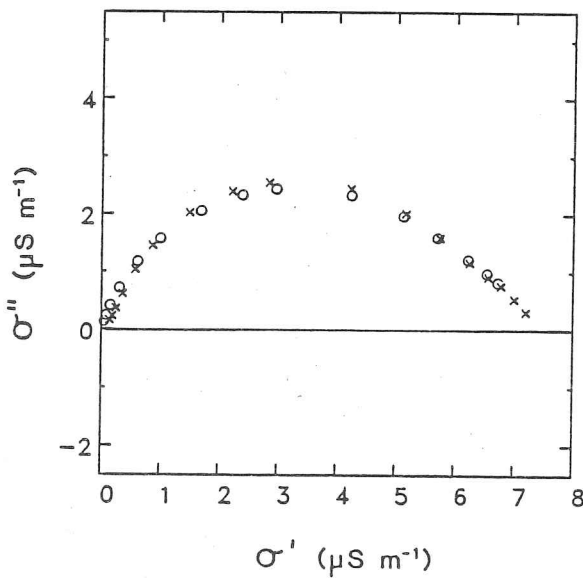
Sample 3



Sample 2



Sample 1



b)

a)

Fig. 4.10 Comparison between experimental data (crosses) and least squares fit (circles) for a model including spectrum 2 and 3. a) $-24.6\text{ }^{\circ}\text{C}$; b) $-44.0\text{ }^{\circ}\text{C}$ (no fit was possible to spectrum 3 for sample 1 at this temperature).

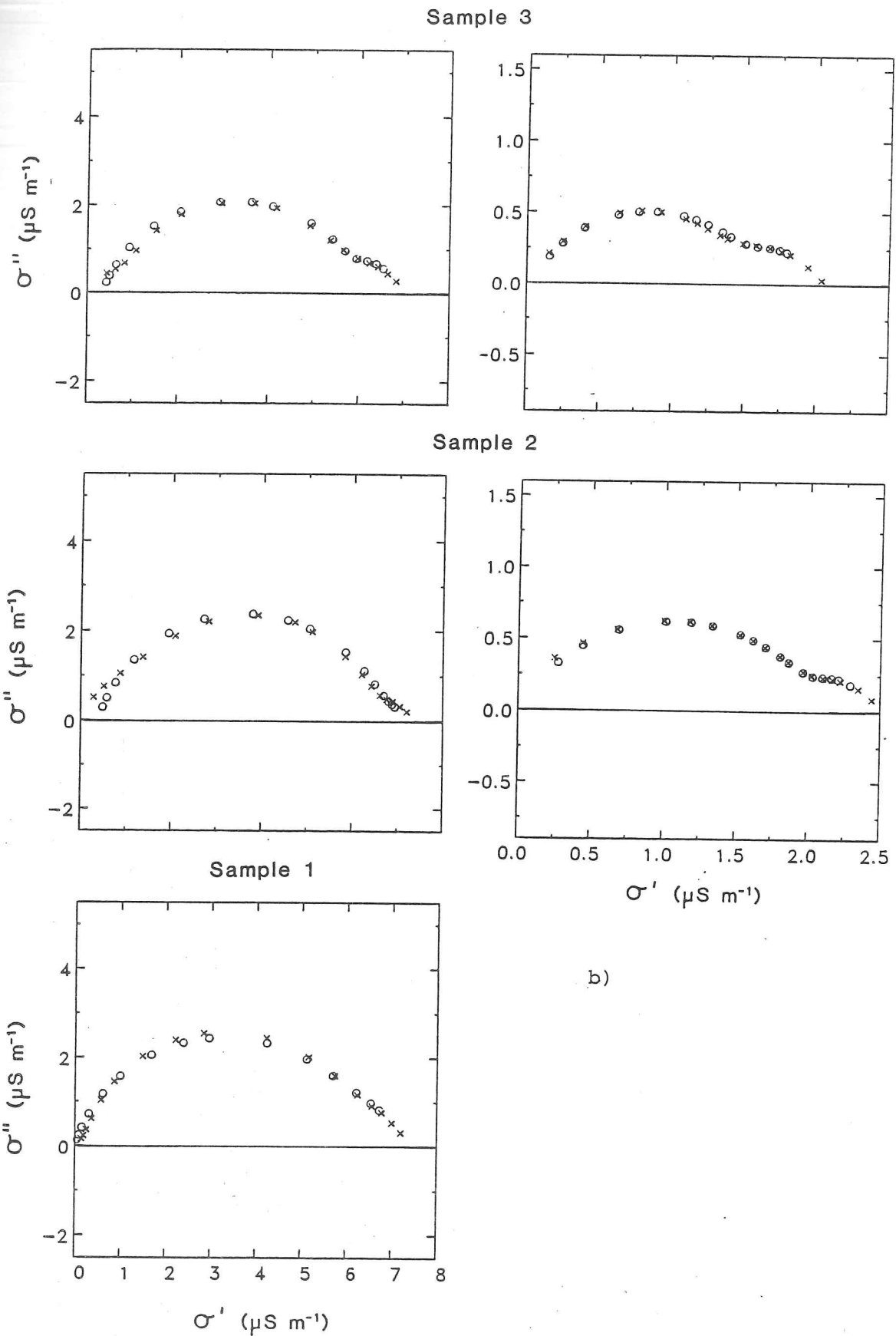


Fig. 4.10 Comparison between experimental data (crosses) and least squares fit (circles) for a model including spectrum 2 and 3. a) $-24.6\text{ }^{\circ}\text{C}$; b) $-44.0\text{ }^{\circ}\text{C}$ (no fit was possible to spectrum 3 for sample 1 at this temperature).

presented in this section, unless otherwise stated, have not been transposed to the equivalent solid ice values, and are those of the actual samples. Sample 1, has a slightly lower density (863 kg m^{-3}) than is typical of deeper ice (e.g. Paterson, 1981) which is nearer 900 kg m^{-3} . The increase in conductivity, for sample 1, if adjusted to this higher density, is approximately 7% and the ratio of hf permittivities is 0.987. For samples 2 and 3, whose densities were 885 kg m^{-3} , the increase in conductivity is about 3% and in permittivity it is negligible.

4.9 Discussion

4.9.1 Spectrum 2

Fig. 4.11 is an Arrhenius plot of $\Delta\sigma_2$ and $\Delta\sigma_3$. A number of interesting features are evident. First, down to a temperature of approximately -25°C all three samples gave similar values for the dispersion strength, $\Delta\sigma_2$, (within 8% of each other), although the relaxation frequency, ${}_1f_{r2}$, of sample 1 (from #145) produced consistently higher values (80–100% greater). The mean value of $\Delta\sigma_2$, at -2.4°C , was $39 \pm 3 \mu\text{S m}^{-1}$. Using the activation energy, $E_{\infty 2}$, (obtained shortly) $\Delta\sigma_2 = 49 \mu\text{S m}^{-1}$ at 0°C . The dc conductivity at this temperature is between 1.1 and $2.8 \mu\text{S m}^{-1}$, raising $\sigma_{\infty 2}$ to $\approx 51 \mu\text{S m}^{-1}$. Ignoring, for the present, the effects of spectrum 3, this value is already greater than a number of commercial and natural ices (from temperate and 'sub-polar' ice masses—Fig. 4.15) but less than a number of 'polar' specimens (Reynolds, 1985; Paren, 1973).

Second, the transition temperature, T_m , occurs at a value close to -20°C for all three samples and below this temperature greater variability in $\Delta\sigma_2$ is seen (presumably due to the differences in extrinsic defect concentration which are believed to dominate the conduction process below T_m (Von Hippel *et al*, 1972)). It is interesting to note that sample 1 shows the greatest change in E_∞ , implying a more 'imperfect' crystal (i.e. more extrinsic defects, or a higher defect mobility). The ion concentrations for the two sections appear to be fairly similar (Fig. 4.3) but the crystal fabrics, however, are significantly different (Fig. 4.4). The mean crystal area for #145 was some 40% greater than that of #209 (Simoes, personal communication), lending weight to the hypothesis that sample 1 was less perfect than either 2 or 3. The value of ${}_1\Delta\epsilon_2$, at -2.5°C (Fig. 4.5) was considerably greater than for the other two samples (0.7 compared with 0.2 and 0.3 for samples 2 and 3 respectively). If Von Hippel's (1972) suggestion that this dispersion is due, primarily to crystal imperfections, also applies to dispersion 3 of

presented in this section, unless otherwise stated, have not been transposed to the equivalent solid ice values, and are those of the actual samples. Sample 1, has a slightly lower density (863 kg m^{-3}) than is typical of deeper ice (e.g. Paterson, 1981) which is nearer 900 kg m^{-3} . The increase in conductivity, for sample 1, if adjusted to this higher density, is approximately 7% and the ratio of hf permittivities is 0.987. For samples 2 and 3, whose densities were 885 kg m^{-3} , the increase in conductivity is about 3% and in permittivity it is negligible.

4.9 Discussion

4.9.1 Spectrum 2

Fig. 4.11 is an Arrhenius plot of $\Delta\sigma_2$ and $\Delta\sigma_3$. A number of interesting features are evident. First, down to a temperature of approximately -25°C all three samples gave similar values for the dispersion strength, $\Delta\sigma_2$, (within 8% of each other), although the relaxation frequency, ${}_1f_{r2}$, of sample 1 (from #145) produced consistently higher values (80–100% greater). The mean value of $\Delta\sigma_2$, at -2.4°C , was $39 \pm 3 \mu\text{S m}^{-1}$. Using the activation energy, $E_{\infty 2}$, (obtained shortly) $\Delta\sigma_2 = 49 \mu\text{S m}^{-1}$ at 0°C . The dc conductivity at this temperature is between 1.1 and $2.8 \mu\text{S m}^{-1}$, raising $\sigma_{\infty 2}$ to $\approx 51 \mu\text{S m}^{-1}$. Ignoring, for the present, the effects of spectrum 3, this value is already greater than a number of commercial and natural ices (from temperate and 'sub-polar' ice masses—Fig. 4.15) but less than a number of 'polar' specimens (Reynolds, 1985; Paren, 1973).

Second, the transition temperature, T_m , occurs at a value close to -20°C for all three samples and below this temperature greater variability in $\Delta\sigma_2$ is seen (presumably due to the differences in extrinsic defect concentration which are believed to dominate the conduction process below T_m (Von Hippel *et al*, 1972)). It is interesting to note that sample 1 shows the greatest change in E_∞ , implying a more 'imperfect' crystal (i.e. more extrinsic defects, or a higher defect mobility). The ion concentrations for the two sections appear to be fairly similar (Fig. 4.3) but the crystal fabrics, however, are significantly different (Fig. 4.4). The mean crystal area for #145 was some 40% greater than that of #209 (Simoes, personal communication), lending weight to the hypothesis that sample 1 was less perfect than either 2 or 3. The value of ${}_1\Delta\epsilon_2$, at -2.5°C (Fig. 4.5) was considerably greater than for the other two samples (0.7 compared with 0.2 and 0.3 for samples 2 and 3 respectively). If Von Hippel's (1972) suggestion that this dispersion is due, primarily to crystal imperfections, also applies to dispersion 3 of

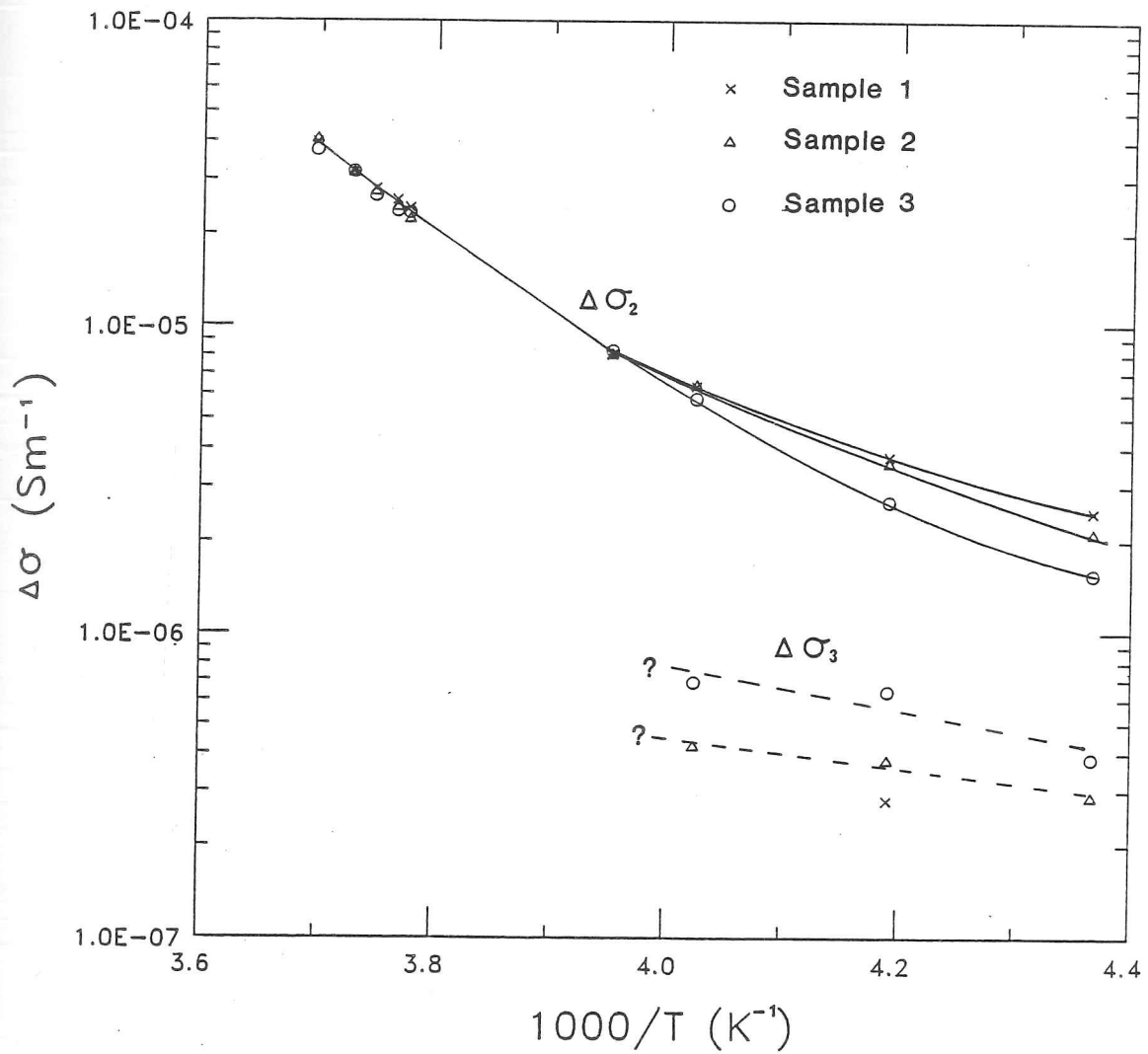


Fig. 4.11 Arrhenius diagram of conductivity dispersion strengths for spectrums 2 and 3. Fitting a curve/line to the data for spectrum 3 is approximate due to the small number of data-points and the large errors associated with them.

these samples then the aforementioned results do indeed suggest that sample 1 has a greater concentration of imperfections. A further observation is that any differences, in this respect, appear to have little effect on the magnitude of $\Delta\sigma_2$ above T_m . At higher temperatures the activation energy, $E_{\infty 2}$, appears to be constant and similar for all three samples with an average value of 0.505 ± 0.006 eV. This is lower than that of laboratory grown pure ice or Paren's Mendenhall Glacier ice (0.57 eV; Paren, 1970; Reynolds, 1985) but significantly greater than that of most 'polar' specimens (≈ 0.25 eV; Reynolds, 1985).

4.9.2 Spectrum 3

Data for this dispersion were much more limited (than for spectrum 2) and values for $\Delta\sigma_3$ and τ_3 were only obtained for the lowest three temperatures (-44.0 , -34.4 and -24.6°C) and had large errors associated with them ($\approx 30\%$; App. 2). They do, however give a good order of magnitude estimate of $\Delta\epsilon$ and τ . The uncertainty in these parameters introduces an error in σ_∞ of between 5 and 10% depending on temperature. The data for $\Delta\sigma_3$ are illustrated in Fig. 4.11 and for f_{r3} in Fig. 4.12. Results were obtained at only one temperature for sample 1 and only two for sample 2. The activation energy, $E_{\infty 3}$, has been, tentatively, estimated to lie between 0.08 and 0.15 eV. If the maximum value is used, (obtained from sample 2) then $\Delta\sigma_3$, at 0°C is found to be $1.1 \mu\text{S m}^{-1}$ and is consequently relatively small compared to $\sigma_{\infty 2}$ ($\approx 2\%$). A validation of the magnitude of $\Delta\sigma_3$, at 0°C , can be made from an estimate of $\Delta\epsilon_3$ and τ_3 , using the relation $\Delta\sigma = 2\pi f_r \epsilon_0 \Delta\epsilon$, which is strictly only true for $\alpha = 0$ but is an adequate approximation for small α . The errors in estimating τ_3 are large but its value can be placed within sensible bounds, based on the frequencies and temperatures at which this dispersion was observed. From the data presented in Fig. 4.12, f_{r3} was estimated to be ≈ 130 kHz (at 0°C) — a similar magnitude to Von Hippel *et al*'s hf spectrum, and consistent with the ϵ_∞ vs. $1/f^2$ data. Assuming $\Delta\sigma_3 = 1-2 \mu\text{S m}^{-1}$ gives $\Delta\epsilon_3 = 0.14$ to 0.28 . The directly calculated values, however, lie between 0.3 and 0.7, however. This suggests a possible error in $\Delta\sigma_3$, by a factor of ≈ 3 , and implies a possible underestimate in σ_∞ of 7%. It does not significantly affect the findings related to radio echo sounding, however, which will now be considered.

Relaxation Freq. vs. Temp.

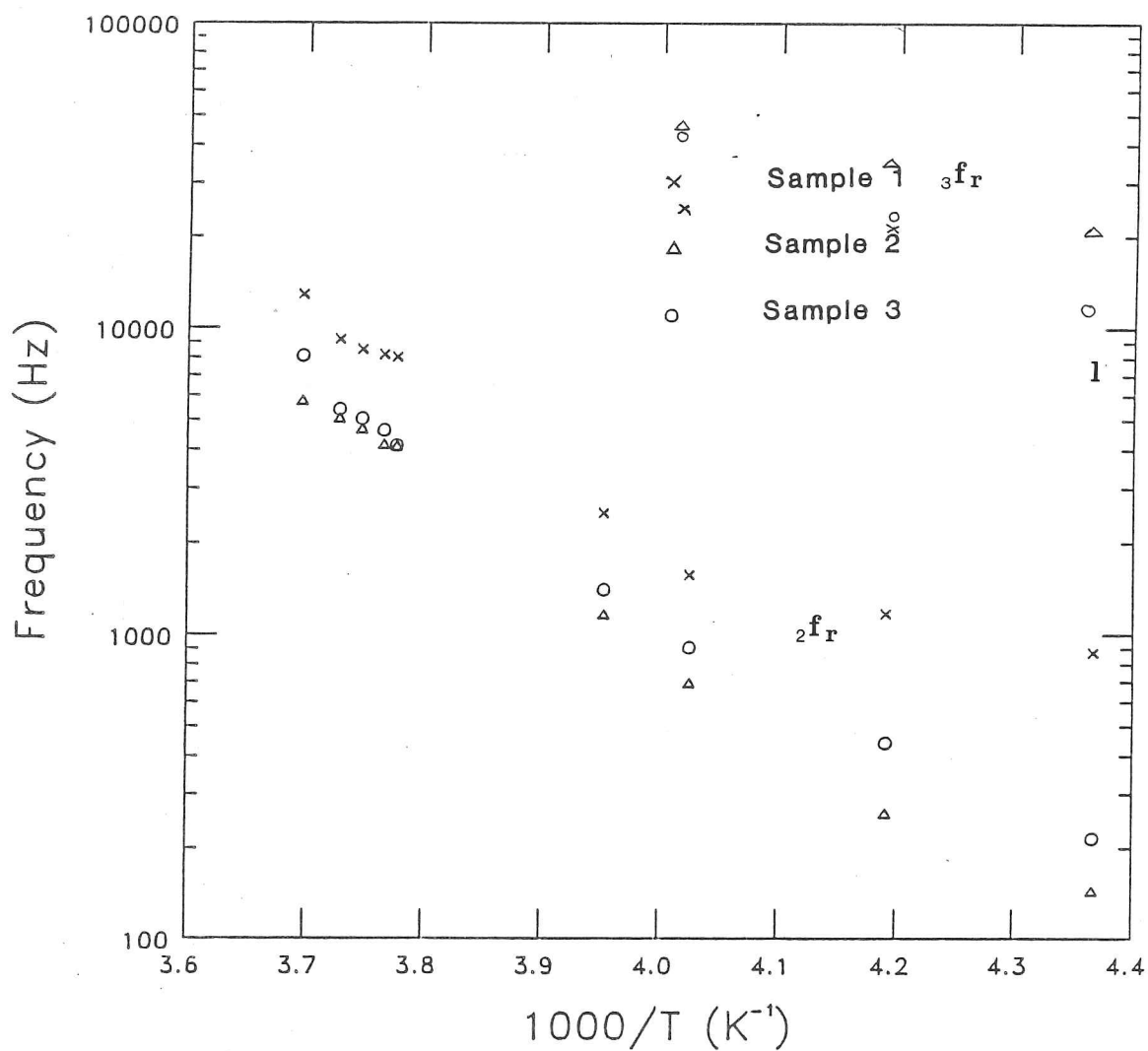


Fig. 4.12 Relaxation frequencies vs. $1/T$ for all three samples. Correction for the differences between values calculated from conductivities as opposed to permittivities has been made (App. 2).

4.9.3 Static Conductivities

The static conductivities are of limited direct relevance to radio echo sounding. Their values are usually no more than 2–3% of σ_{∞} at most. They are, however, one of the parameters that appear to be most sensitive to the thermal environment (Glen and Paren, 1975). They have been found to be up to three orders of magnitude greater for 'polar' glaciers compared with temperate ones (from georesistivity surveys over glaciers). Values, close to 0°C, of the order of $0.01 \mu\text{S m}^{-1}$ to $0.1 \mu\text{S m}^{-1}$ are typical of the latter ice masses (Glen and Paren, 1975) while for the former the range is from about 1 to $10 \mu\text{S m}^{-1}$. The results of the data for the three Spitsbergen samples are illustrated in Fig. 4.13. It is evident that the values of σ_0 fall into the 'polar' category. Considering that σ_0 is most strongly dependent upon the impurity concentration and that the samples were not from a completely temperate zone, this is perhaps not such a surprising result. It is, however, interesting to note that other properties of the samples (specifically the conductivity activation energy) seem to lie closer to the 'temperate' category in their behaviour.

4.9.4 Relevance to RES

It is never possible, with the isolated study of a small sample of ice from one glacier in one location, to determine the generality of specific results and how they might be extended to other glaciers with possibly different thermal regimes. This is evidenced by the variability in Westphal's data between his Arctic and Antarctic samples (Jiracek, 1965). There are, however, a number of important conclusions that can be drawn from this study. The first, and perhaps most relevant, is that an entirely independent measurement of the absorption properties, close to the melting point, has produced a value that is consistent with RES measurements of bulk absorption in glaciers believed to be near this temperature for much of their thickness. Fig. 4.14 illustrates the estimated values of absorption with temperature using the mean values of E_{∞} and C_{∞} (the constant in the Arrhenius equation for σ_{∞}) for the three samples. In section 5.2, it is shown that a number of glaciers in Svalbard, believed to be close to their melting points, have bulk absorption values of a very similar value to those obtained in the laboratory (Table 5.1).

Skobreen is not one of the warmest glaciers in Spitsbergen (section 1.5.3). A 10 m temperature of -2.8 was measured for a site close to the equilibrium line, in May at the start of the melt season. It is also a relatively thin glacier (≈ 200 m; App. 1) and probably lies in between

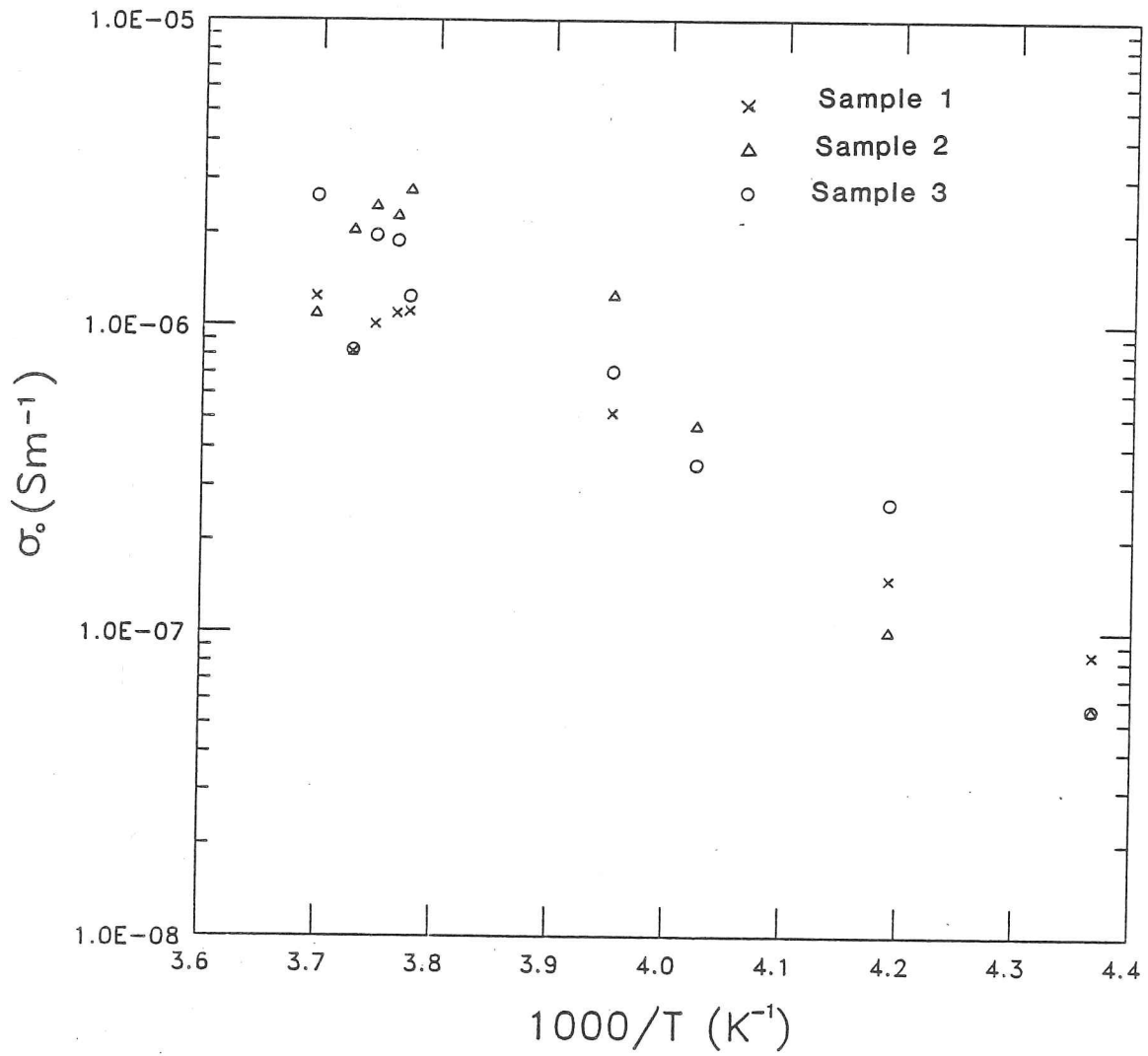


Fig. 4.13 dc conductivities vs. $1/T$ for all three samples.

Absorption vs. Temperature

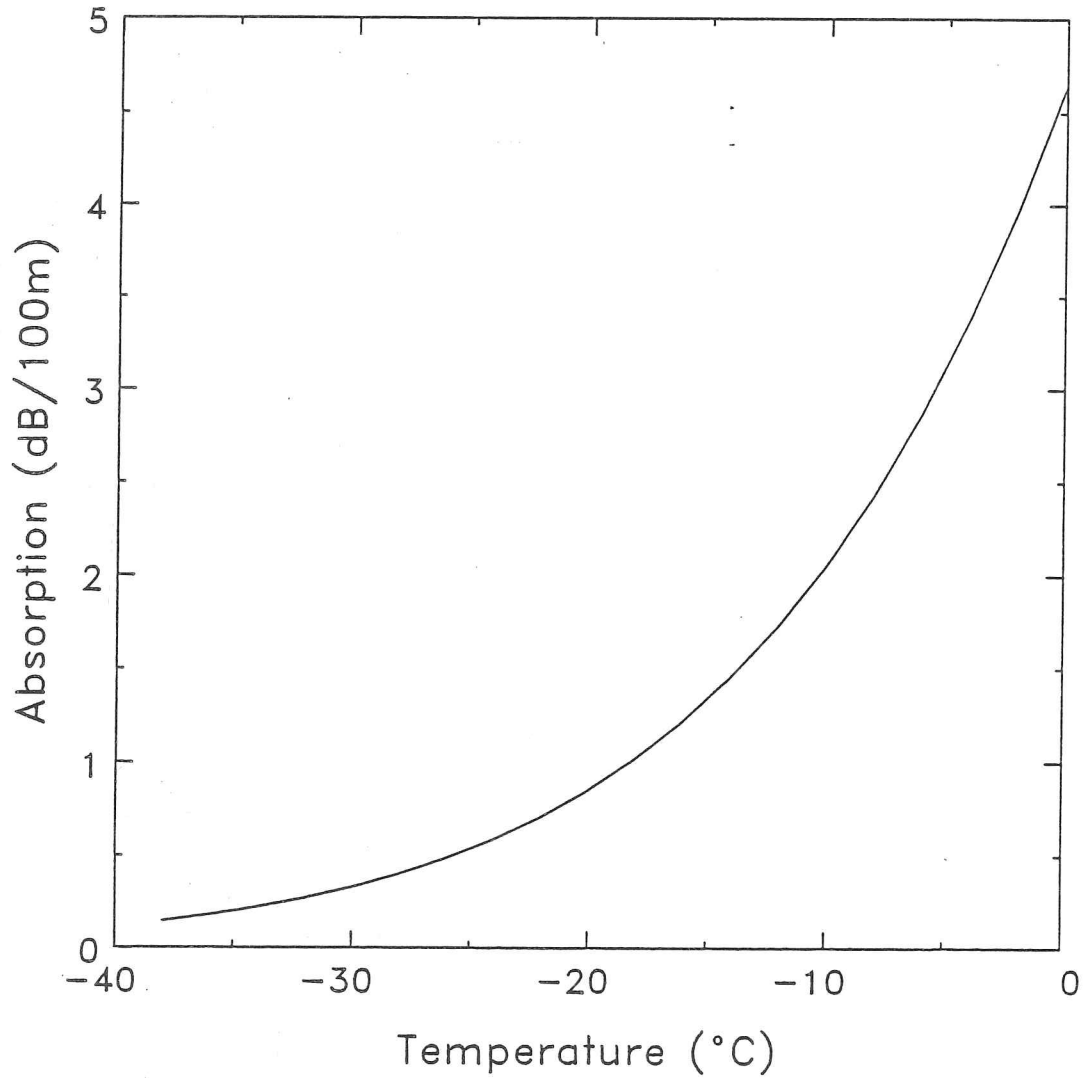


Fig. 4.14 Estimated hf absorption vs. temperature. Curve is average of the three samples, and no correction to density has been made.

the two extremes of thermal regime found in Svalbard.

'Polar' or Temperate

As has already been implied, and would be expected, the dielectric properties of these samples appear to be intermediate in their behaviour. The activation energy displays this most clearly, having a relatively low transition temperature and a value lying in between the 'polar' and temperate extremes. It is illustrated in Fig 4.15—an Arrhenius plot of σ_∞ comparing the Skobreen ice with 10 other samples, including mono and polycrystalline commercial and natural specimens. Curve 11 represents the data obtained in this study (average of the three samples) and it can be seen that the activation energy (above $\approx -20^\circ\text{C}$) is close to the 'pure ice limit'. The magnitude of σ_∞ is greater than that of the temperate and commercial ices shown in Fig. 4.15. This is due to the presence of the hf dispersion and a relatively high σ_0 . If $\Delta\sigma_2$ alone, is considered, it is found to be close to the values of σ_∞ for samples 6–10. Hence the main dispersion would appear to have properties akin to the 'temperate (or pure ice) limit' and it is only the presence of spectrum 3 and a high σ_0 that have shifted the dielectric behaviour away from this.

4.10 Summary and Conclusions

The similarity in results of the two samples from #209 indicate that the preparation technique did not have a significant effect on the dielectric properties (or if it did then it was identical for both). The impurity and dislocation concentration is known to influence the dielectric properties, especially of the hf dispersion (if it exists) (Von Hippel *et al*, 1972). Given the obvious differences in the crystal fabric and air bubble content between #145 and #209 (Fig. 4.4) it would, consequently, seem unlikely that their properties, below T_m in particular, would be identical. Sample 1 (from #145) indeed showed characteristics of greater multicrystallinity (and hence imperfection)—its relaxation times (for the main dispersion) were consistently greater than for the other two samples and the gradient of $\log\Delta\sigma$ vs. $1/T$, below T_m , less.

Three dispersions were observed in all the samples. The low-frequency spectrum was not investigated, but was believed to be most probably due to space charge effects as found by a number of other authors (e.g. Camplin and Glen, 1973; Von Hippel *et al*, 1972). The form of spectrum 2 (due to intrinsic volume polarization in the ice) was successfully modelled with a least squares fit to the equation of a depressed arc (applied to the modified conductivity data).

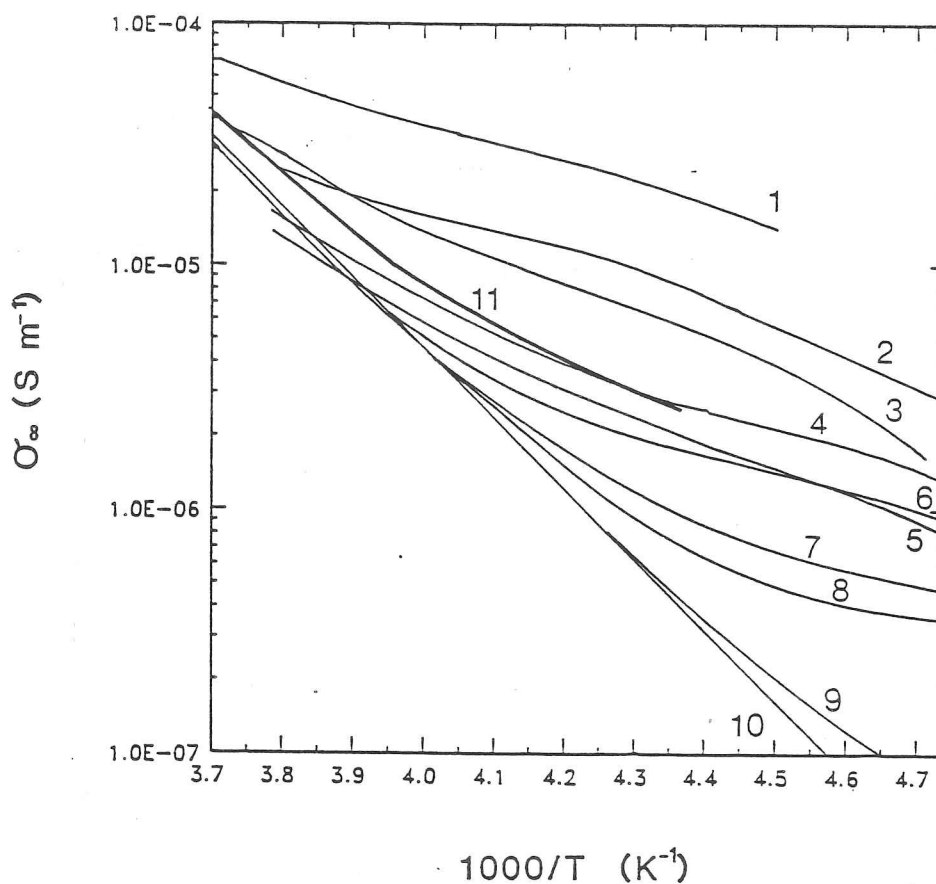


Fig. 4.15 Arrhenius diagram of the high-frequency conductivity (at 100 kHz unless otherwise stated) for a number of different ice samples compared with data from the Skobreen specimens (average of 3 samples at a density of 920 kg m^{-3} and including the effects of spectrum 3). Source Reynolds (1985).

- 1) Little America (Westphal, 300 MHz).
- 2) Wormald Ice Piedmont, Antarctic Peninsula (Reynolds, 1985).
- 3) Ward Hunt Ice Shelf (Westphal, 300 MHz); Camp Century and Site 2, Greenland (Paren, 1973); Byrd Station, Antarctica (Fitzgerald and Paren, 1975).
- 4) George VI Ice Shelf (Reynolds, 1985); 5) Palmer Land plateau (Reynolds 1985); 6) Polycrystalline "commercial" ice (Paren, 1970).
- 7) Ice from Tuto Tunnel, Greenland (Paren, 1970). 8) Polycrystalline ice (Camp et al, 1969). 9) Monocrystal, (Ruepp, 300 kHz).
- 10) Mendenhall Glacier monocrystal (Glen and Paren, 1975); monocrystal K70 of (Ruepp, 300 MHz).
- 11) Polycrystalline samples from Skobreen.

Spectrum 3, believed to be due to impurities and imperfections in the ice (Von Hippel *et al*, 1972) was more difficult to define and only limited 'order of magnitude' data describing this dispersion were obtained.

Above $\approx -20^\circ\text{C}$ σ_∞ is well described by an Arrhenius equation with a single activation energy, estimated to have a mean value of 0.505 ± 0.006 eV. The average value of σ_∞ at 0°C has been estimated to be $51 \pm 3 \mu\text{S m}^{-1}$ which corresponds to a radar absorption of 4.7 dB/100 m. In the next chapter it will be shown that this value is in good agreement with *in situ* RES measurements of absorption from glaciers in Spitsbergen which are believed to be close to their melting points. The static conductivities appear to be 'polar' in magnitude.

These results, combined with RES absorption data (of a more empirical nature) are used in the second part of Ch. 5 to assist in the determination of RCs from internal and ice/bed boundaries.

CHAPTER 5

RADIO ECHO SOUNDING RESULTS

5.1 Introduction

This chapter deals with the results of the various analyses carried out on the RES data described in Ch. 2. The interpretation of the returned echo power is separated into two parts. In the first section an attempt is made to establish, from RES data, the *in situ* absorption properties of the ice. Svalbard glaciers do not fit, easily, into either category of 'polar' or temperate (considered in section 4.4). The effects of meltwater percolation and recrystallisation under stress are obviously strongly dependent on proximity to the melting point (e.g. Duval, 1975, 1979) and, as was seen in Ch. 4, it is conceivable that many of the glaciers in Svalbard will have a dielectric response intermediate between the two extremes.

The second section uses the results of the first part to calculate the dielectric absorption within the ice and hence the RCs of the reflecting boundaries. These data are discussed and from them the nature of the reflecting horizons considered.

5.2 Calculation of In Situ Dielectric Absorption

The analyses that follow are based on determining the relationship (if any) between ice thickness and total absorption. The method adopted was to plot ice thickness against the total attenuation in peak echo power (i.e. that due to dielectric absorption, scattering and reflection losses only) after subtraction of the geometrical spreading and refraction terms. From eqn. 3.21 it can be seen that the gradient corresponds to twice the mean absorption, \bar{B} (assuming scattering losses are negligible), and the intercept to the mean reflection coefficient, \bar{R} .

Inherent in this type of analysis is the assumption that the RC and $B(z)$ remain 'statistically stationary' over the area being considered. These are approximations whose validity can be gauged from the degree of correlation between the two variables. A least-squares linear regression was used to fit the data to a straight line and the correlation coefficient defined as the ratio of the covariance, COV , to the product of the standard deviation, σ , of the two variables; i.e.

$$r = \frac{COV_{xy}}{\sigma_x \sigma_y} \quad (5.1)$$

where the covariance is a measure of the joint variation of the two variables about their mean (Davis, 1973). For a linear regression this gives, in terms of the means of x and y ,

$$r = \frac{\sum_{i=1}^n (x_i - \bar{x})(y_i - \bar{y})}{\sqrt{\sum_{i=1}^n (x_i - \bar{x})^2 \sum_{i=1}^n (y_i - \bar{y})^2}}. \quad (5.2)$$

This is also known as the Pearson product-moment correlation coefficient.

If the dielectric properties of the ice are known then the bulk temperature, \bar{T}_σ , can be estimated from \bar{B} . To do this a value for E_∞ and σ_∞ at a specified temperature must be established. In the discussions that follow these are taken to be 0.57 eV and $46 \mu\text{S m}^{-1}$ (at 0°C) respectively. The former value is used in all calculations, unless otherwise stated, the justification for which comes from the fact that all the temperatures considered are above -10°C in which case, even for polar ice, the activation energy tends to that of 'pure' ice (Ch. 4). The conductivity was calculated from the \bar{B} s for the three glaciers from western Spitsbergen, which are all believed to be close to the melting point but, as will be seen later, the dielectric properties may vary across the archipelago. \bar{T}_σ is not equivalent to the mean ice temperature, \bar{T} , as integration of σ_∞ with respect to depth is not the same as integration of T . However, for a 500 m column of ice with $T_s = -5^\circ\text{C}$ and $T_{bed} = 0^\circ\text{C}$, \bar{T} , for a linear temperature profile, is obviously -2.5°C while \bar{T}_σ is -2.0°C . The smaller the temperature gradient within the ice the lower the difference will be.

5.2.1 Spitsbergen

For many of the glaciers in Spitsbergen the correlation was poor (< 0.8 for approximately 50 data points). The reason for this is more likely to be to variations in reflectivity than in the absorption properties. In section 3.2.1 it was shown that bedrock roughness alone can reduce the mean echo strength by up to 10 dB and can produce random fluctuations of a similar magnitude (Robin *et al*, 1969; Neal, 1977). It is not immediately clear why some glaciers should show much better correlation than others and we shall consider the best correlated data under the assumption that it is sufficiently 'well behaved' to allow meaningful deductions to be made.

The most satisfactory fit was obtained for Borebreen (78.3°N , 14°E , Fig. 5.8). Data from this glacier gave a correlation coefficient of 0.95 for 86 points and these are plotted in Fig. 5.1. The regression coefficient implied a value of 4.2 ± 0.15 dB/100 m for the absorption and the intercept a mean RC of -9.4 ± 0.95 dB for the ice/bed interface. The former value is equivalent

Absorption vs. Ice Thickness

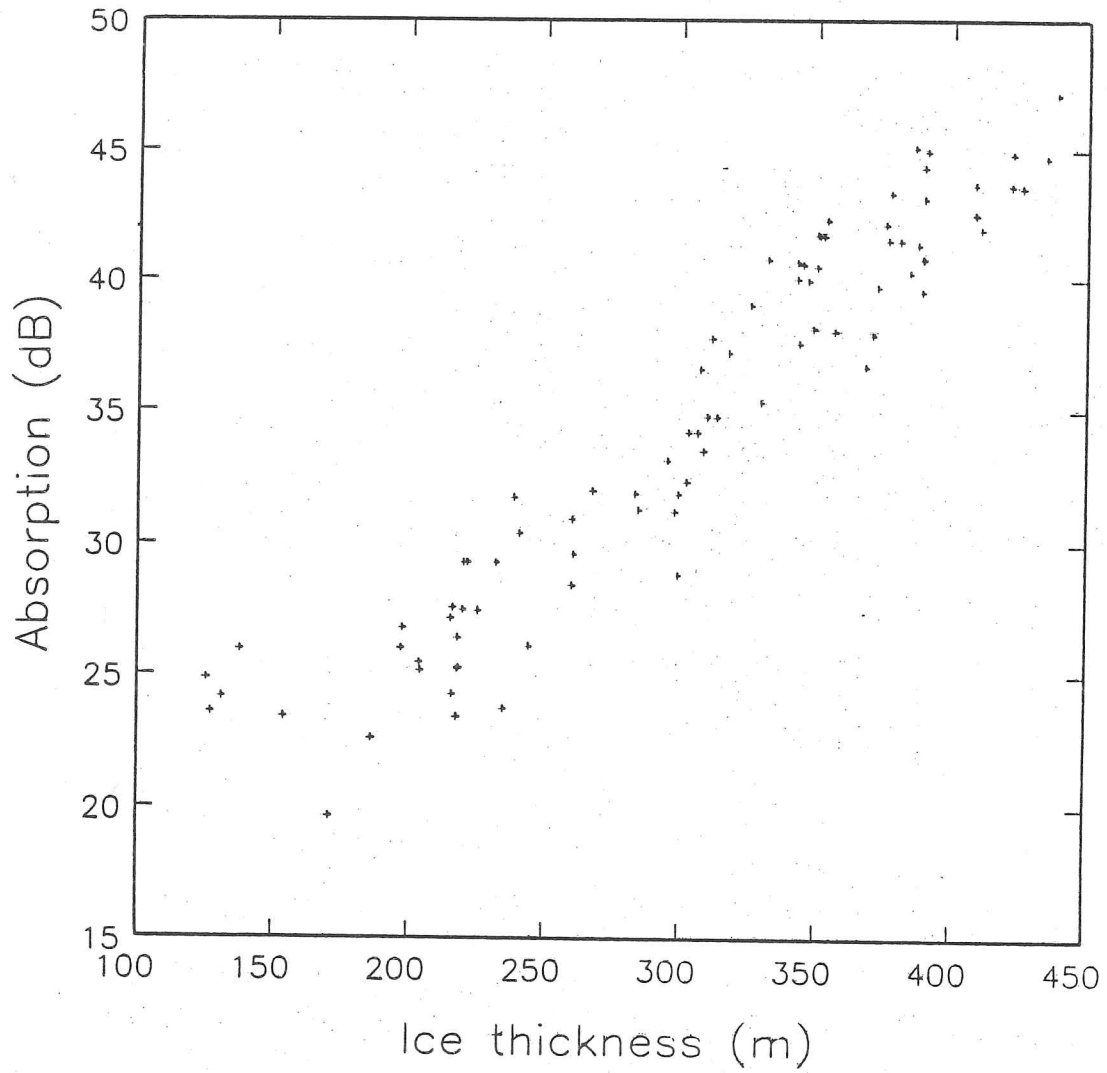


Fig. 5.1 Absorption vs. ice thickness data for Borebreen.

to a mean σ_{∞} of $46 \mu\text{S m}^{-1}$. Borebreen is a glacier that possesses an IRH which extends for 16 km from near the snout to well above the estimated equilibrium line (Fig. 5.8). It is suggested shortly that the existence of this feature indicates the presence of englacial water, implying that the bulk of the ice mass must be close to the melting point. Thus the thermal regime is 'almost' temperate and it is interesting to note that the derived mean σ_{∞} is similar to that deduced from laboratory experiments on temperate ice samples at the melting point (Paren, 1970). The data for the remaining ice masses, which gave meaningful results, are shown in Table 5.1. There is a wide spread in \bar{B} but considering each glacier individually, in terms of its location and thickness a distinct pattern emerges. The lowest \bar{B} s are found with the lowest RCs and come from Ny-Friesland, giving weight to the suggested trend in thermal regime of the glaciers (i.e. that they are the coldest). The glaciers in the table, have been ordered by location. The pattern is not perfectly obeyed—Valhallfonna, Petermannbreen and Negribreen have relatively high \bar{B} s despite lying in the east.

The dataset for Fjortende Julibreen— another glacier possessing an IRH, gave results very similar to that for Borebreen, with $\bar{B} = 4.5 \text{ dB}/100 \text{ m}$. The only other glacier, from west Spitsbergen, which gave reasonable results was Vonbreen ($r = 0.831$). Using data from the IRH (the bed did not provide sufficient data) produced a value of 4.2 for \bar{B} . A number of ice masses in Ny-Friesland showed good correlations, the best of which was Veteranen. In this case $\bar{B} = 3.7 \text{ dB}/100 \text{ m}$ (for the section beyond 189 km along track (Fig. 5.14)).

A reflecting horizon was observed in Veteranen but it is shown later (section 5.5.3) that it has different characteristics to those more commonly found from the western side of the island and may consequently be of a different origin. Hence, it would appear, that despite its thickness ($> 500 \text{ m}$ for several kilometres), much of the ice is significantly below the melting point. The bed, however, may still be at the melting point, as a surface temperature of -5°C would (for a linear temperature profile) give the estimated \bar{T} , requiring a temperature gradient of only 0.001 to $0.002^{\circ}\text{C m}^{-1}$. A very similar result is obtained for adjacent Chydeniusbreen ($\bar{B} = 3.5 \text{ dB}/100 \text{ m}$) which also has a similar profile (Fig. 5.14). The third ice mass from north-east Spitsbergen, is Dunérbreen. Again the glacier has a reflecting horizon but again its properties are not typical. The IRH appears to be composed of a small number of large scattering centres and is clearly not continuous. The mean absorption for this glacier was found to be $3.4 \text{ dB}/100 \text{ m}$. Hence the geographical pattern that emerges is of lower \bar{B} s (and therefore presumably lower \bar{T}_{σ} s) in Ny-Friesland with fairly consistent values for the 'near temperate' valley glaciers in

Table 5.1 Mean absorption values for glaciers from Spitsbergen.

Glacier	Correlation Coefficient	Number of Data	Absorption (dB/100 m)	Conductivity 10^5 S m^{-1}	Refln. Coeff. (dB)
Vonbreen	0.831	109 ¹	4.17±0.3	4.6	21±0.9
Fjortende Julibreen	0.913	33	4.6±0.3	5.0	14±3
Borebreen	0.950	86	4.2±.15	4.6	9.4±0.9
Wahlenbergbreen	0.878	55	5.0±0.4	5.5	13±3
Petermannbreen	0.880	93	5.3 ± 0.3	5.8	18 ± 1
Negribreen	0.820	81	4.8 ± 0.4	5.3	17 ± 1
Olav V land	0.775 ²	584	4.0±0.2	4.4	25.9±0.6
Veteranen	0.911	78 ³	3.7 ± 0.2	4.1	30 ± 1.4
Chydenlusbreen	0.834	181	3.5 ± 0.2	3.8	24±1
Valhallfonna	0.800	232	4.5 ± 0.3	4.9	23.6±0.9
Dunerbreen	0.810	46	3.4 ± 0.4	3.7	22 ± 1.7

- 1 The data for Vonbreen are for the IRH, not the bed, as the latter gave a poor correlation.
- 2 The results from this ice mass has a correlation coefficient less than 0.8 but is included because of the large number of data used for the analysis.
- 3 The data for Veteranen were taken from the upper section of the internal reflecting layer so that there was no ambiguity about which surface was being analysed. The RC is, therefore, that of the internal and not the bed.

the west of Spitsbergen, which are close to those deduced from laboratory measurements on temperate ice (Paren, 1970). The geographical trend is not perfectly obeyed, as Valhallfonna has a value of 4.5 dB/100 m and Negribreen and Petermannbreen also have higher values.

The concept of lower temperatures moving north and east (supported by climatological data (Ch. 1)) appears to be correlated with a trend in RCs which generally decrease in this direction (section 5.4; Fig. 5.6; Table 2.2). Although the rock types in north-east Spitsbergen are different from many of those found further west and south (section 1.4) it is shown in section 3.2.1 that this **alone** is unlikely to be sufficient to explain the differences in the bed RCs between regions and it is suggested that the thermal regime is likely to be a contributory factor: warmer glaciers appear to have higher RCs. The analysis of the data from Austfonna (in the next section) also displays this relationship between RCs and \bar{T}_σ (although the \bar{B} s are generally higher probably due to the dielectric, rather than thermal, properties of the ice (section 4.5)). This may also be the case for Negribreen and Petermannbreen which both have relatively high \bar{B} s but which follow the geographical trend in RCs. In this respect (i.e. in terms of the trend in RCs) Valhallfonna, Petermannbreen and Negribreen **do** follow the pattern. Thus it is possible that there are two opposing influences on \bar{B} . One due to the effects of temperature (reducing \bar{B} moving east) and the second due to a change in dielectric properties (increasing \bar{B}). This hypothesis is most strongly supported by the data from Austfonna where it is known that the glacial temperatures are low (relative to those in Spitsbergen (section 1.5)) but where the highest values of \bar{B} are recorded. In Ch. 4 it was seen that 'polar' ice had, in general, a higher σ_∞ than temperate or 'pure' ice at an equivalent temperature. Hence it is possible that there is a gradual transition from temperate to 'polar' dielectric behaviour moving north-east across the archipelago. The $[H^+]$ gradient (Fig. 4.1) may also contribute to this effect (especially on Austfonna where the ion concentrations are at their highest).

5.2.2 Nordaustlandet

Temperature data from Austfonna (section 1.5.3) suggests that it is not close to the melting point for a significant proportion of its volume. The temperature profile in Fig. 1.10 e) shows signs of an inversion near a depth of 100 m, where the temperature is still $-4.8^\circ C$. 10 m temperatures below the firn line are amongst the lowest recorded in the archipelago ($\approx -8.5^\circ C$) and have led to speculation that the ice cap has a 'warm inner core' surrounded by a 'cold' outer ring, frozen to the bed. It has been suggested that this might be the cause of surges

on the ice cap (Schytt, 1969). It is clear that the assumption, made in the previous section, that the absorption properties (and hence the thermal regime) remain constant, is probably not valid over the larger area of Austfonna. Consequently, a slightly different approach is necessary and, if possible, a means of grouping areas with similar thermal regimes must be employed. The most satisfactory method was found to be classification by surface elevation. This parameter influences the MAAT and also separates ablation and accumulation zones quite well (on Austfonna the equilibrium line is estimated to lie at a fairly constant elevation of about 300 m (Schytt, 1964)).

Data were, therefore, grouped into concentric rings spanning a 100 m interval in elevation (i.e. the groupings were < 100 m a.s.l., 100–200 m a.s.l., 200–300 m a.s.l. etc.). The location of the dividing line between each group is somewhat arbitrary and was, consequently, varied to see whether this had any influence on the results. Two sets of data, offset by 50 m from each other, are shown in Table 5.2 and it is evident that the position of the boundary between groups is not significant. Fig. 5.2 shows the attenuation/ice thickness plots for four of the groups.

Discussion

The correlation coefficients are not generally very high but because of the large number of data points in each group the results are far less prone to distortion by local variations in RC, as was the case for the Spitsbergen glaciers. Data from below 100 m a.s.l. (682 points) gave a very poor correlation (0.273) which was probably due to the variability of the bed environment in the marginal zones (Dowdeswell, 1984). r for the next group (100–200 m a.s.l.) was also relatively low, possibly for a similar reason, and it is, therefore, difficult to judge whether \bar{B} for this group is genuinely less than the one above it. However, a general trend is clearly evident: the mean surface elevation, for each group, is plotted against \bar{B} in Fig. 5.3. Excluding data below 200 m a.s.l., a reasonably linear relationship is obtained. Taking the highest \bar{B} to represent ice close to the melting point and assuming an activation energy of 0.57 eV, the bulk temperatures, \bar{T}_σ , can be estimated (Fig. 5.3). A value of 0.008°C/m is obtained for the temperature gradient within the ice, which is remarkably similar to the air–surface lapse rate of 0.007°C reported by Schytt (1964) for Vestfonna. This is a surprising result, considering the 10 m temperatures that have been observed. Further it implies that, contrary to previous suggestions, the bulk ice temperature increases towards the margins and is warmest below the equilibrium line. Whether it is reduced below approximately 200 m a.s.l. is, however, uncertain.

The highest \bar{B} corresponds to a conductivity of 63 $\mu\text{S m}^{-1}$ which would suggest that the

Table 5.2 Mean absorption values for different surface elevation groups on Nordaustlandet.

Surface elevation range (m a.s.l.)	Number of Data	Corrln. Coeff.	Absorption (dB/100 m)	Regression constant (-dB)
100-200	1730	0.687	5.2±.13	16.5±.6
150-250	1869	0.739	5.3±.11	16.8±.5
200-300	2021	0.806	5.4±.09	17.2±.5
250-350	2231	0.830	5.3±.08	18.5±.4
300-400	2192	0.849	5.0±.07	20.4±.4
350-450	2165	0.852	4.7±.06	22.4±.4
400-500	1843	0.858	4.6±.06	22.3±.4
450-550	1890	0.846	4.4±.07	23.6±.4
500-600	2090	0.833	4.4±.07	22.7±.5
550-650	1620	0.852	4.3±.09	24.4±.7
600-700	1035	0.776	3.6±.09	28.1±.8
650-750	843	0.618	3.1±.12	36.9±1.1

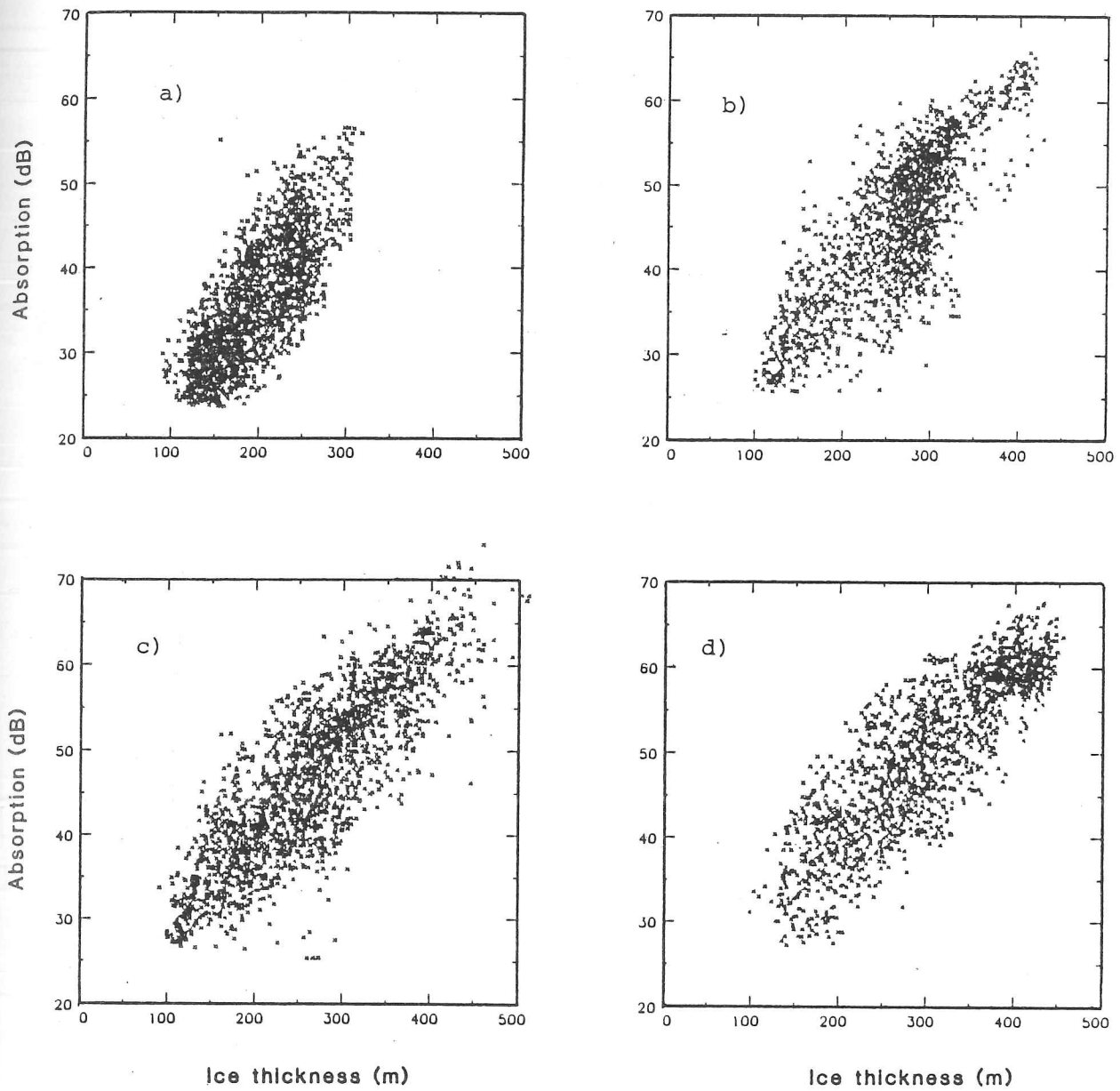


Fig. 5.2 Absorption vs. ice thickness data for four elevation groups on Nordaustlandet. Fig. a) is for data between 200 and 300 m a.s.l.; b) between 300 and 400 m a.s.l.; c) between 400 and 500 m a.s.l.; d) between 500 and 600 m a.s.l.

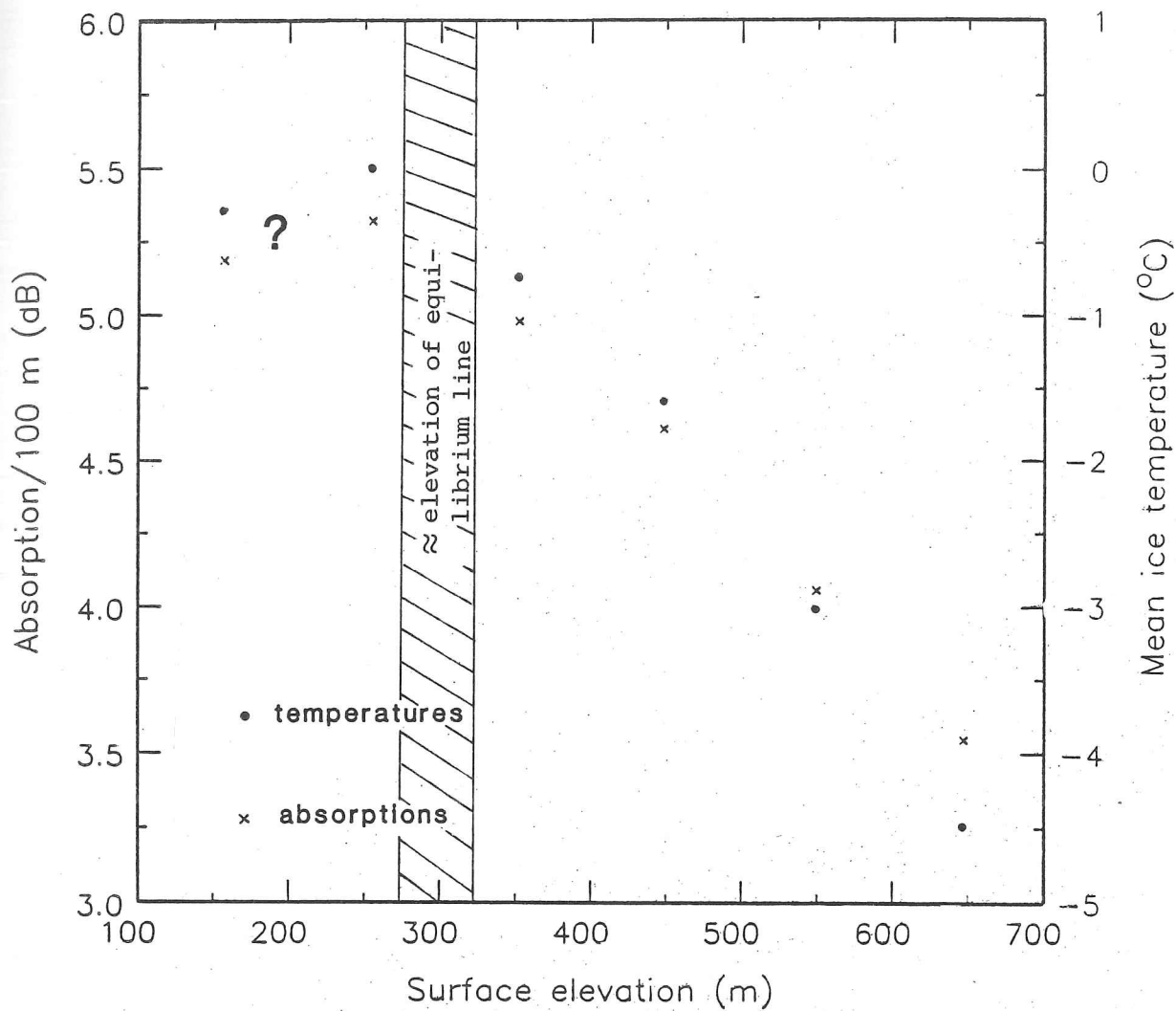


Fig. 5.3 Mean absorption and temperature vs. surface elevation for Nordaustlandet. Temperatures were calculated on the assumption that the highest absorption value represented ice at the melting point.

bulk of the ice in this group must be close to the melting point for it to have such a high value. It is similar to the value of σ_{∞} obtained by Westphal (Jiracek, 1965), for natural 'polar' ice raised near to the melting point, ($59 \mu\text{S m}^{-1}$ at -1°C for his Tuto Tunnel and Little America V samples) and consequently implies that the dielectric properties of this ice are probably closer to the 'polar' category than the temperate. As implied in the last section (and Ch. 4) the reasons for this could be twofold. First, it has been suggested that the removal of meltwater runoff and the extent of recrystallisation of the ice may be important in explaining the differences between polar and temperate ice (Reynolds and Paren, 1980). The extent of these two processes is likely to be markedly different between Nordaustlandet and the glaciers from western Spitsbergen. The colder MAATs and deep ice temperatures in Nordaustlandet (Ch. 1) imply that the degree of surface melting and strain rates will be reduced. Second, the considerably higher impurity and H^+ concentrations (Semb *et al*, 1984; Fig. 4.1) may also play a rôle (section 4.5). If the variations in $[\text{H}^+]$, observed by Semb *et al* are found at depth, within the ice, then a marked difference in the absorption properties would be expected, independently of any thermal dissimilarity.

It can be concluded, therefore, that ice in the marginal zones of Austfonna is probably close to the melting point and that the temperature gradually decreases moving inland. Dowdeswell (1984) has observed suspended sediment plumes emanating from a number of points along the coastline of Austfonna and Vestfonna. He suggests that these indicate the presence of subglacial meltwater at these locations and this would support the hypothesis developed here that much of the ice in the marginal zones is not frozen to its bed. Dowdeswell also notes that the sources of the sediment plumes are restricted to a limited section of the glacier terminus for each location and he concludes from this that the subglacial meltwater is probably flowing in a small number of major conduits or channels. This might well explain the poor correlation between ice thickness and absorption observed in these regions. A bed with variable amounts of water present would be likely to have a strongly fluctuating RC. Hence the condition that the area investigated should be statistically stationary will not be obeyed.

5.3 Models for Calculating Absorption

The most significant unknown in eqn. 3.21, for calculating RCs, is the integral of $B(z)$. In this section a number of models are proposed to determine this integral, based on the discussions of Ch. 4 and the empirical results of the previous section. It is not possible to apply a single model to every ice mass because their thermal regimes are so varied and as a consequence the dielectric properties also vary. The glaciers are divided into four broad categories which are considered below.

- 1) Valley glaciers possessing IRHs and considered to be close to the melting point throughout a significant percentage of their mass. The results from Borebreen, Fjortende Julibreen and Vonbreen are assumed to be typical of glaciers in this category and the absorption is taken as 4.3 dB/100 m. The advantage of this approach is that it requires no assumptions about either the thermal regime or the dielectric properties of the ice, both of which are poorly defined for the majority of the glaciers sounded in Svalbard. For those ice masses which had a sufficiently high correlation coefficient ($r > 0.8$; i.e. those shown in table 5.2) a mean value of B deduced for the specific glacier was used.
- 2) Valley glaciers not in the previous category. Ice masses in this group generally lie away from the west coast of Spitsbergen and are probably subject to a more continental climate (Hisdal, 1985). For these glaciers a linear temperature profile was adopted, requiring a number of boundary conditions to be specified, the most important of which are σ_{∞} , at $0^{\circ}C$, and the surface temperature, T_s . The former was estimated from the results from Borebreen while the latter was taken to be similar to an average 10 m temperature calculated from the data presented in section 1.5.3. The choice of T_s is somewhat arbitrary but it will be shown shortly that it does not have a very significant effect on the total absorption values calculated. The other boundary condition is the geothermal gradient, assumed to be $0.025^{\circ}C/m$ from values reported by Liestøl (1976). If the temperature reaches the melting point above the bed then this value was reduced so that the gradient produced the melting point at the bed. A simple temperature profile was employed for two reasons. First, it simplifies the numerical integration of the conductivity, which is an exponential function of temperature. Second, more sophisticated models require additional boundary conditions and considering the large uncertainties involved in estimating these, the benefits of such a model are lost.

- 3) The high altitude, thin ice cover in north-east Spitsbergen. This includes the two sections of track on Olav V Land (23 and 34), Åsgårdfonna (37) and Balderfonna (41). The model used for these ice masses was similar to that of 2) above except that the values of σ_{∞} were assumed to be similar to those deduced for Austfonna because it is believed that these ice masses are closer in thermal regime to Austfonna than to the warmer glaciers of the west coast (sections 1.5.3 and 5.2.2).
- 4) Austfonna. This ice cap was treated separately, because the analysis of section 5.2.2 enables a satisfactory estimate of \bar{B} from the surface elevation data; i.e. the gradient and intercept from Fig. 5.3 may be used to determine \bar{B} at any point, given the surface elevation.

5.3.1 Errors

Errors in estimating the total absorption are dependent upon the model used and are discussed below.

If $60 \mu\text{S m}^{-1}$ is taken as being the maximum value of σ_{∞} , at 0°C , for the glaciers in group 1, a value of 5.5 dB/100 m for \bar{B} is derived which would give a 2 dB/100 m error for the calculated value of total absorption. For example, in a 200 m thick ice column this would give a 4 dB error in the RC.

For glaciers in group 2 there is the same uncertainty in the value of σ_{∞} but the effects of changing the surface temperature and type of profile used can be investigated. In Fig. 5.4 a) experimentally simulated absorption data for a number of different models are plotted. The ice thickness data from Borebreen was used and the results of the different models are shown against the real data for comparison.

Model 1) was obtained using a mean value of \bar{B} (4.2 dB/100 m). Model 2) was calculated using a linear temperature profile with $T_s = -4^{\circ}\text{C}$ along its entire length; 3) was as for 2) but with $T_s = -1^{\circ}\text{C}$. 4) was calculated using a steady state temperature profile (Clarke *et al*, 1977) which takes into account ice advection and includes a term for strain heating, added to the geothermal heat flux. If melting takes place then, a new basal temperature gradient is found so that T_{bed} does not exceed the melting point. The flow law parameters were taken from Paterson (1981) and the accumulation rate was assumed to be 1.0 m/yr at 600 m a.s.l., decreasing linearly with elevation. The equilibrium line was assumed to be 300 m a.s.l. so that the ablation rate, at sea level, was -1 m/yr. T_s was the same as for model 1), -4°C . The

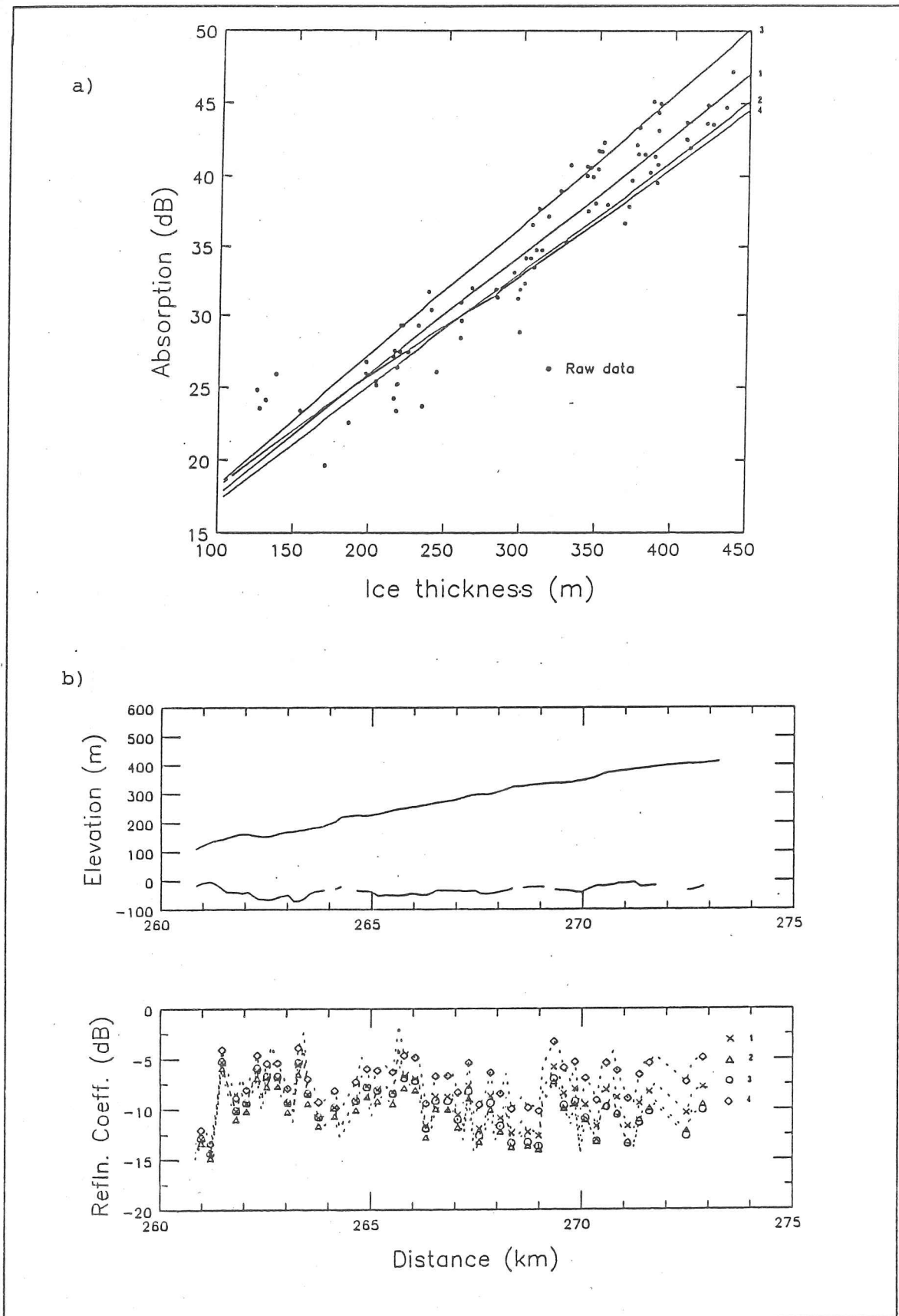


Fig. 5.4 Plot of absorption vs. ice thickness for the four models described in the text. These are shown with the experimental data from Borebreen. Fig. b) indicates the effects of the different models on the estimation of RCs.

activation energy used was 0.57 eV and the value of σ_{∞} at 0°C was assumed to be $52\mu\text{Sm}^{-1}$.

If model 1) is taken to be the best fit to the data (following the discussion of the previous section) then it can be seen that model 3) provides the next most adequate representation. The maximum deviation from model 1) is 3 dB (for an ice thickness of 450 m), representing a 0.7 dB/100 m error in B . Fig. 5.4 b) is a plot of RCs, for Borebreen, using the four different models. Near the snout, where the ice thickness is at its lowest, the differences are relatively small ($< 2\text{dB}$) and gradually increase along glacier reaching a maximum of 6 dB (between models 2) and 3)).

The errors for glaciers in group three are similar to those in 2. Considering the Nordaustlandet data, Fig. 5.3 implies a total change in \bar{B} of 1.8 dB in an elevation range of 500 m. Hence, the variation is quite small and although an individual estimate of total absorption can have an error of this order, on average it will be smaller than this ($\approx 0.4\text{dB}/100\text{ m}$).

5.3.2 Calculation of Reflection Coefficients

The basic equation to determine RCs is the radar equation given in section 3.1.3 and requires a knowledge of the system parameters (P_t , G and L). However, from the calibration graph for the receiver it is possible to eliminate these constants by using the intercept of the y axis (i.e. when the attenuation= 0) to fix the value of the attenuation calculated from the RES data. The RC is then given as:

$$RC = m(D + C) - 20 \log\left[\frac{\lambda_0}{8\pi(H + Z/n)}\right] + 2 \int_0^Z B(Z)dZ \quad (5.3)$$

where m =gradient of calibration graph, C =intercept and D =digital value of signal strength.

5.3.3 Errors

A least squares fit was applied to the linear part of the calibration data (i.e. below the saturation limit of the receiver), the results of which were, for the 1983 values, $m = 0.609 \pm 0.016$ bits/dB and $C = 223.6 \pm 2.7$ bits. From these values it can be seen that the power resolution of the digital recorder was slightly under one half of a dB and that an error of approximately $2\% \pm 1.6\text{ dB}$ is introduced via calibration errors. They are, however, outweighed by the errors associated with the integral of eqn. 5.3 which are $\pm 2\text{ dB}/100\text{ m}$ maximum and are added cumulatively to the calibration errors. Random errors in digitization are ± 1 bit (0.6 dB).

Loss in signal strength due to bed roughness can reduce the mean RC by between 0 and 15 dB (Neal, 1977) and is not an error as such but must be included when analysing the experimental data.

Hence, for typical values of D , there is a total measurement error of ± 1.8 dB and a depth related error of ± 2 dB/100 m. This latter error expresses the **maximum** uncertainty in B and T , and for those glaciers (from the discussion that follows) whose thermal regime can be adequately surmised and where attenuation plots are satisfactory, the error is nearer half this value. Typically IRHs are between 100 and 200 m below the surface, so that the error in RC, ΔR , is 4 to 6 dB. For the glacier bed it will be between 4 and 12 dB. For those glaciers with a well defined \bar{B} , however, the errors are significantly less than this; 3-4 dB and 3-7 dB respectively.

5.4 Reflection Coefficients

5.4.1 Spitsbergen

The complete set of RC data are presented in App. 1 but are summarised in Table 2.1. Considerable variation in the bed RC is observed and in some cases (e.g. Valhallfonna and Olav V Land) they are less than some of the IRH values (Fig. 5.5). This is a surprising result which, taken in isolation, might suggest a misinterpretation of an IRH for bed. It is important, therefore, to consider whether a bed RC of the order of -40 dB (the lowest value measured for the bed) is physically possible. In north-east Spitsbergen rocks are of the Middle and Lower Hecla Hoek complex and comprise greywackes, quartzites and gneisses (Hjelle and Lauritzen, 1982). Such rocks in general have a typical permittivity of about 5 (with a variation of between 4 and 9 (Parkhomenko, 1967)). For a solid, smooth ice/rock interface this permittivity would produce an RC of -19 dB. The rock types mentioned above are all relatively hard and resistant under normal surface conditions. It would seem reasonable, therefore, for them to possess metre-scale bed roughness which could reduce the echo strength by up to 15 dB (Neal, 1977) at best bringing the RC to -34 dB. A second possibility exists if, instead of a solid boundary, a layer of debris rich ice several metres thick were to be present close to the ice-rock interface. Debris-charged basal ice horizons have been reported from many Svalbard glaciers (e.g. Boulton, 1972; Zagorodnov and Zotikov, 1981) and core drilling through Hoganasbreen by the Norwegian mining company, Der Store Norsk Spitsbergen Kullcompagnie, in 1985-'86 demonstrated the presence of debris in a layer of 30 m thickness above the bed (A. Stensrud, personal communication). Consider a basal ice layer containing 70% ice and 30% rock debris by volume, using the Looyenga mixture formula (eqn. 3.24) an RC, for a smooth surface, of -30 dB and a permittivity of 3.7 are obtained. A contribution for the roughness of the reflecting layer can be added to give a value which could explain the observations. It is possibly more appropriate, however, to use the scattering model discussed in section 3.25. Again for a debris concentration of 30% it is found that the average radius of the rock must be less than 2 cm to obtain an RC of -40 dB. This result is not particularly sensitive to the rock concentration chosen. From these arguments it is possible to infer that the bed may be rough on a metre scale and/or overlain by a layer of debris-rich ice thus explaining the low RCs. It does not, however, eliminate the possibility that returns are IRHs. Comparing IRHs from glaciers that also have an unambiguous bed echo with the profiles in Fig. 5.5, it can be seen that there are clear differences. The bed returns do not remain at a constant depth below the ice surface but vary

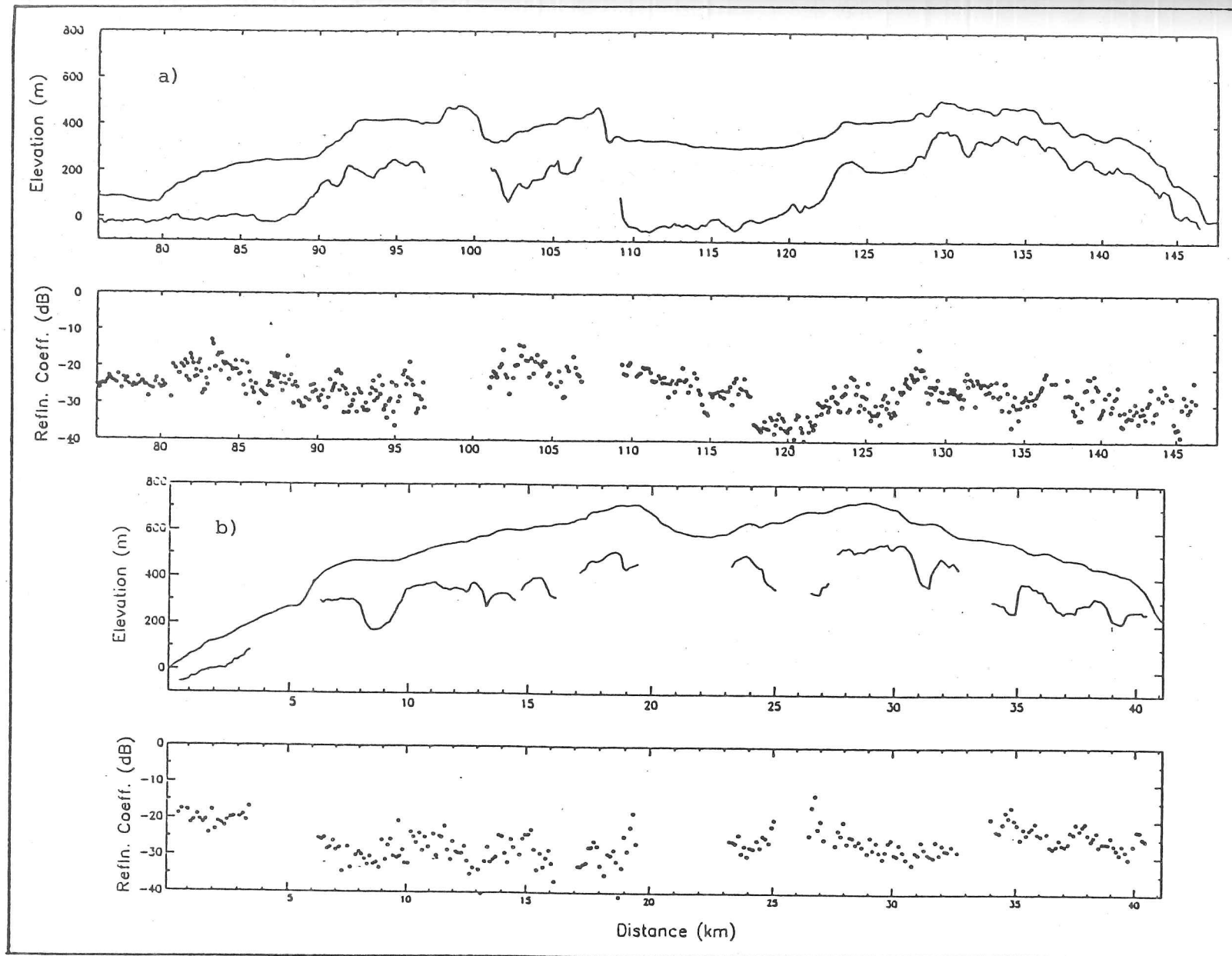


Fig. 5.5 : Glacier profiles and RC data for a) Olav V ice cap and b) Valhallfonna. The RCs are amongst the lowest bed values measured in Spitsbergen.

considerably in their absolute elevation. Oscillograph and 'A' scope records are also markedly different for IRHs and bed echoes (Fig. A1.0 and Fig. 5.8). The explanation for why the bed RCs in this region are some 20 dB less than those of the valley glaciers in the west lies in their different thermal regime and bed environment. It is believed that water is present at the bed of many of the glaciers sounded in western Spitsbergen while for the ice caps in Ny-Friesland it is suggested that they are probably frozen to their beds. In section 3.2.3 the sensitivity of the bedrock RC to the presence of water was demonstrated and the lower RCs virtually preclude the existence of even small quantities. This hypothesis is also supported by the geographical location, altitude and thinness of the ice.

In the following section the high RCs (≈ -10 dB) are investigated. They are observed on many of the valley glaciers in the west of Spitsbergen. The rock types in this region are more variable but are generally softer sedimentary strata. In the north (Albert I Land and Haakon VII Land) Lower Hecla Hoek rocks occur but with a more variable lithology (carbonates and quartzites) and are less resistant than those in the north-east. Further south there is a predominance of Triassic, Middle to Upper Carboniferous and Permian strata—sandstones interbedded with siltstone, shaly siltstone, clay and coal bearing shales. These rocks are less resistant, more soluble and erodable than those in the north-east and also have a higher porosity (M.J. Hambrey, personal communication). The presence of water can increase the bed RC by 10 dB or more (section 3.3.2) depending upon concentration, conductivity and the rock type and the high bed RCs observed on many of these glaciers can be explained by water at the bed although it is also necessary that losses from roughness must be small. Intuitively, these factors appear compatible as warm ice with water at the bed may result in basal sliding—a key factor in erosional (and bed smoothing) processes (Drewry, 1986). The existence of IRHs and heavy internal scattering on many of these glaciers supports the temperate ice hypothesis. The geographical trend in \bar{B} , discussed earlier, is also observed in the RCs. Higher values being found in western Spitsbergen (associated with warmer beds and the presence of water) and the lowest found in Ny-Friesland where the ice is believed to be frozen to the bed and among the coldest in the Archipelago. These results are summarised in Fig. 5.6 which displays the areal distribution of RC strengths across Spitsbergen. It can be seen that RCs > -15 dB are found, almost exclusively, in Oscar II Land and James I Land and those < -20 dB exclusively in north-east Spitsbergen (and Nordaustlandet: Fig. 5.7).

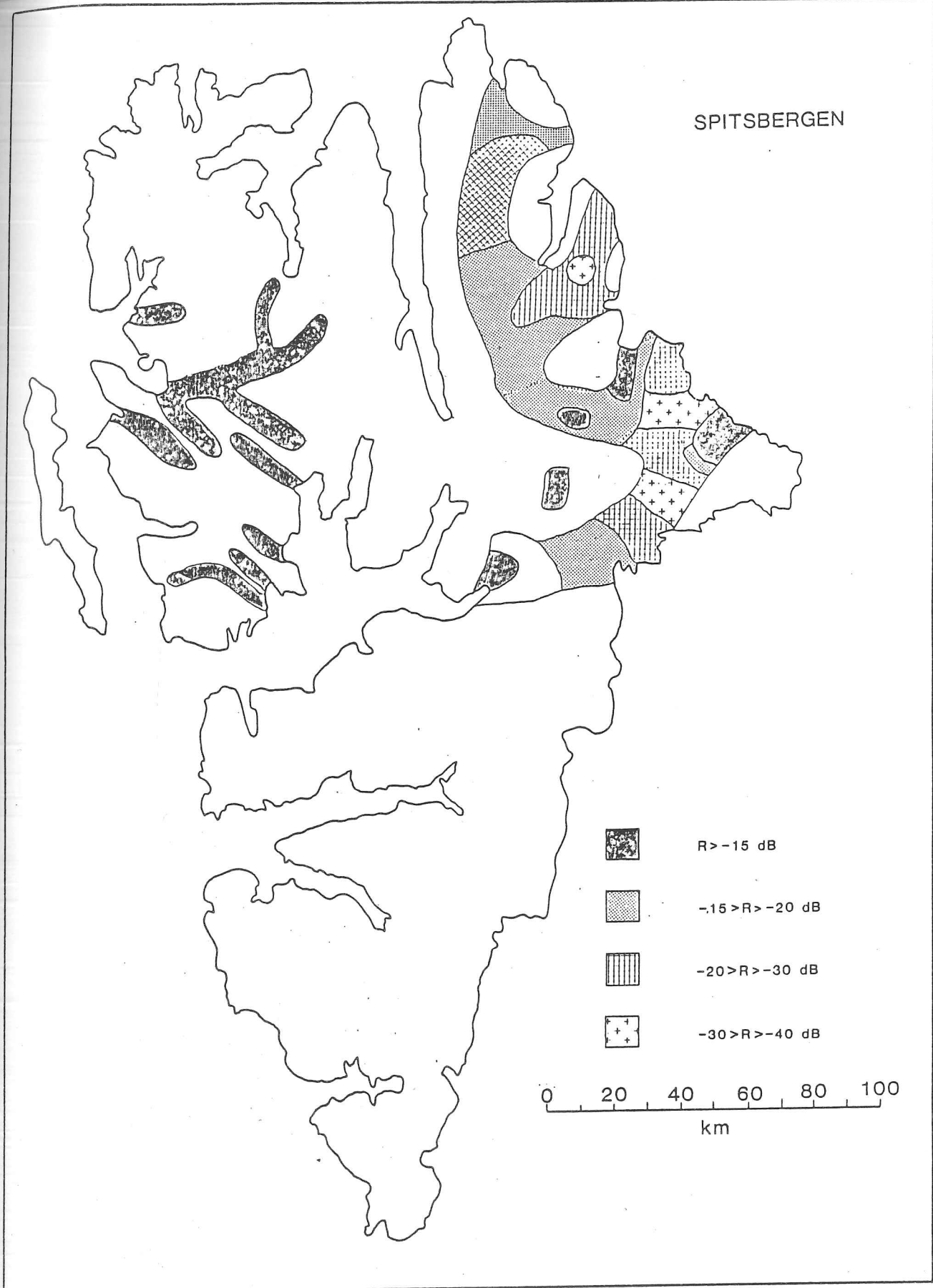


Fig. 5.6 Areal distribution of RC values in Spitsbergen. Unshaded areas had no data.

5.4.2 Nordaustlandet

Fig. 5.7 is a contour map of RCs for Austfonna. Fig. 2.1 b) indicates the high degree of coverage over Nordaustlandet, which has allowed such a representation to be meaningful. Data from Vestfonna were intermittent and difficult to track (Dowdeswell, 1984) and are consequently not shown. The general pattern is one of increasing RCs from the centre of the ice cap towards the margins. It has been suggested that bulk ice temperatures also display this property, so that there would appear to be a proportionality between temperature and RC (as suggested for Spitsbergen). The presence of water in warmer zones maybe to explain. The distribution of sediment plumes around the coast of Austfonna already discussed (Dowdeswell, 1984), suggests that subglacial water is present in most of the areas which have the highest RCs.

The absolute values of RCs from Austfonna are relatively low for typical bed reflections (c.f. Oswald, 1975 and Table 3.1). They are similar to those found for the ice caps and glaciers in Ny-Friesland and Olav V Land and are likely to be due to the same factors that determined those in Ny-Friesland. The Hecla Hoek are of a similar age and include a high proportion of older, harder metamorphics (Hjelle and Lauritzen, 1982). Although water may be present over parts of the bed in Nordaustlandet, the glaciers in western Spitsbergen are likely to possess a greater spatial distribution. This is due to the more temperate nature of the latter ice masses. The greater solubility and carbonate content of the sedimentary rocks also means that the conductivity of the water is likely to be more (M.J. Hambrey, personal communication). Hence its influence is likely to be more limited.

From the discussion above, and the findings of section 5.2.2, it seems reasonable to conclude that bulk ice temperatures become lower moving towards the ice crest and that there is a significant contribution to the RC (≈ 10 dB), in the marginal zones from the presence of water at the bed.

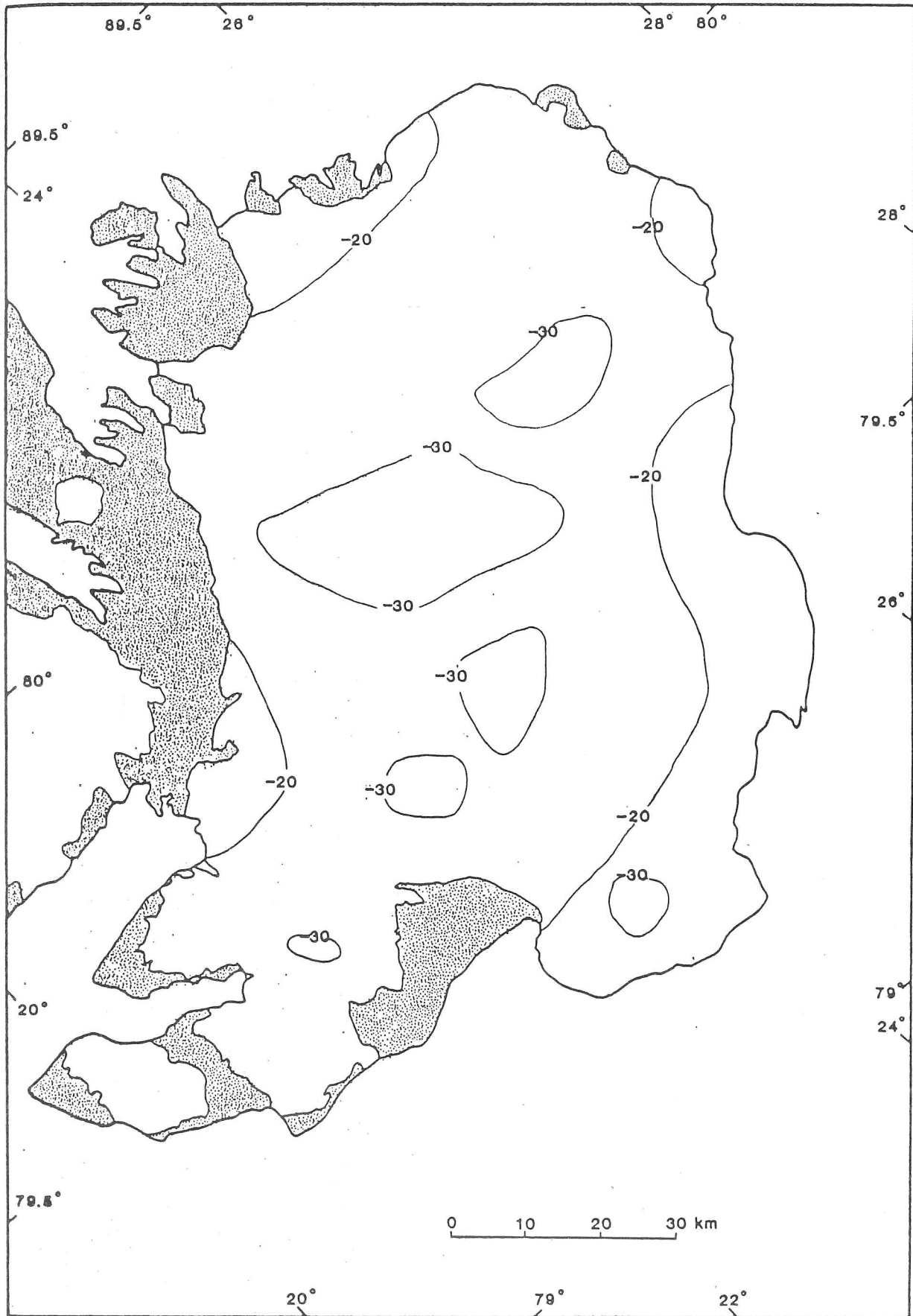


Fig. 5.7 Contour map of RCs in Nordaustlandet.

5.5 Internal Reflecting Horizons

5.5.1 Introduction

The term—internal reflecting horizon (IRH)—is a general descriptor and can encompass a number of different features. Grigoryan *et al* (1985) have tried to categorize those found in Spitsbergen according to their location and continuity within the glacier. IRHs close to the bed (e.g. on Erdmannbreen), they suggest, are due to a moraine layer, which has been verified in cores from Bertilbreen. Those found at greater elevations above the bed were attributed to the existence of a “thermal/hydrological” boundary. Further clues to the origin of an IRH come from its topographic behaviour (i.e. its relationship to the surface and bed, and relative roughness) and its reflecting properties. The former can be used to infer whether the layer is likely to be of a depositional origin (if it follows the flow lines) or if it is some property of the ice which has developed within the ice mass (e.g. temperature, strain history, crystal orientation, air bubble characteristics or water content). The latter (i.e. the reflectivity) can help to elucidate the likely cause of the reflection by considering the effects of a change in ice properties on the dielectric response.

The discussion in this section is directed at those IRHs that appear, on some 60% of the glaciers sounded by SPRI in 1983, as a single continuous horizon ranging in depth from 100–200 m below the ice surface and persisting for up to 20 km along the length of the glacier. They are observed on 19 of the 37 glaciers sounded in 1983 and on a further 10 from 1980. None of the 7 ice caps sounded in '83 indicated their existence. A typical example is shown in Fig. 5.8. It can be seen that the IRH bears a stronger relationship to the surface than the bed, lying at a fairly uniform depth. It does not appear, however, to represent a ‘smooth’ surface (on a radio wavelength scale) and Soviet RES data collected using a frequency of 440 MHz indicate that they may not be continuous on a centimetre scale (Macheret, personal communication). On their records, for some of the glaciers, the IRH appears to be composed of a large number of overlapping hyperbolae (representing individual scattering targets). Sefströmbreen in particular displayed this feature clearly. Another property typical of these IRHs is the presence of internal scattering, often extending for a considerable depth below them, and usually reaching the bed (Fig. 2.6). The geographical distribution of IRHs, conforming to the above description, is shown in Fig. 5.9. The dashed lines indicate glaciers sounded but absent of IRHs and show that the distribution is not an artifact of the areal coverage. There is a greater concentration on the western side of the island, with none being found on the ice caps in north-east Spitsbergen or Austfonna. Vestfonna did not possess any extending over large distances but did have smaller

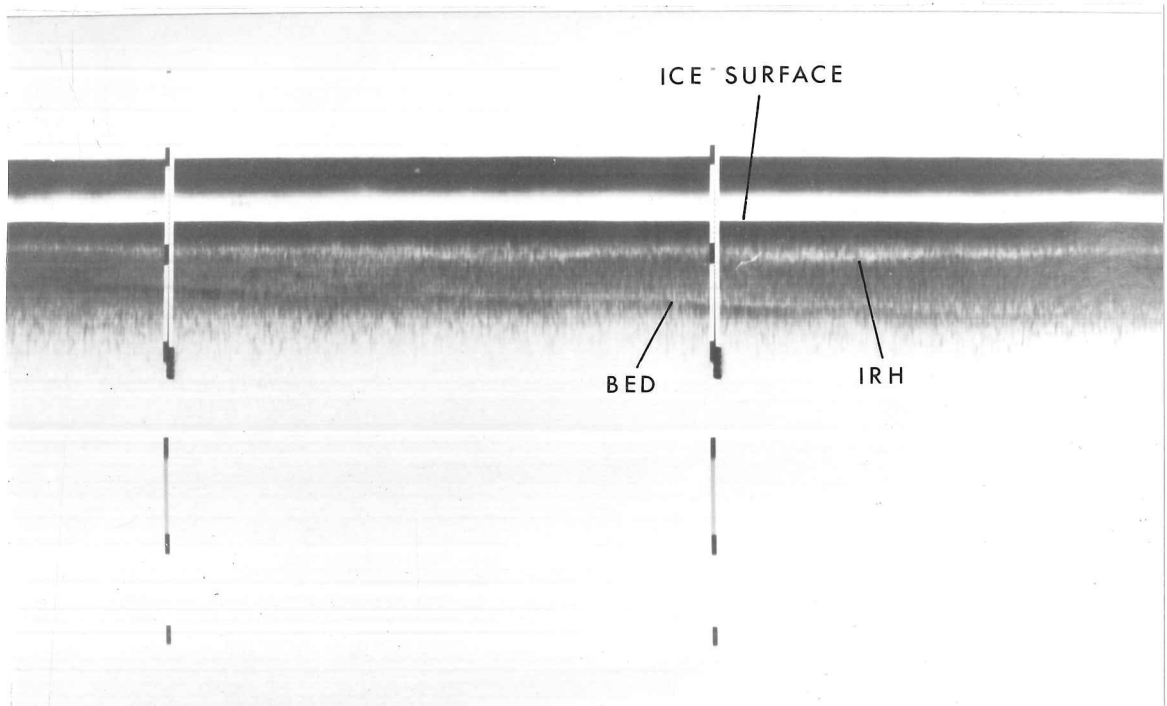
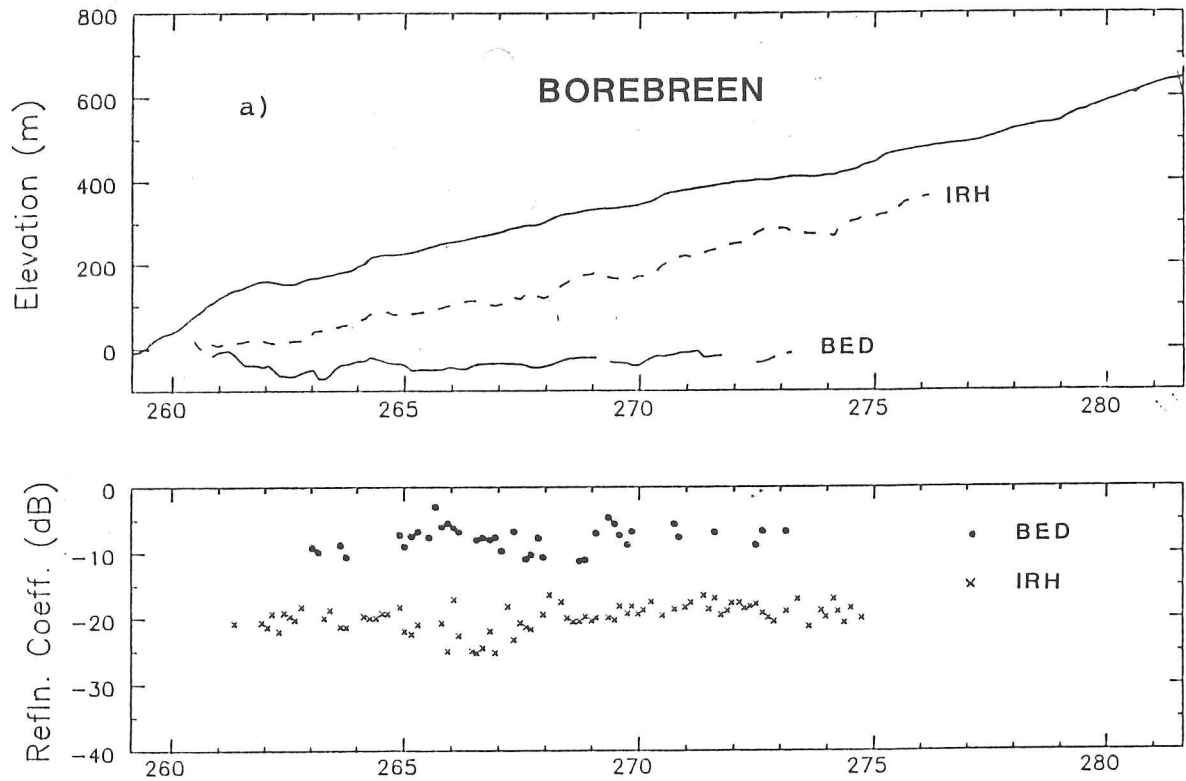


Fig. 5.8 Typical example of an IRH from Spitsbergen. Fig. a) shows the topographic profile with the RC data plotted below. (The convention which will be adopted throughout the thesis is to represent bed by a solid line and solid circles for the RC data and IRHs by a dashed line and crosses for the RC data). Fig. b) is part of an oscillograph record from Borebreen and shows the extended scattering usually found below an IRH.

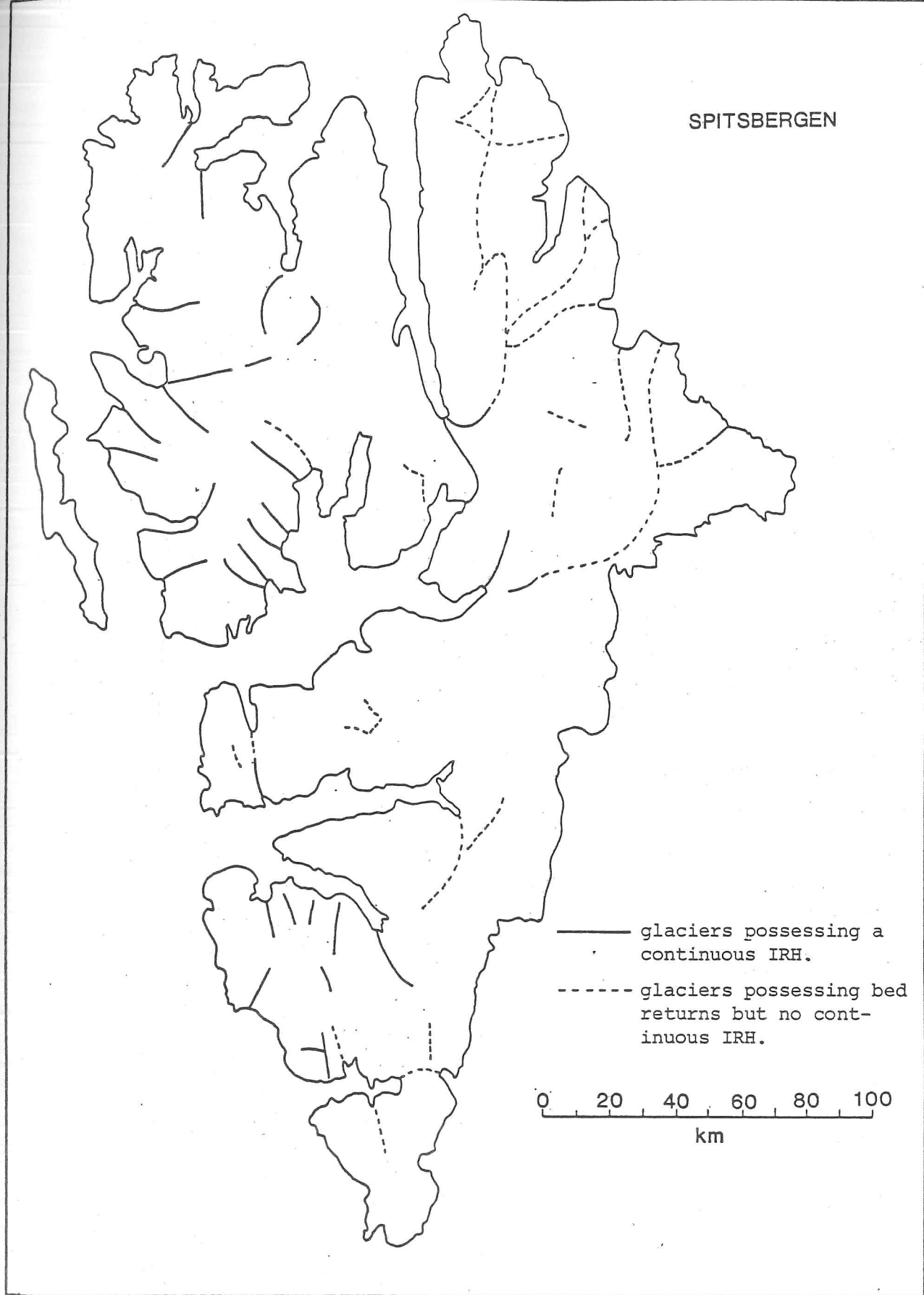


Fig. 5.9 Areal distribution of single, continuous IRHs in Spitsbergen. Data were taken from SPRI field seasons in 1980 and '83 and Soviet soundings. Glaciers with neither bed nor IRH returns have not been included.

segments (< 1 km) located in coastal areas, similar in appearance to those found in Spitsbergen. Typical RCs of the IRHs are about -20 dB.

The characteristics described above are in strong contrast to the depositional type of layer echoes observed in the Antarctic and Greenland (Millar, 1981) which appear to follow the bottom topography or flowlines more closely and which are rarely, if ever, found as single horizons.

5.5.2 Interpretation

Several sources of information have been used in the interpretation of these IRHs including Soviet borehole data and a radio-echo logging experiment (Macheret *et al*, 1984) but the primary dataset are the RCs from SPRI flights. Their values range from between -15 to -30 dB—considerably higher than any other recorded values for an IRH (section 3.2.4) and eliminate the possibility that they could be caused by any of the mechanisms described in that section other than the presence of water. Even considering the maximum possible density variation of solid ice (830 kg m^{-3} to 920 kg m^{-3}) an RC of only -33 dB is possible. It also appears improbable that a layer of depositional origin would persist along the entire length of the glacier, from the accumulation zone almost to the snout. Dirt bands and other depositional discontinuities have even lower RCs (Robin *et al*, 1969; Millar, 1981) and would also be unlikely to persist at such a uniform depth in both the accumulation and ablation zones.

A layer or sheet of water-saturated ice >15 cm thick and of high concentration could generate the observed average values of the RC but it is difficult to envisage how such a sheet could be maintained within the glacier. From this evidence alone, however, it cannot be precluded that the water may be due to a large number of closed-off channels or conduits lying at an impermeable boundary and this concept will be discussed shortly.

5.5.2.1 RC values

The magnitude of the RCs are considered and possible explanations explored. In the following sections calculations are made to estimate the RC from a boundary between wet and dry ice. As explained in Ch. 3, there are two methods of investigating this problem (either as a dielectric boundary or as a scattering phenomenon) and the choice depends primarily on how the water is believed to be distributed.

Nye and Frank (1973) have suggested that the water in temperate glaciers is situated at the crystal grain boundaries, forming a system of interconnecting veins. Lliboutry (1976) has argued otherwise, believing that the veins are broken by the strains in the ice and that all the water is not located at triple grain boundaries. Raymond and Harrison (1975) made observations on the location of water within natural ice samples. They found that it was often present in veins at three-grain boundaries but were not able to verify its continuity because of "interference" by air bubbles. They also observed instances of a high proportion of missing water-filled veins, "pods" and lenses of water. They estimated that the average water content was $\approx 1\%$. Vallon *et al* (1976) also deduced a similar average water concentration in core from an Alpine glacier.

As an approximate indication of the RCs due to a boundary between dry ice and that containing a finite quantity of intragranular water, eqn. 3.25 was used to model the dielectric behaviour of the mixture. The results of the calculation are shown in Fig. 5.10 and imply that unrealistic values for the water content would be necessary to explain the observed RCs by this mechanism.

Combining this result with the observations by Soviet workers on the scattering nature of the IRH it is possible to infer that the water observed may be held in larger 'cavities' or 'conduits'. If a bulk water content of 1% is assumed to be distributed throughout the ice below the level of the IRH then, for a given size the number of 'cavities' present per m^3 may be found. If the cavities are assumed to be spherical then the analysis presented in section 3.2.5 may be used to calculate P_r . The results are shown in Fig. 3.3 where scattering radius, a , is plotted against the effective RC. At a scattering radius of 0.5 m the RC reaches a value of -10 dB. Hence, for sufficiently large 'cavities', the RCs may be explained by this mechanism.

5.5.3 Factors affecting the level of the IRH

It would seem plausible that the IRHs are due to the presence of a finite quantity of englacial water and that this water is most probably distributed anisotropically within the ice. Further support for the latter hypothesis is given when the concepts of classical groundwater hydrology are used to predict the level of the IRH. These are appropriate if the ice is considered to be a porous medium as implied by Nye and Frank's model of water flow. Applying Darcy's law (Fetter, 1980) and Dupuit's assumptions (namely that, for small slopes, the hydraulic head is equal to the surface gradient and that streamlines are parallel to the surface) the piezometric

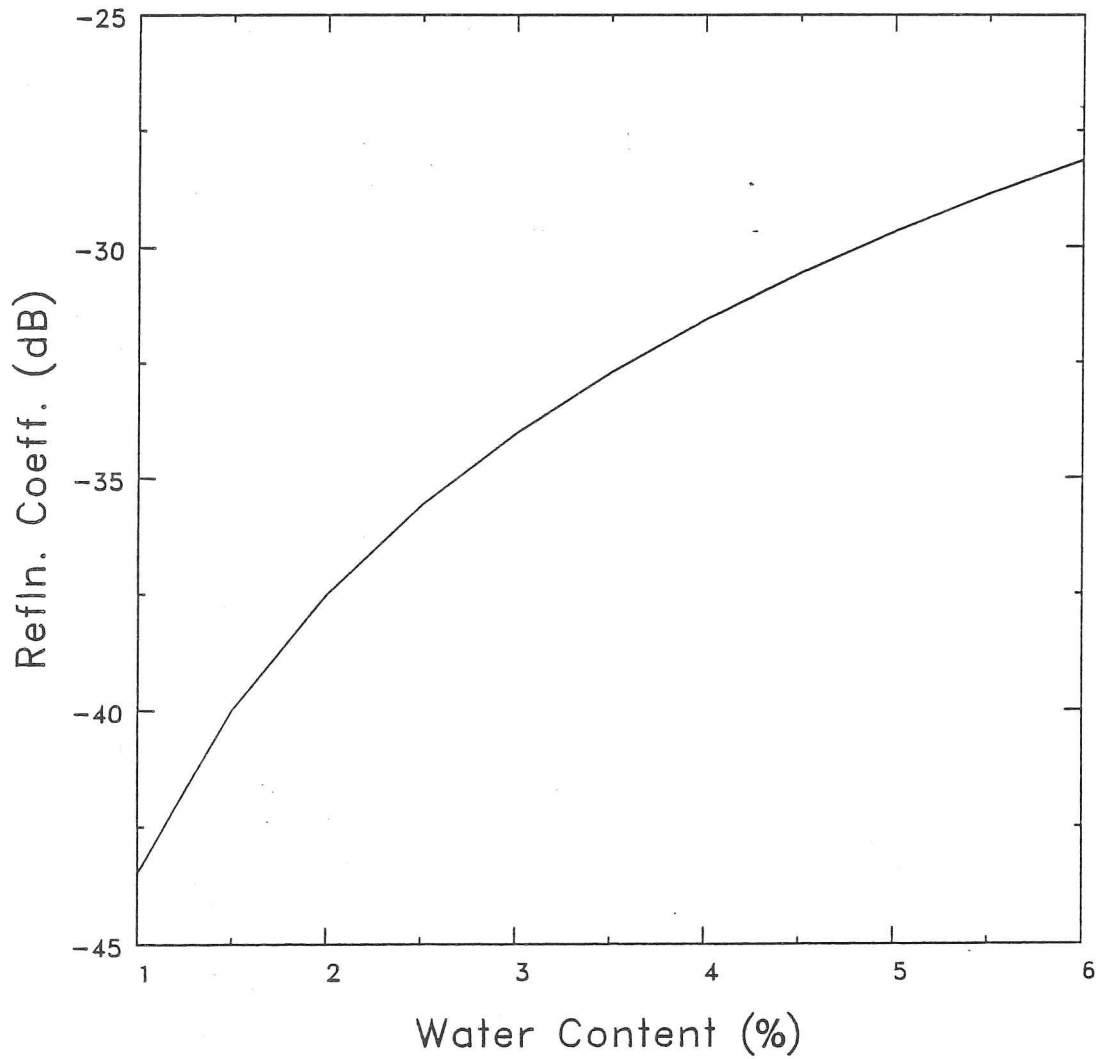


Fig. 5.10 Reflection coefficient vs. water content for a boundary between 'wet' and 'dry' ice. Permittivities were calculated using Rayleigh's mixture formula (eqn. 3.25).

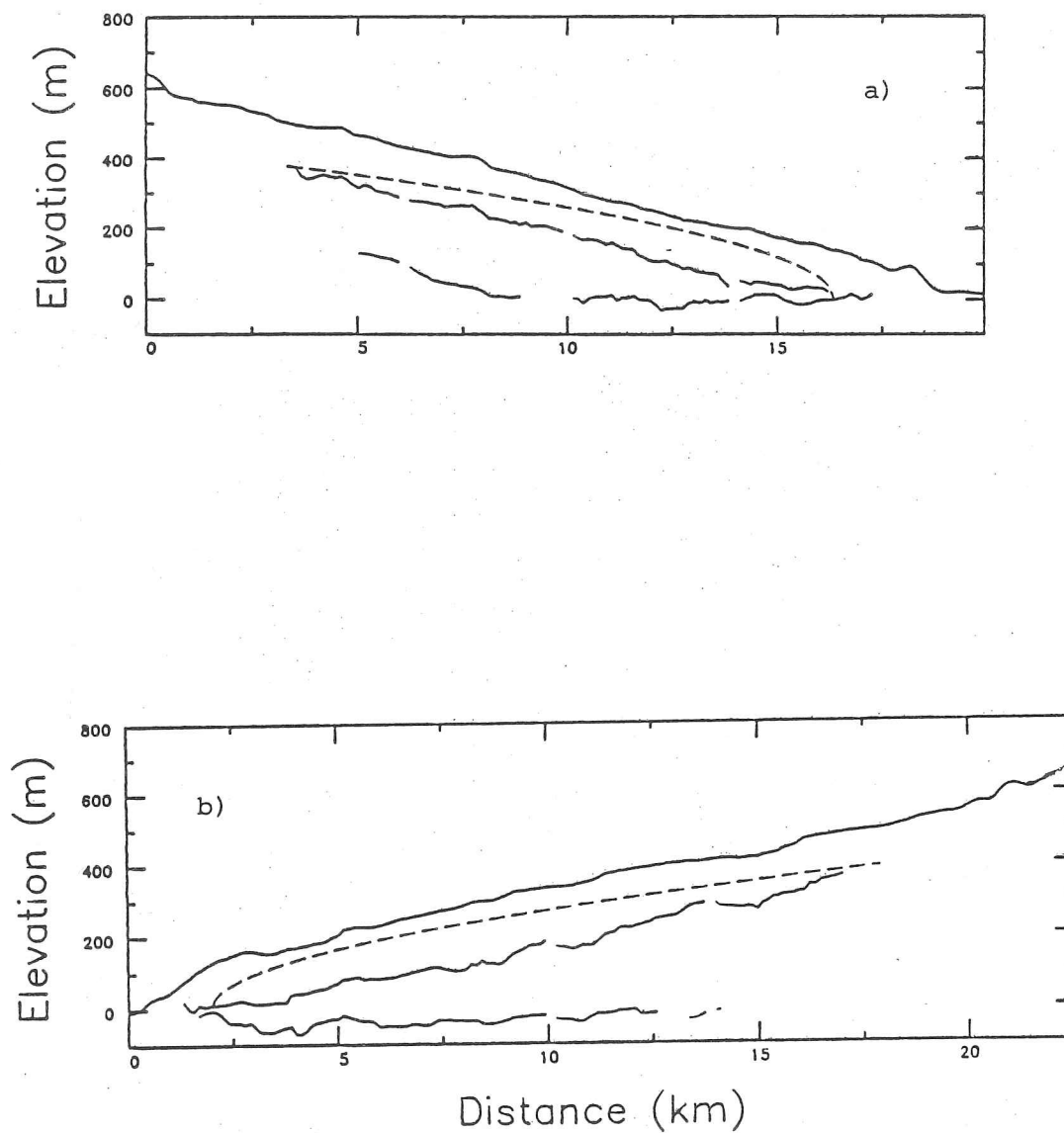


Fig. 5.11 Theoretical 'water table' (dashed lines), calculated from Darcy's law and Dupuit's assumptions, compared with the level of the IRHs in two glaciers- a) Uvêrsbreen and b) Borebreen.

surface of an unconfined aquifer (i.e. the glacier) can be found. If a term is included for drainage at the bed then a depressed parabolic curve is obtained for the hydraulic grade line (i.e. the water level). This is shown in Fig. 5.11 and compared with the real data for Uvêrsbreen and Borebreen. There is poor agreement.

5.5.3.1 R thlisberger Channels

Another model, considered by R thlisberger (1972), is that the water flows in a small number of englacial or subglacial channels. The piezometric surface is now defined by the water pressure within these channels. The equation used to model this hypothesis was

$$\frac{dp}{dx} = \frac{D^{8/11} K^{-6/11} (nA)^{-8n/11} Q^{-2/11} (P - (\rho_i/\rho_w)p)^{8n/11}}{\left[1 - \left(\frac{1}{\rho_w g} D^{8/11} K^{-6/11} (nA)^{-8n/11} Q^{-2/11} (P - (\rho_i/\rho_w)p)^{8n/11}\right)^2\right]^{1/2}} - \rho_w g \tan \beta \quad (5.4)$$

where p = water pressure, $P = \rho_i g z$ (z = ice thickness and ρ_i = ice density), β = bedrock gradient, $D = 3.63 \times 10^{10}$ (Nm^{-2})^{11/8} m^{-3/8} (a physical constant), K = roughness coefficient of the channel, A = flow law constant and n = flow law exponent (assumed to be 3 in this case).

Eqn. 5.4 was integrated numerically to obtain a profile of the piezometric surface along the centre-line of the glacier. This equation describes the water pressure, p , within a gradient conduit¹ and was used because it allows a continuous surface to be calculated, even for negative bed slopes, using the real surface and bed profiles. These latter data were converted into an algebraic form using cubic spline curves, allowing the integral to be evaluated at all points. The flow rate, Q , was estimated by calculating the water produced by strain heating in the lower ice layer and bottom melting due to geothermal heat. It was assumed to vary linearly, reaching a maximum at the snout. Typical values were of the order of 1 m³ s⁻¹.

Springer and Hutter (1981) have suggested a number of modifications to R thlisberger's theory but, as pointed out by Lliboutry (1983), these have little effect upon the hydraulic grade line. Lliboutry (1983) has also suggested modifications which enable more realistic values for the flow law constant to be used. However, as with the previous authors' work, the topographic form is not influenced by these changes. As our primary interest is in the shape of the grade

¹ The topographic form of the piezometric surface for a gradient conduit is similar to that of a subglacial one (R thlisberger, 1972).

line and not the flow law parameters or roughness coefficient, the complications and further unknowns introduced by these modifications are not considered here.

Results of the modelling procedure, for two glaciers possessing IRHs are shown in Fig. 5.12. Different values of the flow law parameter, A , and the roughness coefficient, K have been used to show their effect on the water pressure. It can be seen that they can be altered by a factor of 2 or more without seriously affecting the level of the piezometric surface. Although dp/dx has a weaker power dependence on Q , than either A or K , it is probably the most important parameter as it can vary by several orders of magnitude (Gurnell and Clark, 1987).

It can be seen that the general form of the IRHs is well described by this model. It is not suggested that the values of A or K represent those to be found within the glaciers or that flow will be in a single channel at the hydraulic grade line, but the analysis does indicate that the level of the IRH, along the glacier centre line, has a similar form to that described by a R othlisberger channel. Physically such a model implies that the ice has a large scale network of waterways below the IRH, consisting of conduits and channels, anisotropically distributed within the glacier. These channels will represent discrete radar scatterers.

Evidence for the existence of large scale inhomogeneities, consistent with the model proposed above, comes from a study made by Hodge (1976) on the temperate South Cascade Glacier in Washington state. In the course of drilling a number of boreholes Hodge observed sudden drops in the level of the drill which he associated with the presence of a 'cavity'. The size of these cavities ranged between the limit of detection (0.05 m) to a maximum of 0.86 m with an average value of 0.25 ± 0.21 m. He also observed that the 'cavities' tended to cluster about a line suggesting that this might be related to a R othlisberger gradient conduit. Similar observations have also been made by Schommer (1977) on a temperate glacier in Switzerland.

5.5.3.2 Thermal Regulation

One more factor that may have an important influence on the level of the IRH is heat conduction across its surface. Unlike temperate glaciers, 10m temperatures in Spitsbergen ice can be several degrees below zero and it is possible that the IRH may reflect the pressure melting isotherm. A simple calculation of the temperature gradient needed, to have a significant influence on the water level, suggests that this effect is, however, of a secondary importance. By making an order of magnitude estimate of the maximum heat flux across the surface of the IRH it can be shown that this is insufficient to remove a significant amount of water, and hence

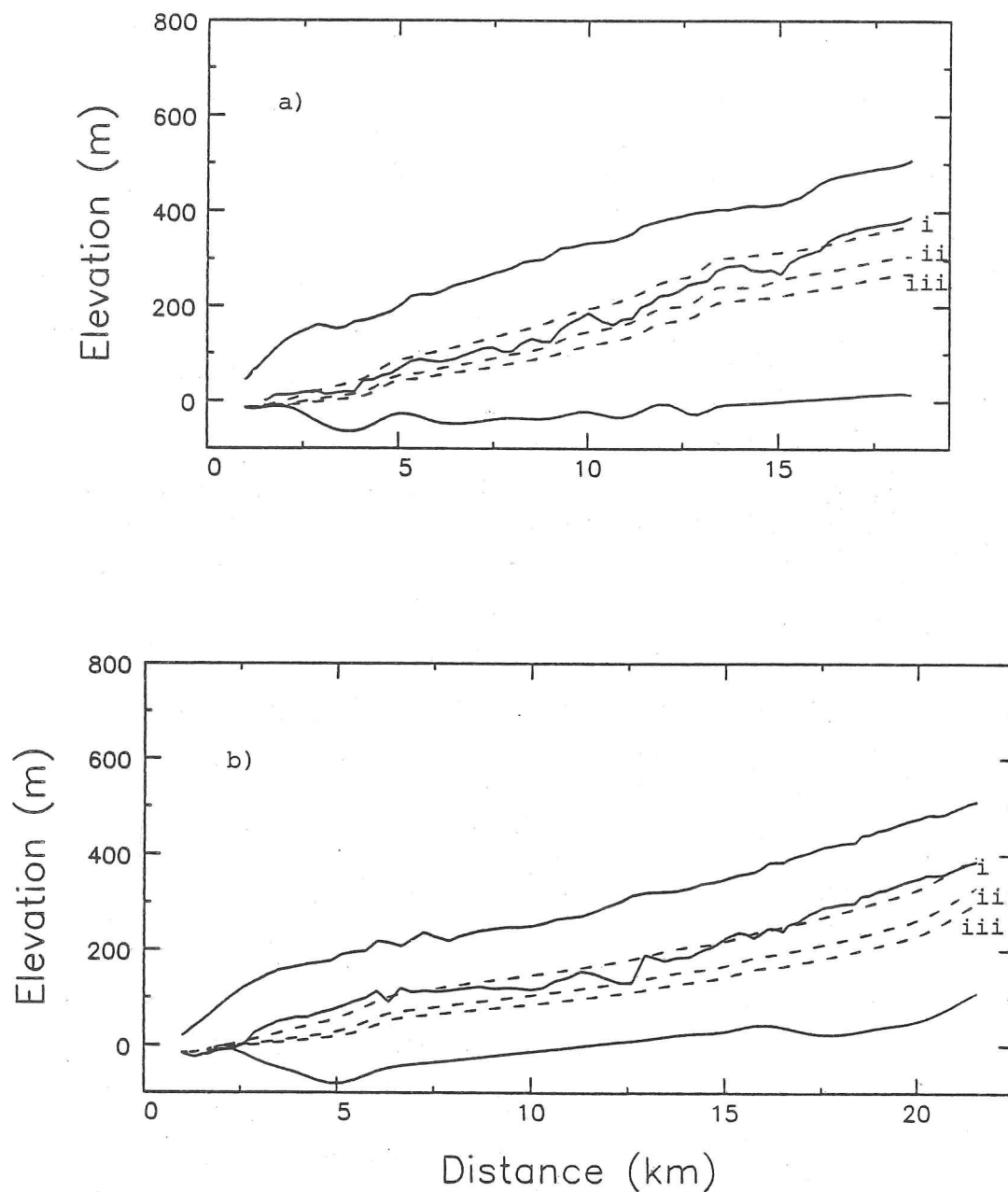


Fig. 5.12 The piezometric surface (dashed) calculated from Röthlisberger's equation for a gradient conduit. Curve i) was calculated using $A=4 \cdot 10^7 \text{ Pa s}^{-\frac{1}{2}}$, $K=100 \text{ m s}^{-1}$; ii) $A=6 \cdot 10^7 \text{ Pa s}^{-\frac{1}{2}}$, K as for i); iii) A as for ii), $K=200 \text{ m s}^{-1}$. The model surfaces are compared with the IRHs from a) Borebreen and b) Eidembreen.

that thermal regulation is unlikely to have a strong and direct influence on the level of the IRH.

The heat involved in freezing 1% of water is $3.4 \times 10^6 \text{ J m}^{-3}$. Let the surface temperature be approximately -1°C and the thickness of ice above the IRH 100 m. The maximum reasonable temperature gradient at the interface is then of the order of 0.1°C . The heat flux across the boundary is 0.21 W m^{-2} . With these values it would take about 165 days to freeze a layer 1 m thick. The water pressure, and hence water level, in temperate glaciers varies by considerably more on a seasonal basis (Hantz and Lliboutry, 1983). If the same is true for Spitsbergen glaciers, it seems unlikely that thermal regulation will be as important as water pressure. The small scale roughness of the IRH supports this conclusion, as a thermally regulated boundary would be expected to be smooth on a 10 metre scale. Although heat conduction across the boundary may not be important in defining its level the fact that the overlying ice may be cold and possibly impermeable as a consequence may be important—the existence of an impermeable boundary would limit the extent to which the water could rise in the network of englacial channels.

In conclusion, it would seem that the IRHs, considered above, consist of a number of englacial water cavities or channels. The upper elevation limit (the piezometric surface) appears to be most adequately described by a Röthlisberger channel which, if located at the bed, implies interconnection, at some time, between the subglacial drainage system and the piezometric surface. The existence of water, at depth, within the glacier has a number of important implications. It suggests that a significant portion of the ice must be close to the melting point. This could have a marked influence on the flow properties of the ice. Duval (1975) has shown that there is an order of magnitude increase in the strain rate for ice with $V_w=0.01$ relative to that with a negligible concentration. The presence of water may also effect the crystal fabric, reducing strain hardening and crystal size (Lliboutry, 1976). If impurities (specifically acids) are concentrated at grain boundaries as has been suggested by Wolff and Paren (1984) then flushing may have an important influence on the purity and hence dielectric properties of the ice (Glen *et al*, 1977). Hence the deduction that a significant volume of water is present within the ice is of considerable glaciological importance.

Having examined some of the more general features of the glaciers sounded, a number of ice masses with atypical properties are considered below.

5.5.3.3 Extraordinary Glacier Profiles

Vonbreen

This glacier shows a discontinuity in both the bedrock elevation (of some 80 m) and the bed RC (5.5 dB) at a track distance of 145 km (Fig 5.13). The oscillograph, from this section, displays a large hyperbola, indicating the presence of a 'corner' reflector or discontinuity. On the geological map a major geological fault has been marked running down the Vonbreen valley. It represents the division between the Lower Hecla Hoek to the east (gneiss, granite) and Devonian (Wood Bay Formation) to the west. It is suggested that the discontinuity seen in Fig. 5.13 marks the location of this fault. The level and strength of the IRH appear to be completely unaffected, at this point, by the existence of the fault, although its behaviour does vary upstream. A similar fault line has been assumed to run along the length of Isachsenfonna (which lies to the west and parallel to Vonbreen) but no bed data were obtained from this ice mass.

Veteranen and Chydeniusbreen

Two anomalous and interesting glacier profiles will be considered here—Veteranen and Chydeniusbreen. Their profiles and RCs are shown in Fig. 5.14 a) and b) respectively. These two glaciers were the deepest sounded in Spitsbergen (the ice thickness on Veteranen reached a maximum value of 656 m) and this in itself may play an important rôle in explaining the observations. As has been seen they are both from a colder and more 'arid' part of the island (Hisdal, 1985) and underlain by harder rocks (Veteranen lies in a valley that separates the Lower from Middle Hecla Hoek the former comprising gneisses and the latter greywackes and quartzites). The bed RCs are intermediate in value (mean value of -23.2 dB) while the level of the IRH in these glaciers is deeper than is typical and far from constant in depth. The two short sections which come within about 150 m of the ice surface are clearly not bed reflections. This can be seen both from the oscillograph records (Fig. 5.15: marked A) and the fact that there is no expression of these features in the ice surface. Their RCs are, however, only about 5 dB less than those assumed to be of the bed. Further, they are some 10 dB stronger than the near-bed internals appearing further up glacier. It seems likely, therefore, that there may be two separate mechanisms responsible for the two types of IRH. One due to the presence of water and the other possibly caused by a moraine layer. The values of the RCs are entirely consistent with these two hypotheses and it is interesting to note that the existence of the near-bed internal

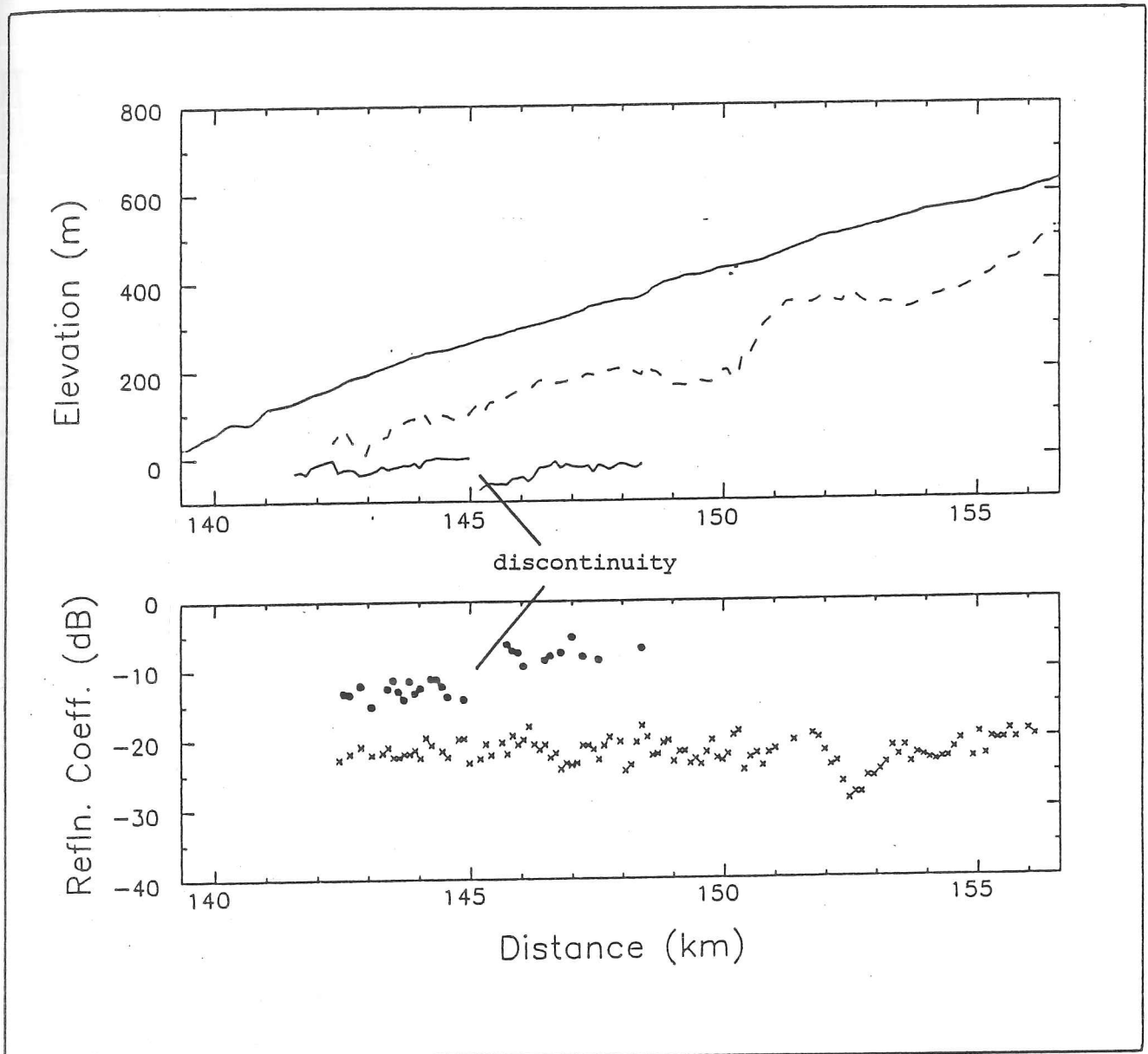


Fig. 5.13 Glacier profile and RC data for Vonbreen indicating the location of the discontinuity.

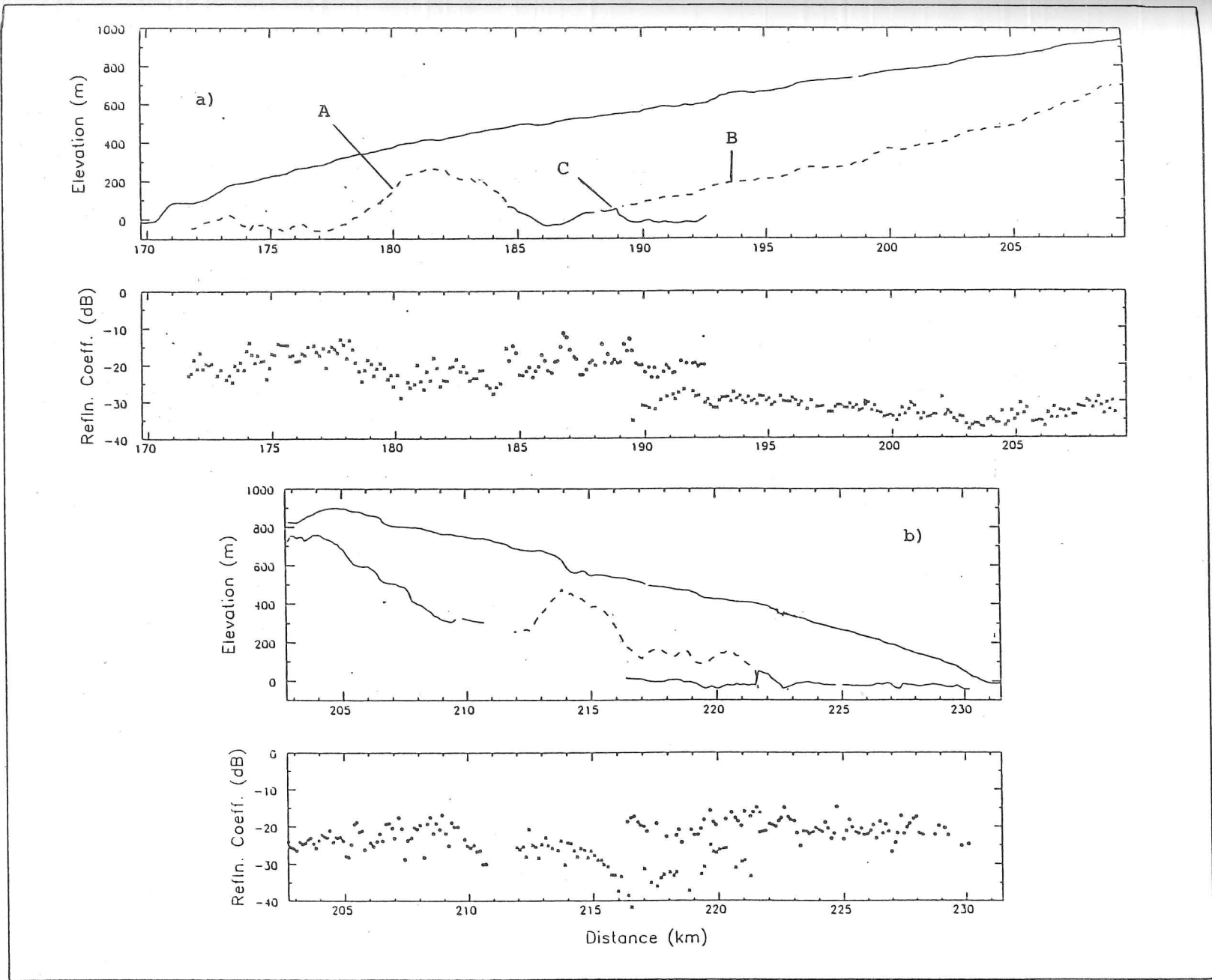


Fig. 5.14 Glacier profiles and RC data for a) Veteranen and b) Chydeniusbreen.

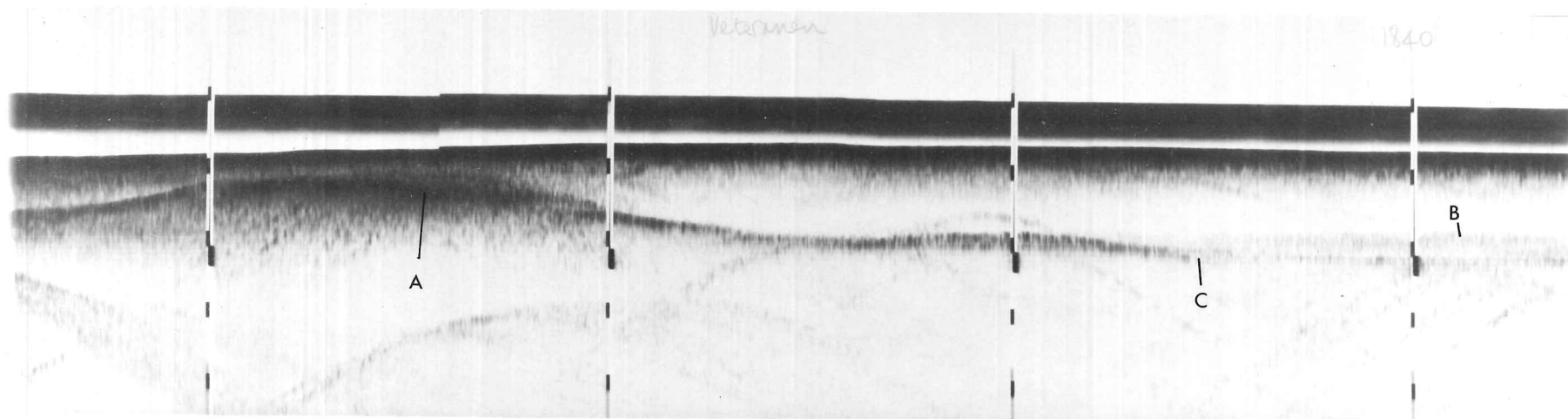


Fig. 5.15 Part of an oscillograph record from Veteranen displaying the extraordinary IRH towards the glacier snout (A) and the near-bed IRH further up glacier (B). The location of the change in reflecting properties, associated with a geological divide can also be seen (C).

coincides with the transition from one rock type to another, on both glaciers. Although it cannot be determined unambiguously how thick the higher elevation internal layer is, it is clear, from the oscillograph, from Chydeniusbreen in particular, that it is not just a surface of scattering bodies but extends to some depth (of the order of 200 m in thickness). It does not, however, appear in this case to reach the bed unlike many of the IRHs from the glaciers in western Spitsbergen.

At an early stage the possibility that the internal horizon on Veteranen, starting at 189 km (Fig 5.15: marked B), might be due to reflections from the side walls of the glacier was dismissed for two reasons. First, on several parts of the oscillograph records valley-wall reflections were visible as discrete targets having a range different to the internal. Second, the internal is too constant in both echo strength and continuity to be due to side-wall scattering. The IRH cannot be due to multiple reflections between the aircraft and surface as it does not have the correct time delay.

Even though the RCs (of the second, deeper IRH; B) are lower than those from western Spitsbergen, they can still only be satisfactorily explained by a limited number of factors. The change in permittivity or conductivity necessary to produce such values are of the order of 0.23 and $7.5 \times 10^{-4} \text{ S m}^{-1}$ respectively. From equation 3.24 it is apparent that a density variation cannot be responsible (an 8% change in bubble volume would be required). The change in $[\text{H}^+]$ necessary to produce the $\Delta\sigma$ quoted above, is of the order of $4 \times 10^{-4} \text{ M}$ (Millar, 1981) and is clearly non-physical. The only mechanisms which are sufficient to produce the high IRHs observed are the presence of water or moraine. In Fig. 5.16 the effective RC of englacial moraine with a permittivity of 9 is plotted against scattering radius, for a volume fraction of 0.01. It can be seen that if the average radius of the debris is ≈ 7 cm then the RCs, for the near-bed internal on Veteranen could be due to this cause. There is a considerable amount of exposed rock in the vicinity of Veteranen that could give rise to the entrainment of moraine. The reflecting power is very invariant locally (more so than typical bed profiles) and the topography of the internal very smooth. All these observations are consistent with a continuous layer of moraine entrained within the ice and emanating near the head of the glacier. There is one major limitation to this hypothesis: the form of the IRH does not appear to follow a typical steady-state flow line, which would be a necessary requirement. Second, aerial photographs of the terminus do not indicate the presence of significant moraine near the snout.

The possibility that the reflection is due to water cannot be dismissed. If the level of the

coincides with the transition from one rock type to another, on both glaciers. Although it cannot be determined unambiguously how thick the higher elevation internal layer is, it is clear, from the oscillograph, from Chydeniusbreen in particular, that it is not just a **surface** of scattering bodies but extends to some depth (of the order of 200 m in thickness). It does not, however, appear in this case to reach the bed unlike many of the IRHs from the glaciers in western Spitsbergen.

At an early stage the possibility that the internal horizon on Veteranen, starting at 189 km (Fig 5.15: marked B), might be due to reflections from the side walls of the glacier was dismissed for two reasons. First, on several parts of the oscillograph records valley-wall reflections were visible as discrete targets having a range different to the internal. Second, the internal is too constant in both echo strength and continuity to be due to side-wall scattering. The IRH cannot be due to multiple reflections between the aircraft and surface as it does not have the correct time delay.

Even though the RCs (of the second, deeper IRH; B) are lower than those from western Spitsbergen, they can still only be satisfactorily explained by a limited number of factors. The change in permittivity or conductivity necessary to produce such values are of the order of 0.23 and $7.5 \times 10^{-4} \text{ S m}^{-1}$ respectively. From equation 3.24 it is apparent that a density variation cannot be responsible (an 8% change in bubble volume would be required). The change in $[\text{H}^+]$ necessary to produce the $\Delta\sigma$ quoted above, is of the order of $4 \times 10^{-4} \text{ M}$ (Millar, 1981) and is clearly non-physical. The only mechanisms which are sufficient to produce the high IRHs observed are the presence of water or moraine. In Fig. 5.16 the effective RC of englacial moraine with a permittivity of 9 is plotted against scattering radius, for a volume fraction of 0.01. It can be seen that if the average radius of the debris is $\approx 7 \text{ cm}$ then the RCs, for the near-bed internal on Veteranen could be due to this cause. There is a considerable amount of exposed rock in the vicinity of Veteranen that could give rise to the entrainment of moraine. The reflecting power is very invariant locally (more so than typical bed profiles) and the topography of the internal very smooth. All these observations are consistent with a continuous layer of moraine entrained within the ice and emanating near the head of the glacier. There is one major limitation to this hypothesis: the form of the IRH does not appear to follow a typical steady-state flow line, which would be a necessary requirement. Second, aerial photographs of the terminus do not indicate the presence of significant moraine near the snout.

The possibility that the reflection is due to water cannot be dismissed. If the level of the

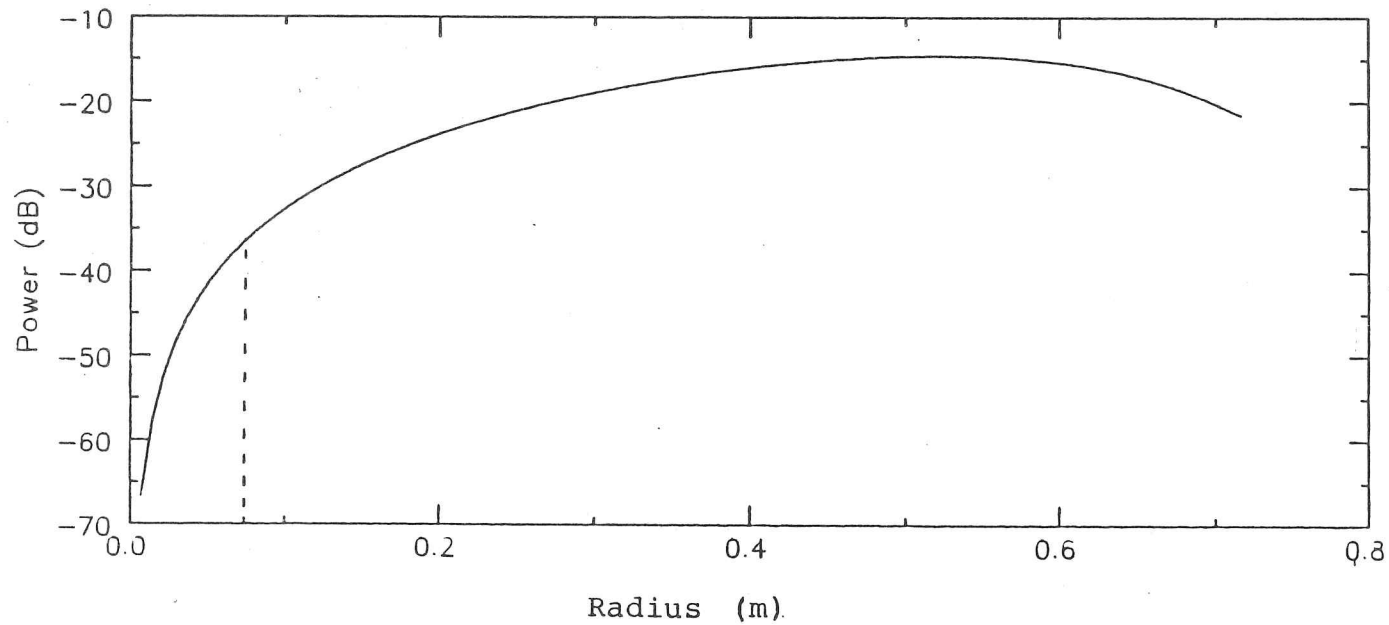


Fig. 5.16 Effective RC (from scattering) vs. scattering particle radius for rock of permittivity 9. The minimum radius required to obtain the observed RCs is indicated by the dashed line. The volume fraction of rock was taken to be 0.01. Changing this value shifts the curve up or down the Y axis.

IRH can still be modelled by a Röthlisberger channel then the fact that it reaches the bed might be explained by the snout being frozen to the bed beyond this point. It is difficult to apply eqn. 5.4 (Röthlisberger's eqn.) to Veteranen because of the lack of bed data beyond 189 km track distance. If, however, a hypothetical bed profile is fitted then an estimate of the piezometric surface can be made. This procedure produced two relevant results. First, to reproduce the shape of the the IRH, a concave (upwards) bed profile was necessary (similar to that of Chydeniusbreen). Second, to obtain the correct absolute elevation, the flow rate required was of the order of $500 \text{ m}^3 \text{ s}^{-1}$ (approximately 500 times that estimated for the glaciers in western Spitsbergen). This value is unrealistic (Gurnell and Clark, 1987) and implies that, if the IRH is due to the presence of water, then its level does not seem to be related to the subglacial water pressure. From the evidence available it is not possible to attribute this deep reflection unambiguously to moraine rather than water and its cause must consequently remain uncertain.

It was noted above that the Veteranen and Chydeniusbreen valleys are split by geological divides and this is now considered, as an additional factor. Examination of the oscillograph record for Veteranen indicated, that at the point where the near-bed internal begins, there is a dramatic change in the nature of the bed echo (Fig. 5.15: marked C). In Fig. 5.17 the digitally recorded waveforms are plotted. Each frame comprises a single 'A' scope separated, in time, by 2 seconds. At a flight time of 183924, the echo begins to become weaker and significantly broader and in a space of 12 seconds (equivalent to 720 m) the signal has been reduced by some 6 dB and is more 'diffuse'. The point along track when this occurs coincides identically (within experimental errors) with the position of what is believed to be a geological boundary between Lower and Middle Hecla Hoek. The former consists of high grade metamorphics (amphibolite, gneiss, psammite and pelites), the latter of quartzites, greywackes, some limestone and volcanics (M.J. Hambrey, personal communication) and consequently have both different chemical and weathering characteristics.

A geological boundary between Middle to Upper Carboniferous rocks and the Middle Hecla Hoek was also crossed on the Chydeniusbreen flight line and although it is not as apparent on the RES records its location does coincide with the start of the 'hummock' observed in the profile.

How these geological divides might influence the existence and location of an IRH is not clear and it is possible that their presence is entirely coincidental. It is conceivable that the

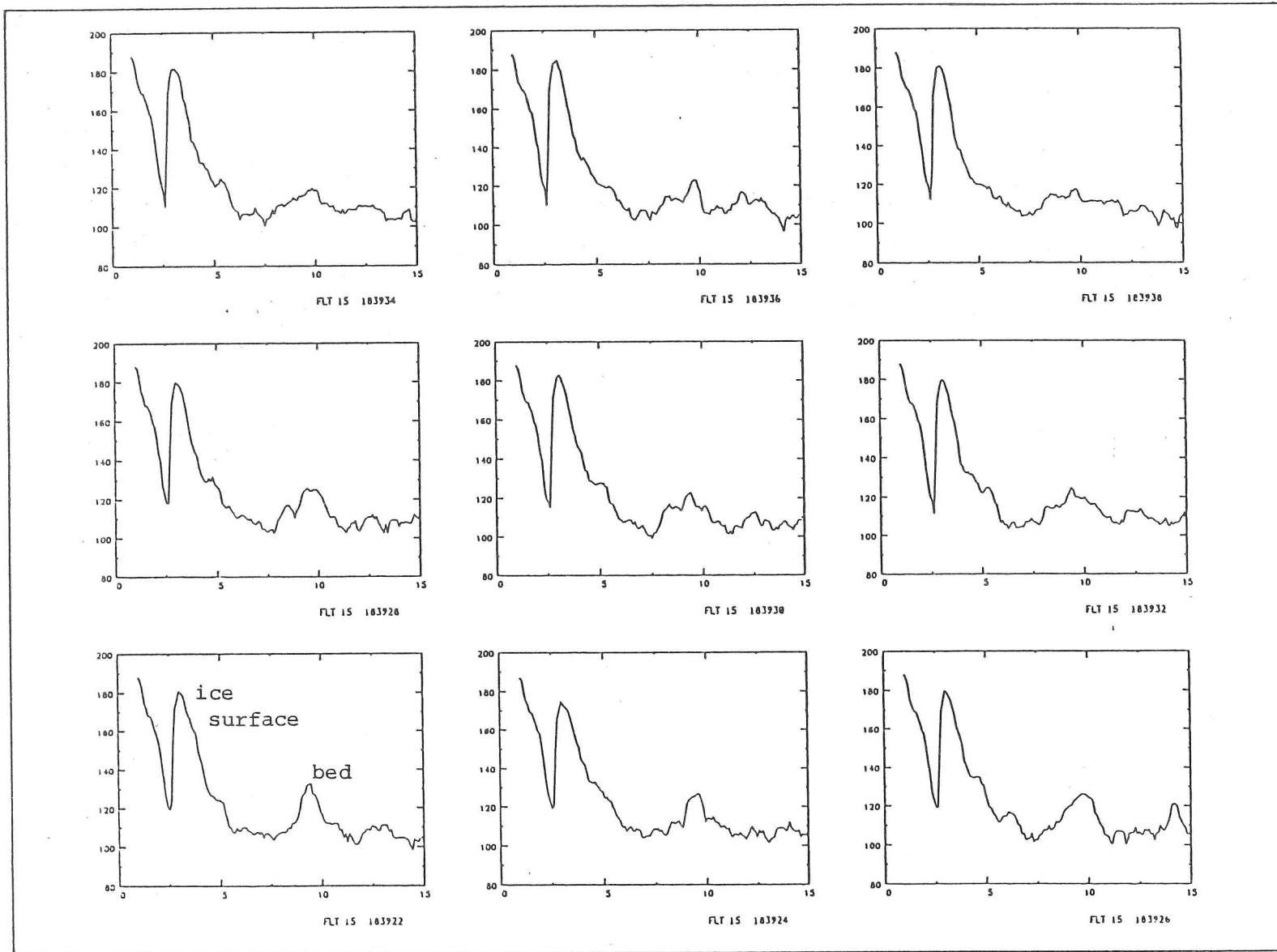


Fig. 5.17 Digitally recorded 'A' scopes for the section of Veteranen where the reflecting properties of the bed undergo a significant change.

change in reflecting properties, indicated in Figs. 5.15 and 5.17, is due to the transition from an area with water present to one where the ice is frozen to the bed. If the geological divide is a boundary between rocks with different heat capacities then it is possible that the slightly different geothermal temperature gradients, either side of the divide, might influence the location of the transition from frozen to wet bed.

In the absence of field data, these hypotheses can only remain speculative. A borehole and/or temperature data would greatly enhance the understanding of the processes governing these two ice masses. Two more conclusions can, however, be drawn. The first is that the short, higher elevation IRHs, in both glaciers, which are present near the snout, must be due to the presence of water. The second conclusion relates to the deduction of the surface temperatures. In the analyses of section 5.2.1 it was shown that the bulk ice temperatures further upstream are significantly lower than 0°C . Using this deduction and assuming that the basal ice temperature in Veteranen is close to the melting point, and applying a linear temperature profile, a surface temperature of approximately -5°C is deduced for the upper part of the glacier (i.e. beyond 189 km along track). If Clarke *et al*'s (1977) temperature profile model is used to calculate the absorption, then this value is nearer -8°C .

5.6 Summary

In this chapter the main findings from the RES field work have been presented. It has been suggested that the low RCs from Valhallfonna, Åsgårdfonna and Olav V ice cap necessitate a rough interface probably consisting of debris laden ice which is frozen to its bed. The high bed RCs found on many of the glaciers in western Spitsbergen, it is argued, are due to a porous erodable interface with significant quantities of water present. Hence these glaciers have the potential to slide. RCs in Nordaustlandet were found to be similar to those from Ny-Friesland, in the central zone, increasing towards the margins. It was suggested that the latter effect was due to the presence of subglacial meltwater. A geographical trend in absorption, RCs and the existence of a particular type of IRH was found. It was suggested that this was linked to the climatic trends (and hence glacier thermal regime) moving east and north. An observed east-west gradient in the concentration of H^+ ions in snow samples was also considered as a possible contributory factor to the regional differences in mean absorption. Higher RCs and a greater concentration of IRHs were found in western Spitsbergen. The lowest RCs and mean absorption values came from Ny-Friesland. Two geological divides were observed from a change

in the reflecting properties of the ice/bed interface.

The only satisfactory explanation for the single, continuous IRHs was found to be the presence of water **within** the ice mass and it was shown that the level of the englacial water can be satisfactorily modelled by a Röthlisberger channel.

APPENDIX 1

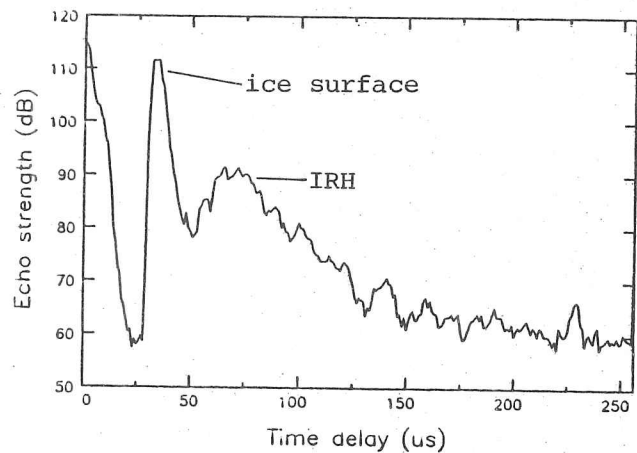
Glacier Profiles and RC data

Glacier profile and RC data obtained from the two RES field seasons in 1983 and '85 are presented. The results have been split into five parts covering the different regions sounded (Fig. A1.1). A map is shown at the beginning of each section covering the area defined by the boxes in Fig. A1.1. The numbering system, for the airborne data, is related to the different flights, starting in the west and moving eastwards. Flight 08 (F08) incorporated profiles 1-13, F09: 14-22, F01: 23-24, F151 (ft. 15 part 1): 31-34 and F152: 35-44.

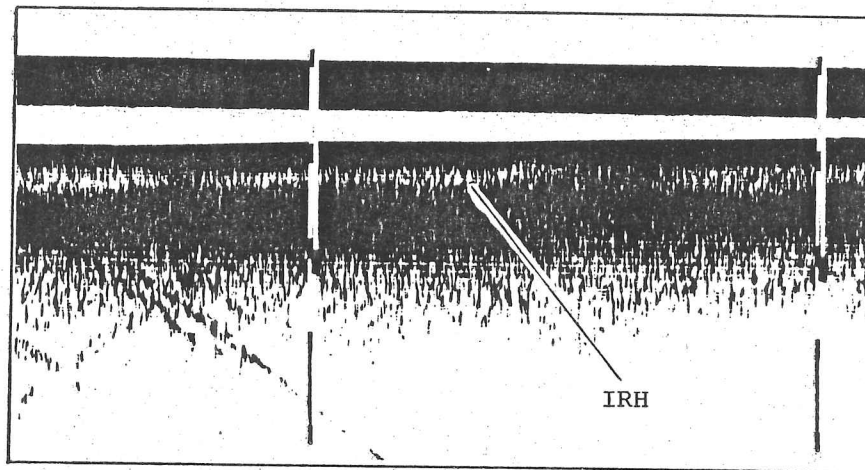
Identification of Bed and IRH Returns

The existence of a strongly reflecting IRH can lead to the misinterpretation of the bed (Dowdeswell *et al.*, 1984a). Ambiguities arise from a combination of the topographic nature and reflectivity of the boundary. Two examples of this problem were discussed briefly in Ch. 2 (namely Negribreen and Holmstrombreen). Such ambiguity can be substantially reduced by examination of all the available RES data (i.e. the digital 'A' and 'Z' scope records and the analogue oscillographs). In general, bed echoes decay more rapidly than IRHs which tend to scatter power for an extended period after the first return. i.e. the bed echoes are 'sharper' and more 'peaked' while the internal echoes are extended and decay slowly. These properties are illustrated in Fig. 2.3. An example of where misinterpretation was possible is shown in Fig. A1.15. Dunérbreen possesses an IRH of a similar reflectivity to the boundary tracked in Åsgårdfonna and the altitudes of the two are also similar. Examination of the 'A' scope and oscillograph data (Fig. A1.0) indicates, however, that they are of a markedly different nature and that the latter has properties more closely resembling that of typical bed echoes.

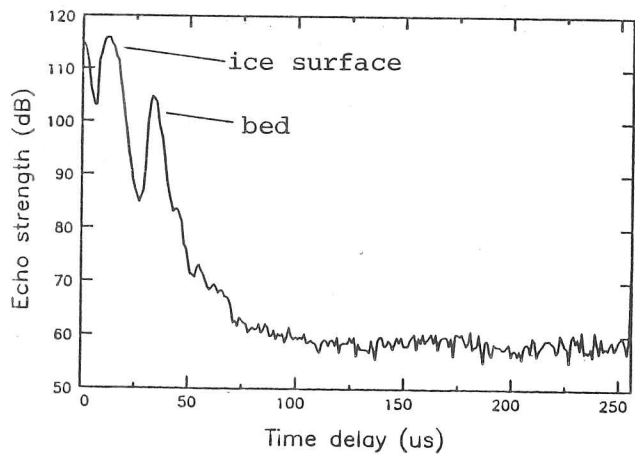
IRHs are shown dashed and the bed as solid lines. For the RCs, crosses represent the former and shaded circles the latter. The location of very approximate equilibrium lines (taken from Fig. 1.7) have been included and are shown by vertical arrows. t_b give an indication of the position of IRH and bed returns in relation to the mass balance zone.



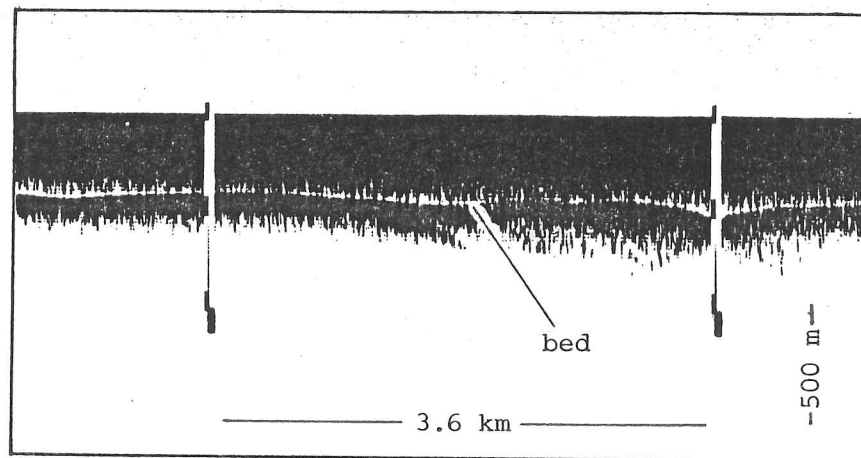
a)



b)



c)



d)

Fig. A1.0 Diagram illustrating the differences between echoes from the bed and an IRH. Fig. a): digital 'A' scope from Dunérbreen; b) oscillograph record from same region; c) and d) as for a) and b) but taken from adjacent Åsgårdfonna.

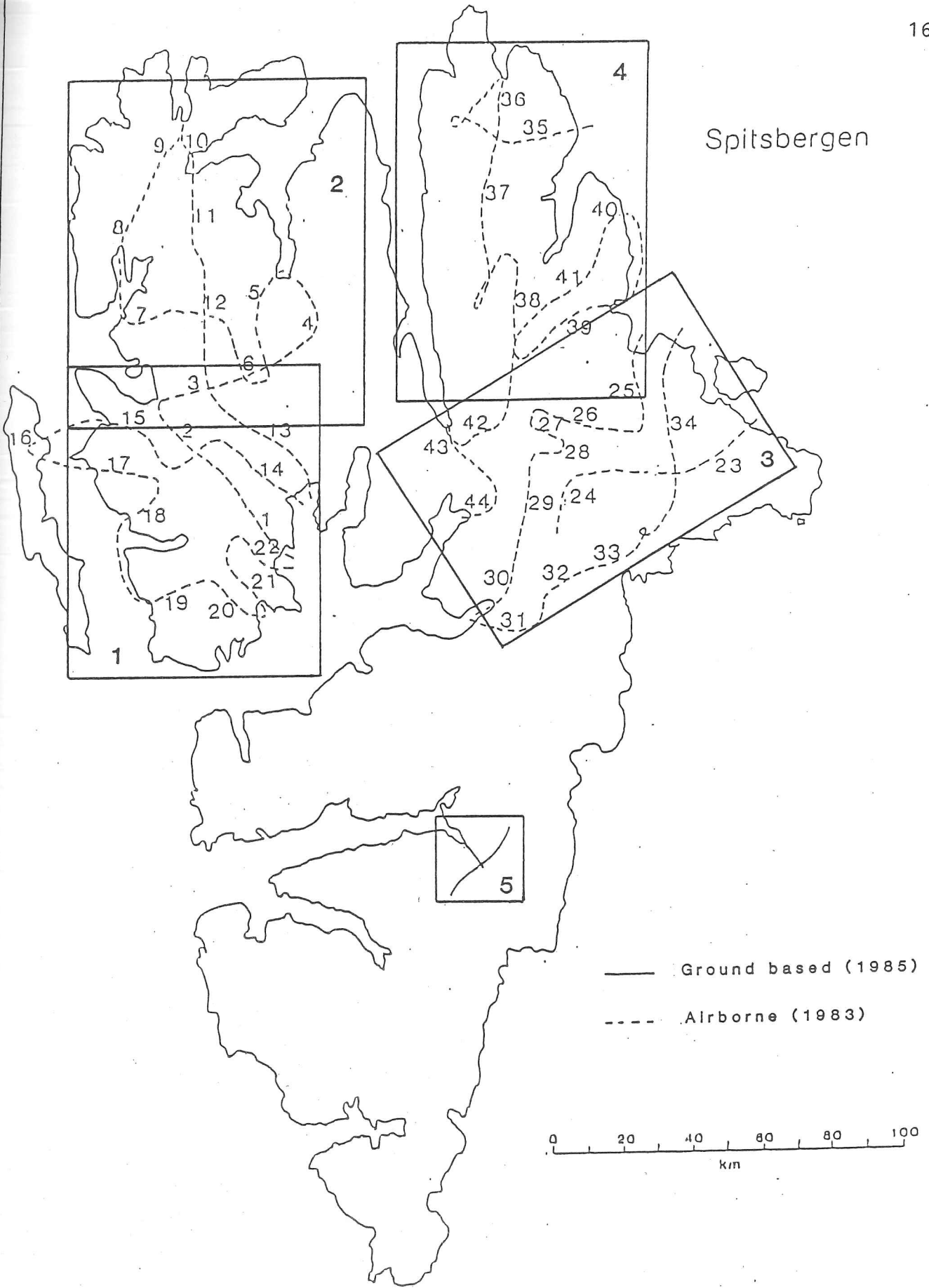


Fig. A1.1 RES flightlines in 1983 (boxes 1-4) and ground-based track in 1985 (box 5).

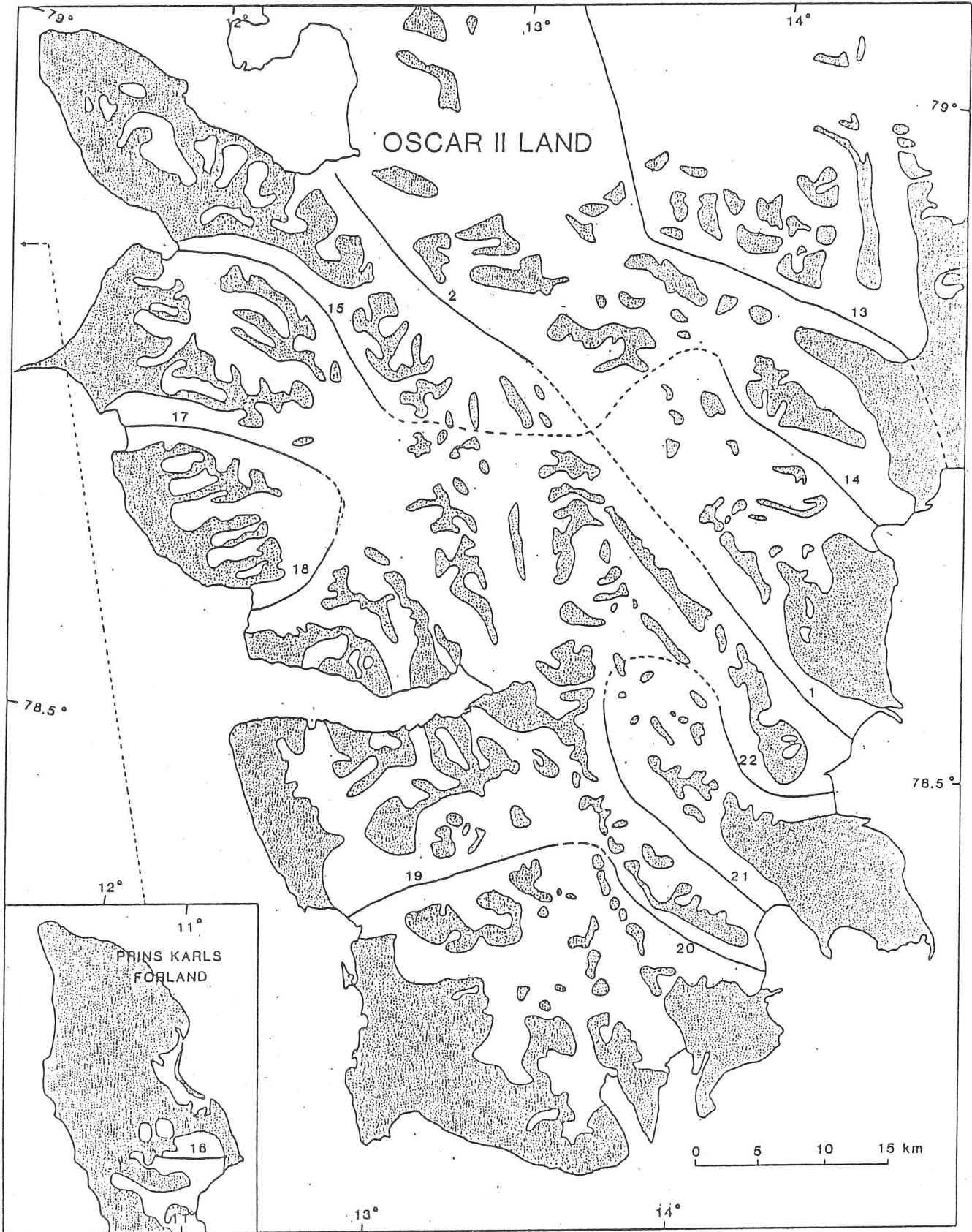


Fig. A1.2 Glaciers sounded in Oscar II Land.

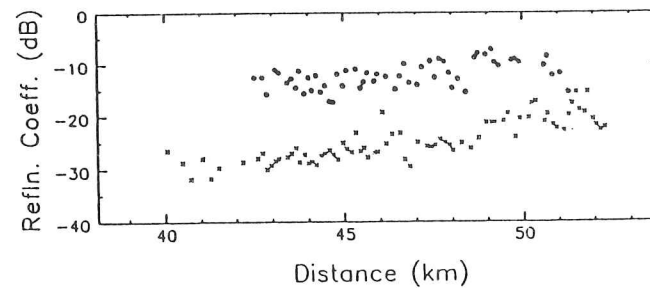
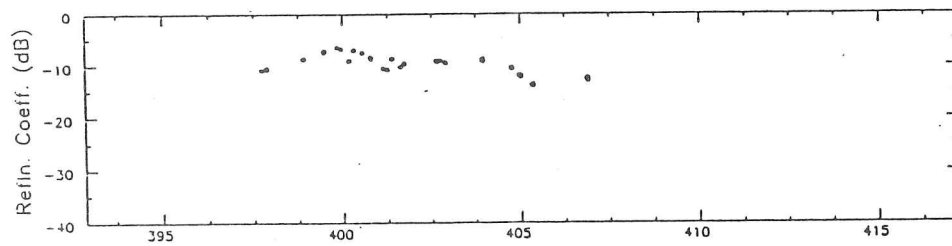
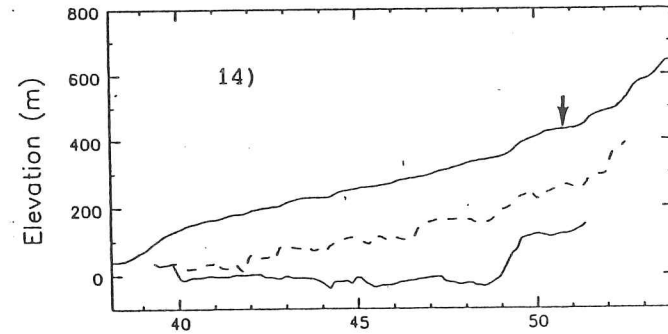
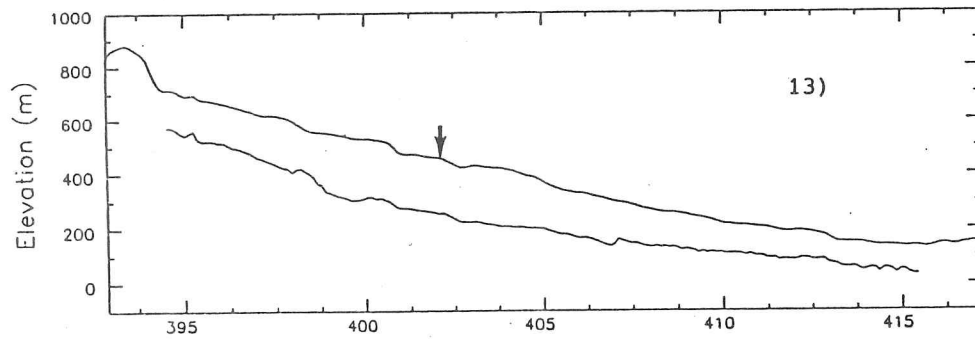
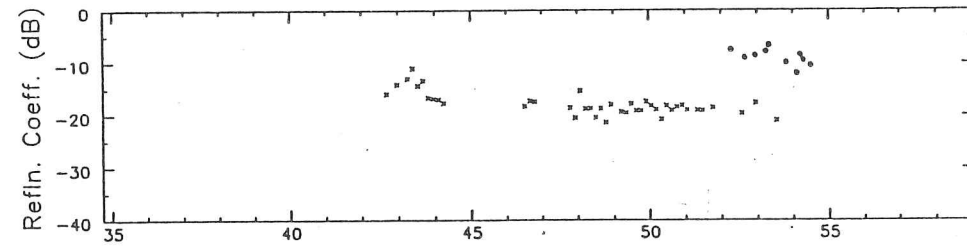
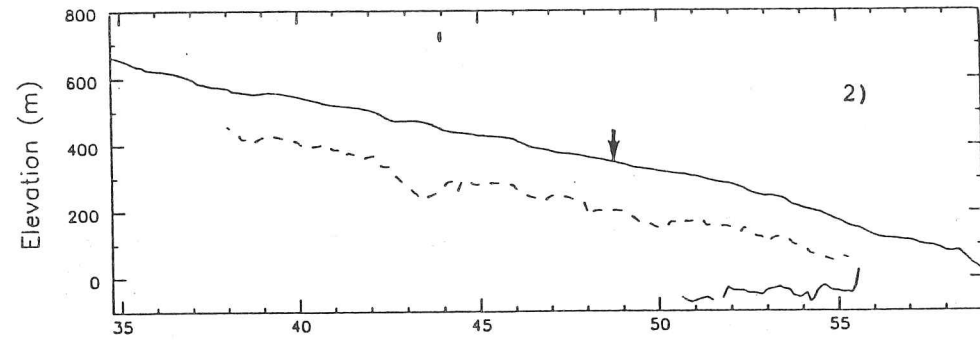
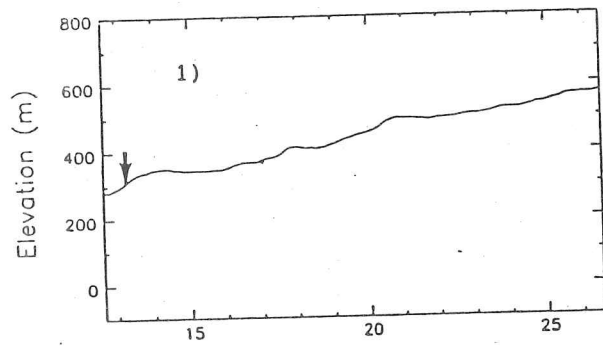


Fig. A1.3 1) Sveabreen; 2) Kongsvegan; 13) Holmstrombreen; 14) Sef strömbreen

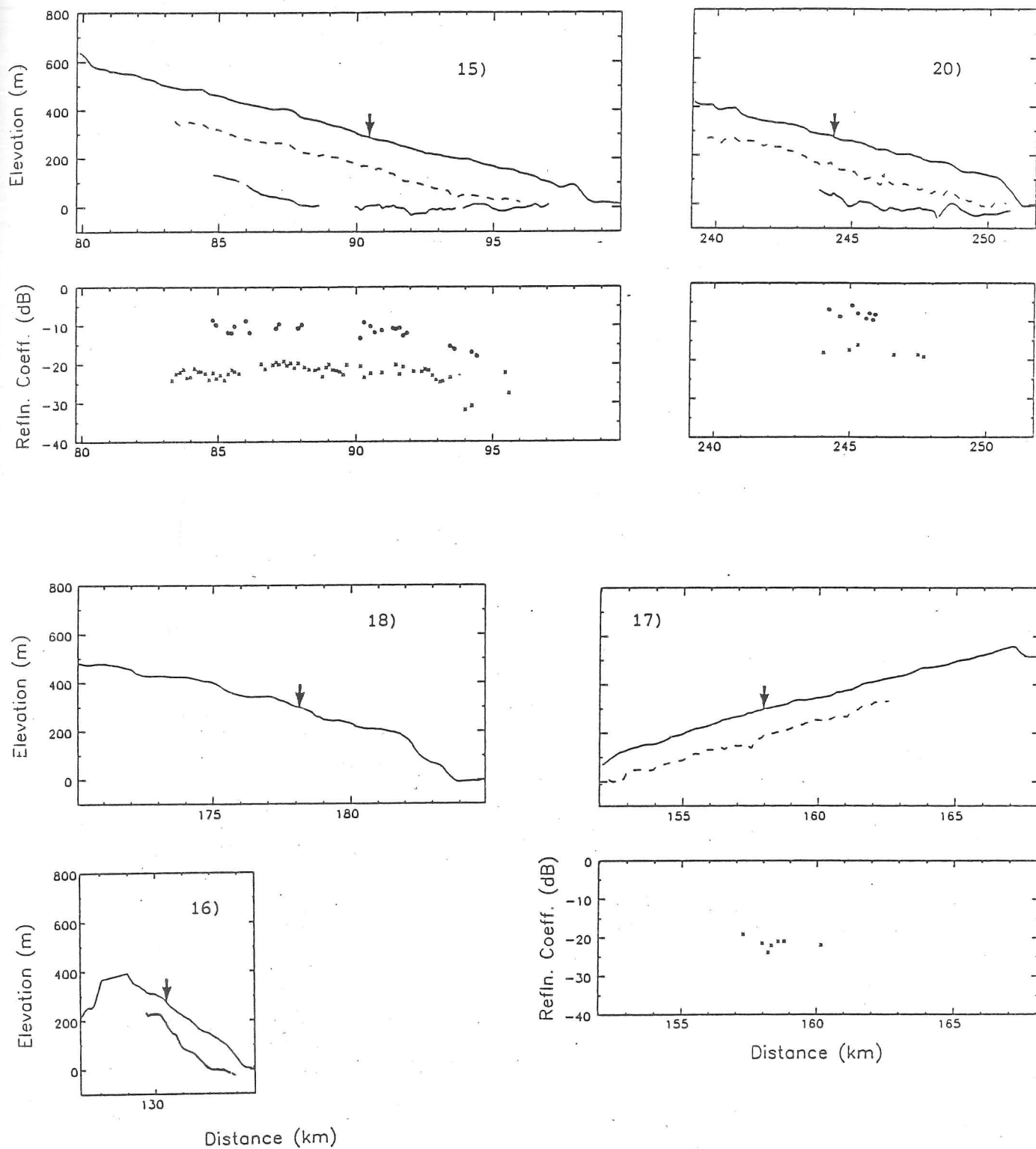


Fig. A1.4 15) Uvêrsbreen; 20) Nansenbreen; 18) Dahlbreen; 17) Aavatsmarkbreen
16) Murraybreen.

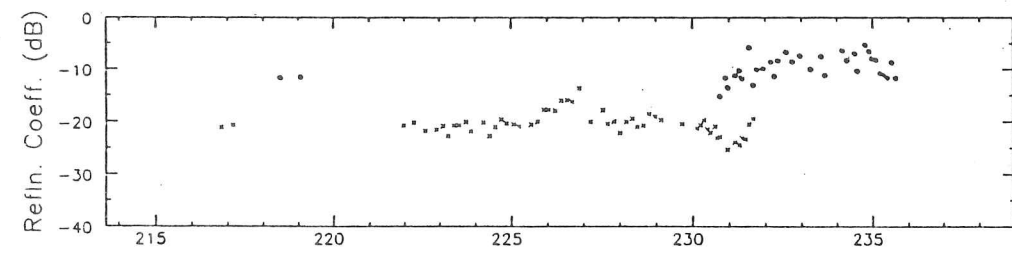
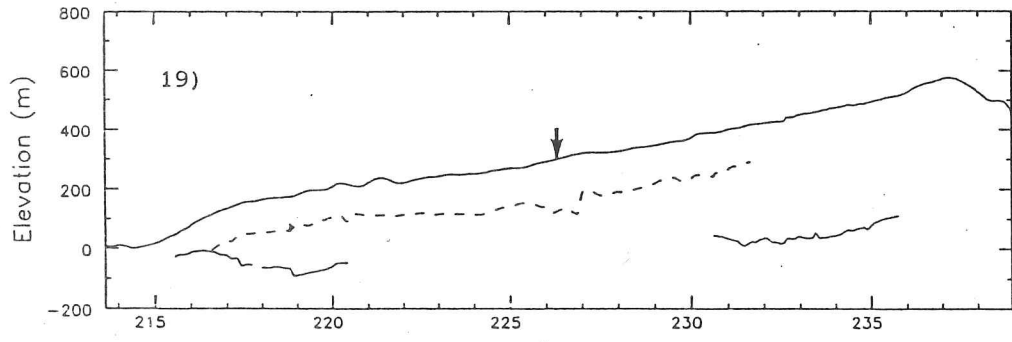
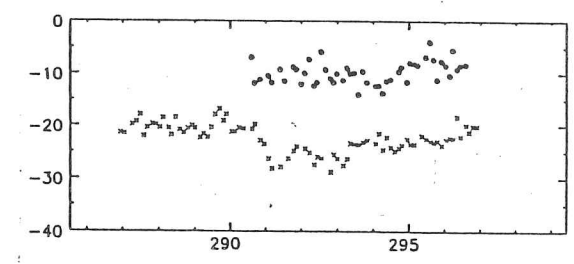
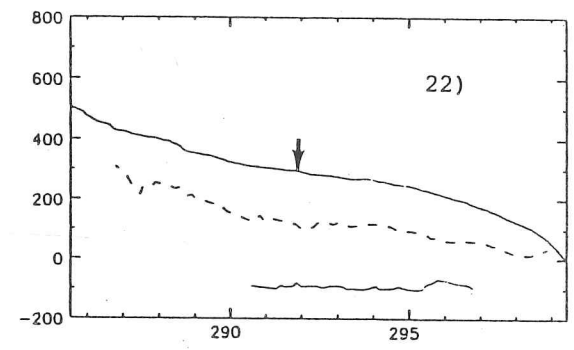
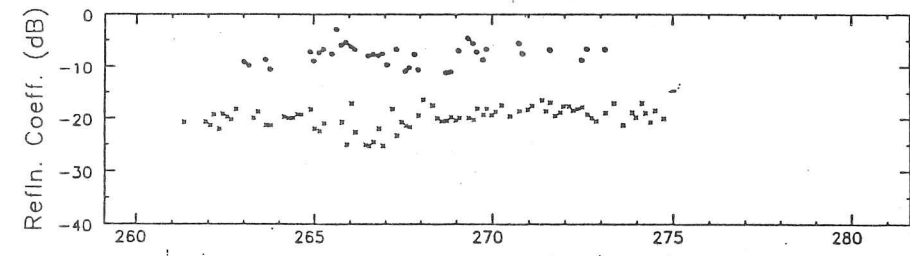
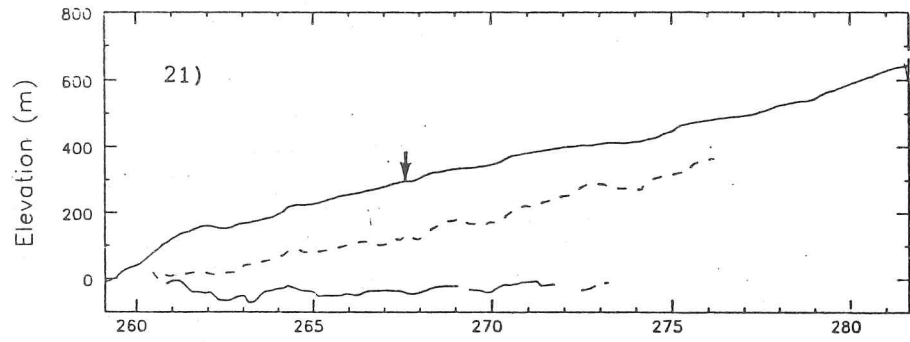


Fig. A1.5 21) Borebreen; 22) Wahlenbergbreen
19) Eidenbreen.

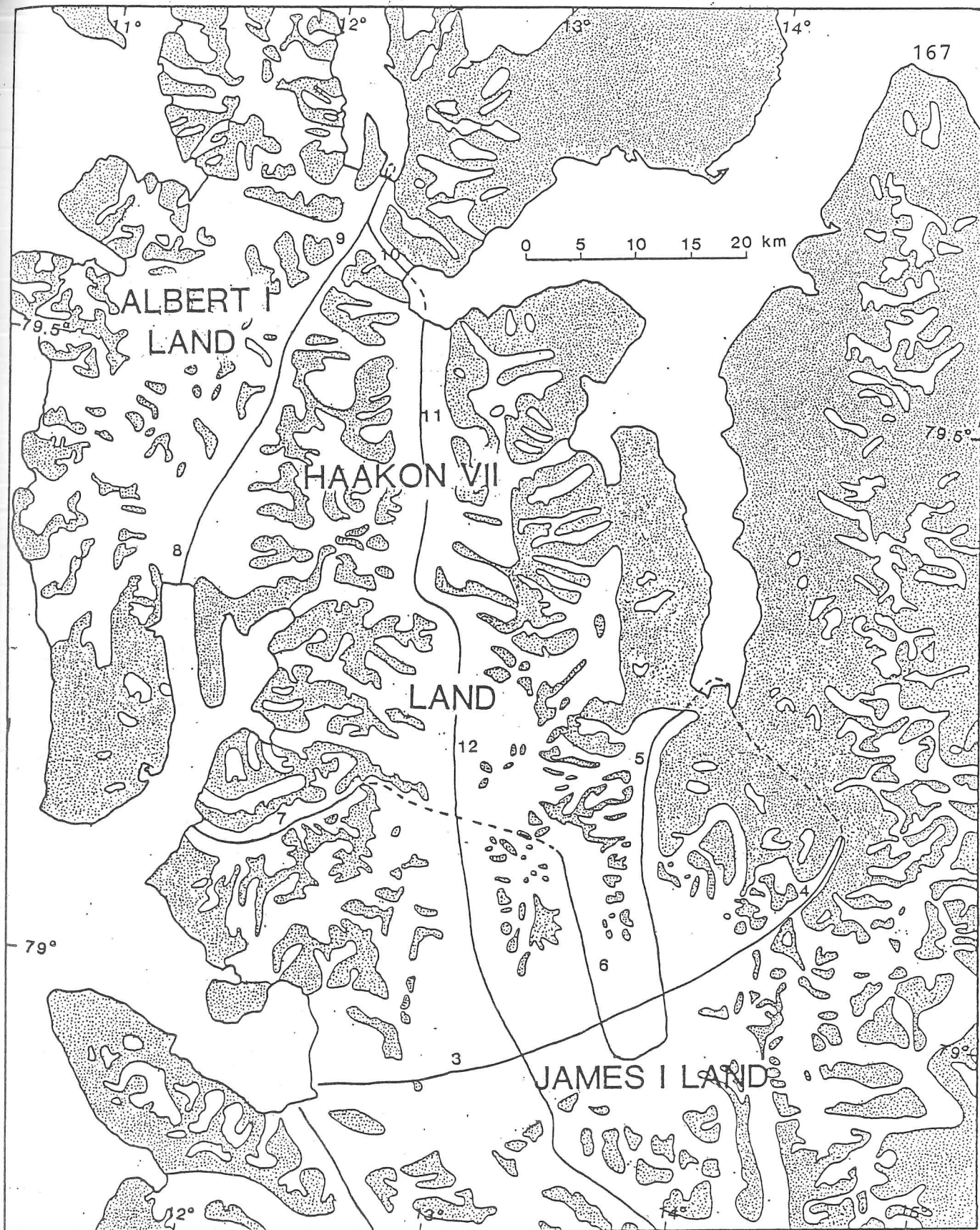
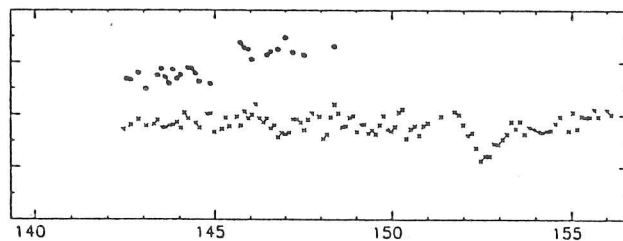
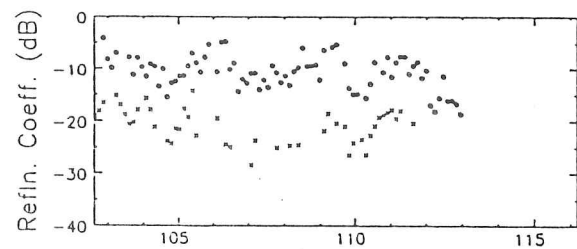
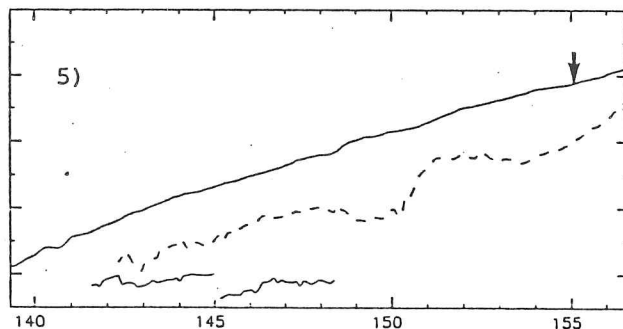
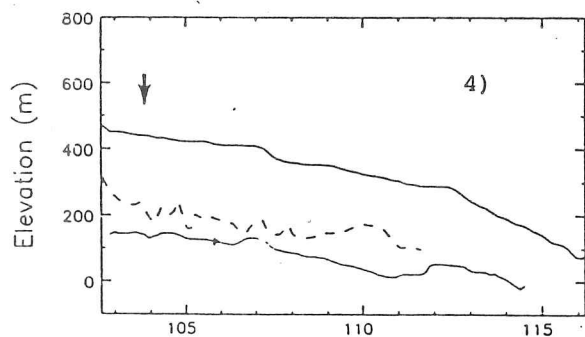
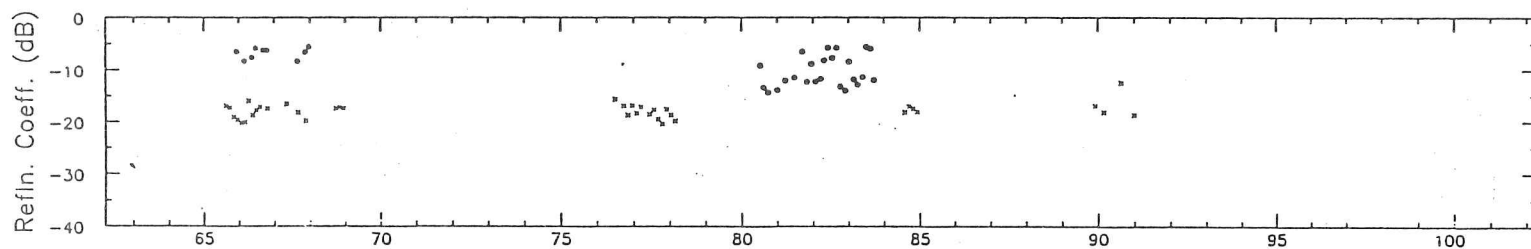
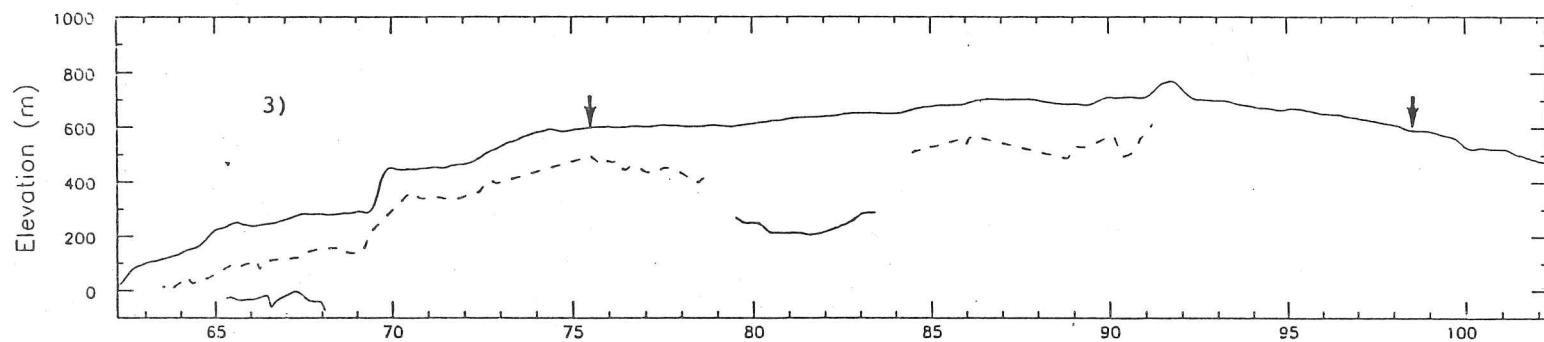


Fig. A1.6 Glaciers sounded in Albert I Land, Haakon VII Land and James I Land.



Distance (km)

Distance (km)

Fig. A1.7 3) Kronerbreven-Holtedahlfonna;
4) Abrahamsenbreen;
5) Vonbreen.

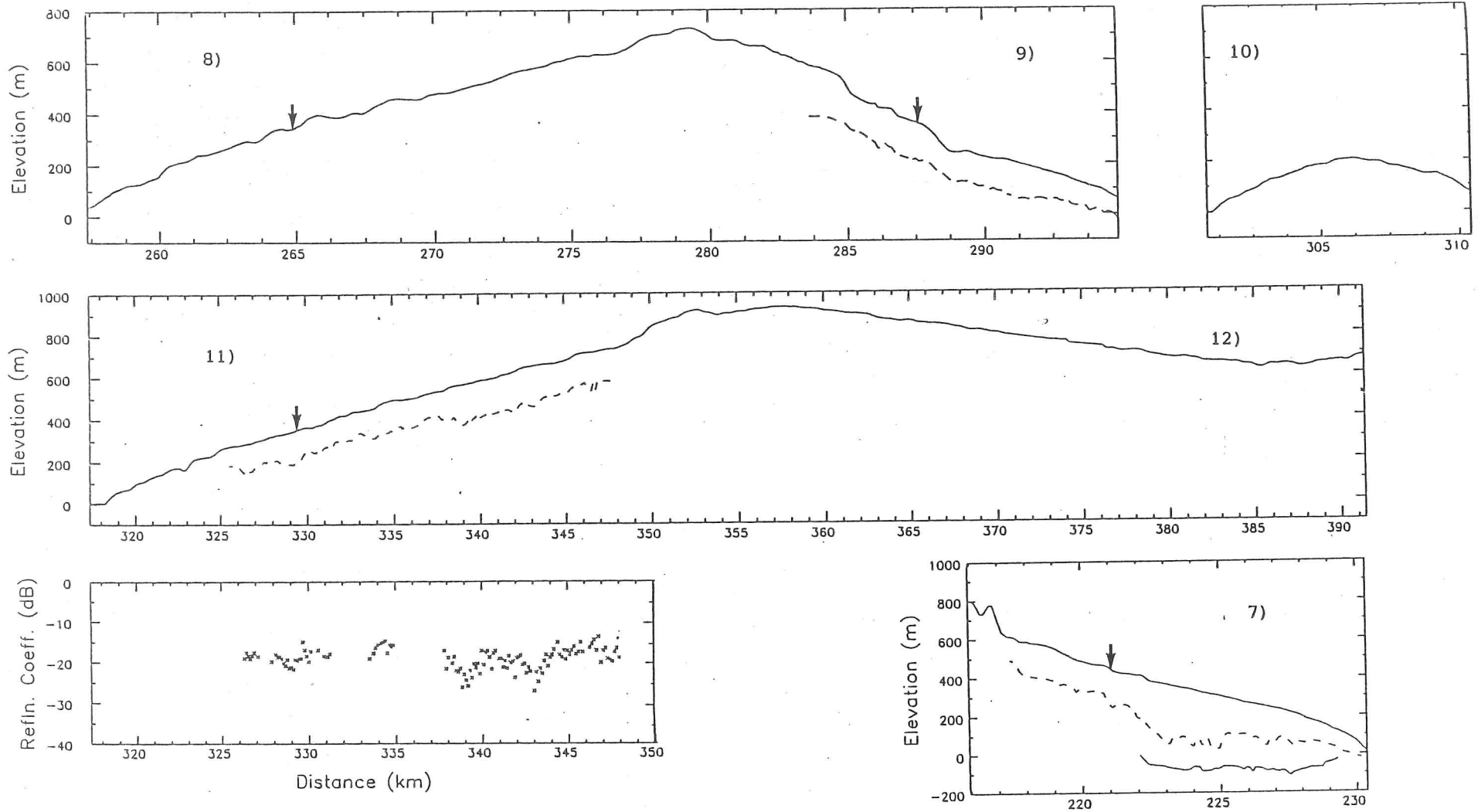


Fig. A1.8 8) Lilliehöökbreen; 9) Raudfjordbreen;
 10) Idabreen; 11) Monacobreen;
 12) Isachsenfonna; 7) Fjortende Julibreen.

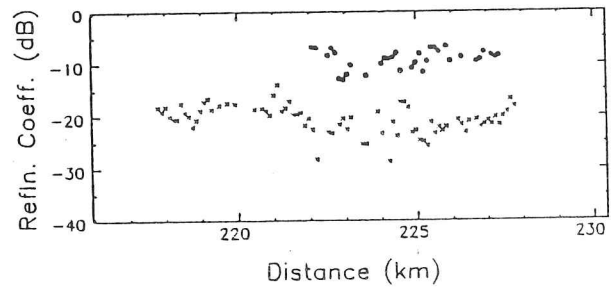




Fig. A1.9 Glaciers sounded in Olav V Land.

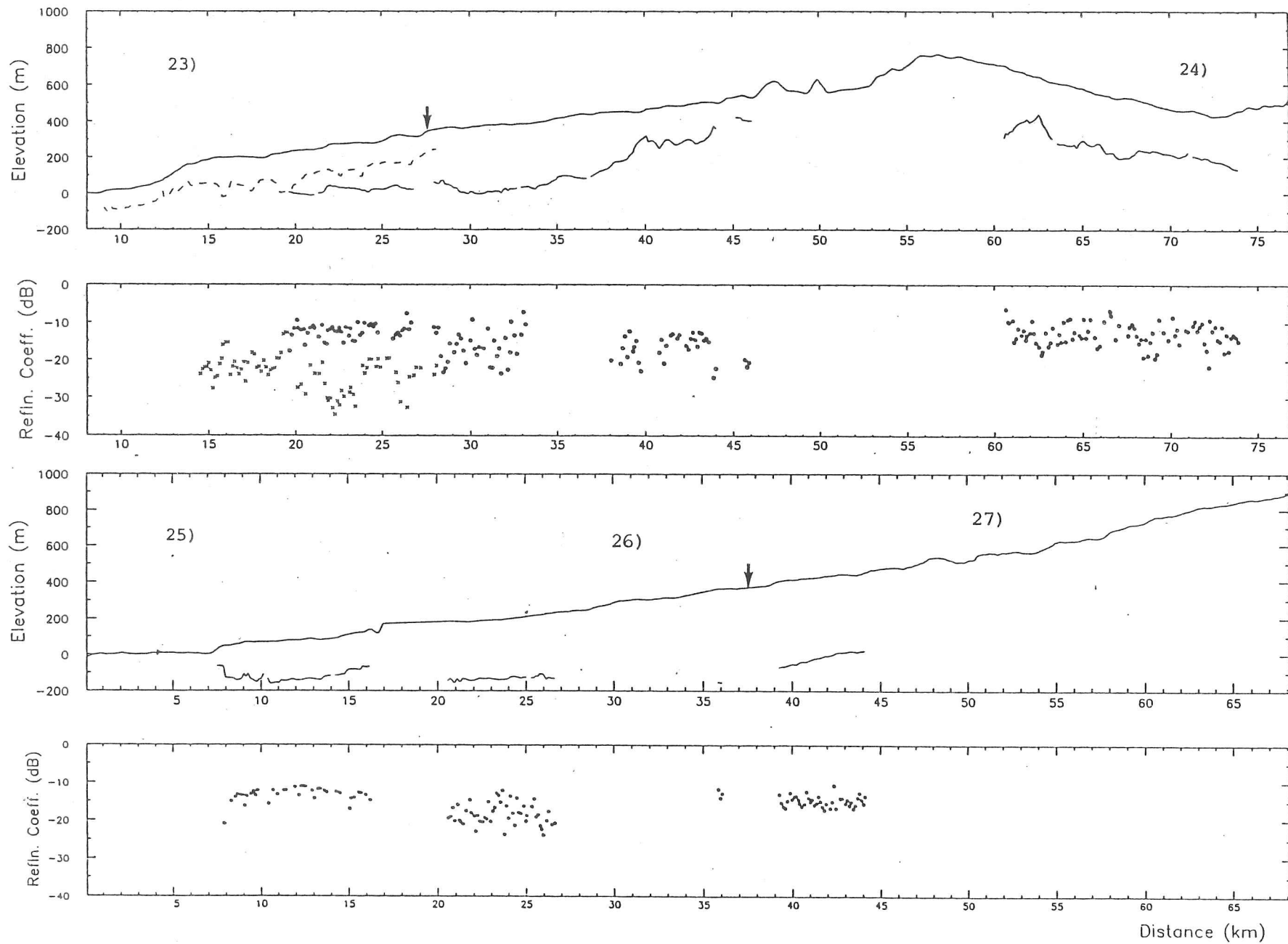


Fig. A1.10 23) Hochsteterbreen- Olav V ice cap; 24) Akademikerbreen;
 25) Hinlopenbreen; 26) Kvitbreen; 27) Russebreen .

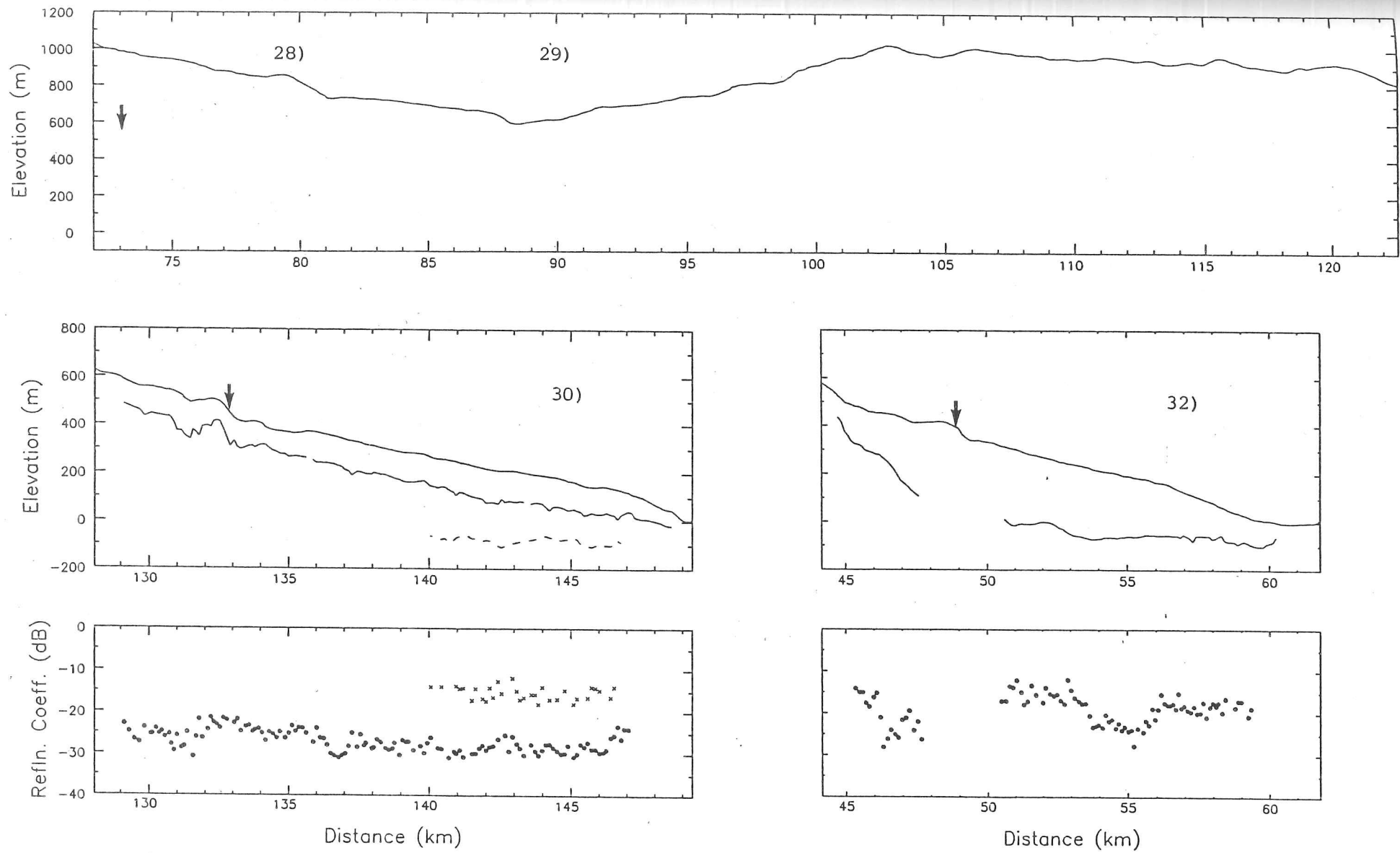


Fig. A1.11 28) Oxfordbreen; 29) Lomonosovfonna; 30) Tunabreen; 32) Petermannbreen.

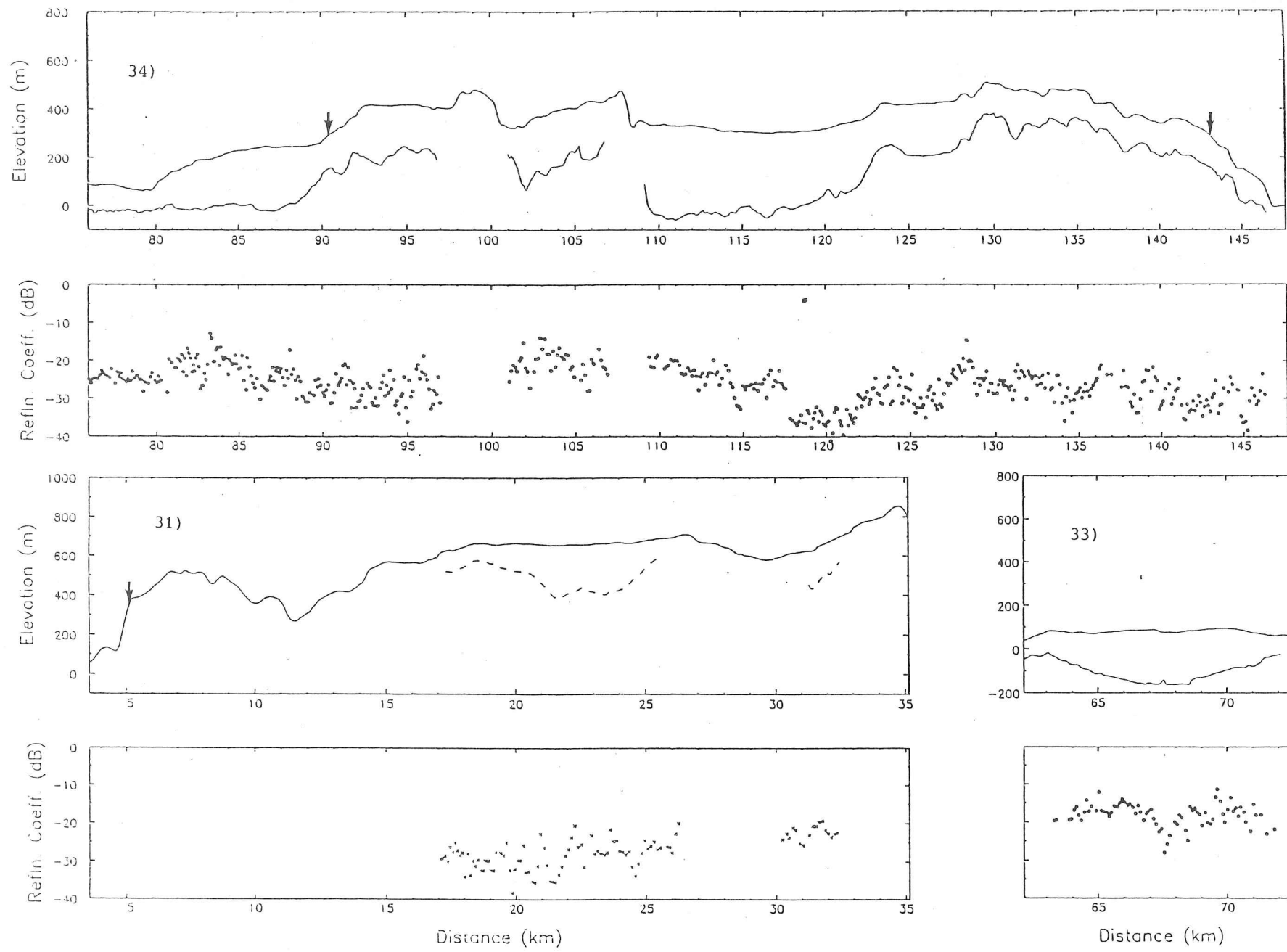


Fig. A1.12 34) Vaigattbreen-Olav V ice cap; 31) Fimbulisen; 33) Negribreen.

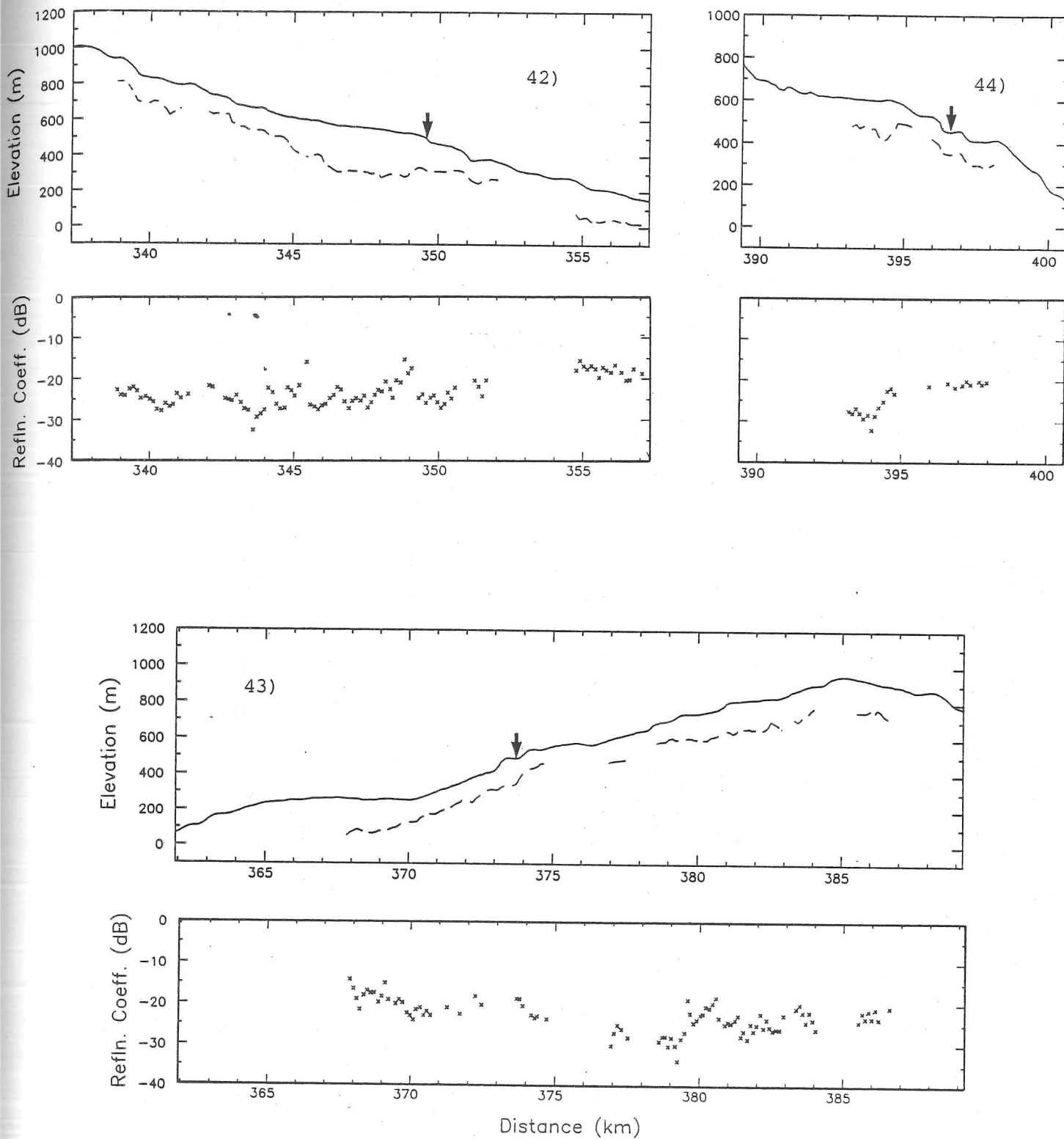


Fig. A1.13 42) Formidablebreen; 44) Nordenskiöldbreen;
43) Mittag-Lefflerbreen.

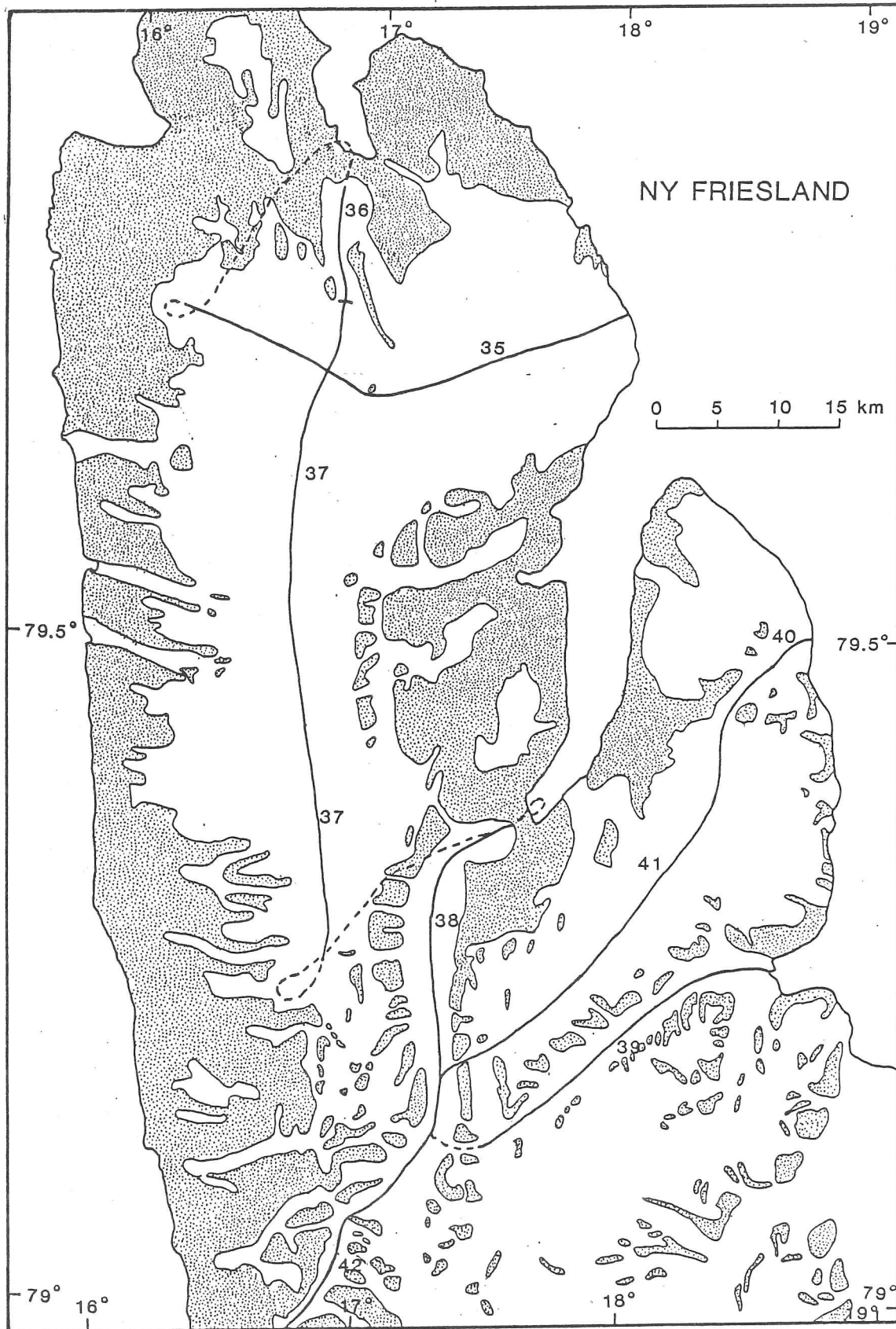
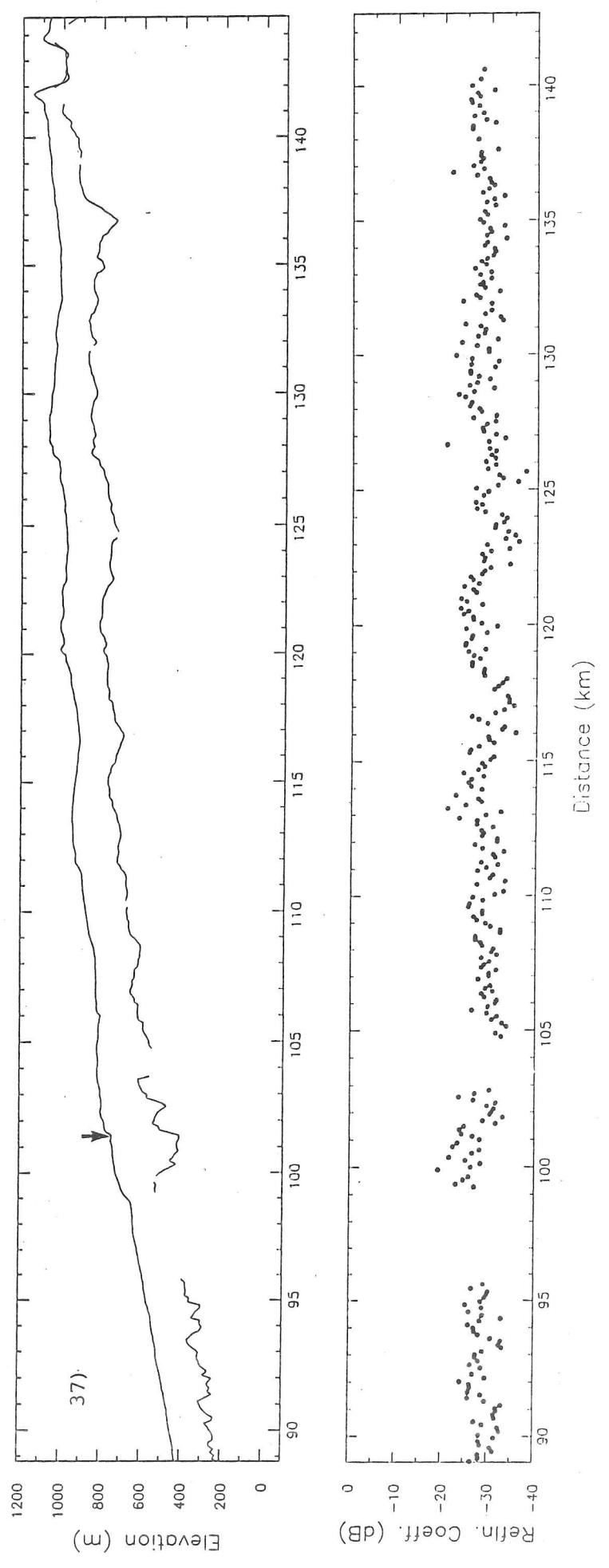
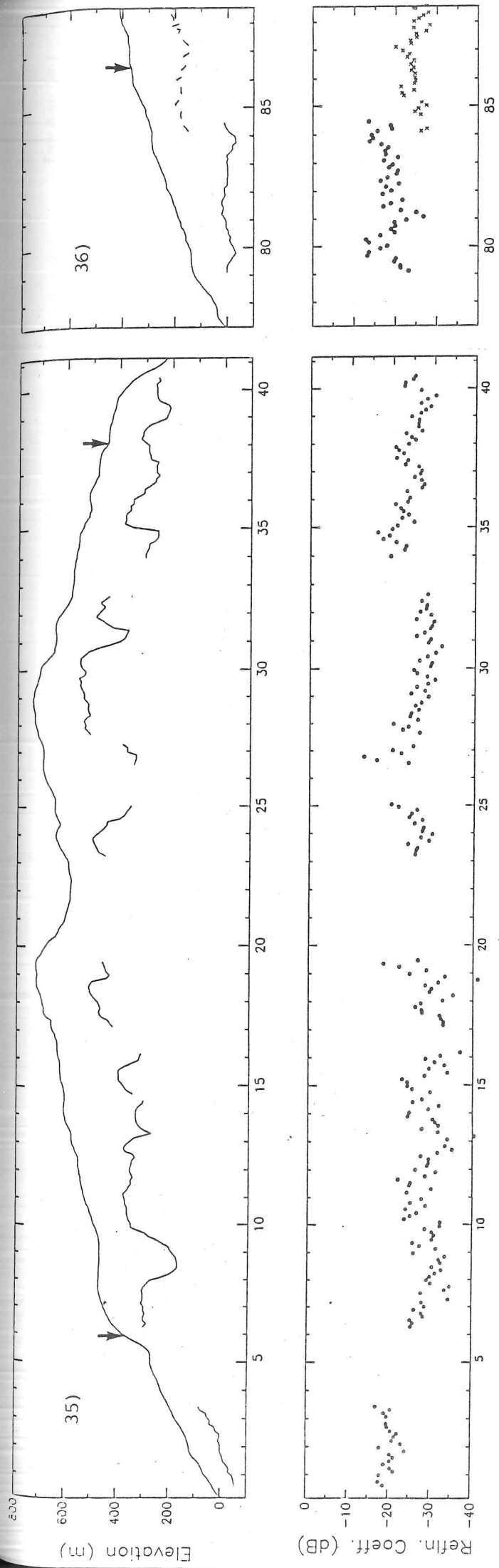


Fig. A1.14 Glaciers sounded in Ny-Friesland.

Fig. A1.15 35) Valhallfonna; 36) Dunér-
breen; 37) Åsgårdfonna.



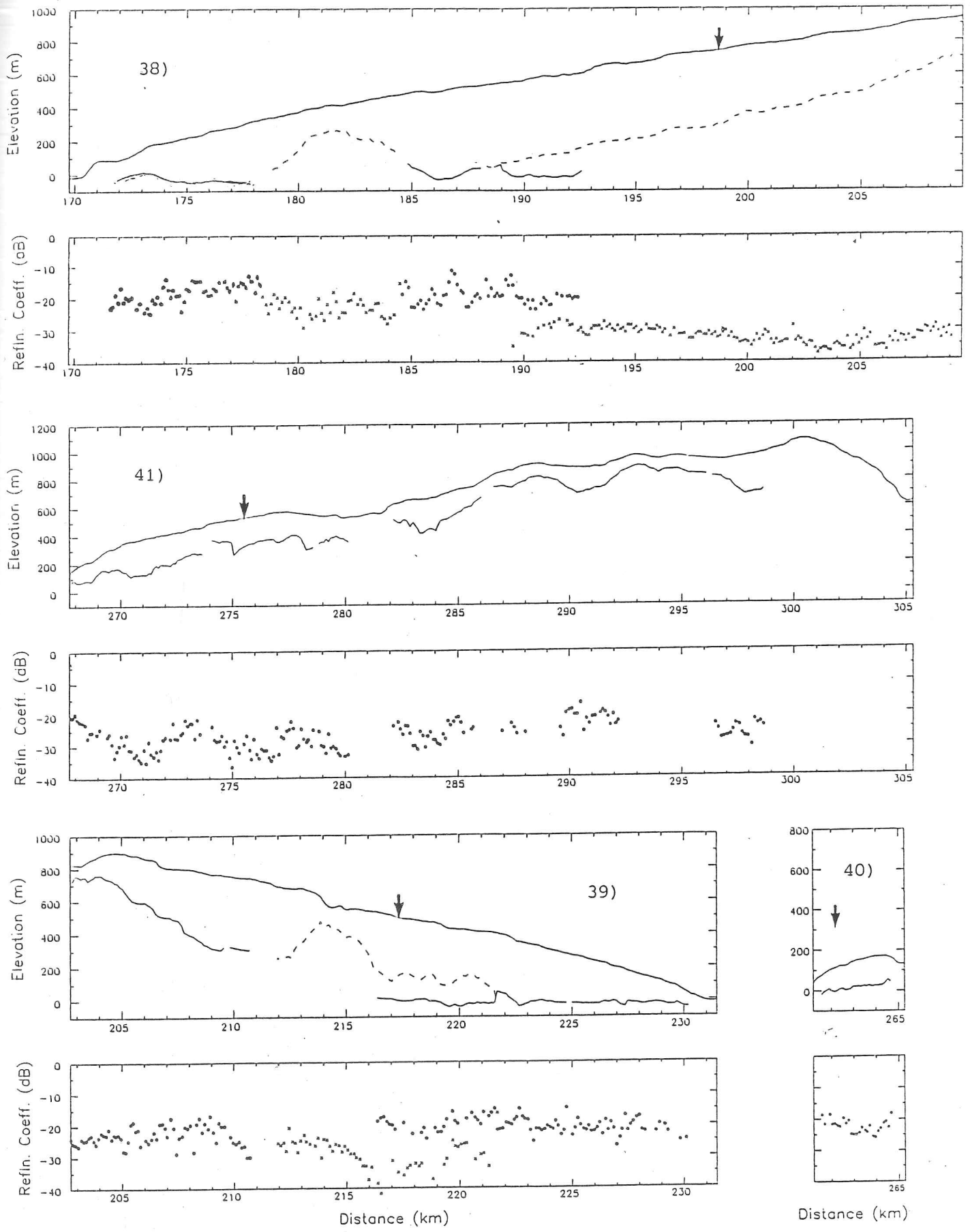


Fig. A1.16 38) Veteranen; 41) Balderfonna; 39) Chydeniusbreen
40) Tommelbreen.

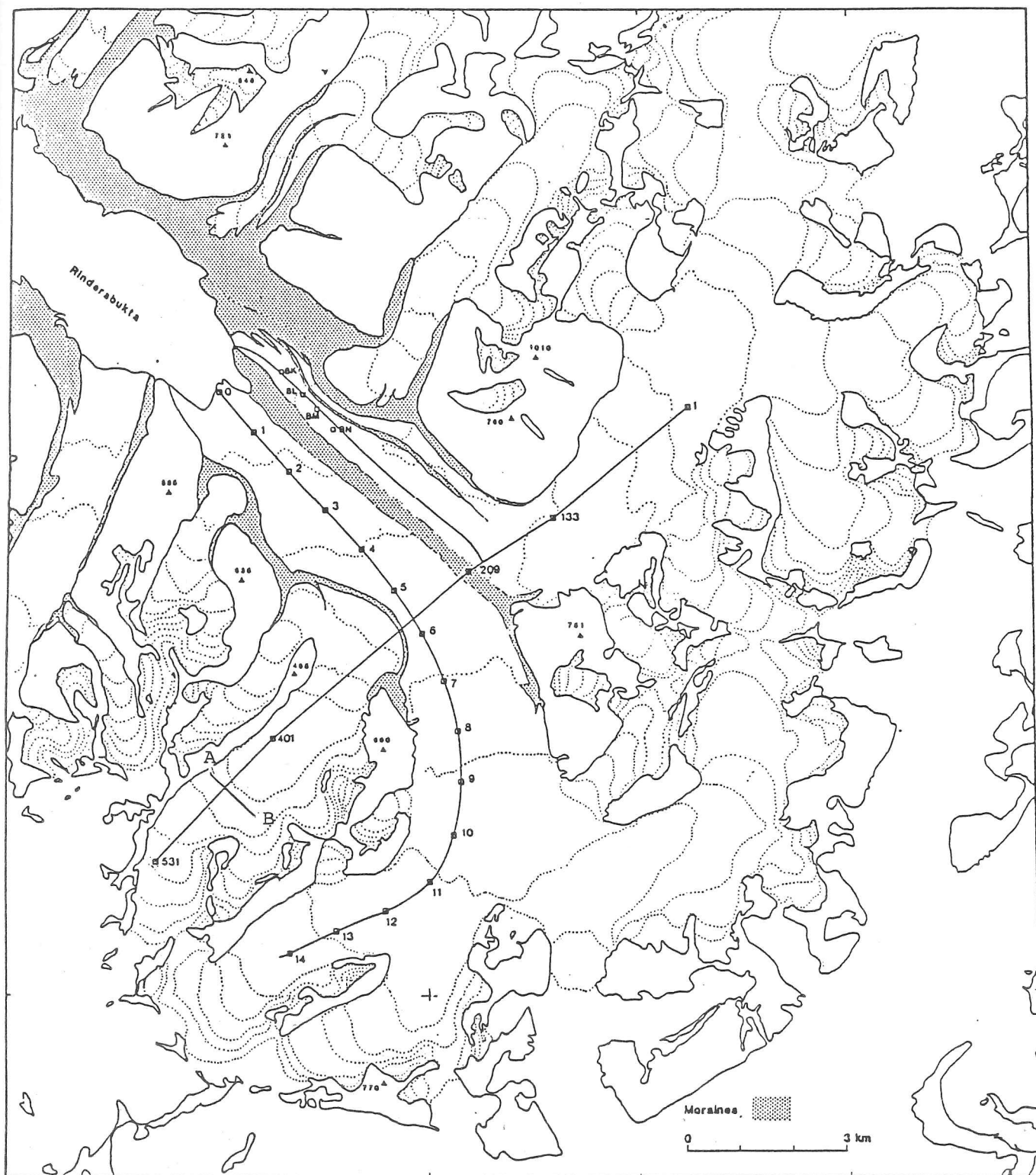


Fig. A1.17 Glaciers sounded in 1985. The numbers running 0-14 (along Paulabreen) are km along track. Those running 1-531 (from Bakaninbreen to Skobreen) are the BP stake numbers (25 m spacing between stakes). The line marked A-B, across Skobreen, shows the location of the cross profile.

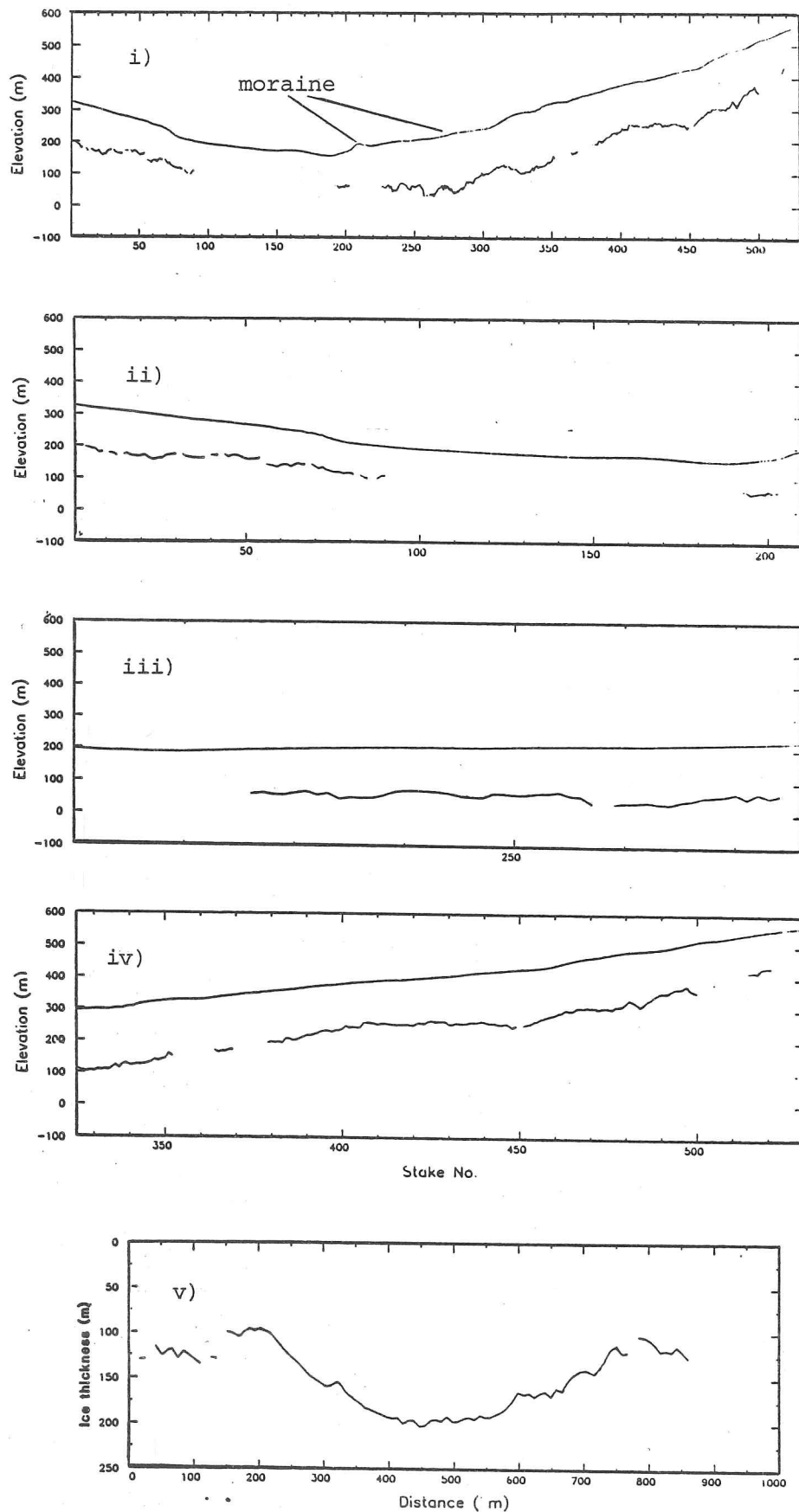


Fig. A1.18 Profiles from 1985. i) complete profile from Bakaninbreen to head of Skobreen; ii) Bakaninbreen; iii) cross profile of Paulabreen; iv) Skobreen; v) cross profile from Skobreen.

APPENDIX 2

Theory and Experimental Procedure for Dielectric Measurements made on a Spitsbergen Core

1 Experimental Procedure

1.1 Apparatus

Three pairs of parallel plate capacitors were made from high grade stainless steel discs (BS 970), approximately 10 mm thick. Each disc was lathed to give a reasonably flat surface and then machine ground on one side only. Considerable care was taken to ensure that only a small thickness of metal ($\approx 25\mu\text{m}$) was removed on each pass of the grinder but despite this the heat produced was found to create stresses in the plate which tended to induce buckling when allowed to rest. Consequently it was necessary to undertake re-lathing and then 'lapping' the plates by hand using 'wet or dry' paper. To avoid this laborious and time consuming task, discs of thickness greater than approximately 15 mm (after the initial lathing) should be used, in which case they may be machine ground without buckling.

The plates were mounted in 10 mm thick tufnel blocks which had been recessed by approximately 3 mm. They were held in place using an epoxy resin. The 'high' electrode consisted of a single disc 9 cm in diameter. The the 'low' plate was made up of a central disc 5 cm across with a 2 cm thick guard ring separated from it by an air gap of 1 mm. Electrical connections with the plates were made by drilling and threading holes through the back of the tufnel and into the metal. Brass screws were then screwed firmly into place. Poor contact was tested for with an ohmmeter but negligible resistances were found for all the plates. All connections between the electrodes, metal case housing them and the bridge were made using RS (spec. URM72) co-axial cable.

Each pair of plates was held in place by four brass rods passing through holes drilled in each corner of the tufnell blocks which were secured by nuts and washers. All these were grounded to the guard ring on the low plate which was in turn connected to the aluminium case (Fig. A2.1). This was fitted with six 100 Ω resistors mounted ^{on} heat sinks, each being capable of dissipating

a maximum of 25 W. These were installed to allow fine adjustment of the temperature when it was close to the melting point, as the freezer cabinet used to store the apparatus was only adjustable to a precision of $\pm 2^\circ\text{C}$.

The rate of heat loss was estimated from the empirical value for the convection rate in still air— $6 \text{ W m}^{-2}\text{ }^\circ\text{C}^{-1}$ (Holman, 1981). From this and an estimate of the heat capacity and surface area of the whole apparatus it was possible to calculate the heat required to maintain a given temperature difference between the box and its surroundings (the freezer cabinet). A value of $2.1 \text{ W }^\circ\text{C}^{-1}$ was obtained and the time constant (i.e. the time for the temperature to have reached $1/e$ of its final value) was found to be 10^3 s so that in 24 hrs the exponential term was 1.8×10^{-4} . Hence by using a power supply with a variable voltage the desired temperature could be obtained in a day. The apparatus described above is illustrated in Figs. A2.1 and A2.2.

1.2 Bridge Measurements

Measurement of capacitance and either the dissipation factor D ($\equiv \tan \delta$) or the conductance G were made using a General Radio bridge, type 1615-A, with a type 1238 General Radio detector and matching oscillator. The measurement of D was, in general, more accurate than G and the equivalent circuit diagram, in this mode, was a resistance, R , and capacitance, C , in **series**. Above a certain frequency (dependent upon the temperature) the D range was insufficient and G had to be measured. In this case the circuit diagram was represented by a resistance and capacitance in **parallel** but it is the series capacitance that is required. The equations relating the different parameters are,

$$D = \omega R_s C_s = G/\omega C_p = 1/\omega R_p C_p \quad (1)$$

$$C_s = C_p(1 + D^2) \quad (2)$$

$$G = 1/R_p = \omega C_s D/(1 + D^2) \quad (3)$$

$$R_s = G/((\omega C_p)^2(1 + D^2)) \quad (4)$$

where subscripts p and s stand for the parallel and series values respectively. The relation of G to the resistance of the decades in the bridge is not linear and this requires that a small correction must be made to the former which is given by,

$$G_{corr} = [G - 2(G/1000)^2] \quad (5)$$

Between 50 Hz and 10 kHz the accuracy of D was $\pm(0.1\% + 10\text{ppm})$ and for G, was $\pm(1\% + 10^{-5}\mu\text{mho})$ for the same frequency range. The bridge sensitivity was found to be best for voltages close to the maximum recommended voltage of 30 V/ kHz but was never set above 50 V.

Part way through the experiment the General Radio oscillator began to malfunction and was replaced by a Philips frequency synthesiser, with a maximum voltage output of 20 V. This meant that it was no longer possible to use the quadrature and phase dials on the detector for the final balance. Despite these limitations it was found that the balance could be found to an equivalent precision.

1.3 Sample Preparation

The samples were prepared in a SPRI cold room at a temperature of approximately -10°C and were handled through polythene gloves. Sections were cut by hand using a teflon coated tenon saw. They were then placed in a specially designed clamp that could be fitted to a microtome. It consisted of a rectangular block of aluminium with a circular section recessed by 1 cm and approximately 2 mm wider than the ice core diameter (Fig. A2.2). Four screws were located in each side of the block and were used to keep the sample in place. Once securely mounted, the surface layers of ice were gradually removed by the microtome blade until flat. The sample was then turned and the process was repeated for the other face. This was carried out several times until the faces of the sample were parallel. To achieve this, it was essential for the clamp to be parallel with the microtome blade and this was accomplished using a surface plate and a pair of parallels (two strips of steel of identical thickness) which were placed on the track on which the blade was mounted. A certain amount of 'give' in the clamp mounting made it difficult to obtain 'perfectly' parallel specimens. Their thicknesses were measured using calipers accurate to 0.01 mm and the maximum variation was 0.4 mm, for sample 1 which was considerably greater than the differences for the other two samples (0.16 mm).

The microtome blade, clamp and electrodes had been scrubbed and then washed in triple distilled water several times before being used and the preparation was designed to prevent contact with any other surfaces.

Once of the desired thickness, the samples were placed in the capacitance cells with a moderate pressure applied by the nuts used to keep the electrodes in place (fig. A2.1). Lateral motion was prevented by four small pads placed around the edges of the sample. The distance

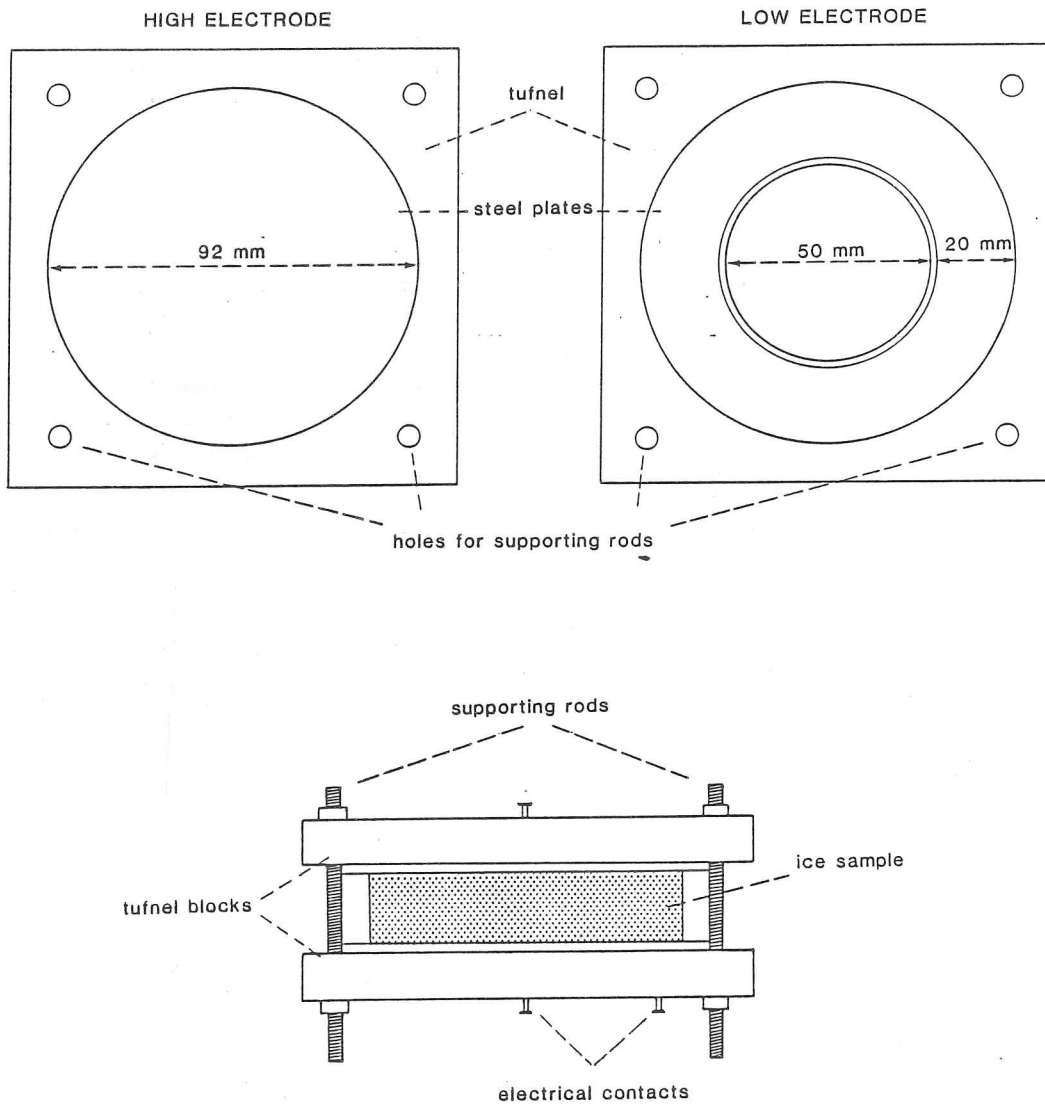


Fig. A2.1 Plan view of the electrodes.

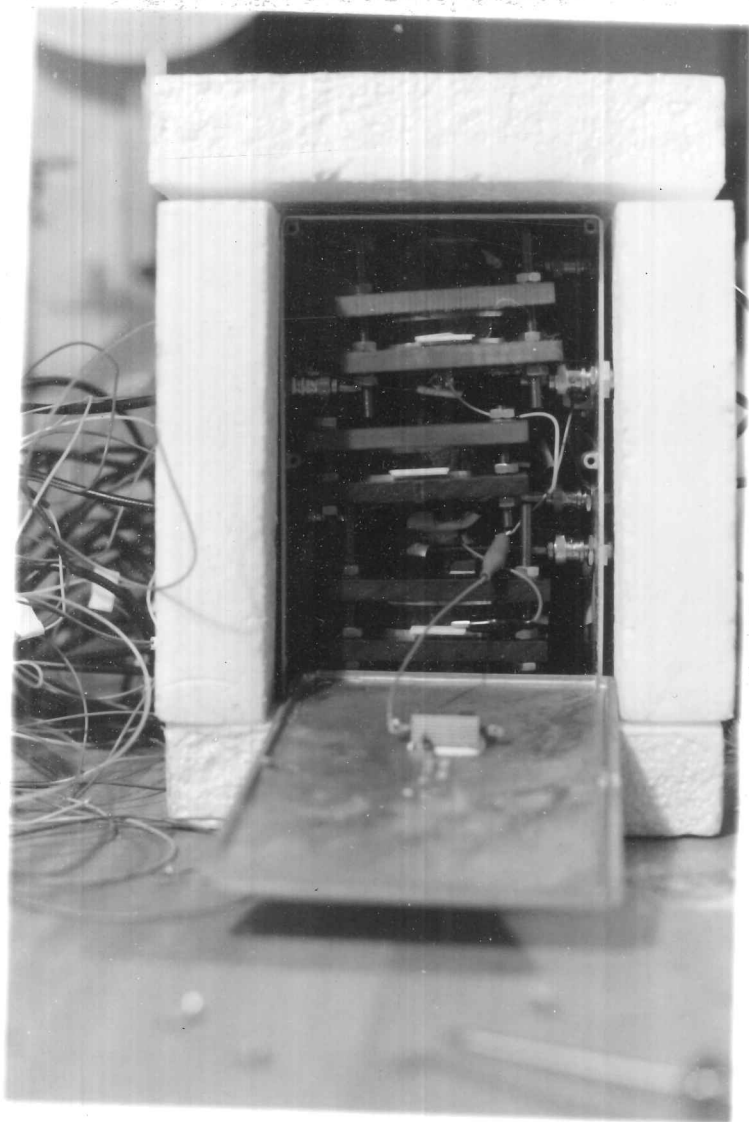


Fig. A2.2 a) Container housing the three sets of plates just before the lid was screwed into place. Co-axial connections are visible.

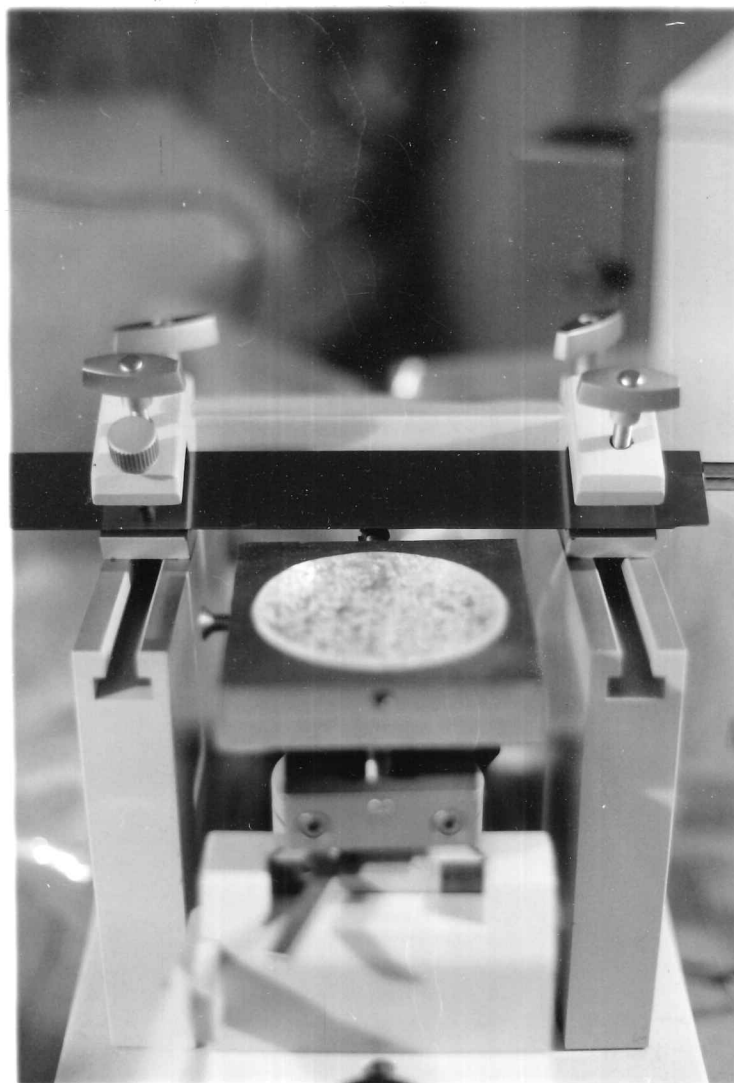


Fig. A2.2 b) Sample preparation using a microtome and specially designed clamp.

between the electrodes was measured to ensure there was no significant difference between the electrode separation and the sample thickness. Fig. A2.2 shows the whole assembly before the lid to the case was screwed into place. The aluminium container used to isolate the electrodes was lagged with 50 mm of polystyrene designed to damp fluctuations in the air temperature within the freezer used to store the apparatus.

1.4 Temperature measurement

The temperature within the box was monitored using two resistance– curve matched thermistors. These were calibrated using a platinum resistance thermometer whose absolute accuracy was 0.1% of the temperature in Kelvins. This was itself calibrated using crushed ice prepared from, and mixed with, distilled water. The temperature coefficient of a platinum resistance thermometer is very well known and if one calibration point can be found with sufficient accuracy then the errors are less than the value above, and are then dependent, on the accuracy with which the resistance can be measured (Kaye and Laby, 1975). The thermistor resistances were measured using a low current ohmmeter accurate to 10Ω ($\equiv 1.3 \times 10^{-3}^\circ\text{C}$) for resistances less than $100 \text{ k}\Omega$. Errors in the estimated temperature were found to be, from the calibration data, $\pm 0.4^\circ\text{C}$. Close to 0°C they are less than this (0.2°C), however, because more calibration data were collected near this temperature than for the lower temperature range.

1.5 Calibration of the Electrodes

The capacitance of a parallel plate air capacitor is

$$C = \epsilon_0 A/d \quad (6)$$

where A =area of the plates and d =separation. The equation for the effective area of a guarded electrode (Von Hippel, 1954) shows that the low electrode is effectively solid to a distance nearly midway between the inner and outer rings (to within 0.2%). The diameter of each low plate was measured using a pair of calipers to an accuracy of $\pm 0.2 \text{ mm}$ ($\equiv 0.27\%$) so that the geometric area was found to within $\pm 0.52\%$.

The effective area was also determined by measuring the capacitance for different values of the separation, d . Not only does this give a second, independent measure of the effective area but it also indicates the magnitude of any stray capacitances that might be present (due to leakage, inefficient isolation etc.).

Calibration Data For Electrodes

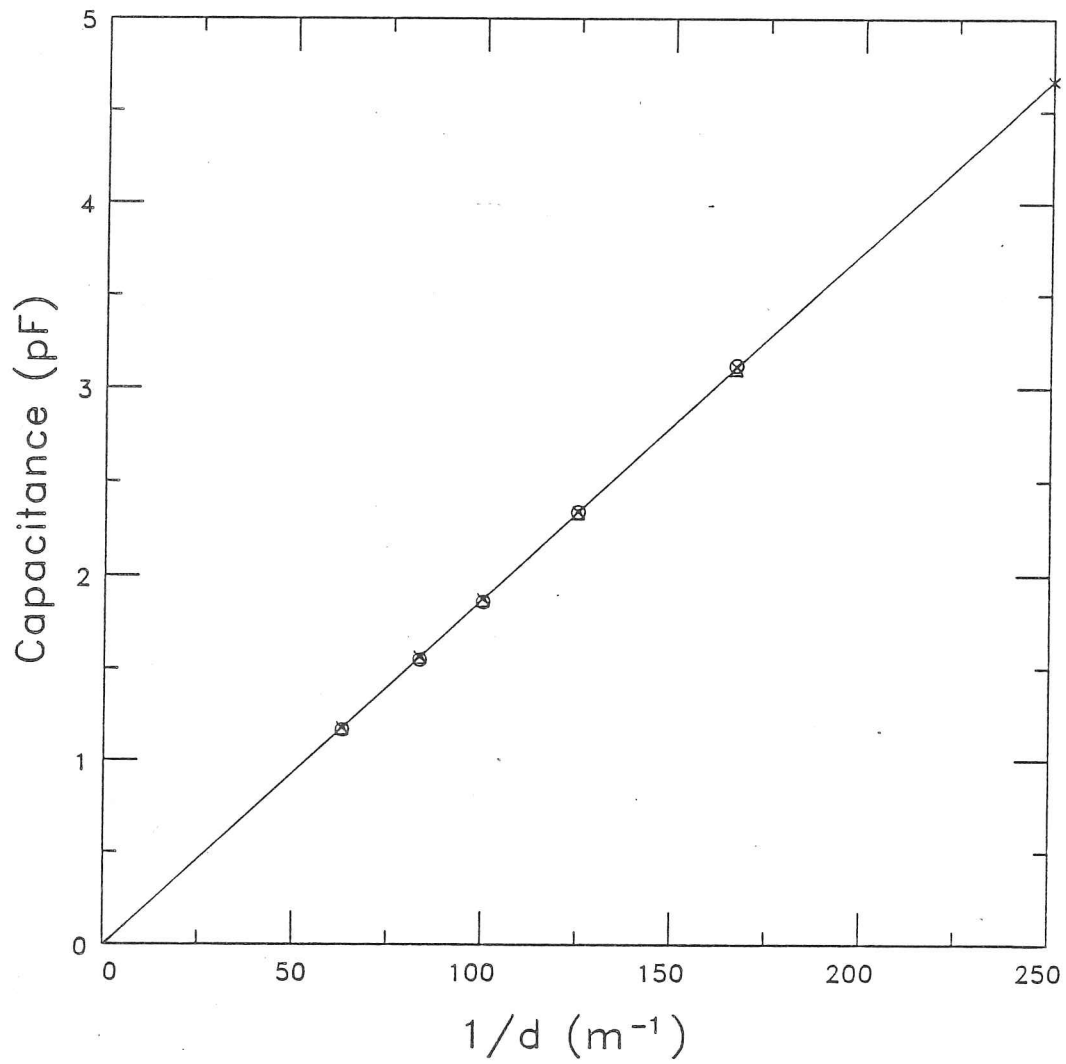


Fig. A2.3 Calibration data for the three pairs of electrodes. Results of a linear regression on the data are given in Table A2.1.

Table A2.1 Calibration Data for Electrodes

	Plate 1	Plate 2	Plate 3
No. of data	6	5	5
Correlation coefficient r	1.000	1.000	1.000
Regression coefficient $\equiv \epsilon_0 A$ (10^{15}F m)	18.626 ± 0.06	18.533 ± 0.06	18.73 ± 0.04
Regression constant (10^3 pF)	6.9 ± 3.0	-1.3 ± 7.2	-9.7 ± 3.7

High tolerance steel ball bearings, whose diameter had been previously measured with a micrometer, were used to fix the separation of the plates to an accuracy of 0.1 mm. The plates and box were arranged in an identical manner to when the ice was present although they were not placed in the freezer as it would have taken too long to reach a stable temperature, for each separation. Six different air gaps, of between 15.88 and 4 mm, were used and the measurements were made at a frequency of 1.2 kHz (Fig. A2.3). For the largest separation the frequency was varied between 200 Hz and 80 kHz but no significant change was observed in the value of the capacitance. A similar procedure was carried out for the smallest air gap and in this case, a 0.1% increase in capacitance was observed between 1.2 and 45.2 kHz. The results were subjected to a linear least squares fit, the results of which are shown in Table A2.1. It can be seen that the stray capacitances estimated are small and within the experimental errors. The difference between the two methods of estimating the area was 0.6%.

1.6 Experimental Procedure

The container, complete with samples was placed in the freezer with several bags of ice, designed to give a more stable thermal environment, and allowed to equilibrate for 24 hours. The initial temperature was -20.0°C . Approximately 15 to 20 different frequencies were used, in the range 20 Hz to 100 kHz. Measurements on all three samples, at a given temperature, took between 3 and 5 hours. During this time the thermistor resistances were monitored at half hourly intervals to see if any significant drift in temperature was taking place. If this did occur the run was abandoned and the conditions in the box allowed to stabilise for another day (the size of drift considered to be unacceptable was $\pm 0.2^{\circ}\text{C}$).

After completion of measurements the temperature of the freezer was adjusted to a new value and left for 24 hours. The temperature was never altered by more than 5°C at any one time, to prevent undue stress on the samples and the possibility of cracking. The additional temperature settings were -15.3 , -11.5 , -8.2 and -6.1°C . Subsequently and over a period of several days the temperature was then reduced to -34.4°C and data taken at this value. The lowest setting was -44.0°C which, despite the greater relevance of values closer to the melting point, was chosen to allow comparisons with the results of other authors (see e.g. Reynolds, 1985) and to reduce the effects of the static conductivity on the main Debye dispersion. The temperature was then raised again, to -24.6°C and then to -7.5°C for comparison with the earlier measurements.

It had been noted that at the lowest temperatures the dispersion was, surprisingly, still not producing a semi circular plot on a Cole-Cole diagram and still appeared to be strongly influenced by the static conductivity. The samples would, most likely, be frozen to the electrodes and it was consequently considered possible that they had cracked. The samples were analysed at -7.5°C which, although not identical to a previous temperature, was close enough to allow comparison with the results at -8.2 and -6.2°C . It was found that no significant differences existed and hence felt that the samples had probably not been damaged. The temperature was then increased to -4.8°C and then to -2.5°C . The measurements at this latter setting were repeated once, after 24 hours, and again after a further 72 hours to determine if annealing would influence the dielectric properties (e.g. Reynolds, 1985). The changes were negligible.

2 Theory

The method used to obtain values of the parameters that describe the dielectric properties of each sample was based upon the analysis of modified complex conductivities;

$$\sigma_m^* = \sigma^* - i\omega\epsilon_0\epsilon_\infty. \quad (7)$$

Prior to obtaining σ_m^* it is necessary to supply a value of ϵ_∞ . In the absence of a reliable experimentally determined value, ϵ_∞ was assumed to be equal to 3.2 at 0°C for ice of density 920 kg m^{-3} and $\partial\epsilon_\infty/\partial T$ to be $1.2 \times 10^{-3} \text{ }^{\circ}\text{C}^{-1}$ (Paren, 1970; Hobbs, 1974).

σ_m^* is described by the equation:

$$\sigma_m^* = \sigma_0 + \sum_{i=1}^3 \frac{\Delta\sigma_i}{1 + (1/i\omega\tau_i)^{1-\alpha_i}} \quad (8)$$

where the subscripts, i , refer to the three dispersions and α is a parameter that defines the angle, $\pi\alpha/2$, subtended by the real axis and the geometrical centre of the dispersion. Separating real and imaginary parts of eqn. A2.8 leads to the relations:

$$\sigma_m' = \sigma_0 + \sum_{i=1}^3 \frac{\Delta\sigma_i(1 + r_i \cos \theta_i)}{\Pi_i} \quad (9)$$

$$\sigma_m'' = \sum_{i=1}^3 \frac{\Delta\sigma_i r_i \sin \theta_i}{\Pi_i} \quad (10)$$

where $r_i = (1/\omega\tau_i)^{\gamma_i}$, $\theta_i = \gamma_i/(2\pi)$, $\Pi = (1 + r \cos \theta)^2 + (r \sin \theta)^2$ and $\gamma_i = 1 - \alpha_i$. There are 10 unknowns in eqn. A2.8. Determination of these parameters was carried out in three

stages. Initial estimates were obtained by graphical means. From these values, it was possible to determine the range of frequencies, at each temperature, for which the low and high frequency dispersions (spectrums 1 and 3) were not significantly influencing the main volume polarization (spectrum 2). A least squares fitting routine (NAG routine E04FDF) was then applied to this limited dataset, to determine the three parameters defining spectrum 2 (i.e. $\Delta\sigma_2$, τ_2 and γ_2) and σ_o . The graphically obtained estimates were used as the starting values for the iteration. The minimization function was of the form:

$$F_{min} = (\sigma'_x + \sigma''_y) - \left(\sigma_o + \Delta\sigma_i \frac{1 + r_i \cos \theta_i}{\Pi_i} + \Delta\sigma_i \frac{r_i \sin \theta_i}{\Pi_i} \right) \quad (11)$$

where σ'_x and σ''_y are the experimental data and the subscript i , refers to the spectrum number.

For each dispersion there are three unknowns: $\Delta\sigma_i$, τ_i and γ_i . Adding to σ_o gives 10 parameters in all, that need to be determined. The variables were normalised to optimise the fitting procedure.

After obtaining the parameters for the main dispersion, its influence was removed by subtracting it from the experimental data, leaving spectrums 1 and 3. Insufficient data were available to determine the parameters defining the former and the latter could only be estimated for the three lowest temperatures. Comparisons between the theoretically deduced conductivities (from eqn. A2.8 and the parameters obtained from the least squares fit) and the experimental data are shown in Fig. 4.9 for two temperatures.

The relaxation times deduced from conductivities are only the same as those determined from permittivities for $\alpha = 0$. Consider eqn. A2.8 in terms of permittivities—

$$\sigma_m^* = i\omega\epsilon_o(\epsilon^* - \epsilon_\infty) \quad \text{which gives} \quad (12)$$

$$\epsilon' = \epsilon_\infty + \frac{\Delta\sigma}{\omega\epsilon_o} \frac{r \sin \theta}{\Pi} \quad (13)$$

$$\text{and } \epsilon'' = \frac{1}{\omega\epsilon_o} \left(\frac{\Delta\sigma(1 + r \cos \theta)}{\Pi} + \sigma_o \right) \quad (14)$$

A maximum occurs in σ'' when $\frac{d\sigma''}{d\omega} = 0$ and similarly for ϵ'' . The equations are expressed in terms of conductivities so, clearly $\frac{d\sigma''}{d\omega} = 0$ when $\omega\tau_\sigma = 0$. Differentiation of ϵ'' , with respect to ω , however, leads to the condition (for the maximum in ϵ''),

$$(\gamma - 1) \cos \theta r^3 + (2\gamma - 1 - 2 \cos^2 \theta)r^2 + (\gamma - 3) \cos \theta r - 1 - \sigma_o / \Delta\sigma = 0. \quad (15)$$

For $\gamma = 1$ (i.e. $\alpha = 0$ — a semi-circular dispersion) the above condition reduces to,

$$r^2 - 1 - \sigma_o / \Delta\sigma = 0 \quad \text{or} \quad \omega\tau_e = (1 + \sigma_o / \Delta\sigma)^{-1/2}. \quad (16)$$

Eqn. A2.15 has been used to transpose the τ_σ s to τ_e s. Both values are given in Table A3.2 which lists the results of the least squares fitting procedure for spectrum 2. Table A3.3 is similar to A3.2 but for spectrum 3.

3 Errors

Qualitative error estimates, for the least squares fitting procedure as a whole, could be inferred from the sum of the squares of the differences (ssd). $\sqrt{ssd/(n+1)}$ (where n is the number of data used) is a measure of the absolute difference between the fitted and experimental data. The errors for individual parameters, however, cannot be determined directly and were estimated by an empirical method. The three parameters defining spectrum 2 and σ_o were forced, one at a time, to have a constant value during a single run of the least squares routine. This value was gradually shifted away from the original estimate to see what influence this would have on the rate of convergence and, more importantly, the sum of the squares of the differences. $\Delta\sigma$ and τ were found to be the most sensitive parameters— varying them by 5% could increase the ssd by up to 20%. γ was found to influence ssd to a smaller degree and is only accurate to about 10%. σ_o had, by far, the weakest effect—changing it by a factor of 2, increased the ssd by only 4%. The errors in this variable are consequently relatively large ($\approx 100\%$) but the values do give a good order of magnitude estimate. It is also worth noting that they follow a reasonably 'well behaved' monotonic relationship with temperature (Fig. 4.13). Errors in the estimate of the parameters defining spectrum 3 are discussed more fully in Ch. 4 and, due to the smaller number of data points covering this spectrum, are relatively high ($> 100\%$).

APPENDIX 3

Dielectric Data

The tables in this appendix represent the data collected on the three samples of Spitsbergen ice that were discussed in Ch. 4. The number of decimal places quoted does not indicate the precision of the data. Table A3.1 provides all the raw data excepting the measurements which were repeated at -2.5°C after 24 and 72 hrs. These were effectively identical to those of the initial measurements. Table A3.2 displays the results of the least squares fitting routine for spectrum 2. Table A3.3 is the same but applied to spectrum 3.

Table A3.1 Complex permittivity data for the three samples at all the temperatures measured. The data have not been corrected for density and are consequently those of the actual samples.

Frequency (kHz)	Sample 1		Sample 2		Sample 3	
	ϵ'	ϵ''	ϵ'	ϵ''	ϵ'	ϵ''
	Temperature		-2.5°C			
0.022	237.811	559.025	515.787	641.631	384.015	806.101
0.044	162.107	328.937	369.802	439.608	262.935	493.186
0.088	111.405	192.967	249.863	300.986	174.800	296.879
0.180	81.751	109.403	167.142	192.754	123.336	170.468
0.360	66.802	63.441	123.084	119.385	98.449	99.034
0.580	60.494	44.563	106.220	85.825	88.497	69.948
1.000	55.418	31.334	94.226	61.600	80.701	50.188
2.000	50.278	23.292	83.082	47.107	71.908	39.606
3.800	44.876	21.917	69.698	46.611	60.750	38.188
6.600	37.968	22.756	51.270	47.976	46.218	39.192
11.000	29.373	23.493	31.848	42.915	30.706	36.039
21.000	17.436	20.812	14.368	29.633	15.181	26.432
35.000	10.338	16.007	7.839	19.569	8.557	18.177
50.000	7.237	12.411	5.646	14.161	6.107	13.397
70.000	5.445	9.392	4.533	10.299	4.806	9.850
100.000	4.425	6.757	3.930	7.255	4.056	7.026

Temperature		-4.8°C				
0.022	259.325	494.668	522.479	566.780	402.901	837.980
0.044	173.271	303.699	377.472	404.045	273.847	512.162
0.088	116.057	183.397	255.165	285.531	181.306	308.265
0.180	83.147	106.061	169.870	187.656	128.058	177.565
0.360	66.657	62.413	123.660	118.611	101.848	104.484
0.580	59.866	44.244	105.798	86.573	91.004	75.059
1.000	54.499	31.528	92.811	63.689	81.692	55.332
2.000	48.998	24.153	79.684	50.589	70.377	45.079
3.800	42.730	23.271	62.955	49.867	55.845	42.582
6.600	34.857	23.735	42.590	47.702	39.327	40.440
11.000	25.624	23.420	24.640	39.490	24.462	34.334
21.000	14.422	19.222	10.991	25.365	11.817	23.225
35.000	8.545	14.048	6.368	16.285	6.954	15.399
50.000	6.159	10.631	4.874	11.661	5.239	11.205
70.000	4.840	7.944	4.127	8.427	4.338	8.178
100.000	4.069	5.734	3.724	5.932	3.826	5.831
Temperature		-6.3°C				
0.022	266.302	602.771	541.010	580.931	444.345	900.980
0.044	166.293	356.699	385.553	408.513	291.684	552.201
0.088	108.149	206.427	251.819	295.027	187.181	334.642
0.180	77.797	115.058	165.886	190.979	130.051	191.202
0.580	57.679	45.791	103.415	87.435	91.545	80.716
1.800	48.557	25.598	78.809	53.024	70.744	48.705
6.600	32.537	24.202	37.603	46.559	35.170	40.668
11.000	23.125	23.136	21.052	36.936	21.092	32.922
16.000	16.561	20.637	13.180	28.617	13.847	26.143
21.000	12.515	18.051	9.481	22.956	10.137	21.332
35.000	7.442	12.770	5.723	14.549	6.427	14.127
50.000	5.508	9.545	4.539	10.404	4.820	10.072
70.000	4.458	7.074	3.947	7.509	4.108	7.342
94.000	3.939	5.387	3.666	5.620	3.756	5.529
Temperature		-7.5°C				
0.025	236.648	450.484	472.032	456.165	386.114	711.038
0.044	169.608	301.806	359.610	356.937	277.204	484.837
0.090	112.335	178.396	242.605	254.153	179.417	291.117
0.240	73.402	84.173	144.060	144.224	114.722	138.148
0.580	58.674	44.132	103.744	83.268	90.233	75.030
1.000	53.324	32.028	90.129	63.665	80.087	57.144
2.000	47.184	25.522	74.485	53.252	66.363	47.425
3.600	40.393	24.386	55.999	51.669	50.409	44.914
5.300	34.513	24.529	41.187	48.613	38.270	42.007
11.000	21.314	22.671	18.010	34.492	18.485	30.866
21.000	11.409	17.045	8.282	20.800	9.003	19.447
35.000	6.932	11.847	5.238	13.047	5.702	12.530
50.000	5.244	8.790	4.289	9.283	4.578	9.035
70.000	4.343	6.514	3.822	6.700	3.985	6.589
90.000	3.950	5.172	3.628	5.241	3.729	5.192
100.000	3.827	4.707	3.571	4.739	3.656	4.705

Temperature		-8.2°C				
0.025	234.904	557.090	477.180	518.429	405.000	797.873
0.090	104.137	202.045	241.730	271.358	185.870	318.856
0.240	69.018	90.072	141.280	149.583	0.000	0.000
0.580	56.580	45.696	101.840	85.231	90.501	80.903
1.300	49.743	29.257	82.644	59.667	74.421	55.941
3.720	38.538	25.210	51.939	51.732	47.016	46.034
5.322	32.794	24.726	38.144	48.059	35.516	42.375
10.900	19.769	22.362	16.611	33.387	16.997	30.242
22.320	9.732	15.597	7.219	18.595	7.805	17.611
89.100	3.785	4.786	3.583	4.954	3.661	4.919
Temperature		-11.5°C				
0.036	185.307	427.519	388.487	372.843	335.961	538.688
0.097	92.275	194.276	224.959	235.601	173.861	274.684
0.267	62.029	81.276	132.066	131.051	107.991	128.494
0.668	52.353	40.790	94.818	78.148	83.282	72.131
1.664	44.649	27.859	69.595	58.730	62.166	54.024
5.687	34.667	22.870	25.618	42.454	24.845	37.569
16.016	10.143	16.423	7.532	19.651	7.711	18.982
36.077	5.011	8.571	4.238	9.214	4.509	8.931
55.390	4.055	5.807	3.741	6.136	3.866	5.957
75.440	3.714	4.357	3.704	4.666	3.636	4.454
95.780	3.588	3.512	3.498	3.568	3.720	3.834
Temperature		-15.3°C				
0.021	268.163	751.722	492.623	429.044	484.531	650.940
0.041	143.850	433.204	352.094	331.292	299.978	451.601
0.061	106.091	308.060	283.477	280.408	222.440	350.457
0.122	72.367	165.163	190.306	198.580	140.994	211.196
0.222	60.168	96.992	139.021	141.824	107.215	134.928
0.523	51.313	49.320	97.227	89.300	81.970	78.357
1.201	44.120	32.350	69.410	67.637	61.091	58.313
2.237	36.171	28.433	45.946	57.054	41.567	49.096
4.221	25.706	25.662	23.396	42.741	22.869	37.194
12.173	9.428	15.941	8.346	14.121	7.354	17.214
32.310	4.383	7.106	3.914	7.441	4.088	7.148
Temperature		-20.0°C				
0.031	110.323	305.979	391.885	329.290	342.230	468.646
0.061	77.960	167.965	272.281	256.371	200.853	308.970
0.110	64.389	100.532	194.161	196.250	135.544	202.360
0.210	55.790	59.049	136.179	140.991	99.330	126.633
0.521	48.213	33.162	88.142	91.526	71.714	74.199
2.210	30.381	26.007	29.650	51.936	27.752	43.258
4.220	18.316	22.367	13.796	33.411	14.007	28.926
12.000	6.192	11.575	5.034	13.299	5.325	12.037
22.040	4.274	7.012	3.912	7.453	4.171	7.122
42.040	3.605	3.874	3.552	3.991	3.567	3.754

Temperature			-24.6°C			
0.022	119.778	120.134	408.203	237.586	352.539	354.851
0.044	91.985	76.913	307.310	212.263	219.287	255.037
0.088	75.291	50.918	214.860	179.120	139.861	168.792
0.180	63.465	36.245	143.154	137.499	98.176	107.847
0.360	54.133	28.713	96.625	104.069	73.755	76.165
0.580	47.847	26.932	71.248	87.393	58.237	64.132
1.000	39.364	26.800	45.232	70.252	39.897	53.111
1.500	31.735	26.528	29.465	56.633	27.600	44.163
2.000	25.979	25.532	21.002	45.920	20.549	37.481
3.800	14.657	19.984	10.030	27.659	10.471	23.238
6.600	8.605	14.051	6.088	16.916	6.499	14.604
11.000	5.731	9.387	4.538	10.497	4.830	9.249
21.000	4.118	5.346	3.763	5.661	3.906	5.116
35.000	3.592	3.371	3.522	3.474	3.576	3.201
50.000	3.398	2.438	3.430	2.478	3.441	2.311
70.000	3.261	1.799	3.357	1.812	3.337	1.705
95.000	3.183	1.363	3.313	1.364	3.275	1.292
Temperature			-34.4°C			
0.022	105.416	108.103	371.140	205.933	253.912	249.724
0.044	83.728	68.143	269.218	193.457	163.784	178.944
0.088	69.971	46.996	173.216	167.018	109.203	122.490
0.180	58.319	35.217	105.268	127.532	74.437	86.509
0.360	47.388	30.795	58.965	93.123	47.079	64.476
0.580	38.817	29.597	36.332	71.050	31.235	51.032
1.800	16.844	22.318	10.506	30.167	10.073	23.309
2.000	15.222	21.131	9.482	27.494	9.154	21.350
3.800	8.365	13.849	5.740	15.348	5.778	12.168
6.600	5.536	8.914	4.425	9.193	4.531	7.425
11.000	4.304	5.738	3.885	5.683	3.887	5.174
16.000	3.822	4.108	3.665	3.997	3.702	3.356
21.000	3.602	3.220	3.560	3.102	3.569	2.635
35.000	3.347	2.038	3.424	1.935	3.394	1.676
50.000	3.227	1.487	3.352	1.404	3.304	1.226
70.000	3.153	1.100	3.302	1.035	3.245	0.912
Temperature			-44.0°C			
0.022	83.030	30.496	294.956	203.698	171.495	125.507
0.044	70.791	27.152	192.622	181.038	121.642	102.224
0.088	60.075	24.860	117.704	138.716	83.990	82.214
0.180	50.307	24.538	65.276	99.859	52.251	63.456
0.260	44.717	25.345	45.870	81.453	38.339	54.303
0.360	39.008	26.122	32.708	66.383	28.067	45.876
0.580	29.590	25.337	19.556	47.249	17.191	33.815
0.750	24.502	24.221	14.933	38.757	13.283	28.054
1.000	19.182	22.136	11.160	30.575	10.094	22.318
1.500	13.170	18.255	7.783	21.612	7.276	15.914
2.000	10.053	15.288	6.295	16.742	6.038	12.403
3.800	5.954	9.473	4.540	9.301	4.543	7.042
6.600	4.392	5.908	3.924	5.518	3.945	4.309
11.000	3.716	3.759	3.632	3.437	3.619	2.742
16.000	3.451	2.684	3.504	2.436	3.464	1.974
21.000	3.325	2.101	3.434	1.903	3.381	1.556

Table A3.2 Parameters obtained from least squares fit for dispersion 2

Sample number	$f_{r\sigma}$ (kHz)	$f_{r\epsilon}$ (kHz)	γ	$\Delta\sigma_2$ $\mu\text{S m}^{-1}$	σ_0 $\mu\text{S m}^{-1}$	Sum of squares	Sum of differences
1 -2.5°C	17.387	12.774	0.906	39.455	1.231	11557.781	0.796
2	7.827	5.726	0.906	40.316	1.082	14574.852	5.893
3	10.590	8.087	0.937	37.334	2.633	13085.230	1.090
1 -4.8°C	12.498	9.153	0.926	31.685	0.814	7032.918	2.829
2	6.619	5.026	0.932	31.467	2.026	10074.535	0.538
3	7.394	5.396	0.893	31.763	0.827	6701.496	2.029
1 -6.3°C	11.500	8.494	0.915	27.965	1.001	6363.227	0.466
2	5.979	4.640	0.944	27.265	2.425	8687.184	0.074
3	6.583	5.040	0.921	26.566	1.954	3998.278	0.278
1 -7.5°C	11.004	8.173	0.906	25.697	1.085	3863.963	0.012
2	5.294	4.123	0.936	24.250	2.256	4869.484	0.080
3	6.000	4.618	0.915	23.643	1.873	2764.845	0.027
1 -8.2°C	10.775	8.020	0.889	24.246	1.101	2504.019	0.151
2	5.101	4.072	0.950	22.144	2.739	3431.213	0.106
3	5.500	4.123	0.876	23.343	1.234	3118.562	0.141
1 -11.5°C	5.400	3.813	0.861	22.092	0.000	2517.004	0.373
2	2.500	1.793	0.949	3.551	0.000	2157.202	0.501
3	2.700	1.907	0.863	26.362	0.000	2671.973	4.955
1 -20.0°C	3.300	2.504	0.906	8.053	0.516	223.941	0.021
2	1.400	1.162	0.875	8.019	1.241	342.047	0.044
3	1.800	1.408	0.792	8.272	0.704	273.432	0.106
1 -24.6°C	2.251	1.577	0.819	6.349	0.000	116.206	0.107
2	0.900	0.692	0.811	6.375	0.468	230.583	0.009
3	1.200	0.909	0.792	5.786	0.352	122.380	0.013
1 -34.4°C	1.596	1.177	0.836	3.761	0.148	51.040	0.006
2	0.360	0.260	0.700	3.560	0.100	70.474	0.002
3	0.550	0.443	0.742	2.683	0.263	43.005	0.001
1 -44.0°C	1.194	0.875	0.843	2.479	0.084	25.873	0.030
2	0.198	0.143	0.673	2.109	0.055	30.231	0.000
3	0.294	0.215	0.721	1.555	0.056	16.339	0.001

Table A3.3 Parameters obtained from least squares fit for dispersion 3

Sample number	$f_{r\sigma}$ (kHz)	$f_{r\epsilon}$ (kHz)	γ	$\Delta\sigma_3$ $\mu\text{S m}^{-1}$	Sum of differences	Sum of squares
1 -24.6°C	37.796	26.781	0.879	0.906	0.196	389.204
2	54.072	46.308	0.762	0.421	0.080	547.224
3	43.084	43.084	1.000	0.689	0.040	444.522
1 -34.4°C	23.003	23.488	0.938	0.280	0.154	162.264
2	36.868	36.868	1.000	0.378	0.008	164.758
3	25.701	24.961	0.896	0.642	0.226	116.480
1 -44.0°C	0.000	0.000	0.000	0.000	0.000	0.000
2	20.626	20.626	1.000	0.287	0.000	68.589
3	16.073	12.515	0.898	0.385	0.006	37.562

REFERENCES

- Abramowitz, M. and Stegun, I.A., 1964: Handbook of Mathematical Functions. *Applied Mathematics Series vol. 55* Washington Bureau of Standards, 1045 pp.
- Ackley, S.F. and Keliher, T.E., 1979: Ice sheet internal radio-echo reflections and associated physical property changes with depth. *Journal of Geophysical Research*, vol. 84 no. B10, p. 5675-5680.
- Ahlmann, H.W:son, 1935: The stratification of the snow and firn on Isachsen's Plateau. *Geografiska Annaler*, v 17, p 47-68.
- Archie, G.E., 1942: The electrical resistivity log as an aid in determining some reservoir characteristics. *Transactions AIME*. v 146 p 54.
- Auty, R.P. and Cole, R.H., 1952: Dielectric properties of ice and solid D₂O. *Journal of Chemical Physics*, v 20, no. 8, p 1309-14
- Baranowski, S., 1975: Glaciological investigations and glaciomorphological observations made in 1970 on Werenskioldbreen and in its forefield. *Acta Universitatis Wratislaviensis*, no. 251, 94 pp.
- Baranowski, S. and Jahn, A. (ed), 1975: Results of investigations of the Polish scientific Spitsbergen expedition 1970-74, *Acta Universitatis Wratislaviensis*, no. 251, 196 pp.
- Berry, M.V., 1973: The statistical properties of echoes diffracted from rough surfaces. *Phil. Trans. Roy. Soc. London (A)*, v 273, no. 1237, p 611-658.
- Bilgram, J.H., 1970: Segregation of hydrogen fluoride in ice single crystals. *Physics of Condensed Materials*, v 10, p 317-325.
- Bilgram, J.H. and Gränicher, H., 1978: Interaction of point defects in ice. *Journal of Glaciology*, v 21, no. 85, p 115-122.
- Blindow, N. and Thyssen, F., 1986: Ice thickness and inner structure of the Vernagtferner (Ötztal Alps): Results of electromagnetic reflection measurements. *Zeitschrift Für Gletscherkunde Und Glazialgeologie*, v 22, no. 1, p 43-60.
- Bogorodski, V.V., Bentley, C.R. and Gudmandsen, P.E., 1985: Radioglaciology. D. Reidel, Lancaster, 1985, 254 pp.

- Boulton, G.S. , 1970: On the origin and transport of englacial debris in Svalbard glaciers. *Journal of Glaciology*, v 9, no. 56, p 213-229.
- Camplin, G.C. and Glen, J.W., 1973: The dielectric properties of HF-doped single crystals of ice. In Whalley, E. and others (ed). *Physics and Chemistry of Ice, Ottawa, Canada, August 1972*. Edited by E. Whalley, S.J. Jones, L.W. Gold, Ottawa, Roy. Soc. of Canada, p 256-261.
- Camplin, G.C., Glen, J.W. and Paren, J.G., 1978: Theoretical models for interpreting the dielectric behaviour of HF-doped ice. *Journal of Glaciology*, v 21, no. 85, p 123-142.
- Clarke, G.K.C., 1976: Thermal regulation of glacier surging. *Journal of Glaciology*, v 16, p 231-250.
- Clarke, G.K.C., Nitsan, U., and Paterson, W.S.B. , 1977: Strain heating and creep instability in glaciers and ice sheets. *Rev. Geophys. Space Phys.* , v 15, p 235-247.
- Clarke, G.K.C., Collins, S.G. and Thompson, D.E., 1984: Flow, thermal structure, and subglacial conditions of a surge-type glacier. *Canadian Journal of Earth Sciences*, v 21, p 232-240.
- Collins, D.N. and Young, G.J., 1981: Meltwater hydrology and hydrochemistry in snow and ice-covered mountain catchments. *Nordic Hydrology*, v 12, p 231-247.
- Davis, J.C., 1973: *Statistics and data analysis in geology*. John Wiley, Chichester, 1973, 550 pp.
- Davis, J.L., 1973. The problem of depth sounding temperate glaciers. *Unpublished M.Sc. thesis* University of Cambridge, 106 pp.
- Dowdeswell, J.A., 1984: Remote sensing studies of Svalbard glaciers. *Unpublished Ph.D. thesis*, University of Cambridge, 250 pp.
- Dowdeswell, J.A., Drewry, D.J., Liestøl, O. and Orheim, O., 1984a: Radio-echo sounding of Spitsbergen glaciers: problems in the interpretation of layer and bottom returns. *Journal of Glaciology* , v 30, p 16-21.
- Dowdeswell, J.A., Drewry, D.J., Liestøl, O. and Orheim, O., 1984b: Airborne radio echo sounding of sub-polar glaciers in Spitsbergen. *Norsk Polarinstitutt Skrifter* , no. 182.
- Drewry, D.J., 1986: *Glacial Geologic Processes*. Edward Arnold, London 1986, 276 pp.

- Drewry, D.J. , Liestøl, O., 1985: Glaciological investigations of surging ice caps in Nordaustlandet, Svalbard, 1983. *Polar Record* , v 22, no. 139 p 359-378
- Duval, P., 1975: The role of water content on the creep rate of ice. In *Isotopes and Impurities in Snow and Ice*, IAHS-IASH Publ. 118 p 263-271, International Association of Hydrological Sciences, Gentbrugge, Belgium.
- Duval, P., 1979: Creep and recrystallisation of polycrystalline ice *Rev. Mineral.*, v 102, p 80-85.
- Evans, S., 1965: Dielectric properties of ice and snow—a review. *Journal of Glaciology*, v 5, no. 42, p 773-792.
- Evans, S. and Smith, B.M.E., 1969: A radio echo equipment for depth sounding in polar ice sheets. *Journal of Scientific Instruments (Journal of Physics E)* ser. 2, v 2, p 131-136.
- Fetter (Jr), C.W., 1980: Applied Hydrogeology. Charles E. Merrill, Columbus, 1980, 488 pp.
- Fitzgerald, W.J. and Paren, J.G., 1975: The dielectric properties of Antarctic ice. *Journal of Glaciology*, v 15, no. 73, p 15-38.
- Glen, A.R., 1937: The Oxford University Arctic Expedition, North-East Land 1935-36. *Geographical Journal*, v 90, p 193-222 and p 289-314.
- Glen, J.W., and Paren, J.G., 1975: The electrical properties of snow and ice. *Journal of Glaciology* , v 15, no. 73 p 15-37
- Glen, J.W., Homer, D.R. and Paren, J.G., 1977: Water at grain boundaries: its role in the purification of temperate glacier ice. [*Union Géodésique et Géophysique Internationale. Association Internationale des Sciences Hydrologiques. Commission des Neiges et Glace.*] Actes du colloque de Grenoble, août/septembre 1975, p 263-271. (IAHS-AISH Publ. no. 118).
- Goodman, R.H., 1975: Radio echo sounding on temperate glaciers. *Journal of Glaciology*, v 14, no. 70, p 57-69.
- Gränicher, H., 1969: Evaluation of dielectric dispersion data. In *Physics of ice: proceedings of the international symposium on physics of ice, Munich, Germany, Sept 9-14 , 1968.* Edited by N. Riehl, B. Bullemer, H. Englehardt., Plenum Press, New York p 527-533.
- Grigoryan, S.S., Bozhinskiy, A.N., Krass, M.S., Macheret, Y.Y., 1985: Yavleniye

- vnuttrennego razogreva "kholodnykh" lednikov i obrazovaniye lednikov perekhodnogo tipa [The phenomenon of internal warming up of "cold" glaciers of a transitional type]. *Materialy Glyatsiologicheskikh Issledovaniy. Khronika. Obsuzhdeniya*, no. 51, p 105-110.
- Gross, G.W., Hayslip, I.C. and Hoy, R.N., 1978: Electrical conductivity and relaxation in ice crystals with known impurity content. *Journal of Glaciology*, v 21, no. 85, p 143-160.
- Gurnell, A.M. and Clark, M.J., (ed) 1987: Glacio-Fluvial sediment transfer—An Alpine perspective. John Wiley, Chichester 1987, 524 pp.
- Hantz, D. and Lliboutry, L., 1983: Waterways, ice permeability at depth and water pressures at Glacier d'Argentière, French Alps *Journal of Glaciology*, v 29, no. 102, p 227-239.
- Harland, W.B., 1985: Caledonide Svalbard. In Gee, D.G. and Stuart, B.A. (eds) *The Caledonide Orogen—Scandinavia and related areas*. J. Wiley, Chichester, 1985 p 999-1016.
- Harrison, C.H., 1972: Radio echo propagation effects in glaciers. *Unpublished Ph.D thesis*, University of Cambridge 193 pp.
- Hisdal, V., 1985: Geography of Svalbard. *Norsk Polarinstitutt Polarhandbok*, no. 2, 75 pp, 2nd edn.
- Hjelle, A. and Lauritzen, Ø., 1982: Geological map of Svalbard 1:500,000 sheet 3G, Spitsbergen northern part. *Norsk Polarinstitutt Skrifter*, no. 154C 15 pp.
- Hobbs, P.V., 1974: Ice physics. Clarendon Press, Oxford 1974, 836 pp.
- Hodge, S.M., 1976: Direct measurement of basal water pressures: a pilot study. *Journal of Glaciology*, v 16, no. 74, p 205-218.
- Holman, J.P., 1981: Heat transfer. McGraw Hill, New York 1981, 2nd edn.
- Horvath, E. and Fahn, C., 1975: Glaciers of Svalbard. In Field, W.O. (ed), *Mountain glaciers of the northern hemisphere*, v 2 p 879-932.
- Husebye, E.S., Sørnes, A. and Wilhelmsen, L.S., 1965: The determination of the thickness of Finsterwalderbreen, Spitsbergen, by gravity measurements. *Norsk Polarinstitutt Årbok*, 1963, p 129-136.

- Jaccard, C., 1959: Étude théorique et expérimentale des propriétés électriques de la glace. *Helvetica Physica Acta*, v 32, p 89-128.
- Jaccard, C., 1964: Thermodynamics of irreversible processes applied to ice. *Physics of Condensed Materials*, v 3, p 143-151.
- Jiracek, G.R., 1965: Radio echo sounding of Antarctic ice. *Unpublished Ph.D thesis*, University of Wisconsin, 1965.
- Johari, G.P., 1976: The dielectric properties of H₂O and D₂O ice 1h at MHz frequencies. *Journal of Chemical Physics*, v 64, no. 10, p 3998-4005.
- Johari, G.P., 1981: The spectrum of ice. *Contemporary Physics*, v 22, no. 6, 613-642.
- Johari, G.P. and Charette, P.A., 1975: The permittivity and attenuation in polycrystalline and single-crystal ice 1h at 35 and 60 MHz. *Journal of Glaciology*, v 14, no. 71, p 293-302.
- Johari, G.P. and Jones, S.J., 1976: Dielectric properties of polycrystalline D₂O ice 1h (hexagonal). *Proc Roy. Soc. London A* v 349, p 467-494.
- Johari, G.P. and Whalley, E., 1981: The dielectric properties of ice 1h in the range 272-133 K. *Journal of Chemical Physics*, v75, no.3, p 1333-1340.
- Jones, A.S., 1979: The flow of ice over a till bed. *Journal of Glaciology*, v22, p 393-395.
- Kaye, G.W.C. and Laby, T.H., 1975: Tables of physical and chemical constants. Longman Press, London, 14th edn.
- Kröger, F.A., 1964: The chemistry of imperfect crystals. Vol. 2. North Holland Publishing Co. Ch. 18, "ice", p 750-767.
- Lamb, J. and Turney, A., 1949: The dielectric properties of ice at 1.25 cm wavelength. *Proc. Phys. Soc., section B*, v 62, part 4 p 272-273.
- Liestøl, O., 1969: Glacier surges in west Spitsbergen. *Canadian Journal of Earth Sciences*, v 6, p 895-897.
- Liestøl, O., 1974: Glaciological work in 1972. *Norsk Polarinstitutt Årbok, 1972* p 125-135.
- Liestøl, O., 1976: Glaciological work in 1974. *Norsk Polarinstitutt Årbok, 1974* p 183-194.
- Liestøl, O., 1977: Pingoos, springs and permafrost in Spitsbergen *Norsk Polarinstitutt Årbok, 1975*. p 7-9.
- Liestøl, O., 1984: Glaciological work in 1983. *Norsk Polarinstitutt Årbok, 1983* p 35-45.

- Lliboutry, L., 1976: Physical processes in temperate glaciers. *Journal of Glaciology*, v 16, no. 74 p 151-158
- Lliboutry, L., 1983: Modification to the theory of intraglacial waterways for the case of subglacial ones. *Journal of Glaciology*, v 29, no. 102, p 216-226.
- Lysne, P.C., 1983: A model for the high-frequency electrical response of wet rocks. *Geophysics*, v 48, no. 6, p 775-786.
- Maeno, N., 1974: Investigations of electrical properties of deep ice cores obtained by drilling in Antarctica. In *Kyokuchihyō shāhyō no butsuriteki kagakuteki kenkyū (Physical and Chemical Studies on ices from glaciers and ice sheets)*. Monbushō Kagaku Kempī Sōgō Kenkyū (A) Hokukusho, 1973 p 45-56.
- Macheret, Y.Y. and Zhuravlev, A.B., 1982: Radio echo sounding of Svalbard glaciers. *Journal of Glaciology*, v 28, p 295-314.
- Macheret, Y.Y., Vasilenko, Y.V., Gromyko A.N., Zhurahlev, A.B., 1984: Radiolokatsionnyy karotazh skvazhiny na lednike Fridtof, Shpitsbergen [Radio echo logging of the borehole on the Fridtjov Glacier, Spitsbergen]. *Materialy Glyatsiologicheskikh Issledovaniy. Khronika. Obsuzhdeniya*, no. 50 p 198-203.
- Macheret, Y.Y., Zhuravlev, A.B. and Bobrova, L.I., 1985: Thickness, subglacial relief and volume of Svalbard glaciers based on radio echo sounding data. *Polar Geography and Geology*, v 9, p 224-243.
- Maxwell, J.C., 1891: A treatise on electricity and magnetism. Dover Publns., Dover revised edn 1954, vol 1 519 pp, vol 2 507 pp.
- Millar, D.H.M., 1981: Radio echo layering in polar ice sheets. *Unpublished Ph.D thesis*, University of Cambridge 177 pp.
- Mogensen, O.E. and Eldrup, M., 1978: Vacancies in pure ice studied by positron annihilation techniques. *Journal of Glaciology*, v 21, no. 83, p 85-99.
- Muller, F., 1963: Englacial temperature measurements on Axel Heiberg Island, Canadian Arctic archipelago. *IASH 61*, p 168-180.
- Neal, C.S., 1977: Radio echo sounding studies of the Ross Ice Shelf *Unpublished Ph.D thesis*, University of Cambridge 87 pp.
- Nye, J.F., and Frank, F.C., 1973: Hydrology of the intragranular veins in a temperate

- glacier. *Union Geodesique et Geophysique Internationale. Association Internationale d'Hydrologie Scientifique. Commission de Neiges et Glaces. Symposium on the Hydrology of Glaciers, Cambridge, 7-13 Sept 1969, p157-161.*
- Oswald, G.K.A., 1975: Radio echo sounding of polar glacier beds *Unpublished Ph.D thesis, University of Cambridge 1975.*
- Paren, J.G., 1970: Dielectric properties of ice. *Unpublished Ph.D thesis, University of Cambridge 233 pp.*
- Paren, J.G., 1973: The electrical behavior of polar glaciers. In Whalley, E. and others (ed). *Physics and Chemistry of Ice, Ottawa, Canada, August 1972.* Edited by E. Whalley, S.J. Jones, L.W. Gold, Ottawa, Roy. Soc. of Canada p 262-267.
- Paren, J.G., and Walker, J.C.F., 1971: Influence of limited solubility on the electrical and mechanical properties of ice. *Nature* v 230, no. 12, p 77-79.
- Paren, J.G., and Robin, G. de Q., 1975: Internal reflections in polar ice sheets. *Journal of Glaciology*, v 14, no. 71 p 251-259.
- Paren, J.G. and Glen, J.W., 1978: Electrical behaviour of finely divided ice. *Journal of Glaciology*, v 21, no. 85, p 173-192.
- Parkhomenko, E.I., 1967: Electrical properties of rocks, translated by G.V. Keller, Plenum Press, New York 1967.
- Paterson, W.S.B., 1981: *The Physics of Glaciers.* Second edition, Pergamon, Oxford, 380pp.
- Punning, J.M.K., Vaykymae, R.A., Kotlyakov, V.M. and Gordiyenko, F.G., 1980: Izotopno-kislorodnye issledovaniy kerna s ledorazdela lednikov Gren'ord i Frit'of (o Zapadnyj Shpitsbergene). [Isotope-hydrogen investigations of an ice core from the ice divide of Grønffjordbreen-Fridtjovbreen (Island of Spitsbergen)]. *Materialy Glyatsiologicheskikh Issledovaniy. Khronika. Obsuzhdeniya*, v 37, p 173-177.
- Raymond, C.F., and Harrison, W.D., 1975: Some observations on the behaviour of the liquid and gas phases in temperate glacier ice. *Journal of Glaciology*, v 14, no. 71 p 213-232.
- Reynolds, J.M., 1985: Dielectric behaviour of firn and ice from the Antarctic peninsula, *Antarctica Journal of Glaciology*, v 31, no. 109, p 253-262.

- Reynolds, J.M. and Paren, J.G., 1980: Recrystallisation and electrical behaviour of glacier ice. *Nature* v 283, no. 5742, p 63-64.
- Robin, G. de Q., 1975: Velocity of radio waves in ice by means of a borehole interferometric technique. *Journal of Glaciology*, v 15, no. 73, p 151-160.
- Robin, G. de Q. (ed), 1985: The climatic record in polar ice sheets. CUP, Cambridge 1985, 212 pp.
- Robin, G. de Q., Evans, S. and Bailey, J.T., 1969: Interpretation of radio echo sounding in polar ice sheets. *Phils. Trans. Roy. Soc. London (A)* v 265, no. 1166, p 437-505.
- Robin, G. de Q. and Weertman, J., 1973: Cyclic surging of glaciers. *Journal of Glaciology*, v 12, p 3-18.
- Röthlisberger, H., 1972: Water pressure in intra- and subglacial channels. *Journal of Glaciology*, v 11, no. 62 p177-203
- Schommer, P., 1977: Wasserpiegelmessungen im firn des Ewigschneefeldes (Schweizer Alpen) 1976. *Zeitschrift Für Gletscherkunde Und Glazialgeologie*, v 12, no. 2, p 125-141.
- Schytt, V., 1964: Scientific results of the Swedish Glaciological Expedition to Nordaustlandet, Spitsbergen, 1957 and 1958 parts I and II *Geografiska Annaler*, v 46, p 243-281.
- Schytt, V., 1969: Some comments on glacier surging in eastern Svalbard. *Canadian Journal of Earth Sciences* v 6, p 867-873.
- Semb, A., Brøekkan, R. and Joranger, E., 1984: Major ions in Spitsbergen snow samples. *Geophys. Res. Let.* v 11, no. 5, p 445-448.
- Sillars, R.W., 1937: The properties of a dielectric containing semi-conducting particles of various shapes. *Journal of the Institute of Electrical Engineers (London)* v 80, p 378.
- Slatt, R.M., 1972: Geochemistry of meltwater streams from nine Alaskan glaciers. *Geological Society of America Bulletin* v 83, p 1125-1132.
- Smith, B.M.E., 1971: Radio echo sounding studies of glaciers. *Unpublished Ph.D. thesis*, University of Cambridge pp 157.
- Smith, B.M.E. and Evans, S., 1972: Radio echo sounding: absorption and scattering by water inclusions and ice lenses. *Journal of Glaciology*, v 11, no. 61, p 133-146.
- Spring, U. and Hutter, K., 1981: Numerical studies of jökulhlaups. *Cold Regions Science*

- and *Technology*, v 4, no. 3 p 227-244.
- Steffenson, E., 1982: The climate at Norwegian Arctic stations. *Klima* no. 5, 44 pp.
- Sverdrup, H.V., 1935: The temperature of the firn on Isachsen's Plateau and general conclusions regarding the temperatures of the glaciers on West-Spitsbergen. *Geografiska Annaler*, v 17, p 53-58.
- Vallon, M., Petit, J.R., and Fabre B., 1976: Study of an ice core to the bedrock in the accumulation zone of an alpine glacier. *Journal of Glaciology*, v 17, no. 75 p 13-28.
- Van Beek, L.K.H., 1967: Dielectric behaviour of heterogeneous systems. In Birks, J.B., ed. *Progress in Dielectrics. Vol. 7* Heywood books, London, 1967 p69-114.
- Van de Hulst, H.C., 1957: Light Scattering by small particles. Dover Publ., New York 1957, 470 pp.
- Vaykymae, R.A., Gordieyenko, F.G., Zagorodnov, V.S., Michalëv, V.I., Punning, Ya. M.K. and Rayamyae, R.A., 1977: Izotopnye, geochimičeske i stratigrafičeske issledavanija na ledorazdele lednikov Grënfjord v Fridtjov (O. Zapadnyj Shpitsberge). [Isotopic, geochemical and stratigraphic investigations on the ice-divide of the Grøn fjord and Fridtjov glaciers.] *Materialy Glyatsiologičeskikh Issledovaniy. Khronika. Obsuzhdeniya*, v 30, p 77-87.
- Von Hippel, A., 1971: Transfer of protons through "pure" ice 1h single crystals II. Molecular models for polarization and conduction. *Journal of Chemical Physics*, v 54, p 145-149.
- Von Hippel, A., Mykolajewycz, R., Runck, A.H. and Westphal, W.B., 1972: Dielectric and mechanical response of ice 1h single crystals and its interpretation. *Journal of Chemical Physics*, v 57, no. 6, p 2560-2571.
- Von Hippel, A., Runck, A.H. and Westphal, W.B., 1973: Ice chemistry: Is ice 1h a proton semiconductor? In Whalley, E. and others (ed). *Physics and Chemistry of Ice, Ottawa, Canada, August 1972*. Edited by E. Whalley, S.J. Jones, L.W. Gold, Ottawa, Roy. Soc. of Canada p 236-241.
- Wagner, K.W., 1914: Erklärung der dielektrischen nachwirkungsvargange auf Grund Maxwellscher varstellungen. *Arch. Elektrotech* v 2, p 371.
- Watts, R.D. and England, A.W., 1976: Radio echo sounding of temperate glaciers: ice properties and sounder design criteria. *Journal of Glaciology*, v 17, p 39-48.

- Winsnes, T.S., Heintz, A. and Heintz, N., 1962: Aspects of the geology of Svalbard. *Norsk Polarinstitutt Meddelelser* no. 87, 35 pp.
- Wolff, E.W., and Paren J.G., 1984: A two-phase model of electrical conduction in polar ice sheets. *Journal of Geophysical Research* , v 89, no. B11 p 9433-9438.
- Yevseyev, A.V., Korzun, A.V., 1985: O khimicheskom sostave lednikovogo pokrova na Severo-Vostochnoy Zemle [On the chemical composition of ice cover on Nordaustlandet]. *Materialy Glyatsiologicheskikh Issledovaniy. Khronika. Obsuzhdeniya*, v 52, p205-209.
- Zagorodnov, V.S., and Zotikov, I.A., 1981: Kernovoye bureniye na Shpitsbergene [Ice core drilling on Spitsbergen]. *Materialy Glyatsiologicheskikh Issledovaniy. Khronika. Obsuzhdeniya*, v 40, p 157-163.
- Zagorodnov, V.S., and Zotikov, I.A., 1981b: Vnutriledikovyye kanaly [Capillary channels in glaciers]. *Materialy Glyatsiologicheskikh Issledovaniy. Khronika. Obsuzhdeniya*, v 41, p 200-202.